N72-30897

A THERMAL SCALE MODELING STUDY FOR APOLLO AND APOLLO APPLICATIONS

VOLUME 2

D180-15048-1

FINAL REPORT

CONTRACT NAS9-8332

JUNE 1972

Prepared by

THE BOEING COMPANY

Research & Engineering Division

Seattle, Washington

PREPARED FOR

NATIONAL AERONAUTICS AND SPACE ADMINISTRATION

MANNED SPACECRAFT CENTER

HOUSTON, TEXAS

D180-15048-1

A THERMAL SCALE MODELING STUDY FOR APOLLO AND APOLLO APPLICATIONS

VOLUME 2

by

Roger L. Shannon

Final Report

Contract NAS9-8332

June 1972

Prepared by

The Boeing Company

Aerospace Group

Research and Engineering Division

Seattle, Washington

Prepared for

National Aeronautics and Space Administration

Manned Spacecraft Center

Houston, Texas

CONTENTS

CONTENTS (Continued)

PART II

CABIN ATMOSPHERE/SPACECRAFT CABIN WALL THERMAL INTERFACE

Table of Contents

Appendices

List of Figures

List of Figures (Continued)

List of Figures (Continued)

List of Figures (Continued)

List of Figures (Continued)

List of Figures (Continued)

List of Tables

Nomenclature

A	area
c	specific heat
C, C_1	constants in convective heat transfer correlations
$\vec{e}$	unit vector
F	radiation exchange factor
g	acceleration of gravity
Gr	Grashof number $\rho^2 g\beta L^3 To/\mu^2$
h	heat transfer coefficient
k	thermal conductivity
K	conductance per unit area
L	characteristic length
Nu	Nusselt number hL/k
m	Pr exponent in forced convection correlation
m_1	Pr exponent in free convection correlation
M	molecular weight
n	Re exponent in forced convection correlation
n_1	Gr exponent in free convection correlation
P	pressure
P_*	nondimensional pressure $\rho L^2 \rho/\mu^2$
Pr	Prandtl number $\mu c/k$
q_s	heating rate per unit area
q_v	heating rate per unit volume
Q	heating rate or heating rate per unit area
Re	Reynolds number $\rho\bar{v}L/\mu$
t	time
T	temperature

Nomenclature (cont.)

T_o	characteristic temperature
v	velocity
v_*	nondimensional velocity $v/\overline{v}$
w	mass flow rate

Greek Symbols

α	heat transfer area/cross-sectional flow area
β	coefficient of thermal expansion
δ	thickness
Θ	nondimensional temperature T/To
Θ_f	nondimensional fluid temperature $(T_f - \overline{T}_f)/To$
μ	viscosity
δ	density
σ	Stefan-Boltzmann constant
τ	nondimensional time $kt/\rho cL^2$

Operators

∇	gradient operator $\vec{e}_i \frac{\partial}{\partial x_i}$
∇_*	nondimensional gradient operator $L\nabla$

Subscripts

e	environment
f	fluid
g	gas
L	laminar
m	model
n	surface normal
o	characteristic value

Subscripts (cont.)

p prototype

r reference

s surface

T turbulent

w wall

superscript * refers to model to prototype parameter ratio

Average values denoted by bar

Other symbols defined where used in text

II.1 SUMMARY

This section of the Final Report documents the Task II #1 "Cabin Atmosphere/ Cabin Wall Thermal Interface" unit study area investigation.

The thermal scale modeling criteria applicable to radiation-conduction-convection systems are derived.

Detailed consideration is given to four possible scale modeling techniques.

- Modified Material Preservation
- Temperature Preservation
- Scaling Compromises
- Nusselt Number Preservation

The most promising techniques (scaling compromises and Nusselt number preservation) were chosen for an experimental investigation.

Full scale and 1/4 scale models of a configuration, in which radiation, conduction and convection heat transfer effects are important, were built and tested.

The full scale and 1/4 scale model temperatures were correlated for scaling compromises of mass flux and heat transfer coefficient preservation.

A thermal math model was developed for use in conjunction with the Nusselt number preservation technique. A Nusselt number correlation was developed for the free convection tests using the 1/4 scale model data. However the investigation of the Nusselt number preservation technique was not completed due to a lack of time and funds.

It was concluded that either preservation of mass flux or heat transfer coefficient may result in adequate thermal similitude depending on the system being modeled. For manned spacecraft heat transfer coefficient preservation should give good thermal similitude for both steady state and transient conditions. The Nusselt number preservation technique is workable however it is costly and difficult to implement.

II.2 INTRODUCTION

Most spacecraft thermal scale modeling studies have dealt with systems involving only the radiation and conduction modes of heat transfer. These studies range from the verification of scale modeling techniques using relatively simple configurations (see for example references 1-4) to the thermal scale modeling of an actual spacecraft concept (reference 5). Thermal scale modeling of manned spacecraft involves the convection as well as the radiation and conduction modes of heat transfer. The similitude criteria and discussions of possible scaling techniques have been presented in the literature (see for example reference 6). However, no experimental verification of the scaling techniques has been reported for manned spacecraft. A thermal scale modeling of free convection in heated enclosures has been reported (reference 7). An 8 x 8 x 8 foot prototype room with a convector heater and a 1/4 scale model were built and tested. Radiation-conduction scaling criteria were used for temperature preservation in the 1/4 scale model, however, no attempt was made to modify the convective heat transfer and air at atmospheric pressure was used in both model and prototype.

In order for thermal scale modeling to be a practical tool for manned spacecraft applications effective thermal scale modeling techniques must be developed for the cabin atmosphere/spacecraft cabin wall thermal interface.

This report describes the development and demonstration of practical thermal scale modeling techniques applicable to radiation - conduction - convection systems with particular emphasis on the cabin atmosphere/cabin wall thermal interface.

II.3 SCALE MODELING CRITERIA

The thermal scale modeling criteria may be developed from the equations which govern the system thermal energy balance. The governing equations when written in nondimensional form result in dimensionless groups of parameters. These dimensionless groups must remain invariant for thermal similitude to exist between similar systems.

The heat conduction within the solid elements of the system is governed by the Fourier equation

$$\rho c \frac{\partial T}{\partial t} = k \nabla^2 T + q_v \tag{1}$$

and the heat transfer boundary condition at the solid/fluid interface is given by

$$q_s - k(\vec{e}_n \cdot \nabla T)_w = \int_j \sigma (T^4 - T_j^4) d\mathcal{F}_j - k_f (\vec{e}_n \cdot \nabla T_f)_w \tag{2}$$

If the heat conduction in the solid is two dimensional (in the plane of the surface) then equation (1) is incorporated in equation (2) which becomes

$$q_s - \rho c \delta \frac{\partial T}{\partial t} + k \delta \nabla^2 T = \int_j \sigma (T^4 - T_j^4) d\mathcal{F}_j - k_f (\vec{e}_n \cdot \nabla T_f)_w \tag{3}$$

These equations can be written in nondimensional form as:

Heat conduction

$$\frac{\partial \theta}{\partial \tau} = \nabla_*^2 \theta + \left(\frac{L^2 q_v}{k T_o}\right) \tag{4}$$

Boundary condition at solid/fluid interface

$$\left(\frac{q_s}{\sigma T_o^4}\right) - \left(\frac{k}{\sigma T_o^3 L}\right)(\vec{e}_n \cdot \nabla_* \theta)_w = \int_j (\theta^4 - \theta_j^4) d\mathcal{F}_j - \left(\frac{k_f}{\sigma T_o^3 L}\right)(\vec{e}_n \cdot \nabla_* \theta_f)_w \tag{5}$$

or for two dimensional conduction

$$\left(\frac{q_s}{\sigma T_o^4}\right) + \left(\frac{k \delta}{\sigma T_o^3 L^2}\right)\left(\nabla_*^2 \theta - \frac{\partial \theta}{\partial \tau}\right) = \int_j (\theta^4 - \theta_j^4) d\mathcal{F}_j - \left(\frac{k_f}{\sigma T_o^3 L}\right)(\vec{e}_n \cdot \nabla_* \theta_f)_w \tag{6}$$

Thermal simiItude within the solid elements of geometrically similar systems having identical radiative surface properties is achieved by keeping the following dimensionless groups invariant:

- Heat Conduction: $\left(\frac{k}{\sigma T_o^3 L}\right)$, or $\left(\frac{k\delta}{\sigma T_o^3 L^2}\right)$ for two dimensional conduction
- Volume heat sources: $\left(\frac{L^2 q_v}{k T_o}\right)$
- Surface heat flux: $\left(\frac{q_s}{\sigma T_o^4}\right)$
- Heat transfer to fluid: $\left(\frac{k_f}{\sigma T_o^3 L}\right)$

The invariance of this last dimensionless group $\left(\frac{k_f}{\sigma T_o^3 L}\right)$ assumes that thermal similitude exists for the fluid elements of the systems as well as for the solid elements.

The fluid elements of the system are governed by the energy, momentum and continuity relationships. The energy equation may be written (without internal heat sources, viscous dissipation or radiation) as

$$\rho_f c_f \left(\frac{\partial T_f}{\partial t} + \vec{v}\cdot\nabla T_f\right) = k_f \nabla^2 T_f \tag{7}$$

and the momentum (Navier-Stokes) equation may be written for incompressible flow with buoyancy effects as

$$\rho_f \left(\frac{\partial \vec{v}}{\partial t} + \vec{v}\cdot\nabla\vec{v}\right) = -\nabla P + \mu\nabla^2\vec{v} - \rho_f g \beta (T_f - \bar{T}_f)\,\vec{e}_g \tag{8}$$

The continuity condition for incompressible flow is

$$\nabla\cdot\vec{v} = 0 \tag{9}$$

These equations may be written in non-dimensional form as

Energy

$$\left(\frac{k}{\rho c}\right)\left(\frac{\rho c}{k}\right)_f \frac{\partial \theta_f}{\partial \tau} + Re\,Pr\,\vec{v}_* \cdot \nabla_* \theta_f = \nabla_*^2 \theta_f \tag{10}$$

Momentum

$$\left(\frac{k}{\rho c}\right)\left(\frac{\rho c}{k}\right)_f \frac{Re}{Pr}\frac{\partial \vec{v}_*}{\partial \tau} + Re^2\,\vec{v}_*\cdot\nabla_*\vec{v}_* = -\nabla_* P_* + Re\,\nabla_*^2\vec{v}_* - Gr\,\theta_f\,\vec{e}_g \qquad (11)$$

Continuity

$$\nabla_*\cdot\vec{v}_* = 0 \qquad (12)$$

Thermal (and dynamic) similitude within the fluid elements of similar systems then requires the following dimensionless groups to remain invariant:

- ° Reynolds number: $Re = \dfrac{\rho_f \bar{v} L}{\mu}$
- ° Prandtl number: $Pr = \dfrac{\mu c}{k}$
- ° Grashof number: $Gr = \dfrac{\rho_f^2 g \beta L^3 T_0}{\mu^2}$
- ° Fluid/solid transients: $\left(\dfrac{k}{\rho c}\right)\left(\dfrac{\rho c}{k}\right)_f$

The last dimensionless group $\left(\frac{k}{\rho c}\right)\left(\frac{\rho c}{k}\right)_f$ when kept invariant preserves the relationship between the transient response of the fluid and that of the solid. However, for thermal scale modeling applications involving the manned spacecraft cabin atmosphere-cabin wall thermal interface, the fluid (gas) transients have negligible effect on the spacecraft thermal response. Consequently the invariance of the $\left(\frac{k}{\rho c}\right)\left(\frac{\rho c}{k}\right)_f$ group is not required for thermal similitude in this case.

The thermal scale modeling criteria for the cabin atmosphere - cabin wall thermal interface are summarized in Table II-1.

TABLE II-1 THERMAL SCALE MODELING CRITERIA FOR CABIN ATMOSPHERE - CABIN WALL THERMAL INTERFACE

Cabin Wall	
Heat Conduction	$(k/LT_o^3)^* = 1$
two dimensional conduction	$(k\delta/L^2T_o^3)^* = 1$
Volume Heat Sources	$(q_v\ L^2/k\ T_o)^* = 1$
Surface Heat Flux	$q_s^* = 1$
Transients	$(kt/\rho CL^2)^* = 1$
Cabin Atmosphere	
Heat Conduction	$(k_f/LT_o^3)^* = 1$
Reynolds number	$Re^* = 1$
Prandtl number	$P_r^* = 1$
Grashof number	$Gr^* = 1$
*Transients	$(k_f\ \rho c/k\ \rho_f\ c_f)^* = 1$

*The cabin atmosphere transient effects on the wall are generally small and adequate similitude may be achieved without meeting this criteria.

II.4 SCALE MODELING TECHNIQUES

Four scaling techniques were considered for the cabin atmosphere - cabin wall thermal interface. These are the Modified Material Preservation, Temperature Preservation, Scaling Compromises and Nusselt Number Preservation Techniques. Table II-2 gives a comparison of these techniques. The Modified Material and Temperature Preservation techniques are straightforward attempts to meet the scaling criteria given in Table II-1. The Scaling Compromises technique attempts to achieve thermal similtude without completely satisfying the scaling criteria. The Nusselt Number Preservation technique uses the thermal scale model to experimentally determine the Nusselt number as a function of Reynolds and Prandtl numbers and uses these results in conjunction with a thermal math model to determine the prototype performance.

II.4.1 Modified Material Preservation

The material preservation technique used for radiation-conduction systems keeps the same materials in model and prototype and meets the scaling criteria by increasing the temperature and heat flux in the model. The scaling criteria for systems involving convective heat transfer may be met by a "modified material preservation technique" which accounts for the variation of gas thermal conductivity with temperature. This technique requires the scale model temperature and heat fluxes be increased to a greater extent than does the normal material preservation technique. The required model to prototype temperature ratio is given by

$$T^* = \left(\frac{k_g^*}{L^*}\right)^{\frac{1}{3}} \qquad (13)$$

The temperature requirements as a function of scale ratio are compared in Figure II-1 for these techniques with air at 70°F in the prototype. The modified material preservation technique also requires the wall material to be changed (or in the case of two dimensional wall conduction, the proper selection of wall thickness) to meet the scaling criteria at the higher temperature.

TABLE II-2 COMPARISON OF SCALING TECHNIQUES

Scaling Techniques	Thermal Similitude	Model Temperature	Gas in Model	Simulation of Prototype Gravity Field	
				0-g	1-g
Modified Material Preservation	Exact	Increased(1) over Prototype	Same as Prototype	Good Prospects	Increased Pressure Required
Temperature Preservation	Exact	Same as Prototype	Thermal(2) Conductivity Scaled	Reduced Pressure Required	Good Prospects
Scaling Compromises	Approximate(3)	Same as Prototype	Same as Prototype	Reduced Pressure Required	Good Prospects
Nusselt Number Preservation	Partial(4)	Approximately same as Prototype	Same as Prototype	Good Prospects	Increased Pressure Required

(1) Excessive temperature and heat fluxes in the scale model severely limits use of "Modified Material Preservation."

(2) The availability of suitable gases limits the use of "Temperature Preservation."

(3) Degree of similitude depends on scaling compromise used and system being scaled.

(4) The use of "Nusselt Number Preservation" requires a verified math model for the radiation-conduction aspects of the system.

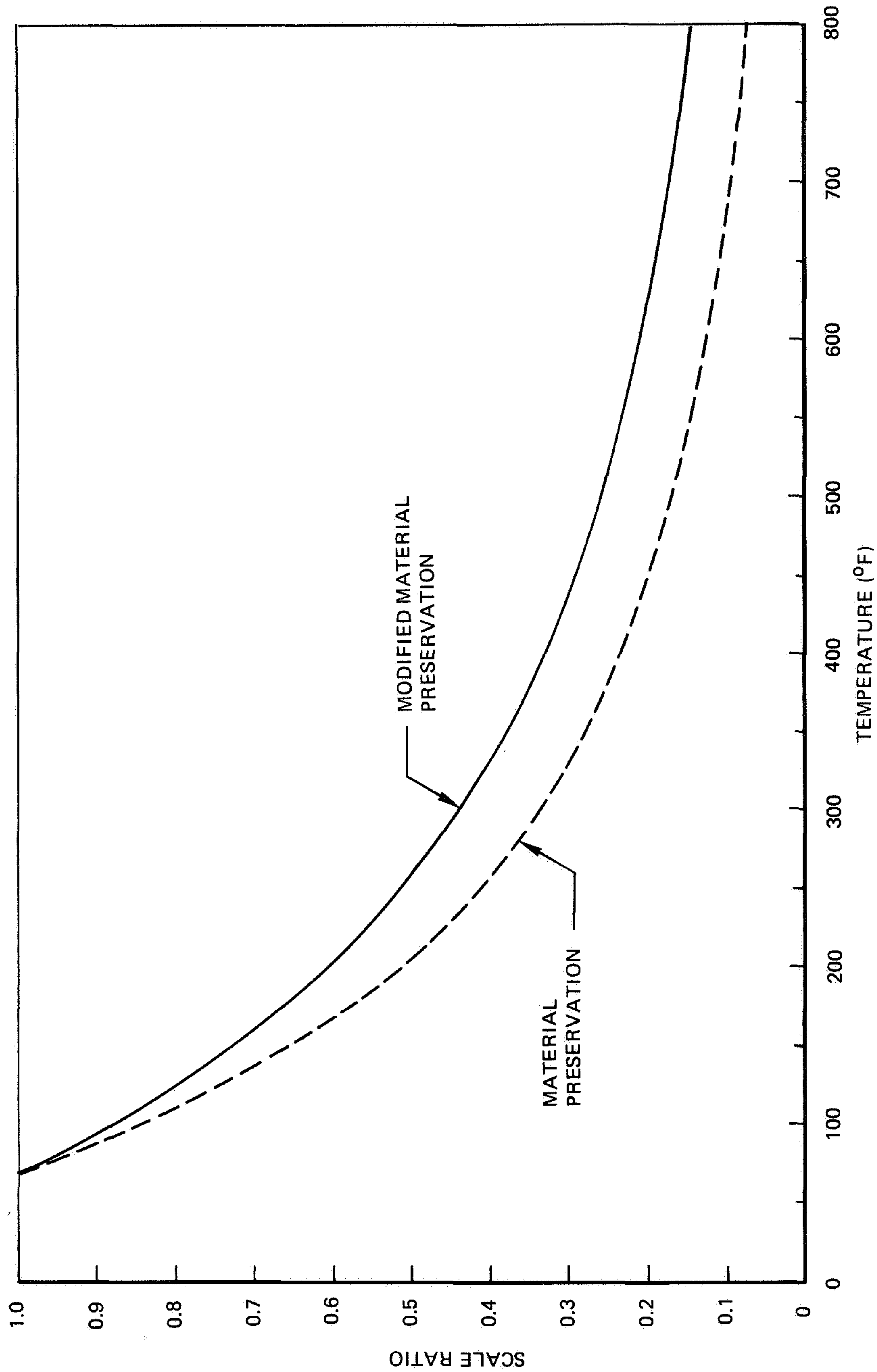

Figure II-1: SCALE RATIO VERSUS CHARACTERISTICS TEMPERATURE – MODIFIED MATERIAL PRESERVATION

Since the Prandtl number does not vary substantially with temperature (or from gas to gas) and since the Reynolds number may be adjusted to the desired value, their preservation in the scale model is easily accomplished. For equal Grashof numbers in the model and prototype the scale model pressure must be increased such that

$$P^* = \mu^* (k_g^*)^{\frac{1}{3}} (g^*)^{-\frac{1}{2}} (L^*)^{-\frac{11}{6}} \tag{14}$$

The scale model pressure requirements for simulating air at 70°F in the prototype is shown in Figure II-2 as a function of scale ratio.

The use of non metals (seals, insulation, etc.) in the scale model effectively limits the use of the Modified Material Preservation technique to scale ratios greater than about 0.5.

II.4.2 Temperature Preservation

The temperature preservation technique maintains equal temperature in the model and prototype and meets the scaling criteria by requiring a reduced thermal conductivity for the model materials. This technique has been used successfully for radiation-conduction systems at various scale ratios, and has considerable flexibiltiy for two dimensional conduction systems where the model material thickness need not be scaled geometrically. The application of this technique to systems involving convective heat transfer depends on the availability of gases with substantially lower thermal conductivities than that of the prototype gas. Figure II-3 shows the thermal conductivities of various gases as a function of temperature. The scale ratios which are possible, using selected gases to simulate air at 70°F, are depicted in Figure II-4.

As with the modified material preservation technique, the preservation of Reynolds and Prandtl numbers in the scale model is easily accomplished. The preservation of the Grashof number in the model requires the model pressure to be set such that

$$P^* = \frac{\mu^*}{M^*} (L^*)^{-\frac{3}{2}} (g^*)^{-\frac{1}{2}} \tag{15}$$

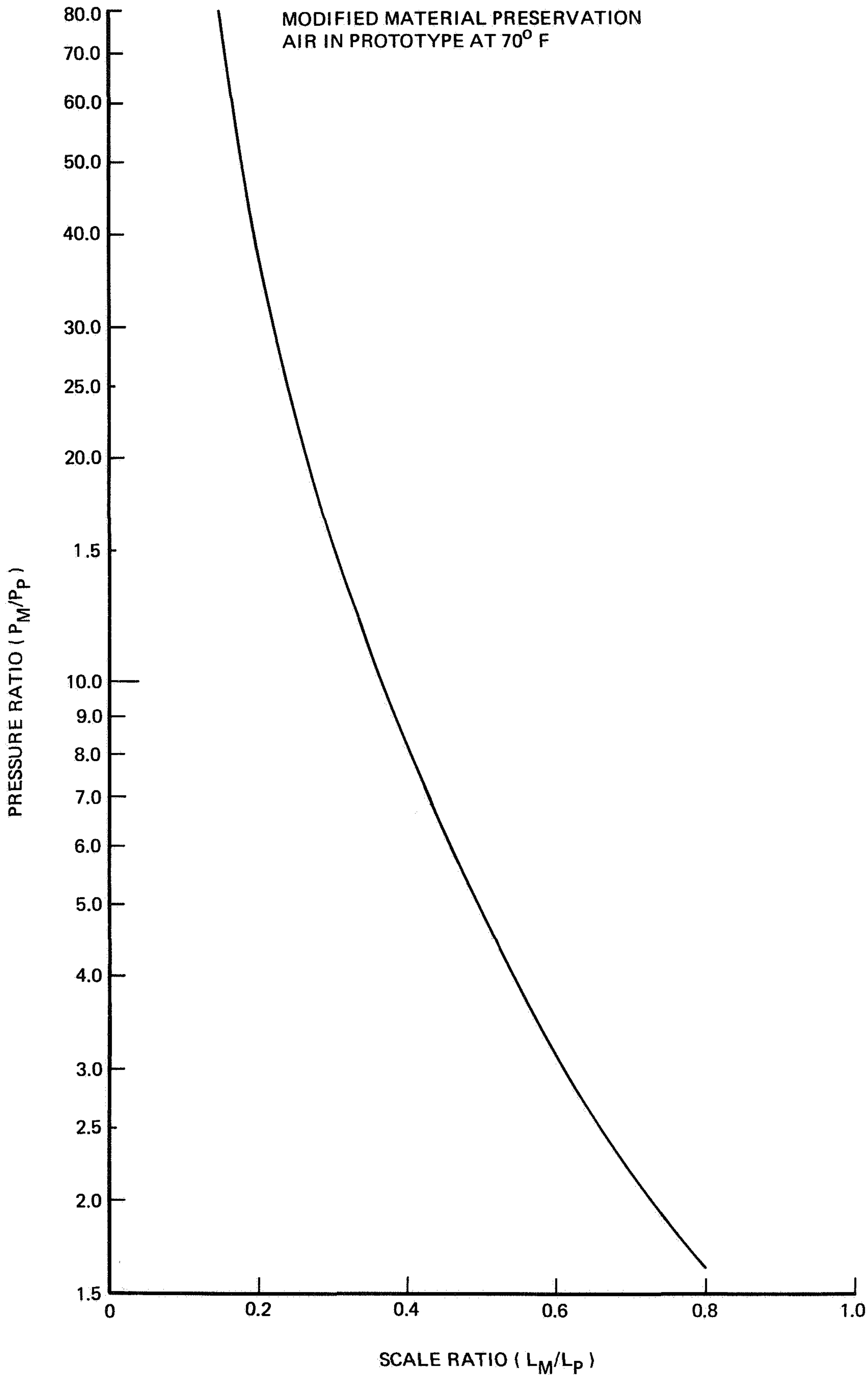

Figure II-2: PRESSURE REQUIREMENTS FOR PRESERVATION OF GRASHOF NUMBER

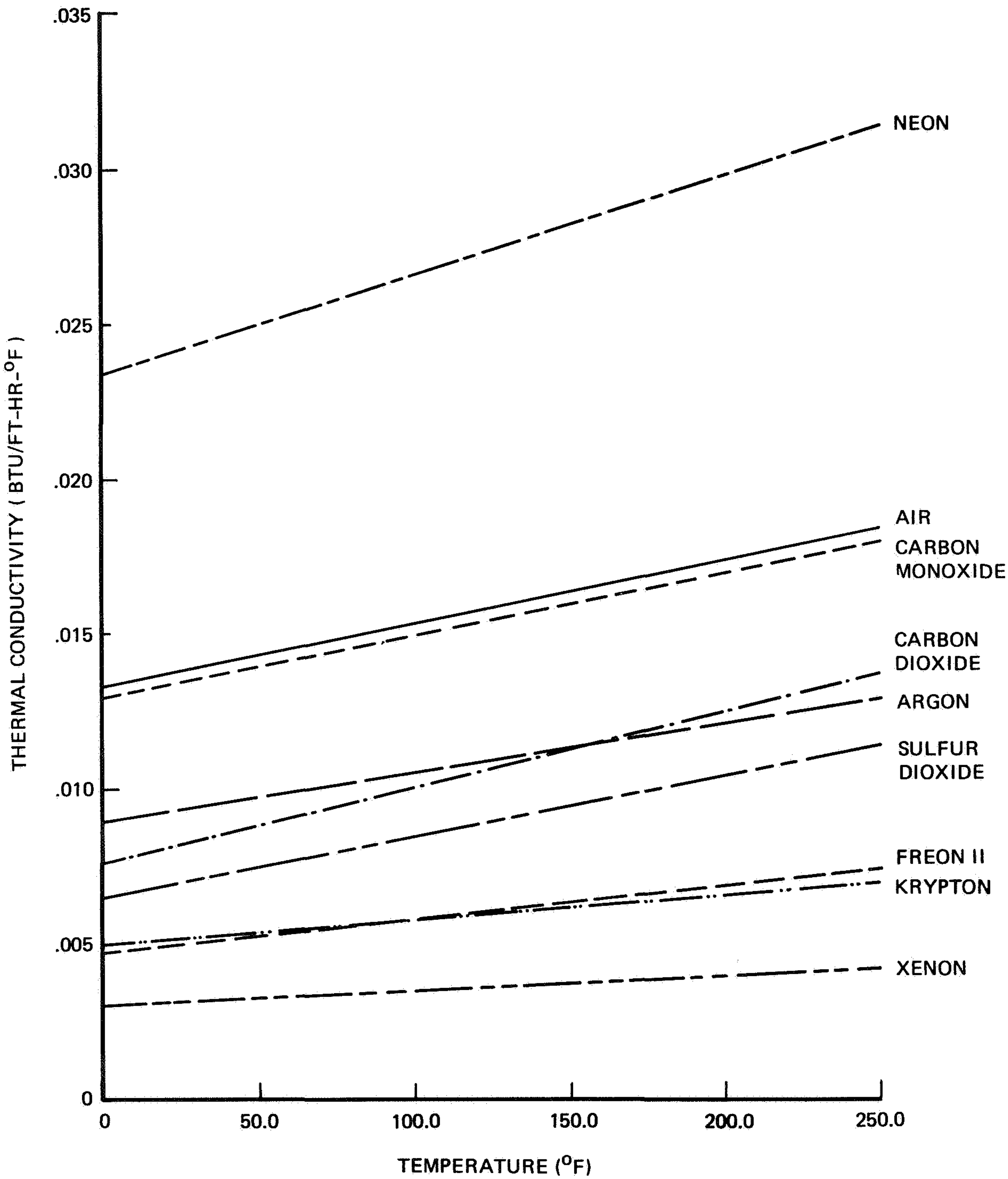

Figure II-3: THERMAL CONDUCTIVITY OF VARIOUS GASES

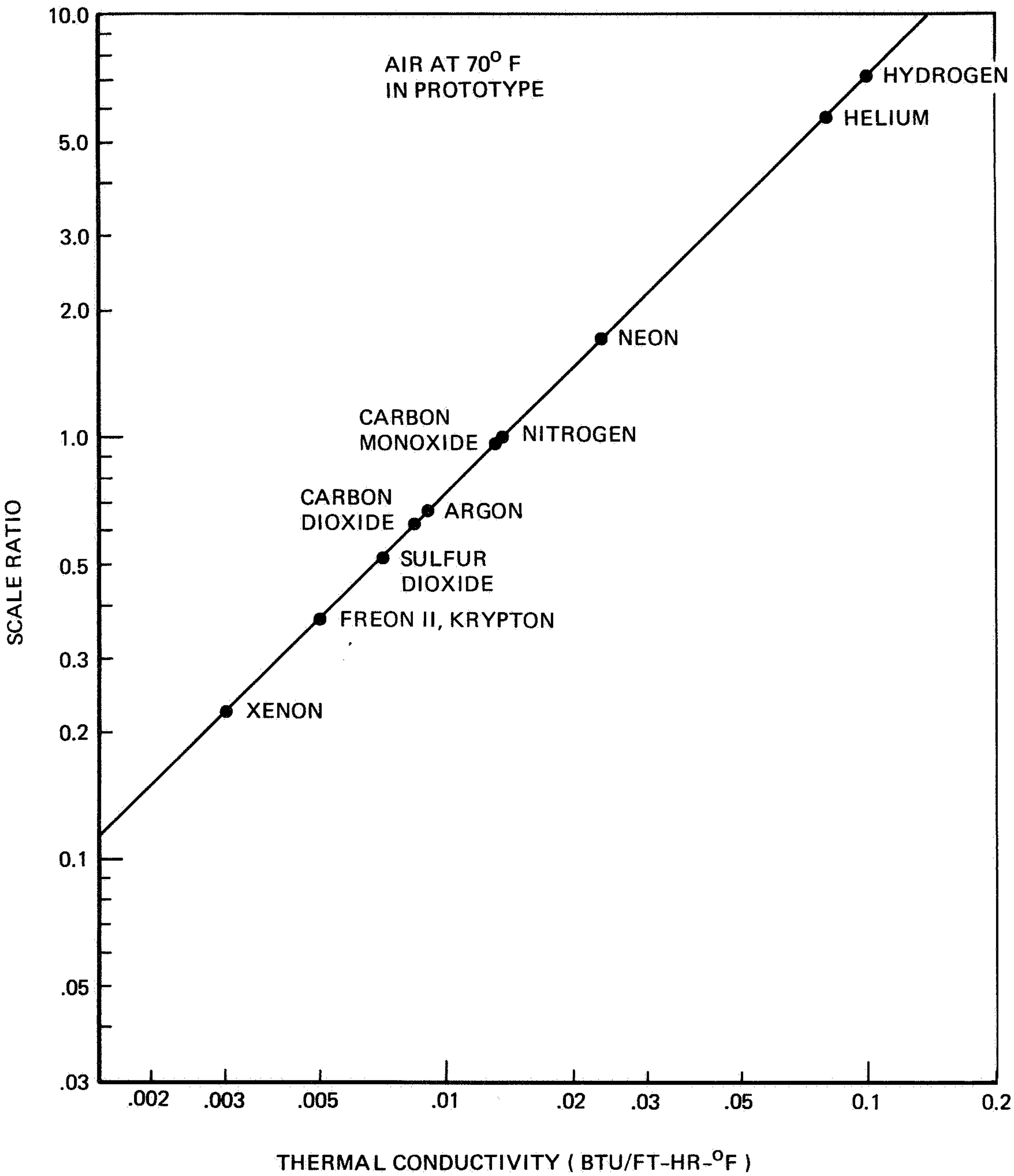

Figure II-4: CANDIDATE SCALE RATIOS – TEMPERATURE PRESERVATION

The model scale ratio and pressure ratio are fixed by the gas in the prototype and the gas chosen for the model. For example a prototype using air at atmospheric pressure could be simulated with a 3/8 scale model with Freon 11 at a pressure of about 0.5 atm.

Application of the "temperature preservation technique" to thermal scale modeling of systems involving convective heat transfer must be evaluated separately for each particular system of interest.

Practical problems that might arise in using this scaling technique include: gas availability, gas toxicity, compatibility between gas and model materials, liquefaction of the gas and lack of reliable thermophysical property data for the gas.

The application of the temperature preservation scaling technique to the cabin atmosphere-cabin wall thermal interface is severely limited by the availability of suitable gases. Of the gases considered, only Freon 11, Krypton and Xenon allow scale ratios less than 0.5. Krypton and Xenon are rare gases and are not readily available. Freon 11 is available, however, it liquefies at 75°F at atmospheric pressure. Low pressure operation of a 3/8 scale model would be feasible using Freon 11 since its boiling point can be reduced to about -30°F by lowering the pressure to 1 psia.

II.4.3 Scaling Compromises

The problems associated with the "modified material preservation and "temperature preservation" scaling techniques limits their usefulness. Consequently other techniques must be sought for thermal scale modeling of systems involving convection.

By allowing scaling compromises it may be possible to achieve adequate thermal similtude while preserving both gas and temperature in the scale model. Thermal similtude for the wall is achieved by preserving the convective heat transfer term in equation (5). This term may be written as

$$\left(\frac{k_g}{\sigma T_o^3 L}\right)\left(\vec{e}_n \cdot \nabla_* \theta_g\right)_w = \frac{q_{conv}}{\sigma T_o^3} \tag{16}$$

Where q_{conv} is the convective heat transfer rate per unit area of surface.

The convective scaling criteria can then be written as

$$\left(\frac{q_{conv}}{T_0^4}\right)^* = 1 \tag{17}$$

The necessary and sufficient conditons for satisfying equation (17) are, of course, given in Table II-1. However, two techniques which approximately satisfy equation (17) are suggested by rewriting this equation with the convective heat transfer in terms of either heat transfer coefficient and the temperature difference between gas and wall, or mass flux and the gas temperature change through the system, i.e., either

$$\left(\frac{h}{T_0^4}\right)^* (T_g - T_w)^* = 1 \tag{18}$$

or

$$\left(\frac{\rho \bar{v} c \Delta T_g}{T_0^4}\right)^* = 1 \tag{19}$$

Temperature preservation using the same gas in model and prototype requires that both the heat transfer coefficient and the mass flux be preserved, i.e.,

$$h^* = (\rho \bar{v})^* = 1 \tag{20}$$

Even though the heat transfer coefficient and mass flux cannot be preserved simultaneously, preservation of either may result in adequate thermal similtude.

Preservation of the heat transfer coefficient may be achieved if its dependence on the system parameters is known. In practical applications the heat transfer coefficient is usually based on analytical, semi-emperical or emperical results for simple flow fields (e.g., flow over a flat plate). These results typically relate the Nusselt number to the Reynolds number for forced convection cases by an equation of the form

$$Nu = c\, Re^n Pr^m \tag{21}$$

and to the Grashof number for free convection cases by an equation of the form

$$Nu = C\, Gr^{n} Pr^{m} \tag{22}$$

The values of the constants in these equations depend on the flow conditions (turbulent or laminar), boundary conditions and the system geometry. If the system to be modeled can be described by these relationships and if the constants are known, then the heat transfer coefficient can be preserved as follows:

a. Laminar flow in model and prototype or turbulent flow in model and prototype

$$Re_m = Re_p \left(\frac{L_m}{L_p}\right)^{\frac{1}{n}}$$ for forced convection and

$$Gr_m = Gr_p \left(\frac{L_m}{L_p}\right)^{\frac{1}{n}}$$ for free convection.

b. Turbulent flow in prototype and laminar flow in model

$$Re_m = \left(\frac{L_m}{L_p}\ \frac{C_T}{C_L}\right)^{\frac{1}{n_L}} Re_p^{\frac{n_T}{n_L}}\, Pr^{\left(\frac{m_T - m_L}{n_L}\right)}$$ for

forced convection and

$$Gr_m = \left(\frac{L_m}{L_p}\ \frac{C_T}{C_L}\right)^{\frac{1}{n_L}} Gr^{\frac{n_T}{n_L}}\, Pr^{\left(\frac{m_T - m_L}{n_L}\right)}$$ for

free convection.

c. Flow transition in either model or prototype

If transitions between laminar and turbulent flow occur in either the model or prototype then it will not be possible to preserve the local heat transfer coefficient.

Preservation of the heat transfer coefficient is most easily achieved for case (a) since only the exponents (n) are needed to determine the scaling criteria, whereas, case (b) also requires the constants (C) and exponents (m) to be known.

The mass flux is easily preserved by adjusting the Reynolds number in the model such that

$$Re_m = \left(\frac{L_m}{L_p}\right) Re_p \tag{23}$$

The free convection heat transfer is preserved for the mass flux as well as for the heat transfer coefficient preservation techniques.

Preservation of either mass flux or heat transfer coefficient results in some loss of thermal similtude. If the mass flux is preserved then the ratio of forced convection heat transfer coefficient between model and prototype is given, for case (a) above, by

$$h^{*} = (L^{*})^{n-1} \tag{24}$$

and conversely, if the forced convection heat transfer coefficient is preserved, then the ratio of mass fluxes between model and prototype is given by

$$(\rho\bar{v})^{*} = (L^{*})^{\frac{1-n}{n}} \tag{25}$$

Mass flux preservation tends to preserve the gas temperature change through the system, whereas, heat transfer coefficient preservation tends to preserve the temperature difference between the wall and gas.

The degree of thermal similitude achieved with the mass flux and heat transfer coefficient preservation scaling techniques may be approximated using the following simplified analysis:

Consider gas flow through an enclosure which is subject to uniform surface heating and coupled to the external environment through a uniform conductance per unit surface area. The thermal balance for the enclosure is given by

$$QA_s = KA_s(T - T_e) + hA_s(T - T_g) \tag{26}$$

where

Q = surface heating rate/unit area

A_s = surface area

K = conductance per unit area to environment

h = heat transfer coefficient

T = enclosure temperature

T_e = environment temperature

T_g = average gas temperature

The average gas temperature may be related to the inlet gas temperature by equating the convective heat transfer rate to the energy transport rate

$$hA_s(T - T_g) = WC\left(T_g^{out} - T_g^{in}\right) \tag{27}$$

where

W = gas flow rate

C = gas specific heat

Setting, $T_g = \left(T_g^{out} + T_g^{in}\right)/2$ and solving for T_g gives

$$T_g = \frac{T_g^{in} + \frac{hA_s}{2WC}T}{1 + \frac{hA_s}{2WC}} \tag{28}$$

Using this result in equation (26) and solving for T yields

$$T - T_r = \frac{T_g^{in} - T_r}{1 + K\left(\frac{1}{h} + \frac{A_s}{2WC}\right)} \tag{29}$$

where the reference temperature T_r is the enclosure temperature when there is no gas flow and is given by

$$T_r = \frac{Q}{K} + T_e \tag{30}$$

Assuming the free and forced convection heat transfer coefficients to be additive the heat transfer coefficient may be written as

$$h = \left(\frac{k_g}{L}\right)\left(C\,Re^n Pr^m + C_1 Gr^{n_1} Pr^{m_1}\right) \tag{31}$$

Using this definition of h and writing WC in terms of RePr equation (29) becomes

$$T - T_r = \frac{T_g^{in} - T_r}{1 + \left(\frac{KL}{k_g}\right)\left(\frac{\alpha}{2RePr} + \frac{1}{CRe^n Pr^m + C_1 Gr^{n_1} Pr^{m_1}}\right)} \qquad (32)$$

where

α = A_s /cross sectional flow area

The prototype and scale model temperatures can be written (for Pr = 1 and preservation of the free convection coefficient) as

Prototype

$$\frac{T_p - T_r}{T_g^{in} - T_r} = \left\{ 1 + \left(\frac{KL_p}{k_g}\right)\left[\frac{\alpha}{2Re_p} + \left(\frac{1}{CRe_p^n + C_1 Gr_p^{m_1}}\right)\right]\right\}^{-1} \qquad (33)$$

Scale Model (Mass Flux Preservation)

$$\frac{T_m - T_r}{T_g^{in} - T_r} = \left\{ 1 + \left(\frac{KL_p}{k_g}\right)\left[\frac{\alpha}{2Re_p} + \frac{1}{C\left(\frac{L_m}{L_p}\right)^{n-1} Re_p^n + C_1 Gr_p^{n_1}}\right]\right\}^{-1} \qquad (34)$$

Scale Model (Heat Transfer Coefficient Preservation)

$$\frac{T_m - T_r}{T_g^{in} - T_r} = \left\{ 1 + \left(\frac{KL_p}{k_g}\right)\left[\frac{\alpha}{2\left(\frac{L_m}{L_p}\right)^{\frac{1-n}{n}} Re_p} + \frac{1}{CRe_p^n + C_1 Gr_p^{n_1}}\right]\right\}^{-1} \qquad (35)$$

Figure II-5 shows the calculated temperature differences between model and prototype as a function of Reynolds number and Grashof number for the two scaling techniques. These calculated results used the following parameters:

$$\frac{L_m}{L_p} = \frac{1}{5}$$

n = 0.5, n_1 = 0.25 and C_1 = C = 0.33 (typical laminar flow values)

$\left(\frac{KL_p}{k_g}\right) = 10$ (representative value for manned spacecraft cabin)

$\alpha = 4$ (value for cylinder with length = radius)

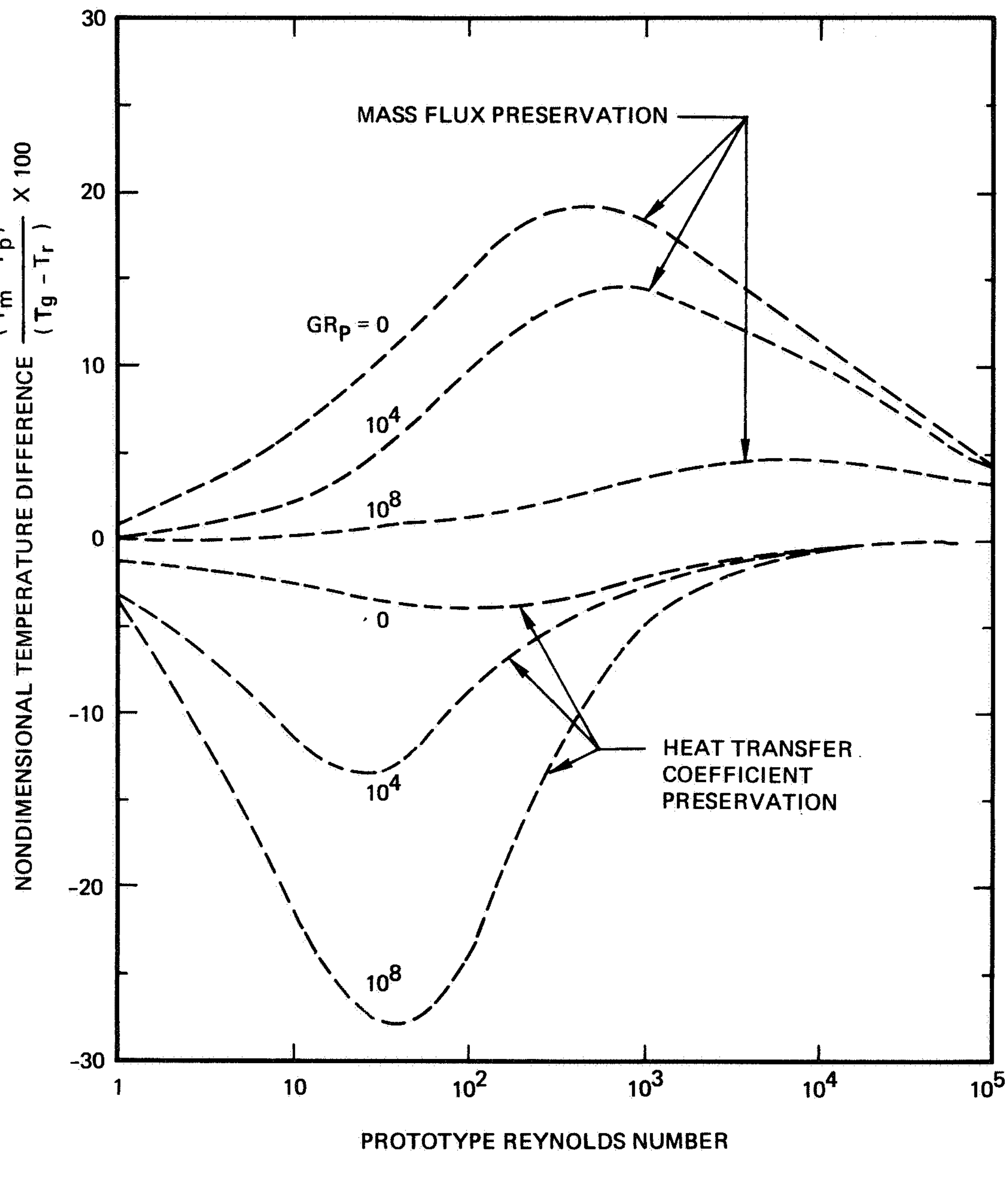

Figure II-5: EFFECT OF SCALING COMPROMISES ON TEMPERATURE FOR 1/5 SCALE MODEL SPACECRAFT

The degree of thermal similitude achieved with either scaling technique is greatest at large Reynolds numbers where the wall temperature approaches the gas temperature and at small Reynolds numbers where the wall temperature approaches the reference temperature. The heat transfer preservation technique gives the best results for pure forced convection (Gr=0) and mass flux preservation gives the best results when free convection dominates.

These scaling compromises also affect the transient response of the spacecraft cabin wall. The transient response may be calculated by substituting for T_r in equation (32) and solving for T, assuming $T=T_r$ at t=0,

$$T - T_r = \frac{T_g^{in} - T_r}{1+\beta}\left[1 - \exp - \left(\frac{1+\beta}{\beta}\right)\left(\frac{K}{M}\right)t\right] \tag{36}$$

where

$$\beta = \left(\frac{KL}{k_g}\right)\left(\frac{\alpha}{2RePr} + \frac{1}{C\,Re^n Pr^m + C_1 Gr^{n_1} Pr^{m_1}}\right) \tag{37}$$

and M=thermal mass per unit area of wall

The characteristic response time is then

$$t_o = \left(\frac{M}{K}\right)\left(\frac{\beta}{1+\beta}\right) \tag{38}$$

Noting that (K/M) corresponds to the $(k/\rho CL^2)$ in the scaling criteria, equation (38) may be written in terms of nondimensional time as

$$\tau_o = \frac{\beta}{1+\beta} \tag{39}$$

The characteristic response time ratio between model and prototype for changes in convective heat transfer is then given by

$$\tau_o^* = \left(\frac{\beta}{1+\beta}\right)^* \tag{40}$$

This response time ratio for the 1/5 scale model spacecraft parameters is shown in Figure II-6 as functions of Reynolds and Grashof numbers for the two scaling techniques.

As would be expected the relative model response is slow with heat transfer coefficient preservation and fast for mass flux preservation.

The heat transfer coefficient preservation technique generally gives better transient simulation except for the lower Reynolds numbers when free convection effects dominate.

The calculated results for this simple model indicate that the prototype temperature remains bounded by the scale model temperatures obtained using mass flux and heat transfer coefficient preservation.

Whether mass flux preservation or heat transfer coefficient preservation gives better thermal similitude depends on the nature of the system to be modeled. Systems with mass flow rates large enough to give a small gas temperature change should be modeled well using the heat transfer coefficient preservation technique. If the free convection mode of heat transfer dominates then the mass flux preservation technique should give good results.

II.4.4 Nusselt Number Preservation

The Nusselt number preservation scaling technique would use the thermal scale model to experimentally determine the Nusselt number for the system as a function of Reynolds number and Grashof number. (If the model uses a different fluid the Prandtl number effects would also have to be determined). This functional relationship would then be used in conjunction with a thermal math model to predict the prototype performance.

The Nusselt number is preserved if thermal and dynamic similitude exist between the fluid elements of the systems. Thermal and dynamic similitude may be achieved by preserving Re and ($Gr\Theta_{fw}$). This keeps the nondimensional velocity $\vec{v}_*$ and fluid temperature $\frac{\Theta_f}{\Theta_{fw}}$ invariant for similar systems. (see equations 10 and 11). The Reynolds number is easily preserved in the scale model, however

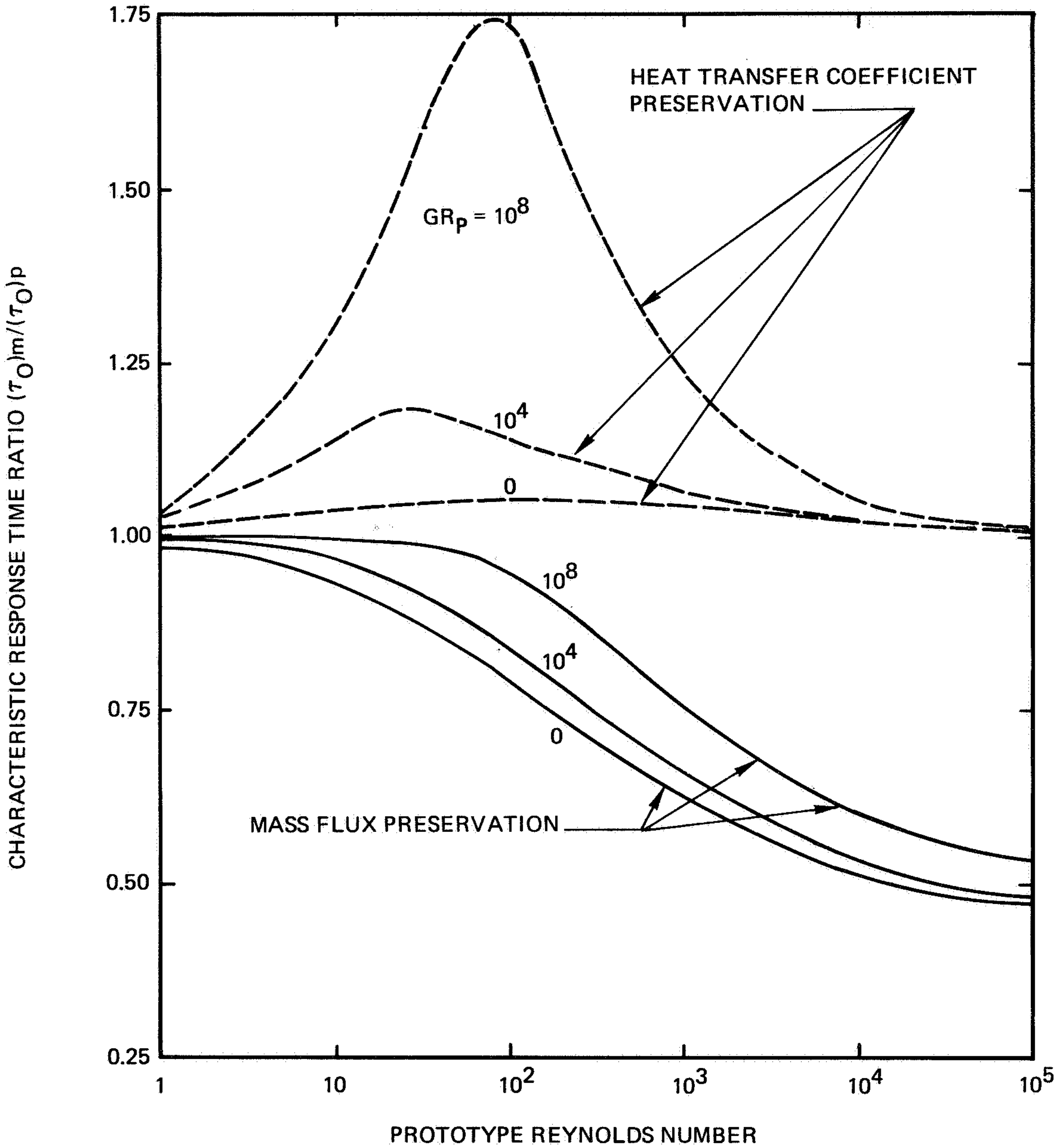

Figure II-6: EFFECT OF SCALING COMPROMISES ON TRANSIENT RESPONSE FOR 1/5 SCALE MODEL SPACECRAFT preservation of the $Gr\theta_{fw}$ term depends on the magnitude of the convective heat transfer. In the limit of no convective heat transfer $\theta_{fw}^* = 1$ and in the limit of only convective heat transfer $\theta_{fw}^* = L^*$. Consequently the model pressure required to preserve the $Gr\theta_{fw}$ term (i.e, the free convection effects) is within the limits

$$(L^*)^{-\frac{3}{2}} \leq P^* \leq (L^*)^{-2} \tag{41}$$

The use of Nusselt number preservation scaling technique can be summarized as follows:

- Use temperature preservation technique for radiation - conduction aspects of thermal scale model.
- Develop math model for radiation-conduction aspects of scale model
- Test model without convection and use results to upgrade math model
- Test model with convection at various pressures for each Reynolds number.
- Use the experimental results in conjunction with math model to determine the convective heat transfer.
- Develop Nusselt number correlation with Reynolds and Grashof numbers
- Expand math model to include convection effects and use in conjunction with the Nusselt number correlation to predict prototype performance.

The Nusselt number preservation technique avoids the problems inherent in the other scaling techniques, i.e., high temperatures and heat fluxes required for the "modified material preservation", the suitable gas required for temperature preservation", and the uncertainties of "scaling compromises."

However thermal scale modeling using Nusselt number preservation requires the use of experimental research techniques whereas use of the other scaling techniques requires only fabrication and testing of the scale model.

II.4.5 Simulation of Zero Gravity Conditions

In order to simulate the pure forced convection which occurs in a zero gravity field, free convection must be reduced to a negligible amount in the ground test simulation. Free convection effects on forced flow are generally related to the magnitude of $\frac{Gr}{Re^2}$ for flow over a vertical surface. If $\frac{Gr}{Re^2} << 1$ forced convection dominates and if $\frac{Gr}{Re^2} >> 1$ free convection dominates.

The Grashof number to Reynolds number squared ratio may be written as

$$\frac{Gr}{Re^2} = \frac{g \beta L (T_g - T_w)}{v^2} \tag{42}$$

Using a characteristic length of 10 feet, temperature differences between wall and gas of 1. to 10.°F and gas velocities of 15 to 45 ft/min as representative for manned spacecraft yields values for $\frac{Gr}{Re^2}$ of 1 to 100 for ground tests of manned spacecraft configurations. This indicates that free convection effects are important, and in fact may dominate, in ground tests of prototype manned spacecraft.

The reduction of free convection effects in thermal scale model tests depends on the scaling technique, scale ratio and gas density. At a given gas pressure the value of $\frac{Gr}{Re^2}$ decreases with smaller scale ratios for the Modified Material Preservation, Nusselt Number Preservation and Mass Flux Preservation Scaling techniques and increases for the Heat Transfer Coefficient Preservation Technique.

The value of $\frac{Gr}{Re^2}$ can be reduced by decreasing the gas density while preserving the Reynolds number. This means that the gas velocity must be increased to compensate for the reduced density. The maximum allowable gas velocity is limited by the onset of compressible flow effects. This reduction in $\frac{Gr}{Re^2}$ could also be obtained in the prototype tests.

The scale model to prototype $\frac{Gr}{Re^2}$ ratio may be written as

$$\left(Gr/Re^2\right)^* = (Re^*)^{-2} (L^*)^3 (M^*)^2 (\mu^*)^{-2} (T^*)^{-2} (P^*)^2 \tag{43}$$

This may be written for the various scaling techniques as follows:

Modified Material Preservation

$$\left(Gr/Re^2\right)^* = \left[\mu^*/(k_g^*)^{\frac{1}{3}}\right]^{-2} (L^*)^{\frac{11}{3}} (P^*)^2 \tag{44}$$

Temperature Preservation

$$\left(Gr/Re^2\right)^* = (\mu^*)^{-2} (M^*)^2 (L^*)^3 (P^*)^2 \tag{45}$$

Mass Flux Preservation

$$\left(Gr/Re^2\right)^* = L^* (P^*)^2 \tag{46}$$

Heat Transfer Coefficient Preservation (Laminar Flow)

$$\left(Gr/Re^2\right)^* = (L^*)^{-1} (P^*)^2 \tag{47}$$

Nusselt Number Preservation

$$\left(Gr/Re^2\right)^* = (L^*)^3 (P^*)^2 \tag{48}$$

The free convection effects in manned spacecraft scale model tests should be eliminated by reducing $\frac{Gr}{Re^2}$ by a factor of 1000. This corresponds to values of 0.001 to 0.1 for the scale model tests. The pressure ratio required for this reduction in free convection effects is shown in Figure II-7 for the various scaling techniques. Even though these required pressure levels result in cabin gas velocities well within the incompressible flow regime, problems in sizing the gas supply and return lines may arise for the techniques requiring the lower pressure levels.

II.4.6 Manned Spacecraft Applications

The "modified material preservation" scaling technique applied to manned spacecraft is limited, by the increased model temperature, to scale ratios greater than about 0.5. The increased model pressure requirements preclude simulation of

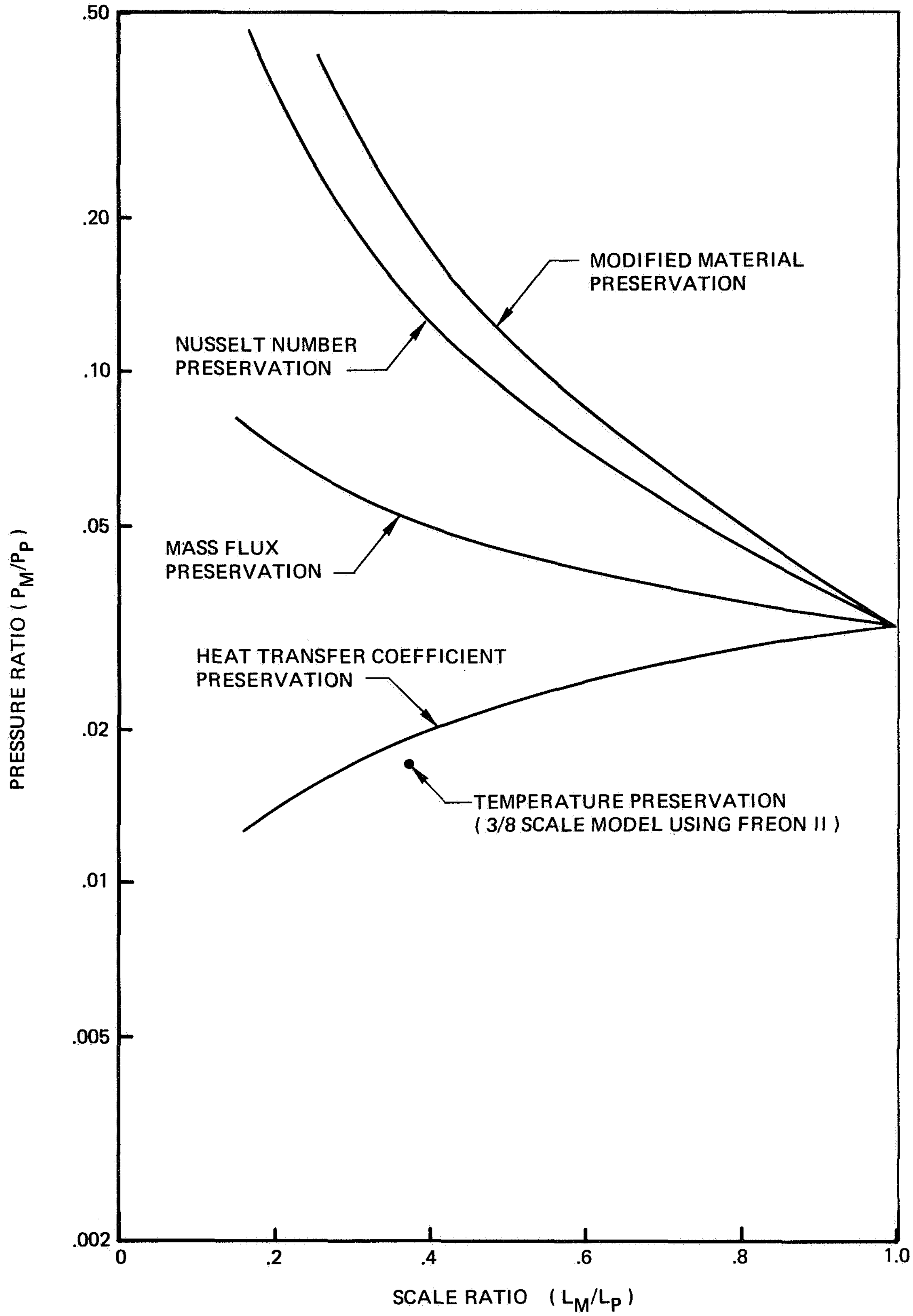

Figure II-7: ***REDUCTION OF FREE CONVECTION EFFECTS***
PRESSURE RATIO REQUIRED TO REDUCE (GR/RE^2) BY FACTOR OF 10^3

1-g prototype gravity field. This technique is well suited for zero gravity simulation.

The "temperature preservation" scaling technique is limited by availability of "suitable gases." A 3/8 thermal scale model of a manned spacecraft appears to be possible using Freon 11. Simulation of a 1-g prototype gravity field is marginal because of possible liquification of the Freon gas. The low model pressure required to simulate zero gravity conditions may result in design problems for the gas supply and return lines.

Scaling compromises using the mass flux and/or heat transfer coefficient preservation scaling techniques may give adequate thermal similitude without limiting the model scale ratio. Use of both techniques should bound the prototype spacecraft performance. Both techniques are suited for simulation of 1-g prototype conditions. However the low model pressure required for simulation of zero gravity conditions using "heat transfer coefficient preservation" may result in design problems for the gas supply and return lines.

The "Nusselt number preservation" scaling technique is unsuited for simulating 1-g conditions in the prototype spacecraft due to the increased pressure requirement. This technique is well suited for simulating zero gravity conditions without limiting the model scale ratio.

Since "scaling compromises," using both mass flux and heat transfer coefficient preservation, and Nusselt number preservation allow a greater range of thermal scale modeling applications these techniques were chosen for an experimental investigation of thermal scale modeling applied to a radiation-conduction-convection system.

II.5 EXPERIMENTAL INVESTIGATION

II.5.1 Objective

The objective of the investigation was to experimentally demonstrate the application of the selected scaling techniques to thermal scale modeling of systems involving radiation-conduction and convection, in particular, to systems representative of the manned spacecraft "Cabin-Atmosphere - Cabin Wall Thermal Interface."

In order to accomplish this objective the following plan was developed:

- Select a model configuration in which radiation, conduction and convection are important.
- Construct full scale and 1/4 scale models using temperature preservation scaling criteria for the radiation and conduction aspects of the configuration.
- Develop a Thermal Math Model (TMM) for the configuration.
- Test the 1/4 scale model without convection at various heating rates and upgrade and/or verify the radiation-conduction aspects of the TMM.
- Test the models for various heating rates and gas convection conditions.
- Use verified TMM in conjunction with 1/4 scale model test results to evaluate the Nusselt number preservation scaling technique.
- Correlate the 1/4 scale model and full scale model test results to evaluate the mass flux and heat transfer coefficient preservation scaling techniques.

II.5.2 Model Configuration

The model configuration chosen for the experimental investigation is shown in Figure II-8. The model basically consists of two concentric cylinders with

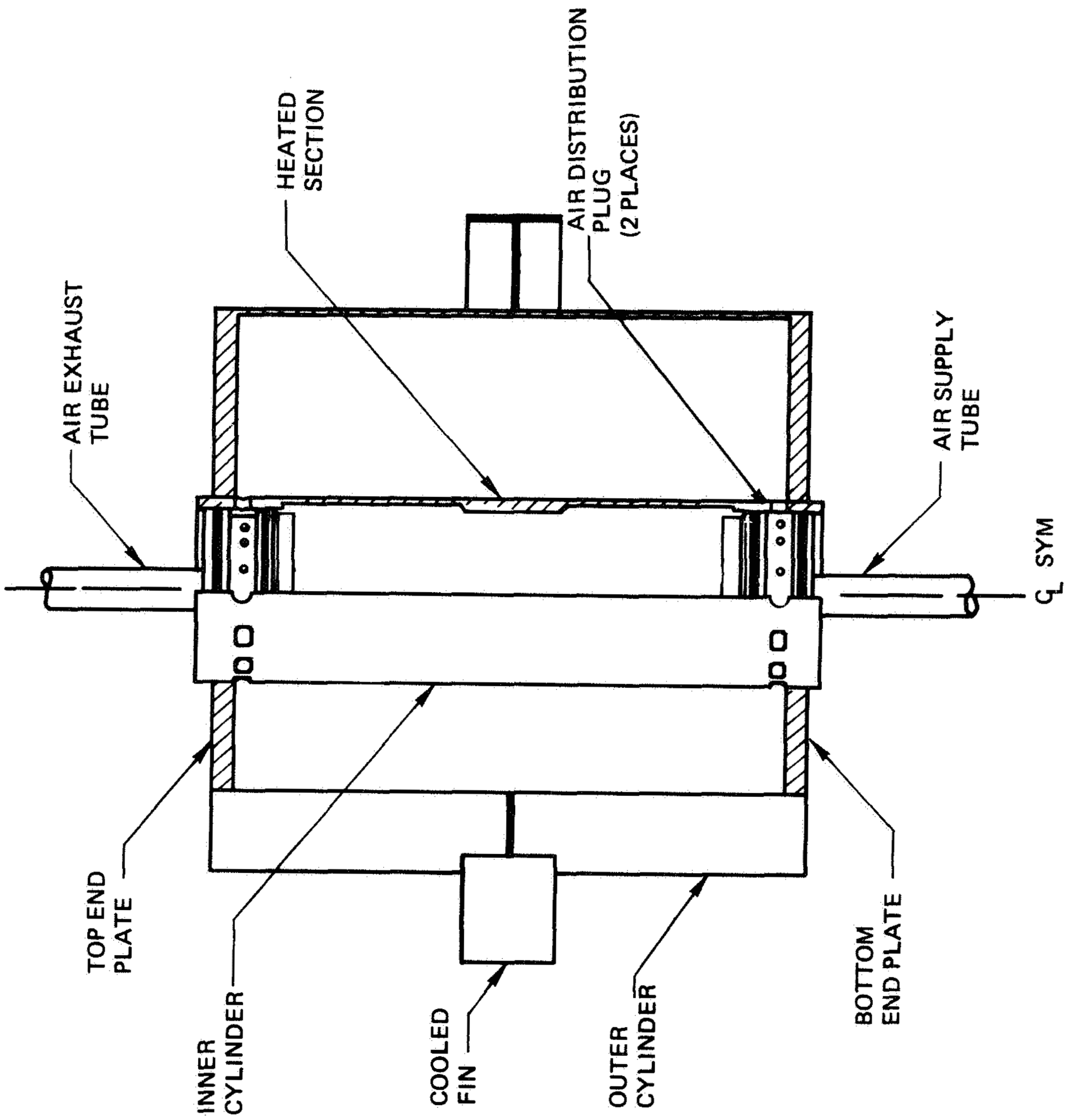

Figure II-8: MODEL CONFIGURATION

end plates closing off the annular region between the cylinders. Thermal gradients are generated by heating the center section of the inner cylinder and cooling the center of the outer cylinder.

The heating is provided by an electrical heater mounted on the inside of the inner cylinder and the cooling by a cooled fin attached to the center of the outer cylinder.

The exposed surfaces in the annular region are painted black to enhance the radiation heat transfer and to provide the same radiation properties for full and 1/4 scale models.

Forced convection is provided by air flow in the annular region. Air is supplied to and exhausted from the model through air distribution plugs in the air inlet and outlet sections of the inner cylinder.

This model configuration was chosen for the following reasons:

- Radiation, conduction and convection modes of heat transfer are important in the thermal response.

- Symmetry of model minimizes the amount of instrumentation and the size of the TMM and also allows the asymmetric convective heat transfer effects to become apparent.

- Air flow distribution is similar to that for manned spacecraft configurations.

- Expensive space chamber testing is avoided by insulating the model and testing at ambient conditions.

- The annular region can be evacuated for radiation-conduction tests and can be pressurized to increase the free convection effects.

- The annular flow region can be kept free of instrumentation and heater leads.

- The inner cylinder can be evacuated to reduce the extraneous heat transfer in this region.

The basic structure of the full scale model uses 6061-T6 aluminum and measures approximately 2 feet in length and diameter. The 1/4 scale model uses type 304 stainless steel and measures approximately 6 x 6 inches. The basic length dimensions for the two models are shown in Figure II-9. The inner cylinders have thicker walls at the center and end sections, where the heater and air distribution plugs are installed. The model material thicknesses and the scaling parameter for two dimensional conduction are given in Table II-3. The conduction scaling parameter agreement is generally within 10 percent over the temperature range of 30 to 350°F. These model dimensions reflect the requirements of pressurization and evacuation while maintaining relatively thin walls to keep conduction from dominating the heat transfer processes.

II.5.3 Basic TMM and Preliminary Analysis

A TMM was developed for the basic configuration and preliminary analyses were made to verify the thermal similitude between the full scale and 1/4 scale models and to determine the experimental accuracy required to implement the Nusselt number preservation scaling technique.

II.5.3.1 Basic TMM

The basic TMM nodal network is shown in Figure II-10. There are 12 equally spaced nodes (401-412) on the outer cylinder and 12 (301-312) on the inner cylinder. Both end plates have 4 equally spaced nodes (101-104 on the air outlet end and 201-204 on the air inlet end). The fin node is 413 and the boundary node at the outer edge of the fin is node 414. The inlet gas temperature boundary node is numbered 500 and the outlet gas node is number 513. The remaining gas nodes (501-512) are equally spaced axially in the annular region between the inner and outer cylinders.

The radiation exchange factors (script F's) between the interior solid nodes (101-104, 201-204, 301-312 and 401-412) were calculated using Boeing's Generalized Radiative Heat Transfer Program (AS2814) (Reference 8) for the surfaces

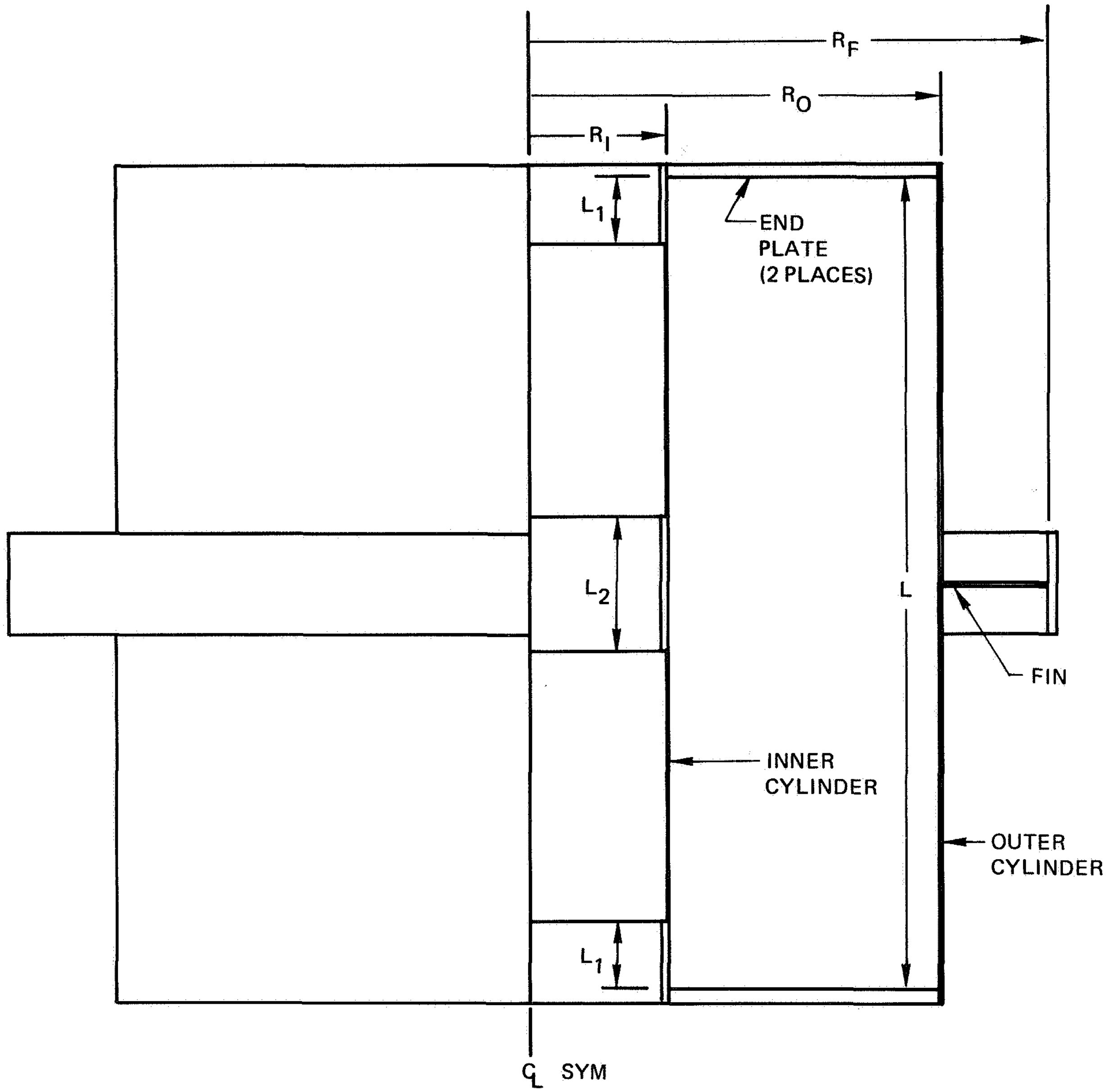

MODEL	L	L_1	L_2	R_I	R_O	R_F
FULL SIZE	24	2	4	4	12	15.063
1/4 SCALE	6	0.5	1	1	3	4.000

Figure II-9: BASIC MODEL DIMENSIONS

TABLE II-3 MODEL MATERIAL THICKNESSES AND SCALING PARAMETERS

Component	Model	Thickness d, inches	Scaling Parameter* BTU/HR-°F 30°F	75°F	200°F	350°F
Outer Cylinder	Full Scale	0.063	.502	.508	.521	.527
	1/4 Scale	0.040	.425	.446	.496	.531
Inner Cylinder Thin Section	Full Scale	0.050	.399	.404	.414	.418
	1/4 Scale	0.032	.339	.366	.396	.424
Thick Section	Full Scale	0.125	.998	1.010	1.035	1.046
	1/4 Scale	0.085	.900	.946	1.052	1.128
End Plates	Full Scale	0.375	3.00	3.02	3.10	3.14
	1/4 Scale	0.250	2.65	2.78	3.10	3.32
Cooling Fin	Full Scale	0.071	2.51	2.52	2.54	-
	1/4 Scale	0.063	2.44	2.50	2.56	-

*Scaling parameter is kd/N^2 for wall components, where k = thermal conductivity, d = wall thickness, N = scale ratio. For the cooling fin the scaling parameter is

$$\left(kd/N^2\right) / \ln\left(\frac{R_F}{R_o + d_o}\right)$$

where R_F = outer radius of fin, $(R_o + d_o)$ = outer radius of outer cylinder.

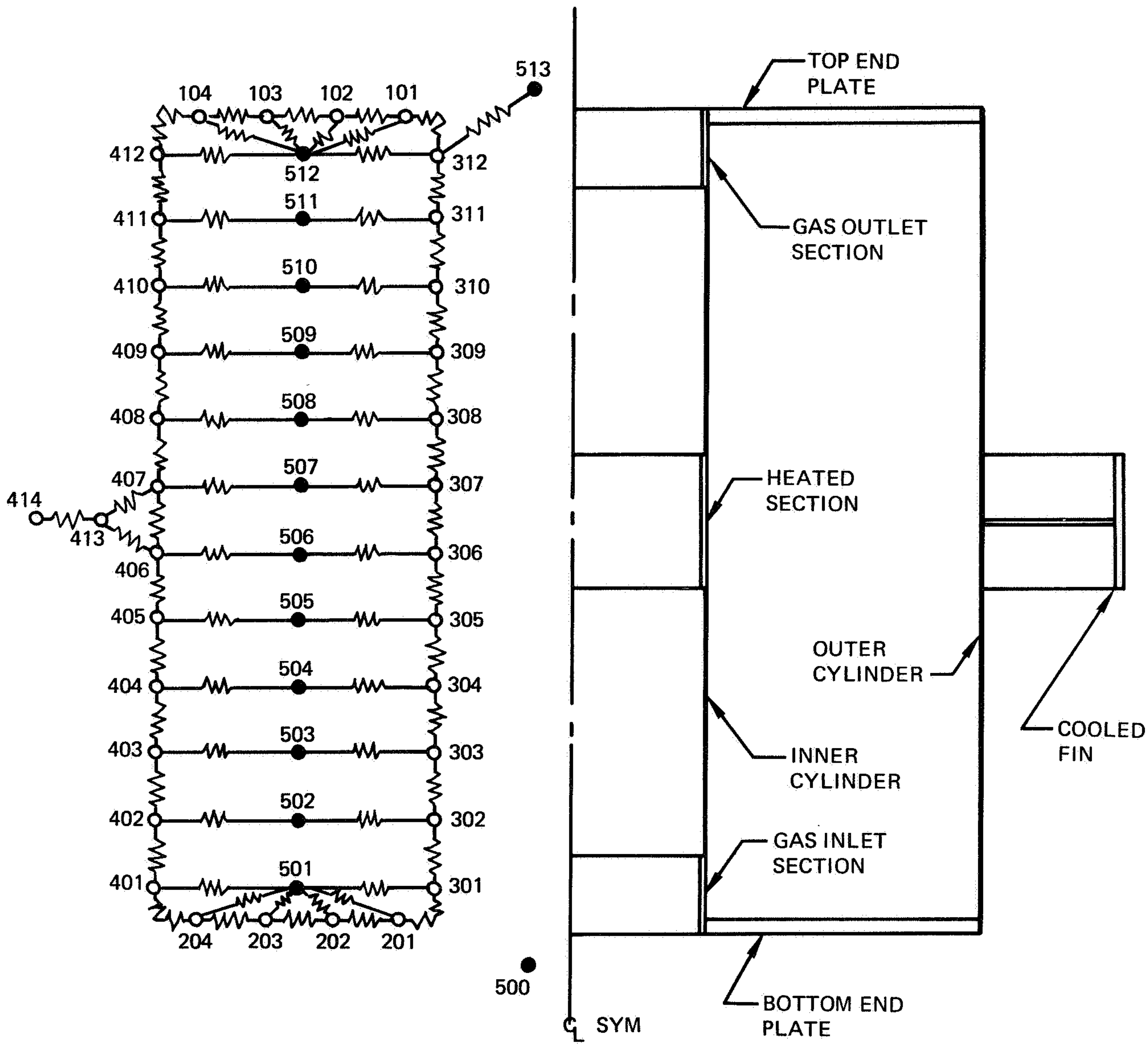

HEAT SOURCE AT NODES 306 & 307

NODES 414 & 500 ARE BOUNDARY NODES

○ SOLID NODES

● GAS NODES

Figure II-10: BASIC THERMAL MATH MODEL painted with black paint ($\varepsilon = 0.88$). These calculations resulted in 496 SAF (σAF) values which were input into the BETA (Boeing Engineering Thermal Analyzer) program (Reference 9).

The gas flow was treated as a source at the gas nodes. The value of the source at node i is given by $S_i = wc \ (T_{i-1} - T_i)$ where w = mass flow rate and c = specific heat of the gas, e.g., $S_{507} = wc \ (T_{506} - T_{507})$. The solid conductors were input as a function of temperature and heat sources input at nodes 306 and 307.

The conductors (hA) between the wall and the gas were based on an approximation of the combined free and forced convection and the gas conduction heat transfer. The forced convection heat transfer coefficient was assumed to be that given for laminar flow over a flat plate

$$h(x) = 0.332\left(\frac{k_g}{L}\right) Re_L^{\frac{1}{2}} Pr^{\frac{1}{3}} \left(\frac{L}{x}\right)^{\frac{1}{2}}$$

and free convection heat transfer assumed to be

$$Nu = 0.04 Gr^{\frac{1}{4}}$$

or basing the Grashof number on the annular spacing ($R_o - R_i$) and the local gas to wall temperature difference

$$h = \frac{0.04 k_g}{R_o - R_i}\left[\frac{\rho_g^2 g (R_o - R_i)^3}{\mu^2}\left(\frac{T_g}{T_w} - 1\right)\right]^{\frac{1}{4}}$$

The total heat transfer coefficient used in the analysis consists of the sum of the forced convection, free convection and gas conduction

$$h = \left| \frac{0.332 k_g Pr^{\frac{1}{3}}}{L} Re_L^{\frac{1}{2}} \left(\frac{L}{x}\right)^{\frac{1}{2}} \pm \frac{.04 k_g}{R_o - R_i}\left[\frac{\rho_g^2 g (R_o - R_i)^3}{\mu^2}\left(\frac{T_g}{T_w} - 1\right)\right]^{\frac{1}{4}} \right| + \frac{k_g}{\Delta X}$$

The + sign is used when the buoyancy acts with the flow and the - sign when it acts against the flow. Along the end plates the buoyancy term is not included and the forced convection term is modified to account for the radial flow of the gas along these plates. These convective heat transfer relationships are only a reasonable guess as to how the convective heat transfer occurs, however; they serve their purpose in the assessment of the experimental configuration.

II 5.3.2 Preliminary Analyses

Thermal analyses, using the math model were made for the full scale model and the 1/4 scale model for the following conditions:

a. Full Size Model (heat input 1000 Btu/hr)
   1. Evaculated (radiation - solid conduction)
   2. Low Pressure (#1 + gas conduction)
   3. 1 atm Pressure (#2 + free convection)
   4. Gas Flow (#3 + forced convection)
      a. Re = 1180 V = 6. fpm
      b. Re = 4720 V = 24. fpm
      c. Re = 18,900 V = 96. fpm

b. 1/4 Scale Model (heat input = 62.5 Btu/hr)
   1. Evacuated
   2. Low Pressure
   3. 1 atm Pressure
   4. Gas Flow
      a. Re = 1180 V = 48. fpm
      b. Re = 4720 V = 192. fpm
      c. Re = 18,900 V = 788. fpm
   5. #3 and #4 repeated at pressures of 4., 8. and 16. atmospheres.

These cases were analyzed for air inlet (where applicable) temperatures of 35 and 80°F. All cases used a cooling fin temperature of 35°F.

The calculated temperature distributions for an air inlet temperature of 80°F are shown in Figures II-11 and II-12 for the full scale and 1/4 scale models respectively. The full scale model temperatures are somewhat lower than those of the 1/4 scale model for the radiation-solid conduction case. It was originally planned to use 6061-T4 alloy aluminum for the full scale model, however, it turned out that 6061-T6 alloy was used instead. This switch in full scale model alloy resulted in model conductances about 10 percent too low. Figure II-13 shows the calculated temperature differences between the 1/4 scale and full scale model for both 6061-T4 and 6061-T6 aluminum alloys. The good agreement with the 6061-T4 curve reflects the intended use of this alloy. The calculated 1/4 scale model temperatures average about 7.5°F warmer than the full scale model constructed of 6061-T6 alloy. The 1/4 scale model fin design was subsequently modified to properly scale the full size model. This change lowers the model temperature by about 5°F. Consequently the imperfect thermal conduction scaling is expected to result in a 1/4 scale model temperature that is too high by about 2.5°F. This represents the largest differences to be expected since the cases analyzed are for the highest heating rates anticipated during radiation-conduction testing.

A subroutine to the TMM BETA program was written to evaluate the experimental accuracy required to implement the Nusselt number preservation scaling technique. This subroutine calculates the convective heat transfer coefficient at each node using a given temperature distribution. When the calculated temperature distribution is used the input heat transfer coefficients are calculated. By using the calculated temperature distribution with the temperatures rounded off to varying degrees of accuracy, the effect of temperature measurement accuracy on the calculated heat transfer coefficients is determined.

The effect of temperature measurement accuracy on the heat transfer coefficient determination was investigated by rounding off the calculated temperatures to the nearest 0.1, 0.2 and 0.4 degrees and using the subroutine to calculate the heat transfer coefficient. Figure II-14 shows a typical comparison between the input heat transfer coefficients and those calculated for the various temperature accuracies. The accuracy of the temperature measurements is most critical in regions where the thermal gradient is small and/or where the wall temperature

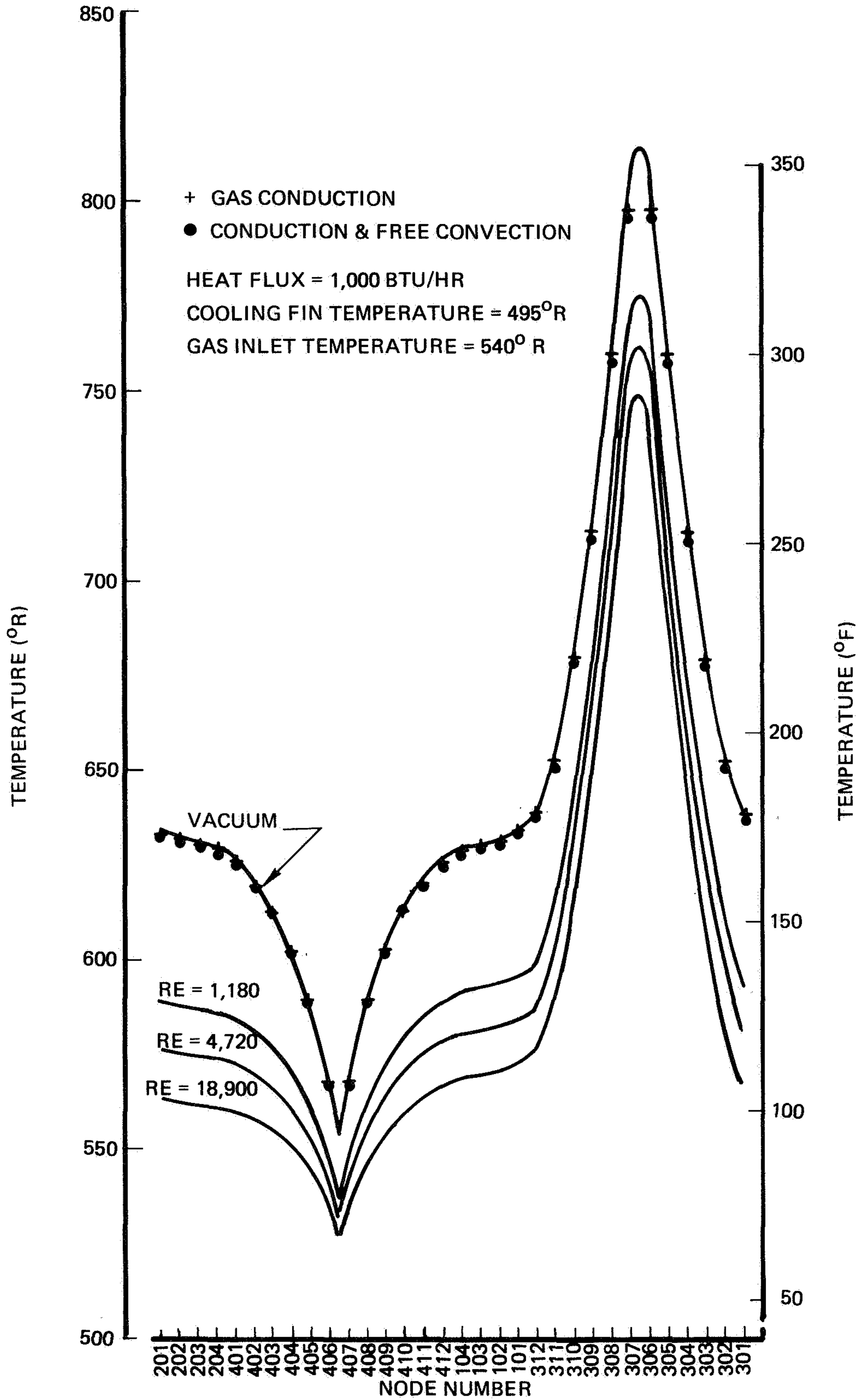

Figure II-11: CALCULATED TEMPERATURE DISTRIBUTION FOR FULL SIZE MODEL

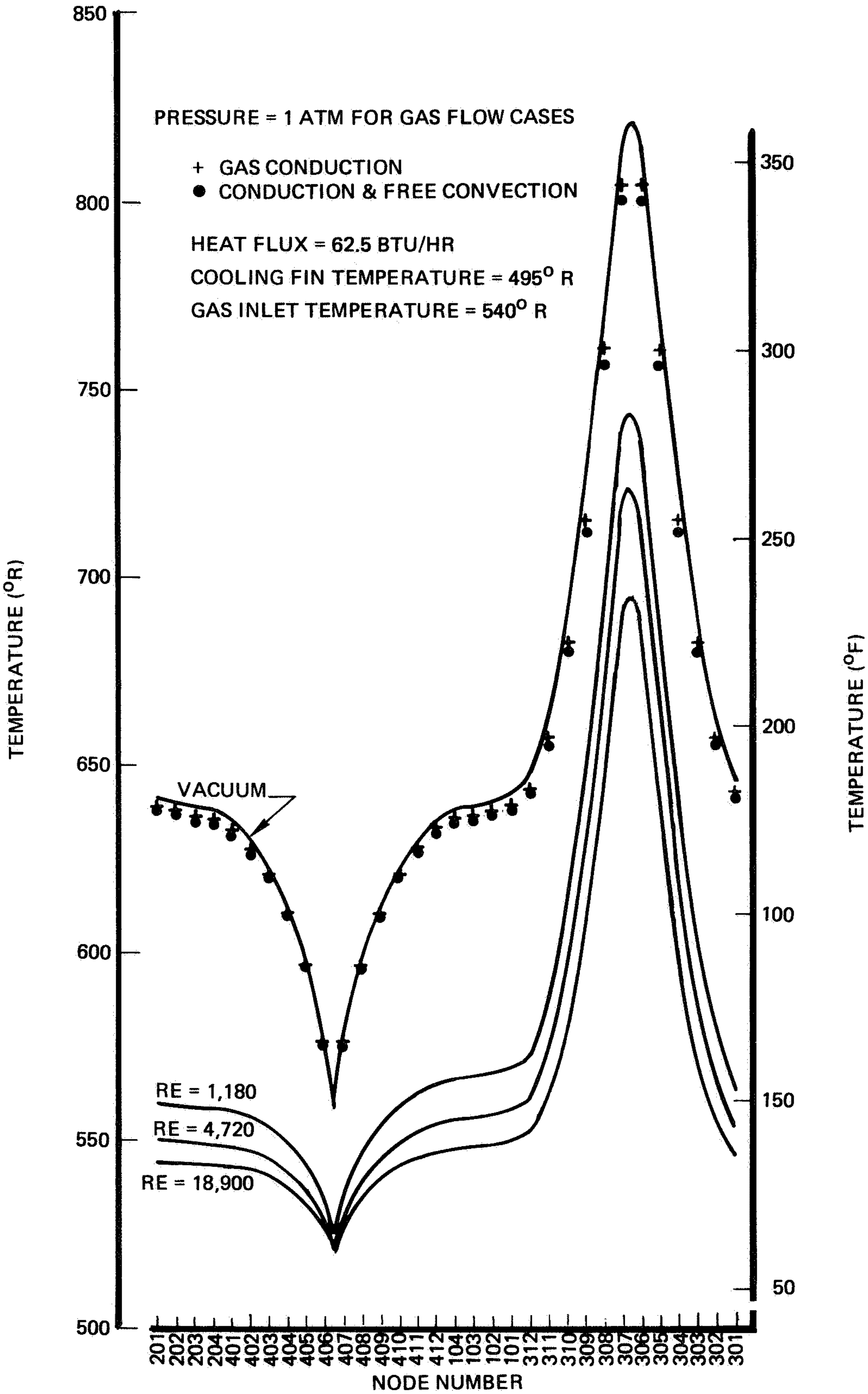

Figure II-12: CALCULATED TEMPERATURE DISTRIBUTION FOR 1/4 SCALE MODEL

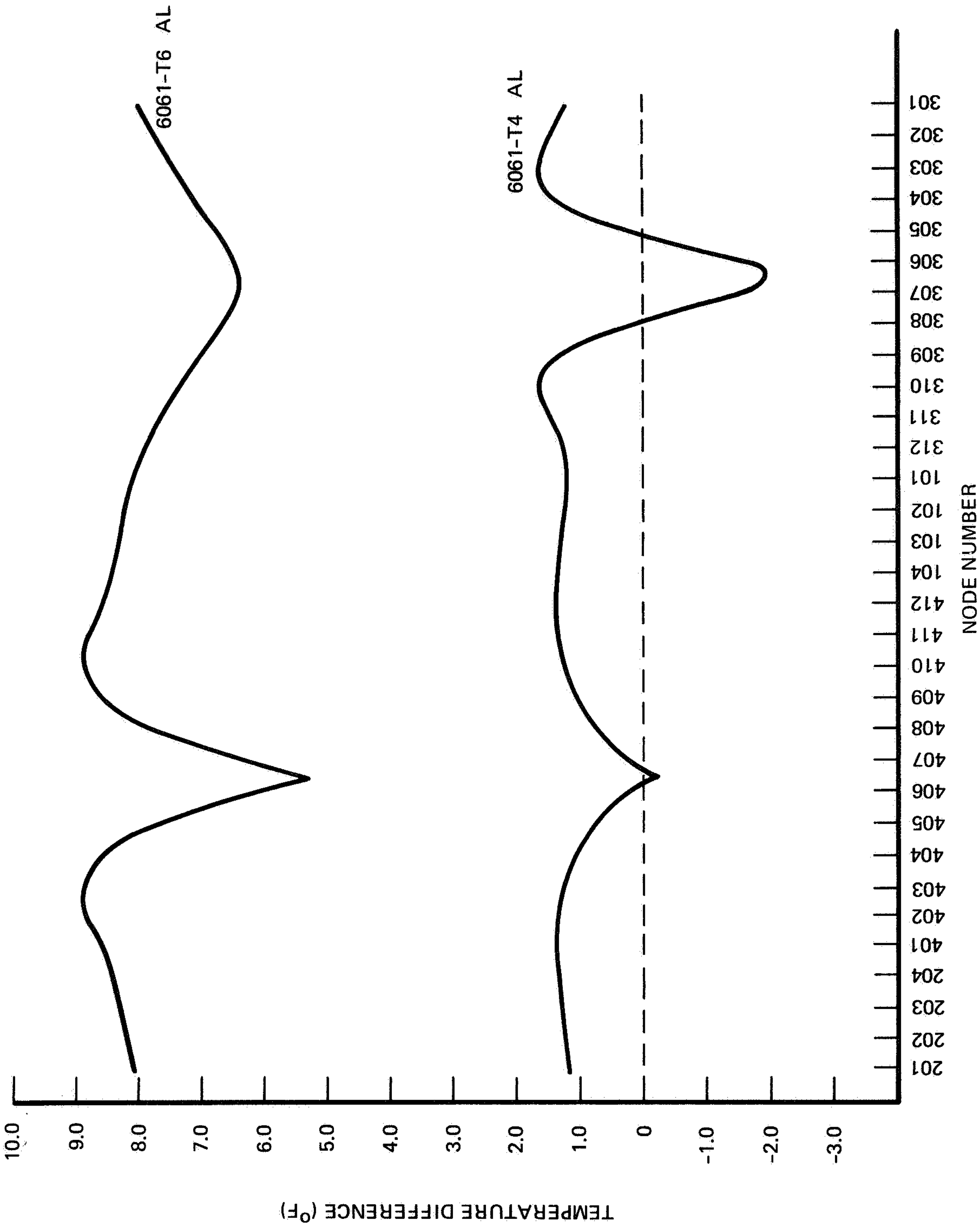

Figure II-13: CALCULATED TEMPERATURE DIFFERENCE BETWEEN 1/4 SCALE MODEL AND FULL SIZE MODEL (RADIATION-CONDUCTION ONLY)

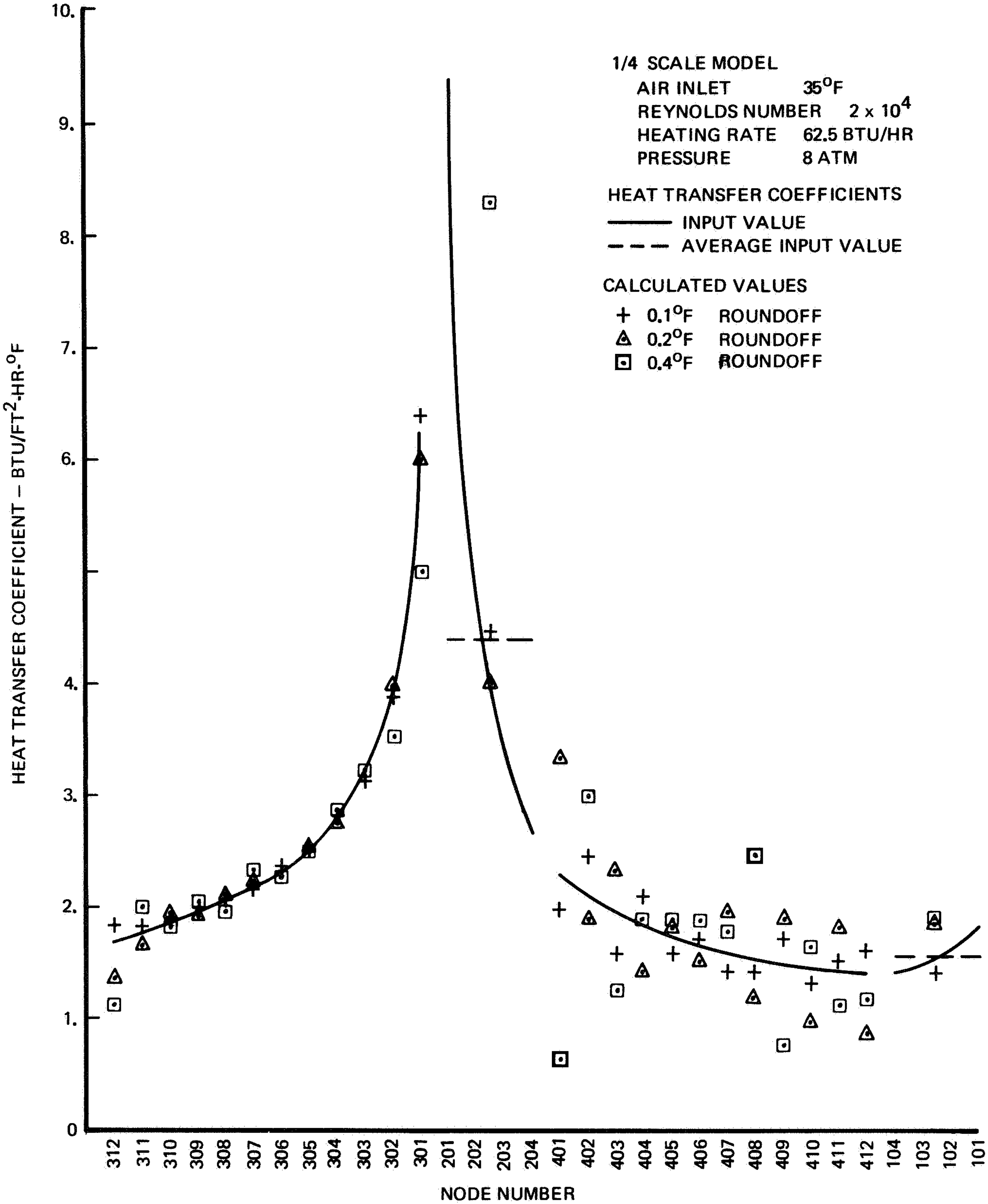

Figure II-14: HEAT TRANSFER COEFFICIENT CALCULATIONS is near to the gas temperature. The results shown in Figure II-14 indicate that the heat transfer coefficient may be determined to within 10 to 15 percent with temperatures measured to $\pm 0.1°F$, to within about 30% for $\pm 0.2°F$ and to within about 80% for $\pm 0.4°F$. These results are for an inlet gas temperature of 35°F. The results for an inlet gas temperature of 80°F show larger uncertainties in the determination of the heat transfer coefficient for the outer cylinder regions where the gas temperature and wall temperature are nearly equal. Consequently it was decided that a temperature measurement accuracy of at least $\pm 0.1°F$ is required to implement the Nusselt number preservation scaling technique.

II.5.4 Thermocouple Calibration

Forty-nine chromel-constantan thermocouples were calibrated for the full scale model and a like number for the one-quarter scale model. The wires are AWG #36 (0.005 in. diameter) with a double layer of stranded fiberglas insulation. All the wires were taken from the same spool. The junctions were made by twisting the leads together and silver brazing.

The calibration consisted of an absolute calibration and a relative calibration. The absolute calibrations were conducted, on samples from the spool, at the Boeing Metrology Laboratory. This calibration has NBS traceability and claims an accuracy of $\pm 0.04°F$ for any particular calibration point. This calibration data is presented in Table II-4. The standard EMF is based on tabulated results of reference 10. The relative calibration consisted of fixing the forty-nine thermocouples earmarked for a particular model on a copper slug. The slug was then put in an insulated oven fixture and all the wires were checked against each other over the entire test temperature range. Other than the transferring of the test junctions from the copper slug to the model, all the thermocouple circuitry for the relative calibration was kept for the model tests. The oven and the thermocouple circuitry are shown in Figure II-15.

Since the preliminary analyses showed that a temperature roundoff (simulated thermocouple error) larger than 0.1°F began to cause scatter in the calculated convective heat transfer coefficient, it was decided to correct all thermocouples to at least this accuracy. For chromel-constantan wire at the test temperatures,

TABLE II-4 THERMOCOUPLE ABSOLUTE CALIBRATION

	Thermocouple EMF (above ice point)		
Temperature (°F)	Standard (m V)	Measured (m V)	Correction (μ V)
32	0	0	0
100	2.2753	2.2708	+4.5
200	5.8724	5.8598	+12.6
300	9.7112	9.6950	+16.2
400	13.7518	13.7378	+14.0

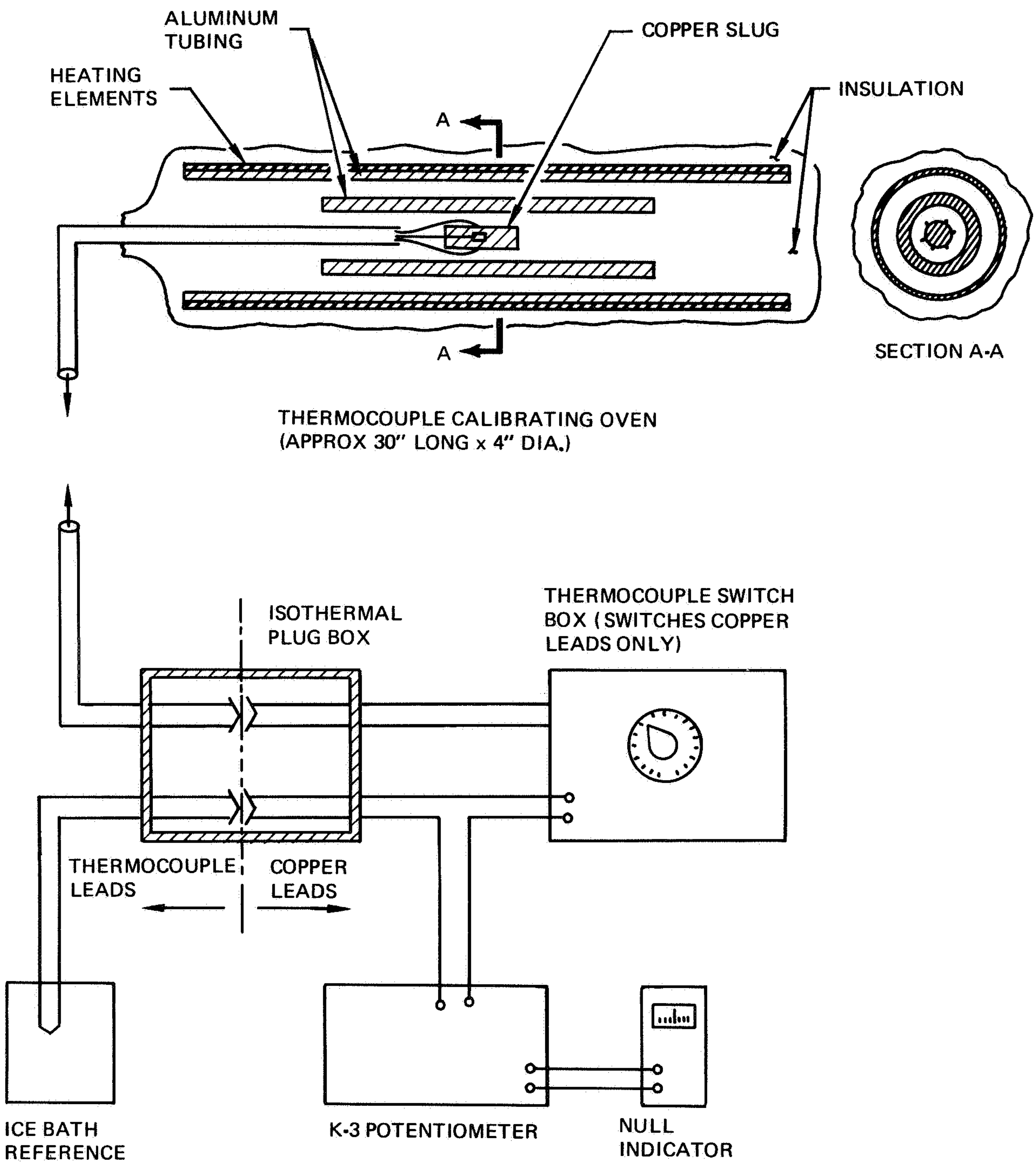

Figure II-15: THERMOCOUPLE CALIBRATION SET-UP AND CIRCUITRY

0.1°F is approximately equal to 3.5 μV of thermocouple emf. This allowed grouping the thermocouples for purposes of generating correction curves. For the full scale model the grouping was six groups of 6, 6, 12, 13, 6 and 6. For the quarter scale the grouping was seven groups of seven each. Each group can then be represented by its own mean and corrected to the mean of the forty-nine wires. The absolute calibration can then be added to the mean of the forty-nine wires. In this way each wire is accurately related to every other wire in the model (± 3 μV) and is also accurate to within approximately 0.5°F of absolute temperature. Note that the ± 3 μV is the maximum error between any two thermocouples and represents a simulated round off of individual temperatures in the math model of approximately 0.05°F. The relative calibration curves for the full scale and the one-quarter scale model are given in Figure II-16.

II.5.5 Model Design, Fabrication and Instrumentation

The basic model designs (outer cylinder, cooling fin, end plates and inner cylinder) were outlined in Section II.5.2. The outer cylinders were fabricated from sheet material which was rolled and seam welded to form the cylinders. The cooling fins were also made from sheet material. The horizontal fins were cut from a sheet and welded to the vertical fins which had been formed by rolling and seam welding. These fin structures were then welded onto the centers of the outer cylinders. The end plates were cut from plate material. The inner cylinder for the 1/4 scale model was machined from a 2.0 inch O.D. by 0.109 inch wall tube. The inner cylinder for the full scale model was fabricated using tubing and sheet material. The thicker sections of the inner cylinder were cut lengths of 8.0 inch O.D. by 0.125 inch wall tubing and the thinner sections were formed from 0.050 sheet material by rolling and seam welding. These sections were then welded together to form the inner cylinder.

Twelve equally spaced holes were cut at each end of the inner cylinders to provide air inlet and outlet passages. These holes were cut such that one side would be flush with the end plates in the final model assemblies. The holes are slots with semicircular ends. The full scale model holes measure 1.344 inches long by 0.625 inches high and the 1/4 scale model holes 0.336 inches long by 0.156 inches high.

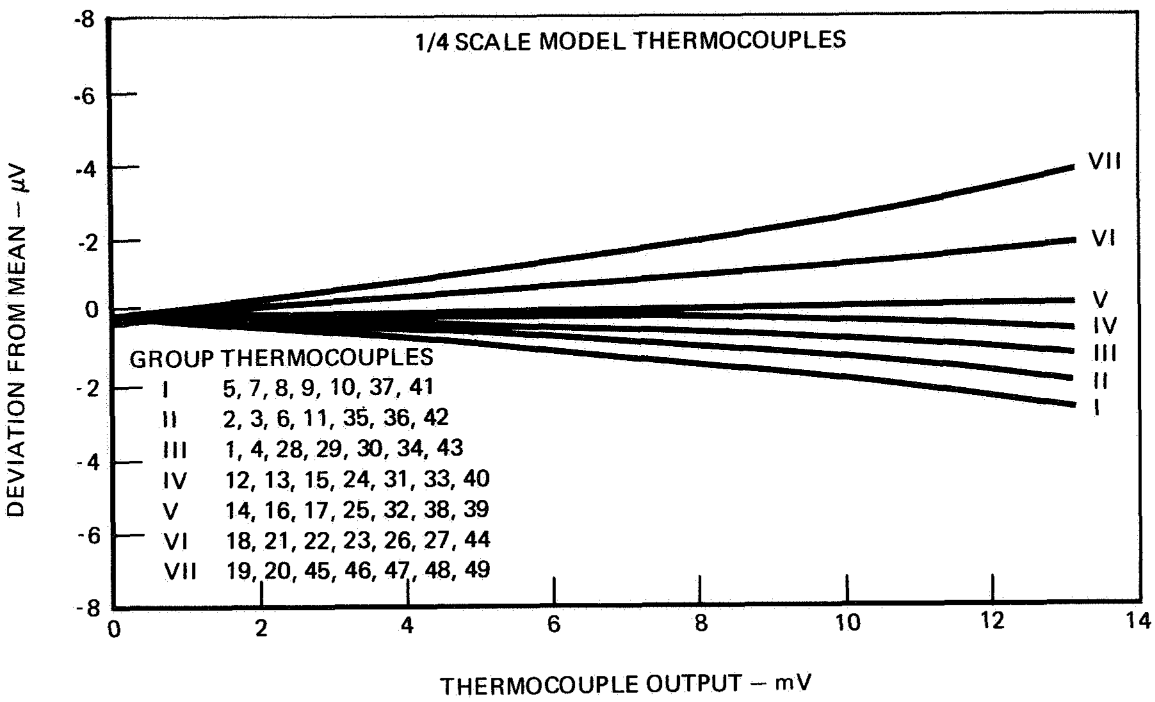

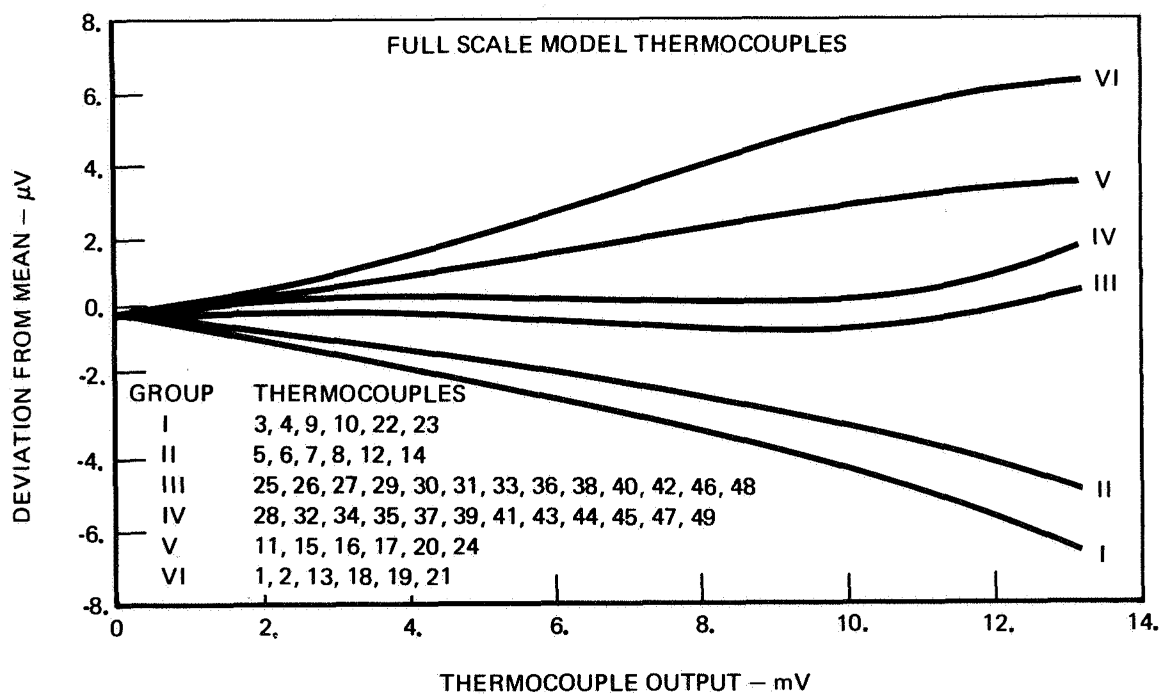

Figure II-16: RELATIVE THERMOCOUPLE CALIBRATING

The air distribution plugs were designed to provide air to the annular region of the models. These plugs also seal off the inner cylinder while providing instrumentation and heater lead feed throughs, as well as providing the capability for evaluating the inner cylinder. No attempt was made to thermally scale model these air distribution plugs since their effects on the thermal performance of the models should be minor. The flow passage geometry was scaled to preserve dynamic similarity. Both full scale and 1/4 scale model plugs were made of phenolic material. Figure II-17 shows the 1/4 scale model air distribution plug that has the heater and thermocouple feed through passages. The other plug is identical with the exception of having only two pass through holes 180° apart which are counterbored to accept 1/4 inch O.D. vacuum lines. Twelve equally spaced 0.156 inch diameter holes drilled radially provide the air distribution passages. The air supply (or exhaust) is provided by a hole in the center of the plug which is threaded to accept a standard fitting for 1/2 inch O.D. tubing. The full scale model air distribution plugs are similar to those for the 1/4 scale model except that only two feed throughs were required for the instrumentation and heater leads.

The model heaters were designed to provide a uniform heat flux to the center section of the inner cylinders. The full scale model heater was fabricated by uniformly wrapping 0.001 x 0.062 inch Nichrome V ribbon on a flat 0.015 inch thick phenolic sheet which was then bonded to a 0.125 inch silicone rubber backing sheet. The exposed heater ribbon was then coated with a layer of RTV silicone rubber approximately 0.006 inches thick. The heater assembly was sized such that when rolled into a cylinder it would fit the inside of the center section of the inner cylinder. The 1/4 scale model heater was fabricated by wrapping 28 turns of Nichrome wire around a threaded heater core that had been machined from a "Transite" block. A 0.059 inch thick layer of RTV silicone rubber was then bonded on the outer surface of the assembly. This assembly was designed to be a press fit inside the center section of the inner cylinder.

Prior to installing the heaters, 24 holes (0.015 inch diameter) were drilled in each inner cylinder for the thermocouple instrumentation. Two holes were drilled 180° apart at 12 axial locations along the inner cylinders. These axial locations correspond to the center of each inner cylinder node of the TMM. An exception to this positioning occurs for the air inlet and outlet sections

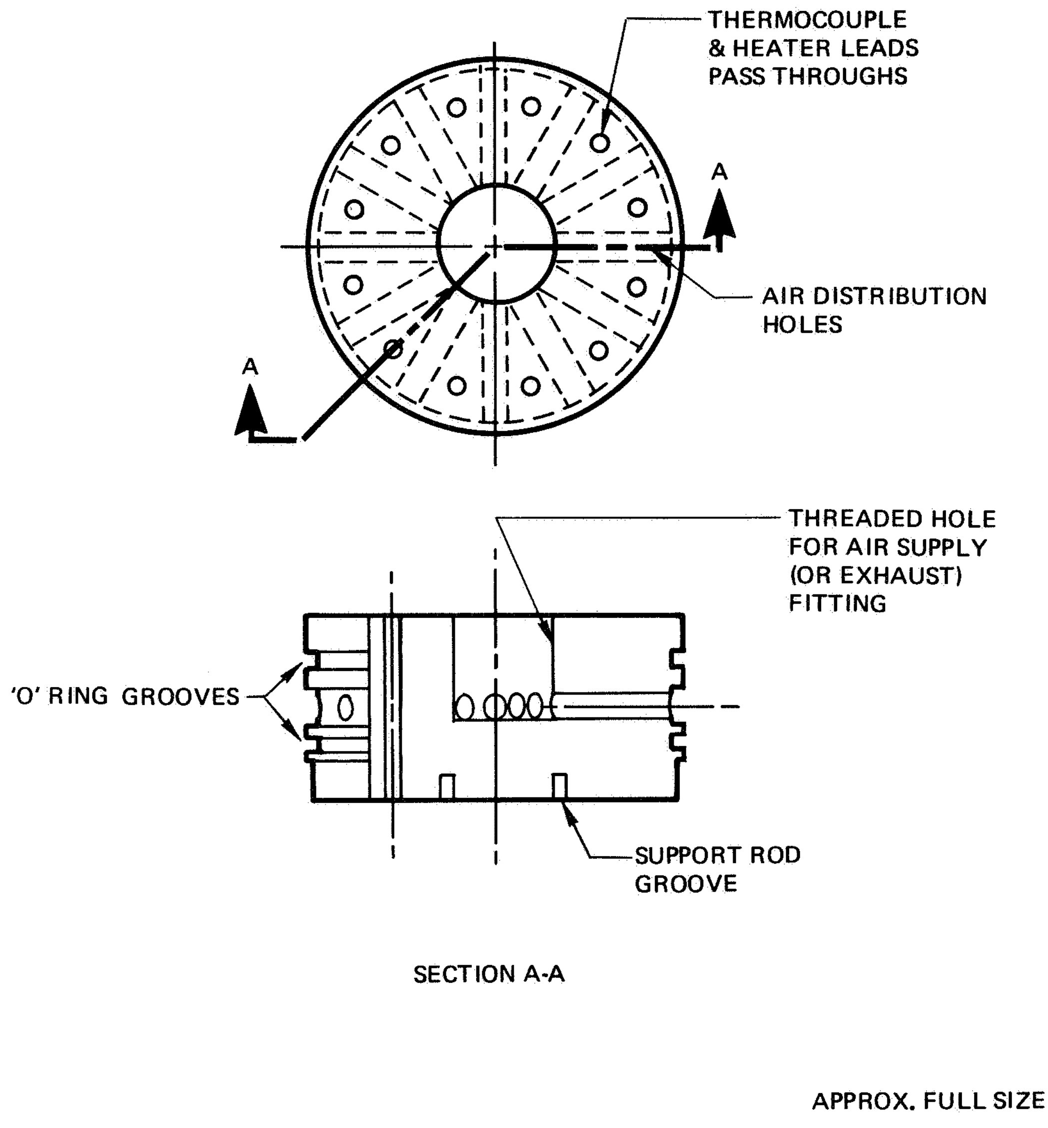

Figure II-17: 1/4 SCALE MODEL AIR DISTRIBUTION PLUG where the air holes interfere. The thermocouple holes for these sections are 75 percent of the node length away from the end plates instead of being at the node center.

The four thermocouples for the center section of the inner cylinders were installed before the heaters were placed in position. These thermocouples (as were all of those for the inner cylinders) were installed by inserting the twisted and silver brazed junctions in the holes, securing them in position by swaging, filing off the junction excess protruding beyond the outer surface of the cylinder and sealing the holes with epoxy resin.

Figure II-18 shows a photograph of the 1/4 scale model components prior to installation of the heater inside the inner cylinder. This figure shows the two end plates, the outer cylinder assembly with the copper coiling coils brazed to the fin, the inner cylinder with the four center section thermocouples installed, the air distribution plugs and the heater assembly. The heater assembly is shown without the 0.059 inch layer of RTV silicone rubber. This layer was bonded to the heater in two pieces leaving two gaps to clear the center section thermocouple leads. After the heater was pressed into place, these gaps were filled with RTV using a hypodermic syringe. The full scale model heater was installed by coating the heater surface with RTV, inserting the heater in place inside the center section of the inner cylinder and holding it tightly in position against the cylinder wall, using an inflatable bladder, until the RTV cured. After the RTV cured the gap in the heater assembly was filled in with RTV. The full scale model heater design and installation is shown in Figure II-19. Following the heater installation, the remaining inner cylinder thermocouples were installed and "bench tests" were made to check out the thermocouple and heater installations.

One end plate was welded to the inner and outer cylinder assemblies, and the radiation surfaces were cleaned and painted with two coats of Fullers Metal Etch Primer (3811 black with 3816 primer). Figure II-20 shows the full scale model at this stage of assembly. The emittance data for the black paint was measured for various painted 6061-T6 aluminum and 304 stainless steel samples.

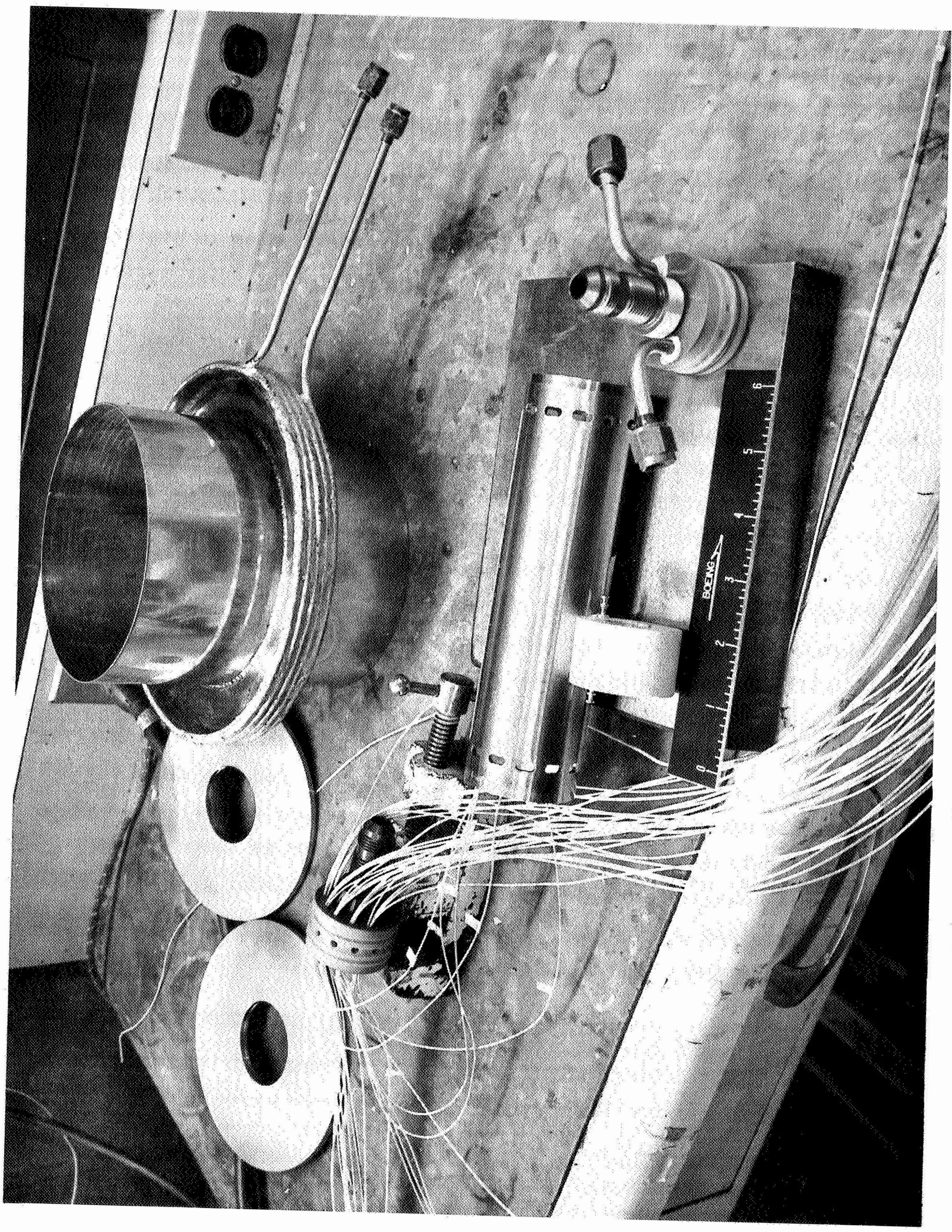

FIGURE II-18 ¼ SCALE MODEL COMPONENT PARTS

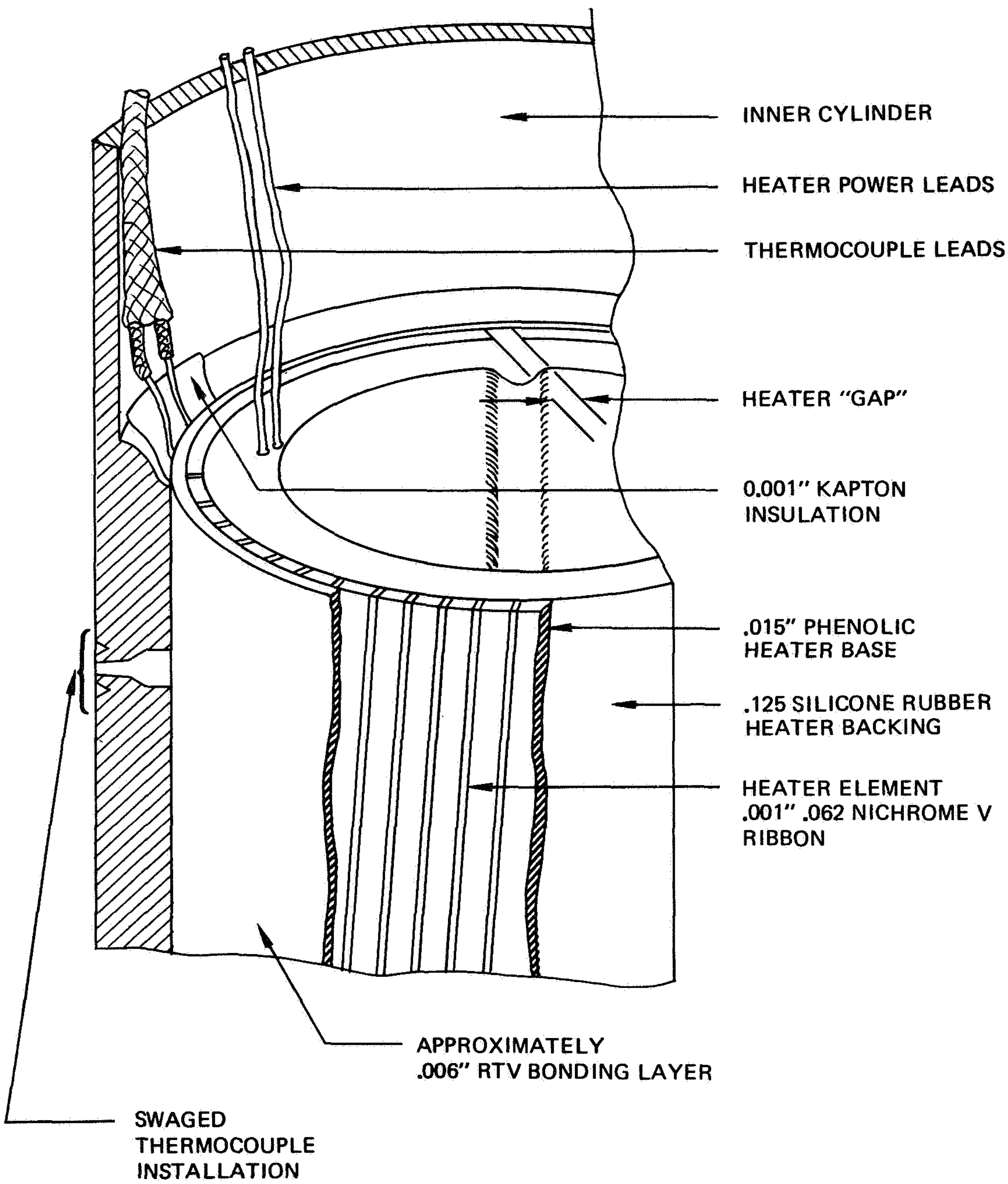

Figure II-19: FULL SCALE MODEL HEATER INSTALLATION

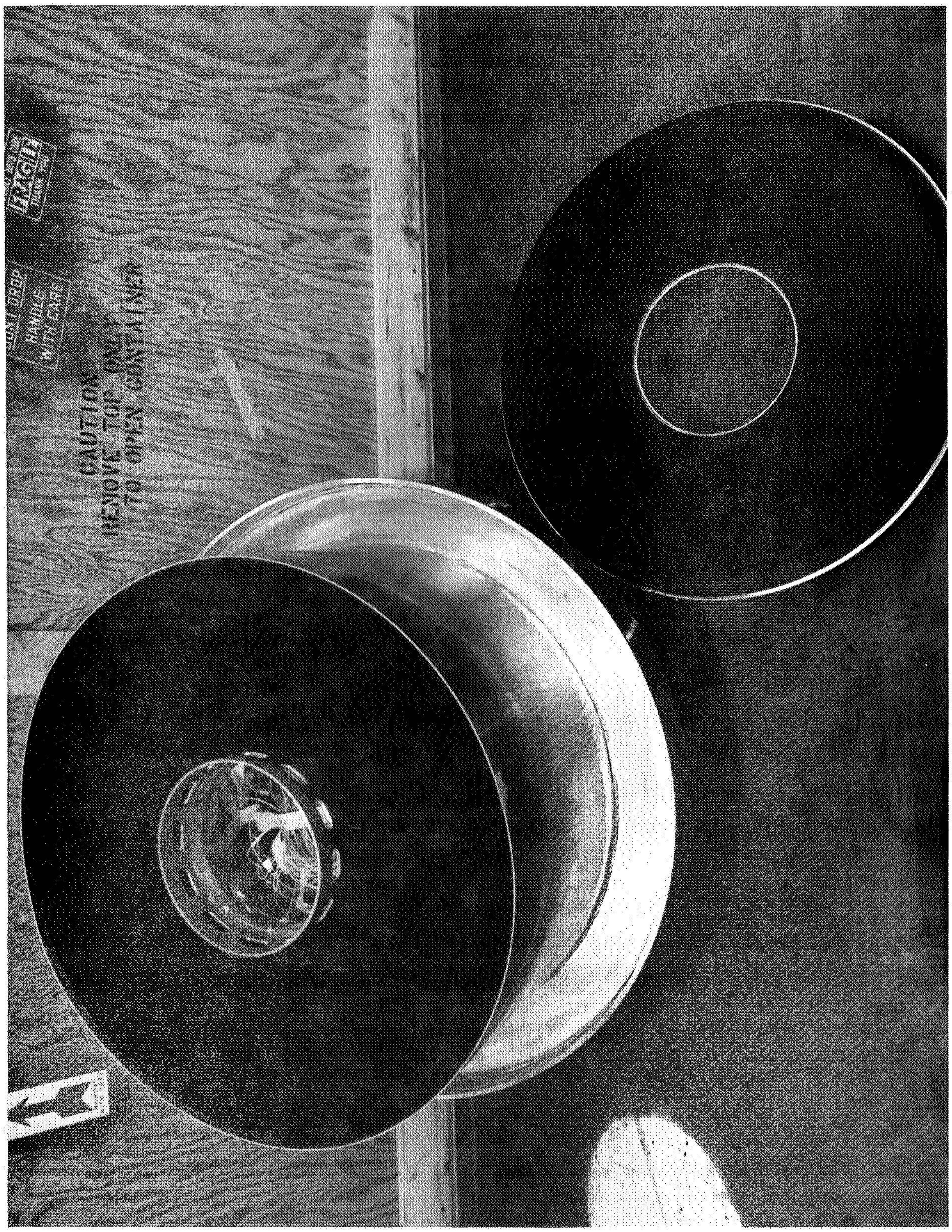

FIGURE II–20 FULL SCALE MODEL BEFORE FINAL WELDING

These data are presented in Table II-5. The preliminary analyses assumed an emissivity of 0.88. The welding of the remaining end plates to the inner and outer cylinders completed the basic structure assemblies. The "O" ring seal surfaces at each end of the inner cylinders were machined after the model assemblies were welded.

The inner cylinder assemblies were completed with the installation of the air distribution plugs. Figure II-21 shows the inner cylinder assembly of the 1/4 scale model. The air distribution plugs are held in position by a 0.75 inch diameter phenolic rod which keeps external pressure from pushing the plugs further into the cylinder. The full scale model uses a 2 inch O.D. by 1/16 inch wall phenolic tube to support the air distribution plugs. At this point, a recheck of the thermocouples revealed that many of the 1/4 scale model thermocouples were broken. Because of the limited working space inside the inner cylinder, the 1/4 scale model was disassembled and reinstrumented. The welds between the end plates and outer cylinder were cut and the inner cylinder assembly with attached end plates was removed from the outer cylinder assembly. The heater and thermocouples were removed, the old thermocouple holes welded closed, and new holes drilled. The thermocouple leads were shortened to reduce the possibility of subsequent damage during handling of the model and new thermocouple junctions fabricated and installed as shown in Figure II-22. Since the old thermocouple leads were used for the new junctions the effect on the calibration curves is insignificant. After brazing the thermocouple junctions the bared lead wires were encapsulated with RTV (silicone rubber) to form tabs about 3/8 inch square by 0.05 inch thick with the brazed functions emerging normal to the tabs. The junctions and adjacent tab surfaces were coated with RTV and the junction were inserted into the drilled holes of the inner cylinder and held in place. The curing of the RTV then bonded the thermocouple assembly in place. The thermocouple leads were wrapped a distance around the inner cylinder wall in the plane of the junction (to reduce the heat leak from the junction) and then routed through the pass through holes in one air distribution plug. The thermocouple and heater leads were sealed in the pass through holes with "Scotchcast 5." Prior to the installation of the air distribution plugs, the inner cylinder was filled with "Micro Quartz" insulation to reduce heat transfer inside the inner cylinder. Before rewelding the end plates to the outer cylinder an extensive vaccum leak check was made for the inner cylinder using a helium leak detector. However, even after sealing all of the leaks that could be found, the minimum pressure that could be obtained in the inner cylinder was about 5×10^{-3} torr at room temperature and 80×10^{-3} torr with the heater at 300°F.

TABLE II-5 EMITTANCE DATA FOR PAINTED SAMPLES

FULLERS METAL ETCH PRIMER (3811 BLACK WITH 3816 PRIMER)

Sample No.	Substrate Condition	Number of Coats (Sprayed)	ε	ε **
1	6061-T6, base	1	0.78	0.73
2	6061-T6, base	2	0.88	0.83
3	6061-T6, roughened	1	0.79	0.75
4	6061-T6, roughened	2	0.90	0.85
9	304 CRES, base	1	0.78	0.78
10	304 CRES, base	2	0.85	0.88
11	304 CRES, roughened	1	0.75	0.76
12	304 CRES, roughened	2	0.84	0.88

*Measured with a Lions Emissometer.

**Value after baking cycle of:

3 1/2 hours at 220°F
1 1/4 hours at 350°F
4 hours at 400°F

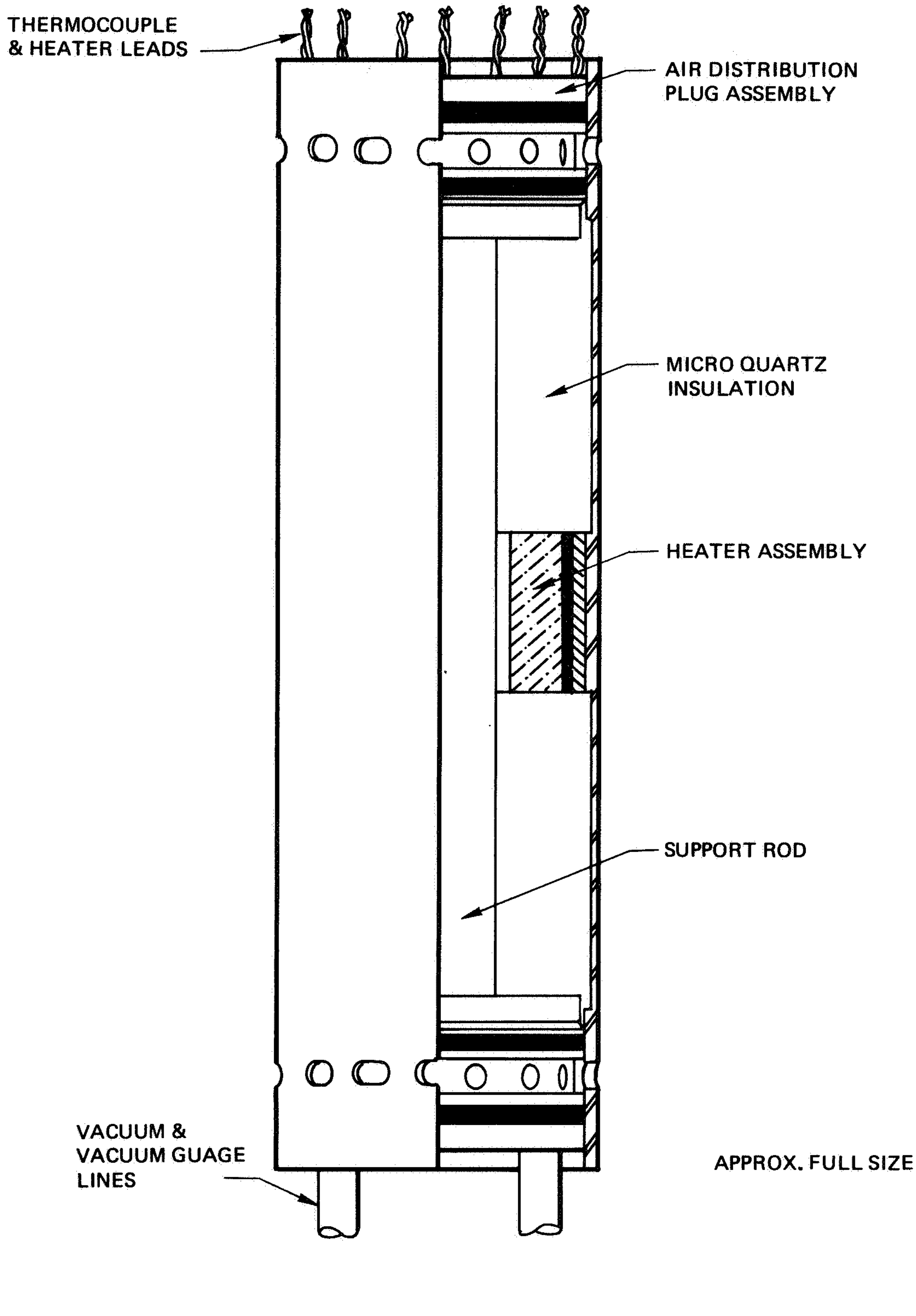

Figure II-21: 1/4 SCALE MODEL INNER CYLINDER ASSEMBLY

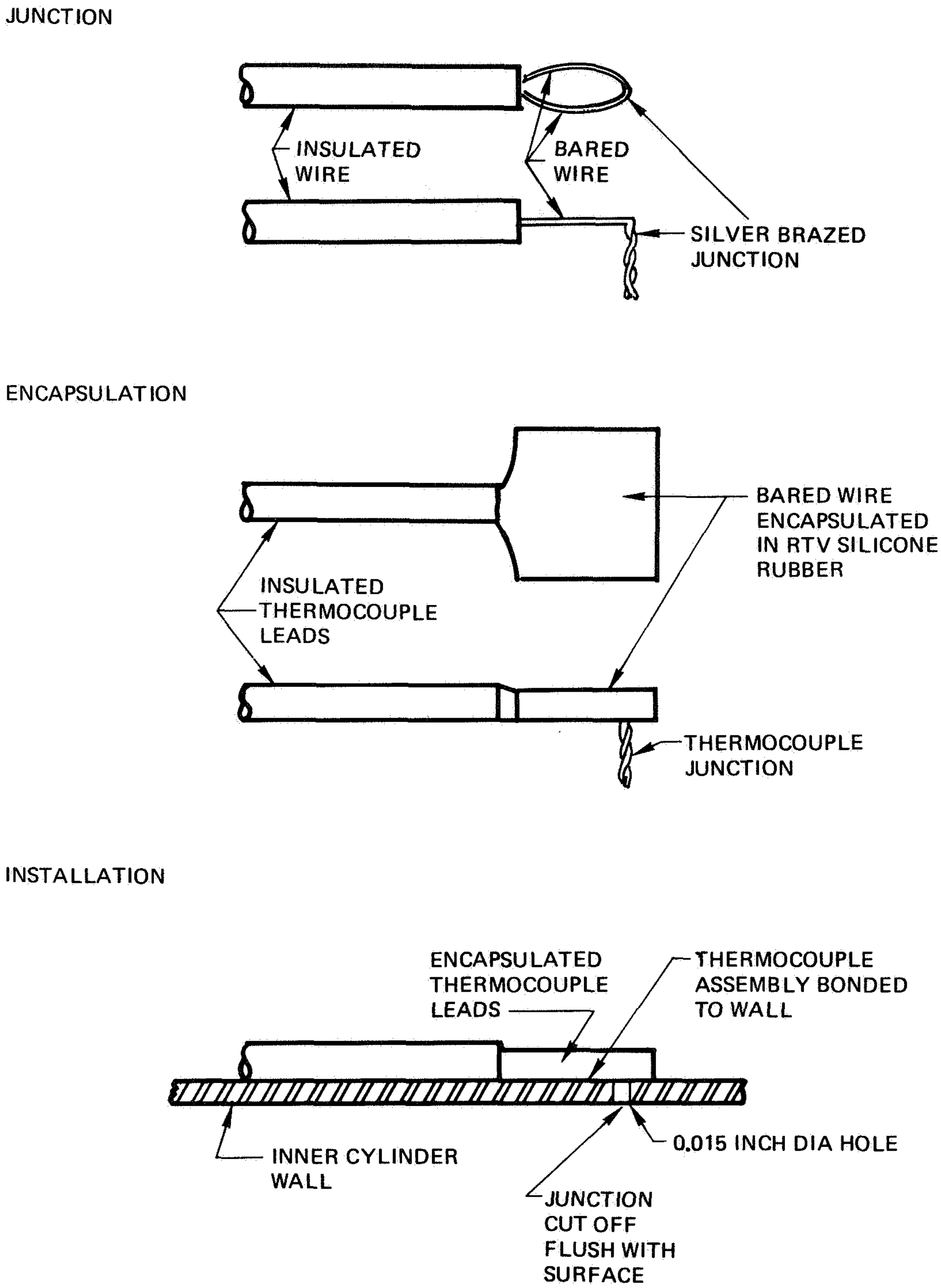

Figure II-22: THERMOCOUPLE INSTALLATION FOR 1/4 SCALE MODEL INNER CYLINDER

The outgasing of the transit heater core and the RTV along with the small pumping line apparently limits the evacuation of the inner cylinder.

Twenty-three thermocouples were attached to the outside of each model at positions corresponding to the TMM node locations. The junctions were spot welded to the model except those on the 1/4 scale model end plates were staked into drilled holes and those on the copper coiling tubes were brazed. The thermocouple installation corresponding to nodes 201-204 and 401-406 is shown in Figure II-23 for the full scale model and Figure II-24 for the 1/4 scale model. The thermocouple installation corresponding to nodes 101-104 and 407-412 is shown in Figure II-25 for the full scale model and Figure II-26 for the 1/4 scale model. The thermocouple installation for node 413 can be seen in Figures II-25 and II-24 for full scale and 1/4 scale models respectively. Two thermocouples were used for node 414, one at the inlet and the other at the outlet of the cooling coil. These may be seen in Figure II-27 for the full scale model and Figure II-26 for the 1/4 scale model. The thermocouple leads were routed around the models to minimize the heat leak from the junctions and were grouped into a single bundle of leads routed away from the model. The routing of the lead bundle away from the models can be seen in Figures II-27 and II-28. The correspondence between the thermocouple numbers and the TMM node numbers is shown in Figure II-29 for the full scale model and Figure II-30 for the 1/4 scale model.

Prior to testing, the models were insulated with polyurethane foam. The models were centered in cylindrical molds and the insulation was foamed between the models and the molds. The foam insulation is shown in Figures II-31 and II-32 for the full scale and 1/4 scale models. The foam thickness was sized to preserve the one-dimensional heat transfer through the insulation. Figure II-33 shows a photograph of the insulated full scale model.

II.5.6 Model Tests

The full scale model was tested at atmospheric pressure under free convection and forced convection conditions. Five heating rates were used in the free convection (no flow) tests. The forced convection tests used three heating rates and three flow rates. The flow rate tests were repeated for the highest

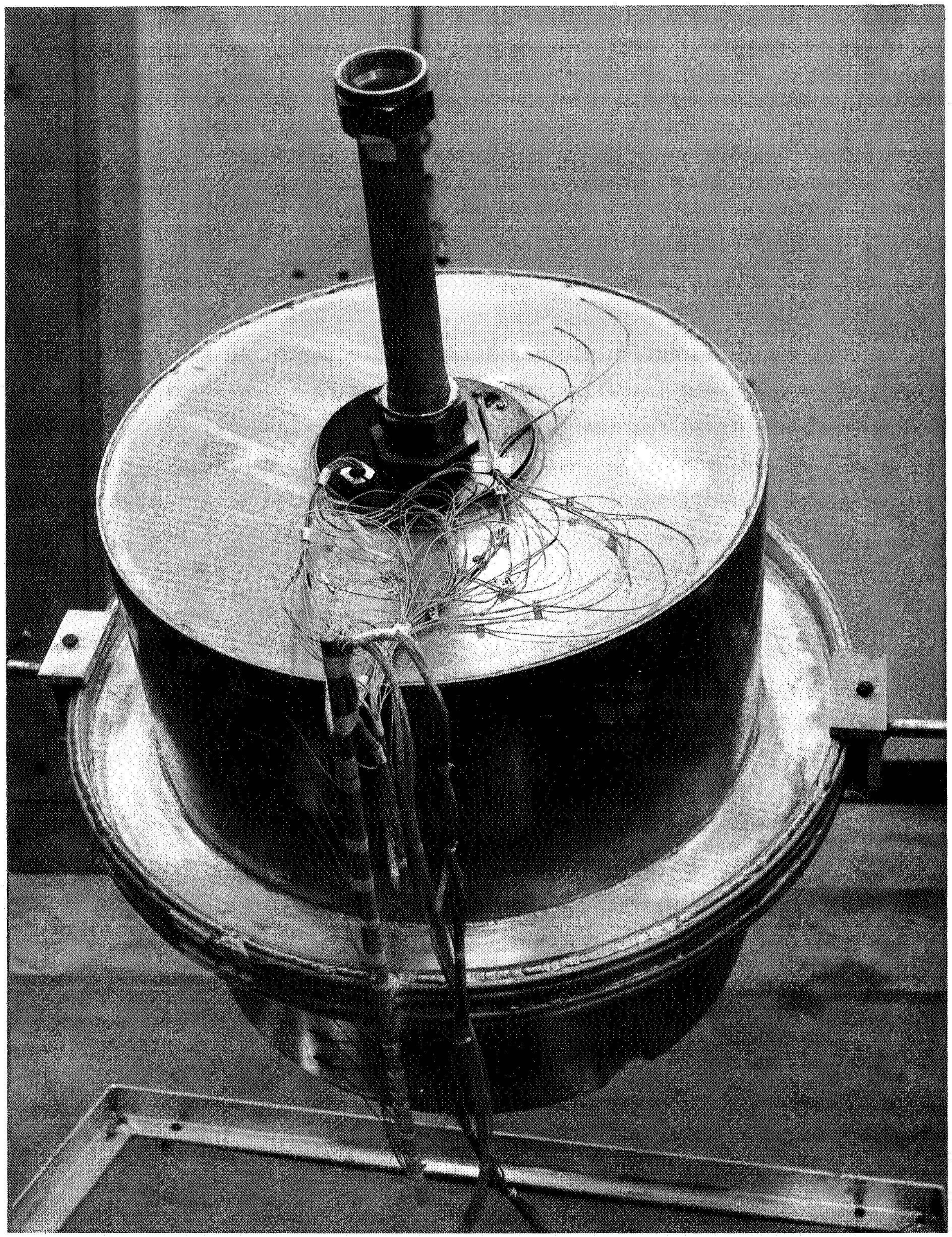

FIGURE II–23 INSTRUMENTED FULL SCALE MODEL

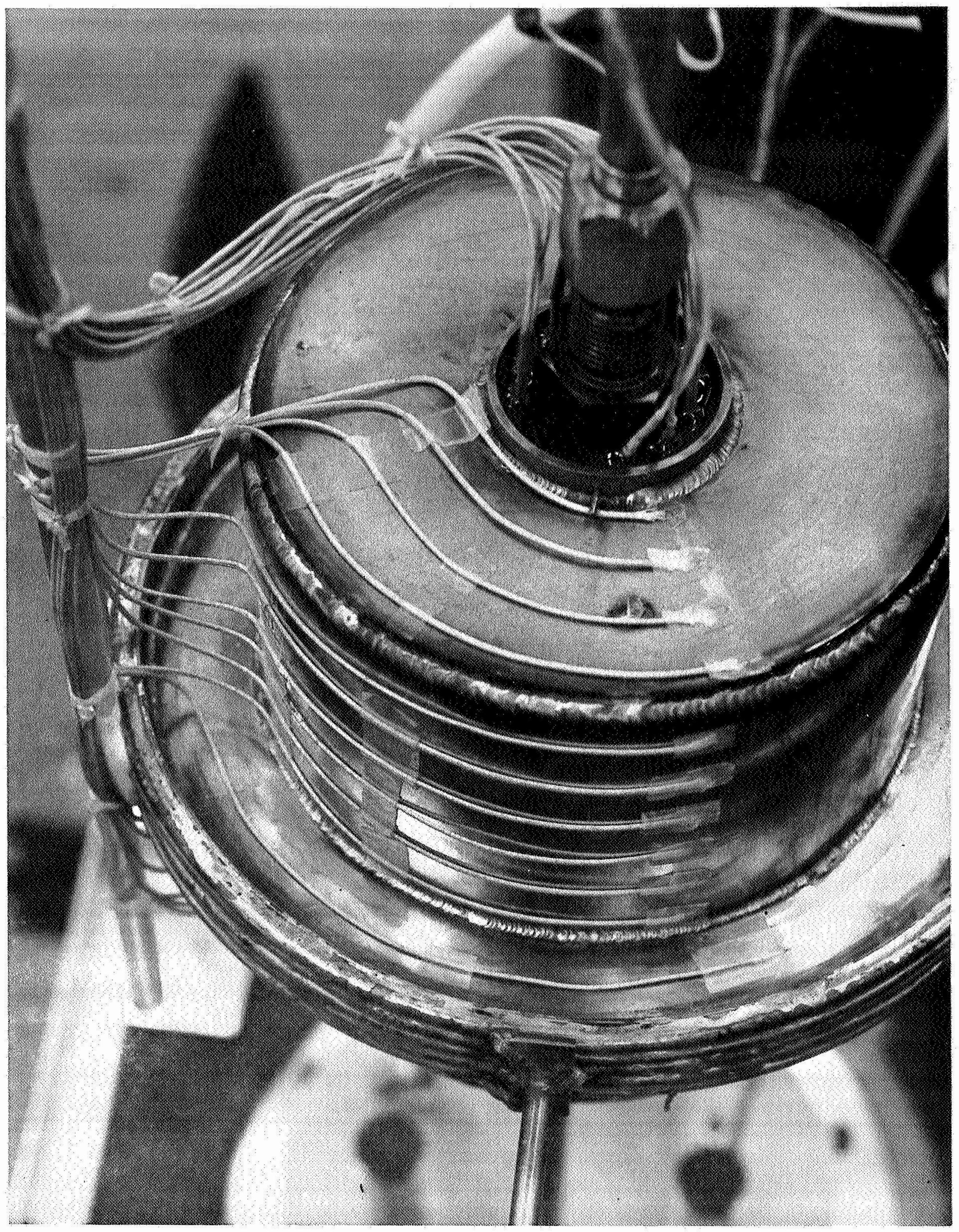

FIGURE II–24 INSTRUMENTED ¼ SCALE MODEL

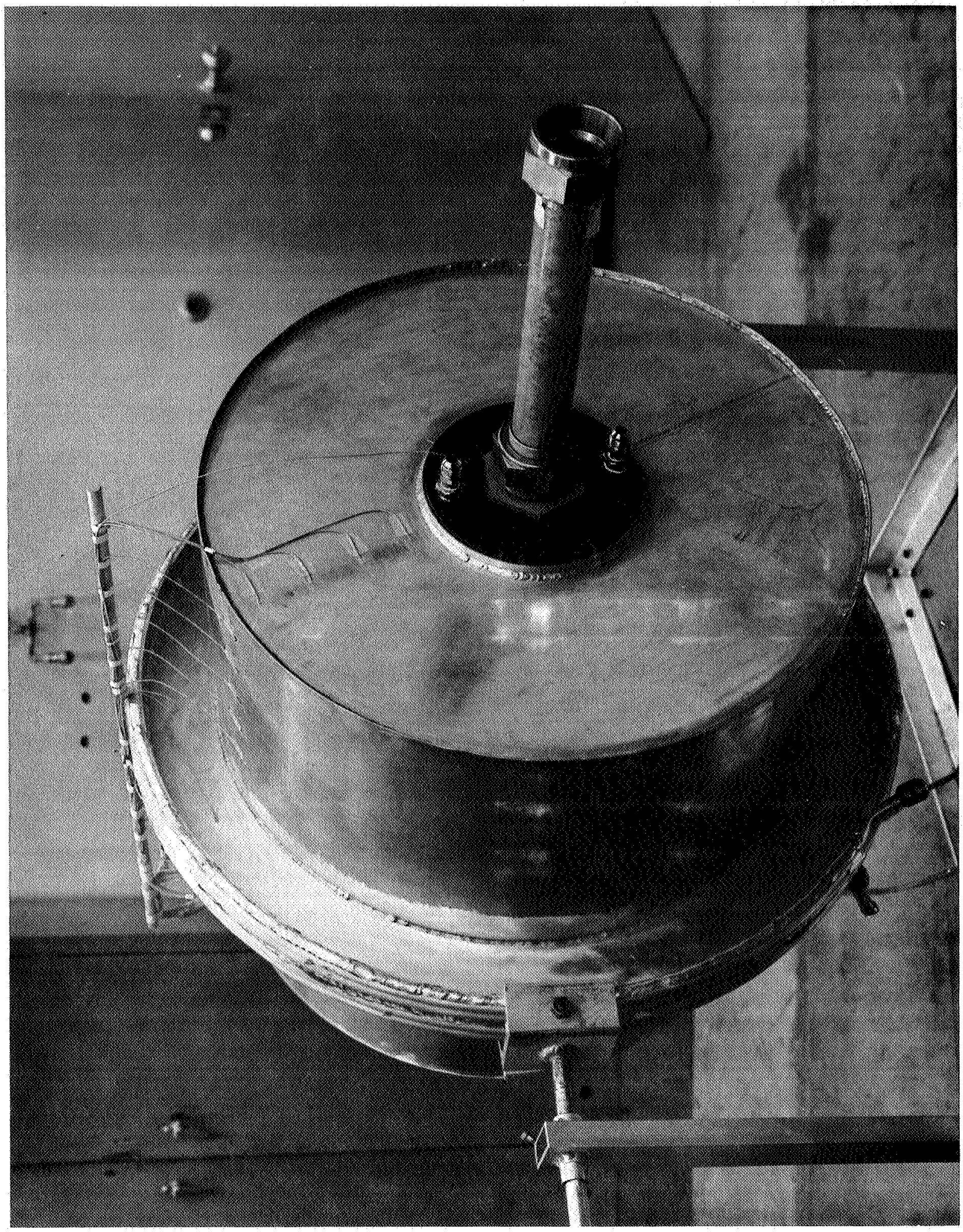

FIGURE II–25 INSTRUMENTED FULL SCALE MODEL

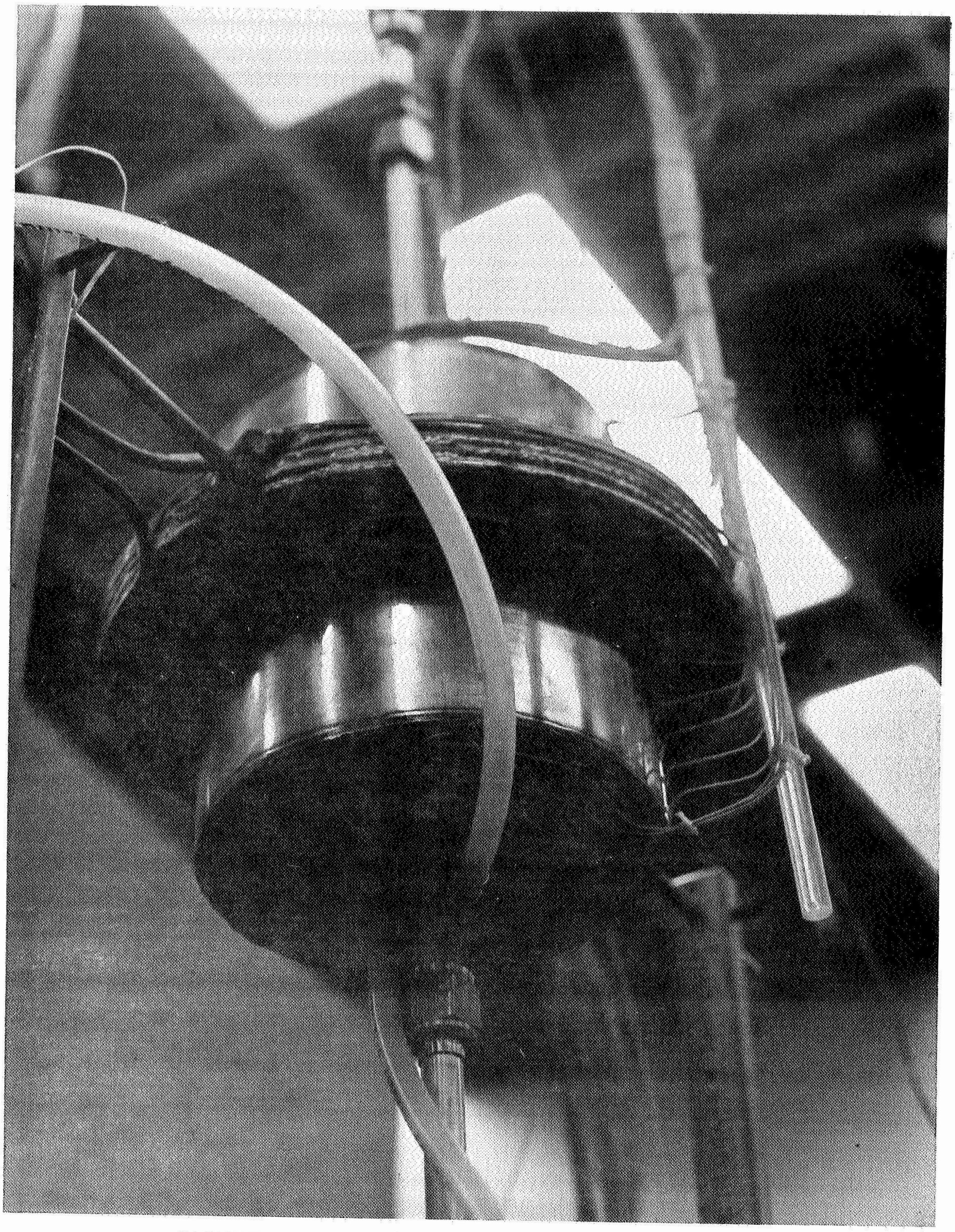

FIGURE II–26 INSTRUMENTED ¼ SCALE MODEL

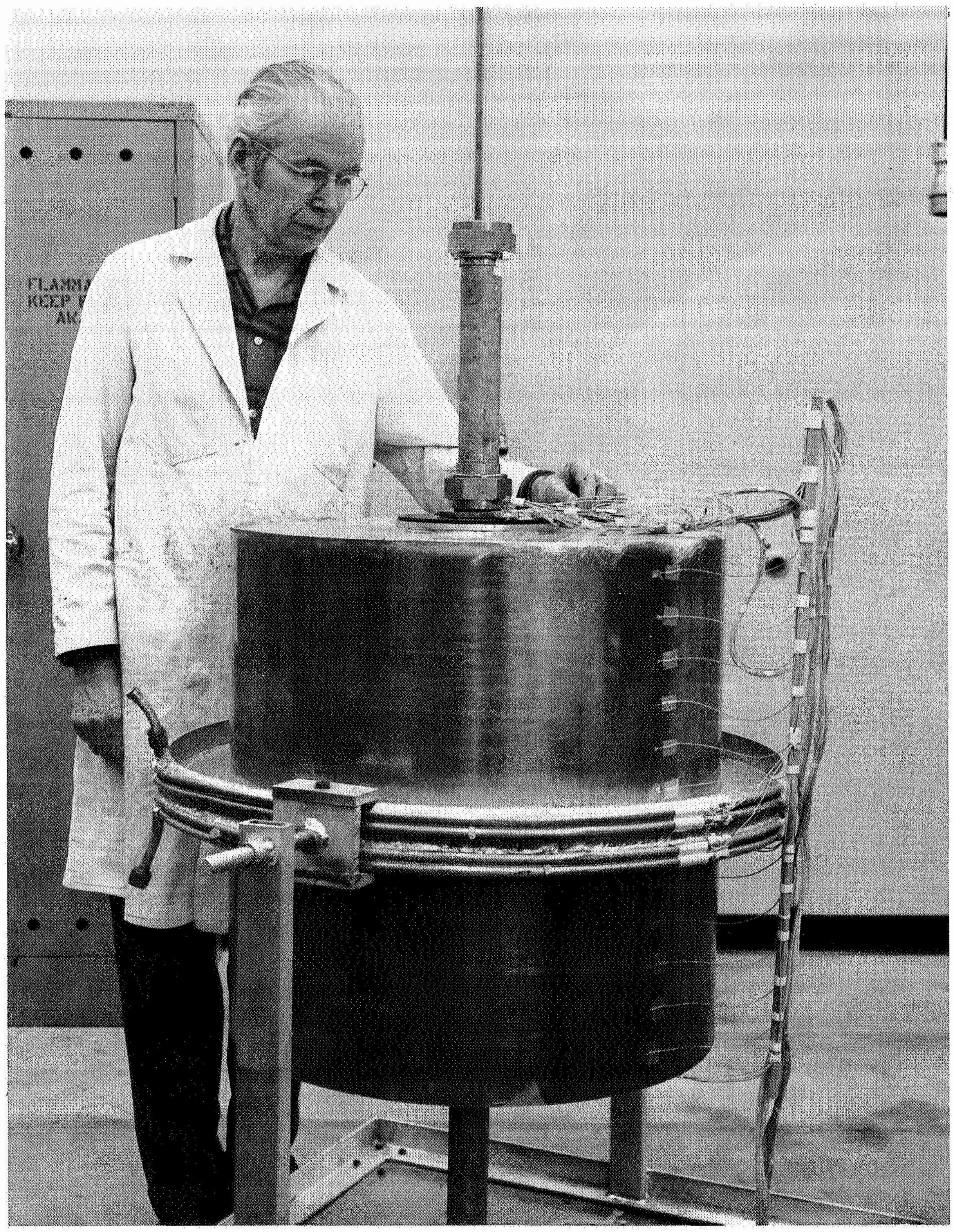

FIGURE II–27 INSTRUMENTED FULL SCALE MODEL

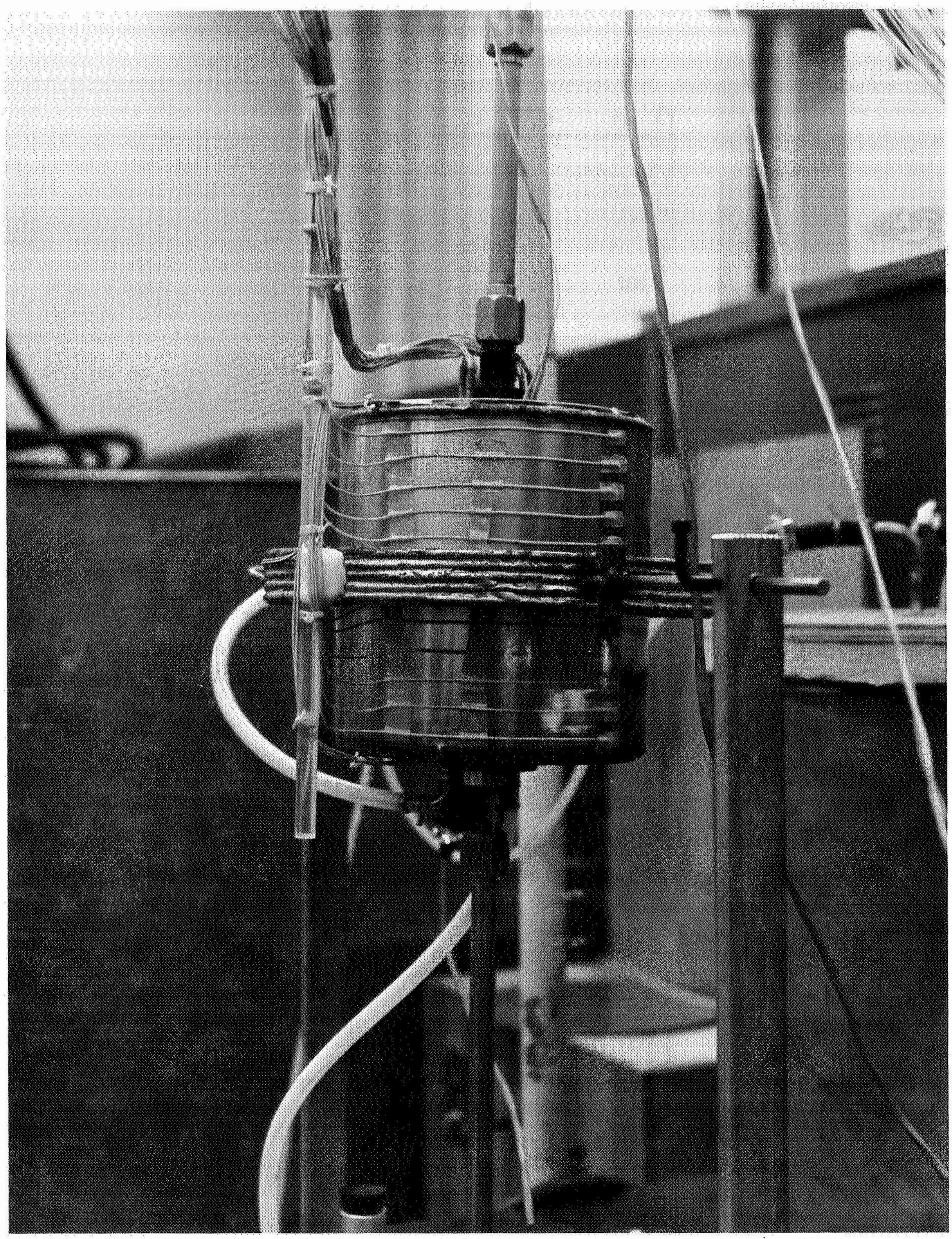

FIGURE II–28 INSTRUMENTED ¼ SCALE MODEL

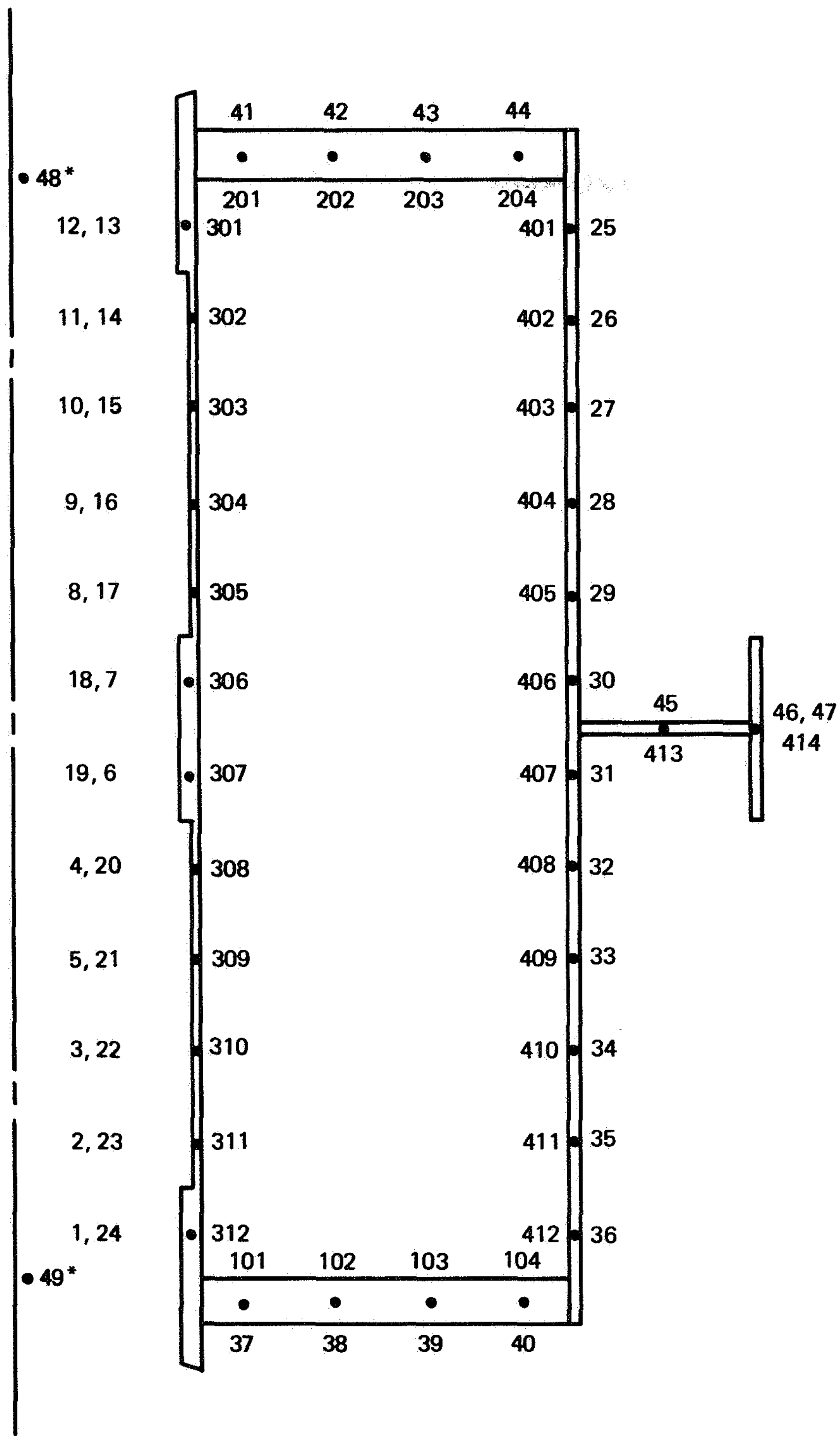

*THERMOCOUPLES INSTALLED IN AIR PASSAGE OF AIR DISTRIBUTION PLUGS

THREE DIGIT NUMBERS REFER TO TMM NODES

Figure II-29: THERMOCOUPLE NUMBERING SYSTEM FOR FULL SCALE MODEL

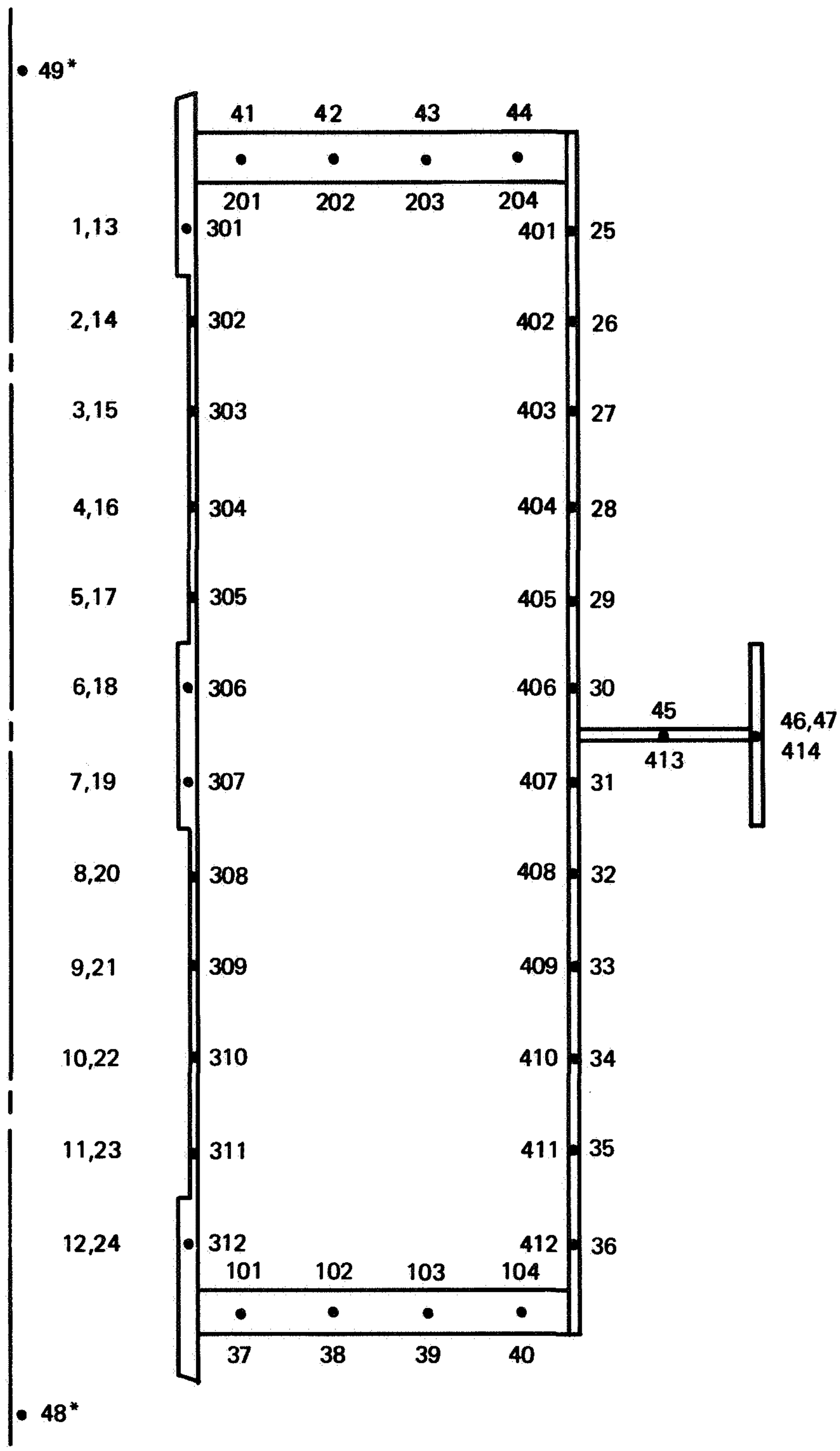

*THERMOCOUPLES INSTALLED IN AIR INLET AND OUTLET TUBES PRIOR TO FORCED CONVECTION TESTS

NOTE: THREE DIGIT NUMBERS REFER TO TMM NODES

Figure II-30: THERMOCOUPLD NUMBERING SYSTEM FOR 1/4 SCALE MODEL

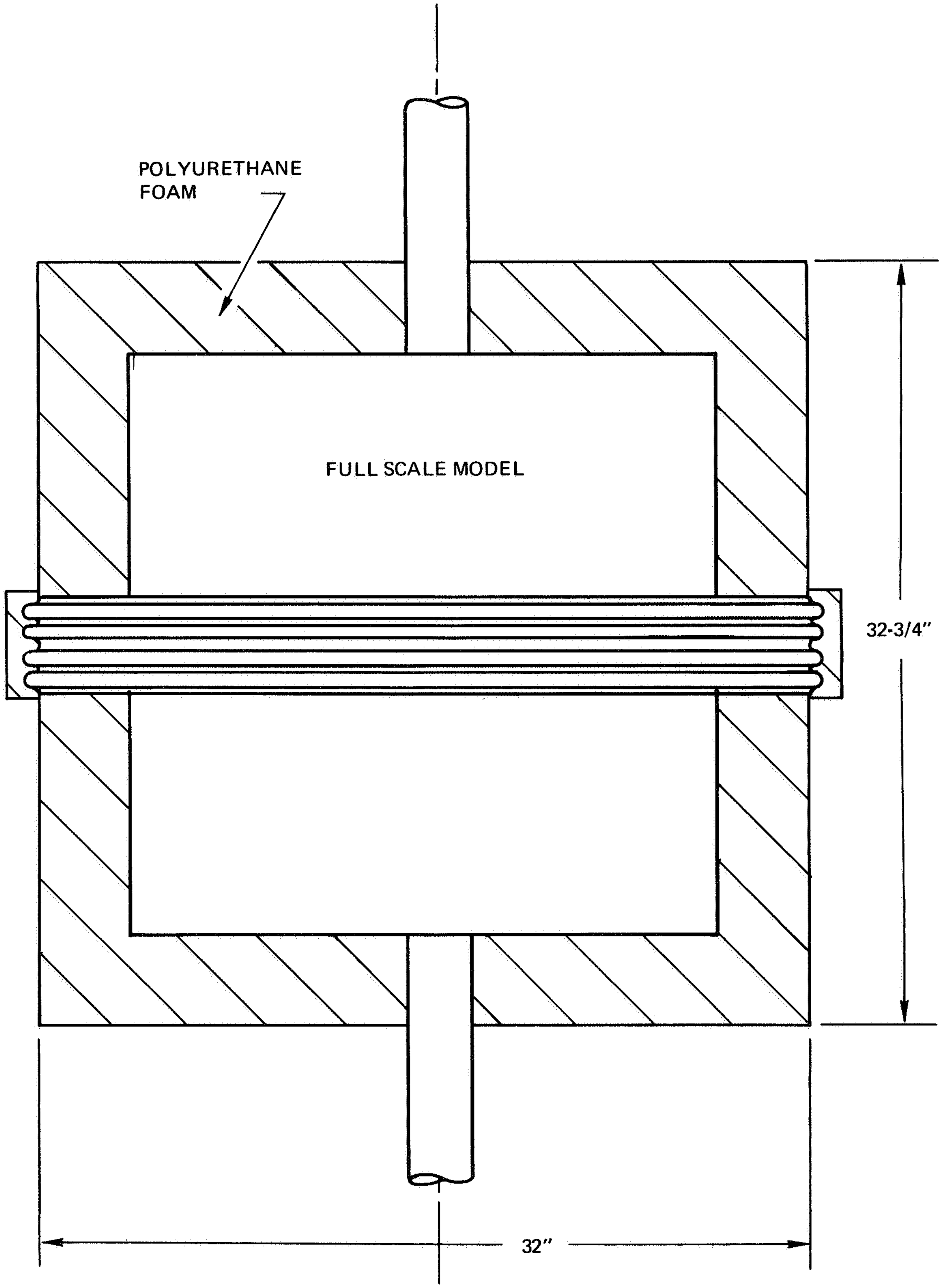

Figure II-31: FULL SCALE MODEL INSULATION

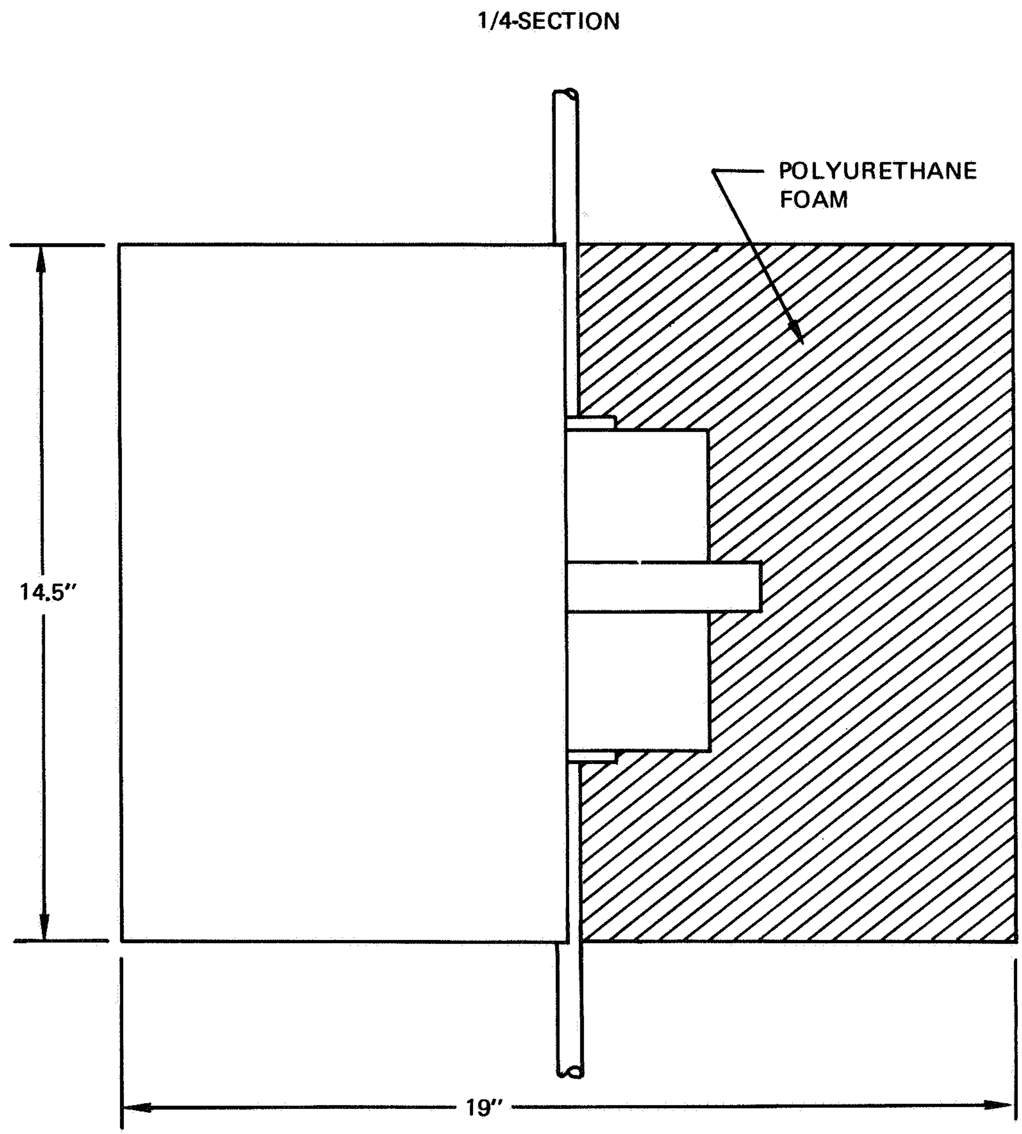

Figure II-32: 1/4 SCALE MODEL INSULATION

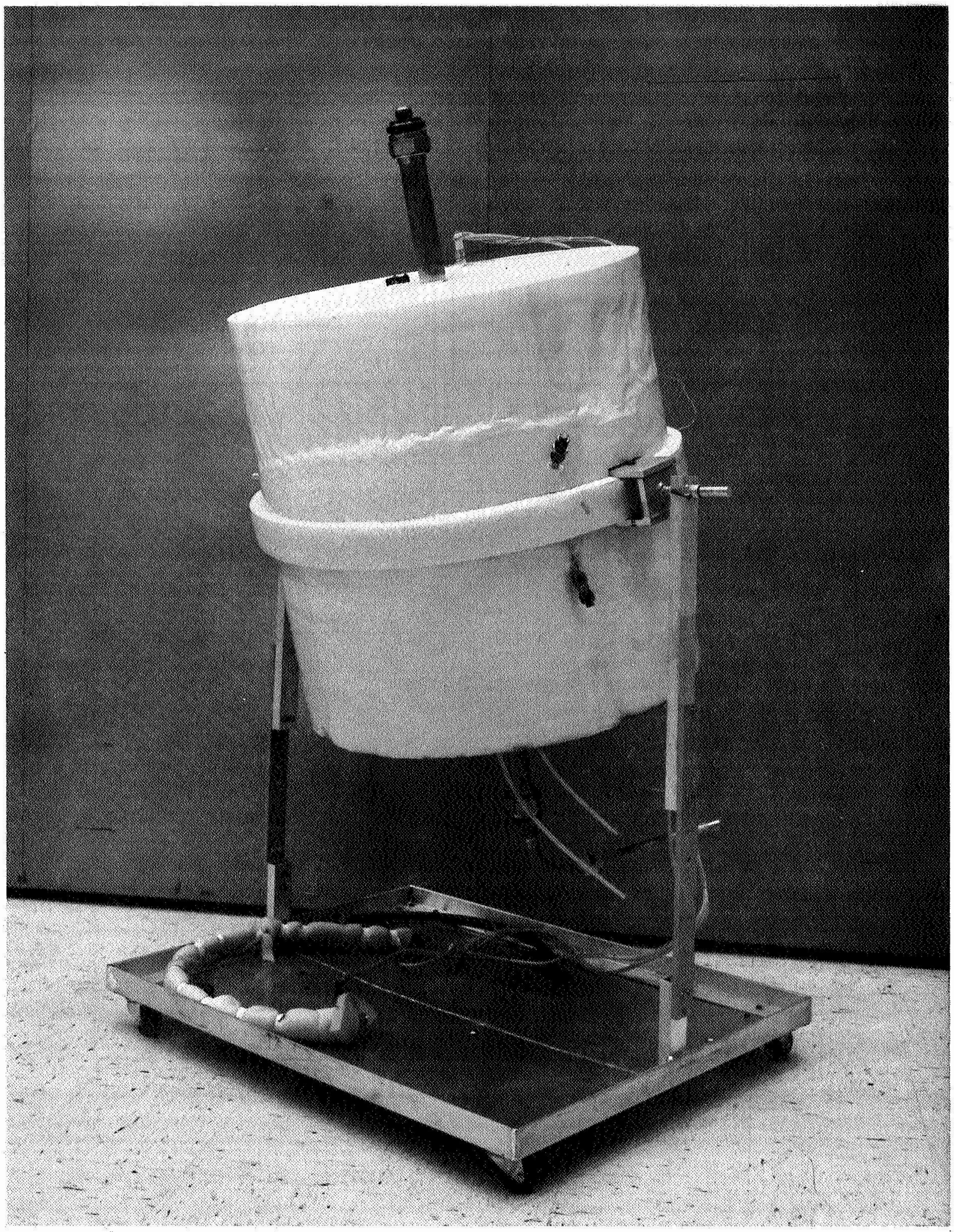

FIGURE II–33 INSULATED FULL SCALE MODEL

heating rate case with the flow direction through the model reversed to see if the flow direction has any effect on the data correlation. To minimize the number of 1/4 scale model tests the full scale model flow rates were chosen to differ by factors of four, i.e., letting w = highest flow rate, w /4 = intermediate flow rate and w /16 = lowest flow rate.

The 1/4 scale model tests consisted of radiation-conduction, free convection and forced convection tests. The purpose of radiation-conduction tests was to obtain data for upgrading the thermal math model. The free convection tests were at five heating rates corresponding to the full scale model heating rates with the heating rate scaled such that

$$Q_m = \frac{1}{16} Q_p$$

These 1/4 scale model tests were made at pressures of 1/2, 1, 2, 4 and 8 atmosheres. The heat transfer coefficient preservation scaling technique uses the 1/2 atmosphere tests to simulate the full scale model tests. This assumes that the free convection Nusselt number is proprotional to the fourth root of the Grashof number. Based on this relationship the 1/4 scale model pressure required to preserve the free convection heat transfer coefficient is

$$P_m = \frac{1}{2} P_p$$

The Nusselt number preservation scaling technique uses all of the tests to determine the Nusselt number as a function of Grashof number.

The 1/4 scale model forced convection tests were made to obtain data to be used for the Nusselt number, mass flux and heat transfer coefficient preservation scaling techniques. The forced convection Nusselt number was assumed to be given by flat plate laminar flow theory (i.e., Nusselt number proportional to the square root of the Reynolds number). Based on the relationship the 1/4 scale model mass flow rate required to preserve the heat transfer coefficient is

$$W_m = \frac{1}{64} W_p$$

The mass flow rate required for mass flux preservation is

$$W_m = \frac{1}{16} W_p$$

and that required for the Nusselt number preservation technique is

$$W_m = \frac{1}{4} W_p$$

Consequently three 1/4 scale model flow rates are required for each full scale model flow rate, however, since the full scale model flow rates differ by factors of four, only five different flow rates were required for the 1/4 scale model tests (i.e., w /4, w /14, w /64, w /128 and w /512). The heat transfer coefficient and mass flux preservation tests were made at 1/2 atmosphere pressure and at the three heating rates corresponding to the full scale tests. The Nusselt number preservation tests were generally made at pressures of 1, 2, 4, and 8 atmosphere pressure. The heating rates for these tests were not restricted to simulating the full scale model heading rates since this is not required for determining the Nusselt number as a function of Grashof number at given Reynolds numbers.

A matrix of the model test runs is given in Table II-6. These are the test runs basic to the data correlation. The runs not shown are the various preliminary and checkout tests.

II.5.6.1 1/4 Scale Model Tests

II.5.6.1.1 Preliminary Tests

Prior to insulating the 1/4 scale model with polyurethane foam a checkout was made of the test setup and model instrumentation. A photograph of the test setup is shown in Figure II-34. Figure II-35 gives a schematic of the test setup. The 1/4 scale model is mounted on top of a vacuum cart which provides the vacuum pumping facility for the model. The heater power is provided by a D.C. power supply. The thermocouple readout apparatus is the same as that used for the thermocouple calibration. The cooling for the fin is provided by water which is colled in an ice-water bath. The ice-water bath is maintained at the ice point by means of an ethylene glycol-water loop connected

TABLE II-6 TEST RUN MATRIX

MODEL	1/4 SCALE MODEL																						FULL SCALE MODEL			
TEST SERIES	RADIATION-CONDUCTION	FREE CONVECTION					FORCED CONVECTION																FREE CONVECTION	FORCED CONVECTION		
FLOW RATE	0	0					$\dot{m}_1$				$\dot{m}_2$				$\dot{m}_3$				$\frac{\dot{m}_1}{16}$	$\frac{\dot{m}_2}{16}$	$\frac{\dot{m}_3}{16}$	0	$4\dot{m}_1$	$4\dot{m}_2$	$4\dot{m}_3$
PRESSURE ATM	10^{-3}	1/2	1	2	4	8	1	2	4	8	1	2	4	8	1	2	4	8	1/2	1/2	1/2	1	1	1	1
Q_1	17	18	19																			105			
Q_2	16	21	20B	37B	38B	39																104			
Q_3	15	22	23	34	35B	36									68	69	70	67	77	85.1	82	101	108	111	112
Q_4	10	25	24	31C	32B	33					58		57		63	64	65	66	78	84	81	102	107	110	113
Q_5	14	26B	27B	28	29B	30	74	43.1 75	76		49 50	51	52	48	62	61	60	59	79	83	80	103	106	109	114
Q_6							45	44	46 46.1	47	54	55	56.1	53											
$^*Q_5$							86		87		89		88	90	95	96	94	93	97	98	99		117	116	115

*Air flow direction reversed for these tests (air flow downward).

NOMINAL VALUES

**HEATING RATE WATTS	FLOW RATE LB/MIN
$Q_1 = 5.82$	$\dot{m}_1 = 1.25$
$Q_2 = 8.75$	$\dot{m}_2 = 0.290$
$Q_3 = 11.70$	$\dot{m}_3 = 0.075$
$Q_4 = 14.0$	
$Q_5 = 18.2$	
$Q_6 = 28.0$	

**Heating rate given for 1/4 scale model. Heating rate for full scale model is 16 times the values given.

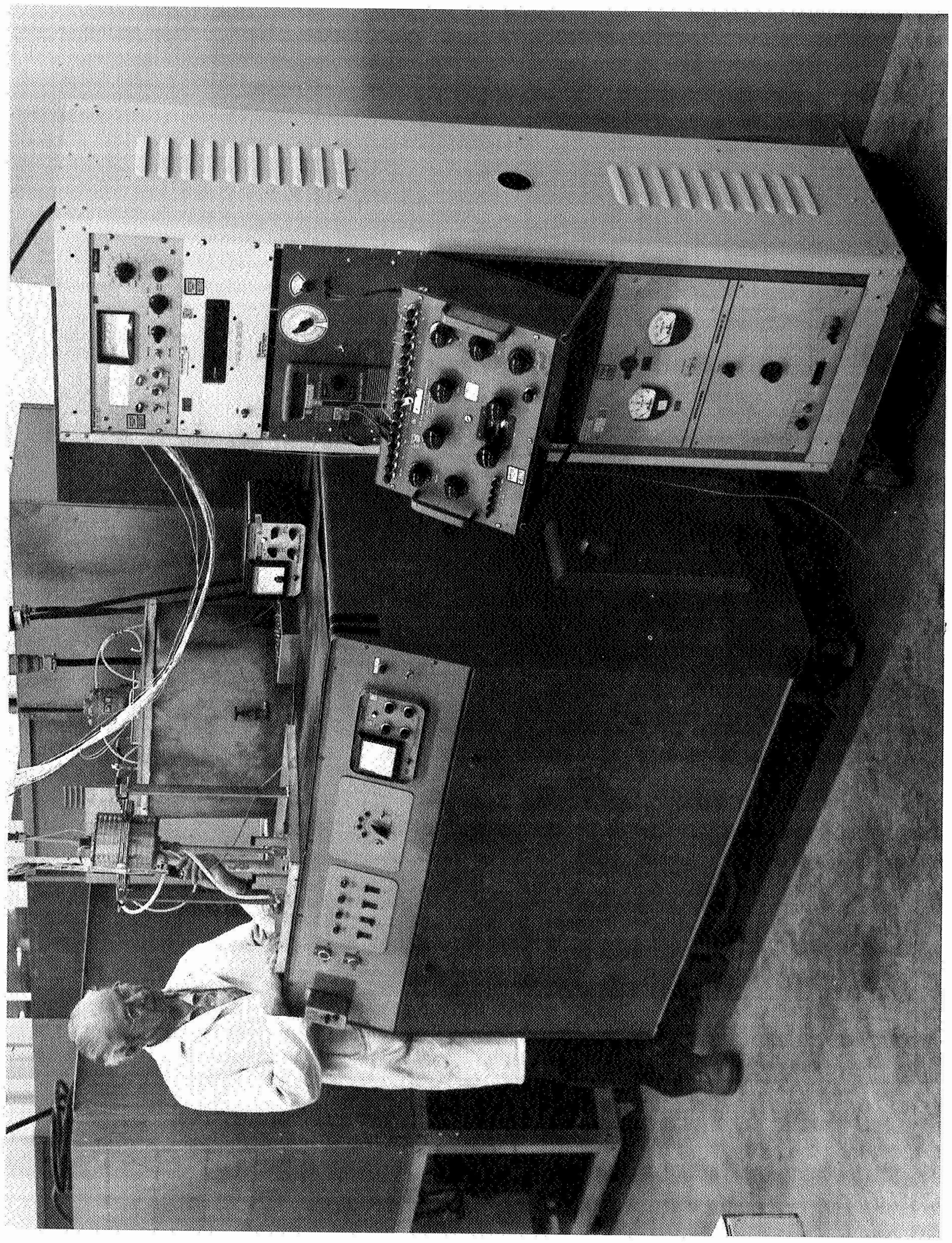

FIGURE II–34 ¼ SCALE MODEL PRELIMINARY TEST SETUP

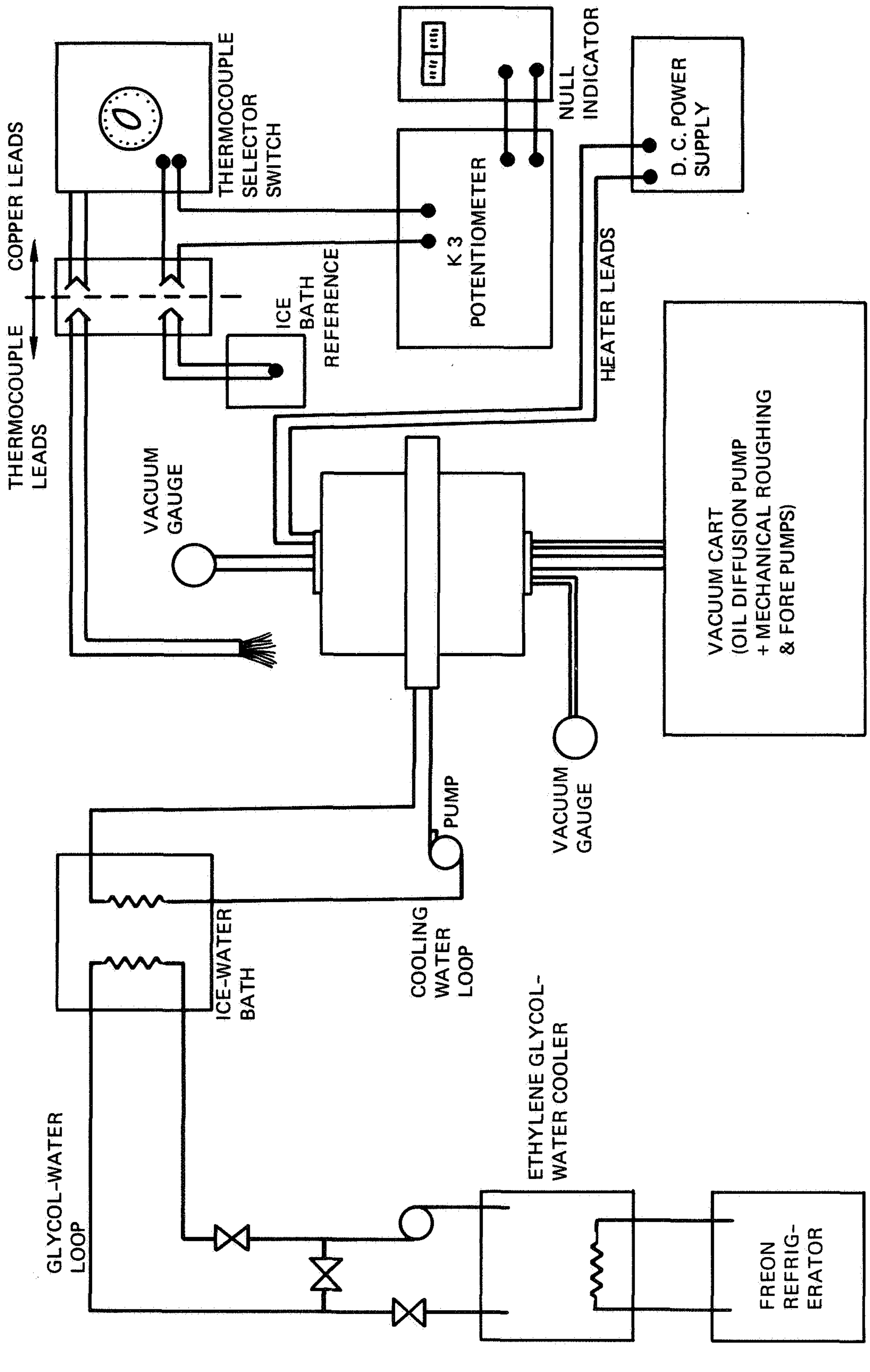

Figure II-35: PRELIMINARY TEST SETUP SCHEMATIC to a Freon refrigerator. Figure II-36 shows another view of the test setup with the full size model along side the 1/4 scale model to give a direct size comparison.

In order to checkout the test setup and model instrumentation, the 1/4 scale model was temporarily insulated with approximately one inch thickness of foam rubber, and preliminary tests were made with the vacuum system, cooling system and the heater turned on. These preliminary tests resulted in the following observations:

- The outgassing of the paint in the annular region between the inner and outer cylinders slows the pump out of this region.

- The cooling system is adequate to maintain the fin temperature at a constant value between 33 and 34°F.

- Thermocouple numbers 14, 18 and 24 not giving any reading. Thermocouple number 12 reading erroneously. All other thermocouples give repeatable readings with the differences between adjacent thermocouples repeatable to within about 1 microvolt ($\approx$0.03°F). The heater section thermocouples show some discrepancies. Thermocouple number 6 is apparently reading correctly, however, numbers 7 and 19 appear to be reading a temperature away from the cylinder wall and closer to the heater core.

- The copper vacuum lines on one of the air distribution plugs provide a significant heat leak path and need to be shortened.

After these preliminary tests the air distribution plug containing the copper vacuum lines was removed and the tubes were shortened. With the air distribution plug removed an inspection of thermocouple numbers 12 and 24 revealed nothing abnormal with 12, however, 24 was broken near the junction (the junction was repaired and the thermocouple reinstalled).

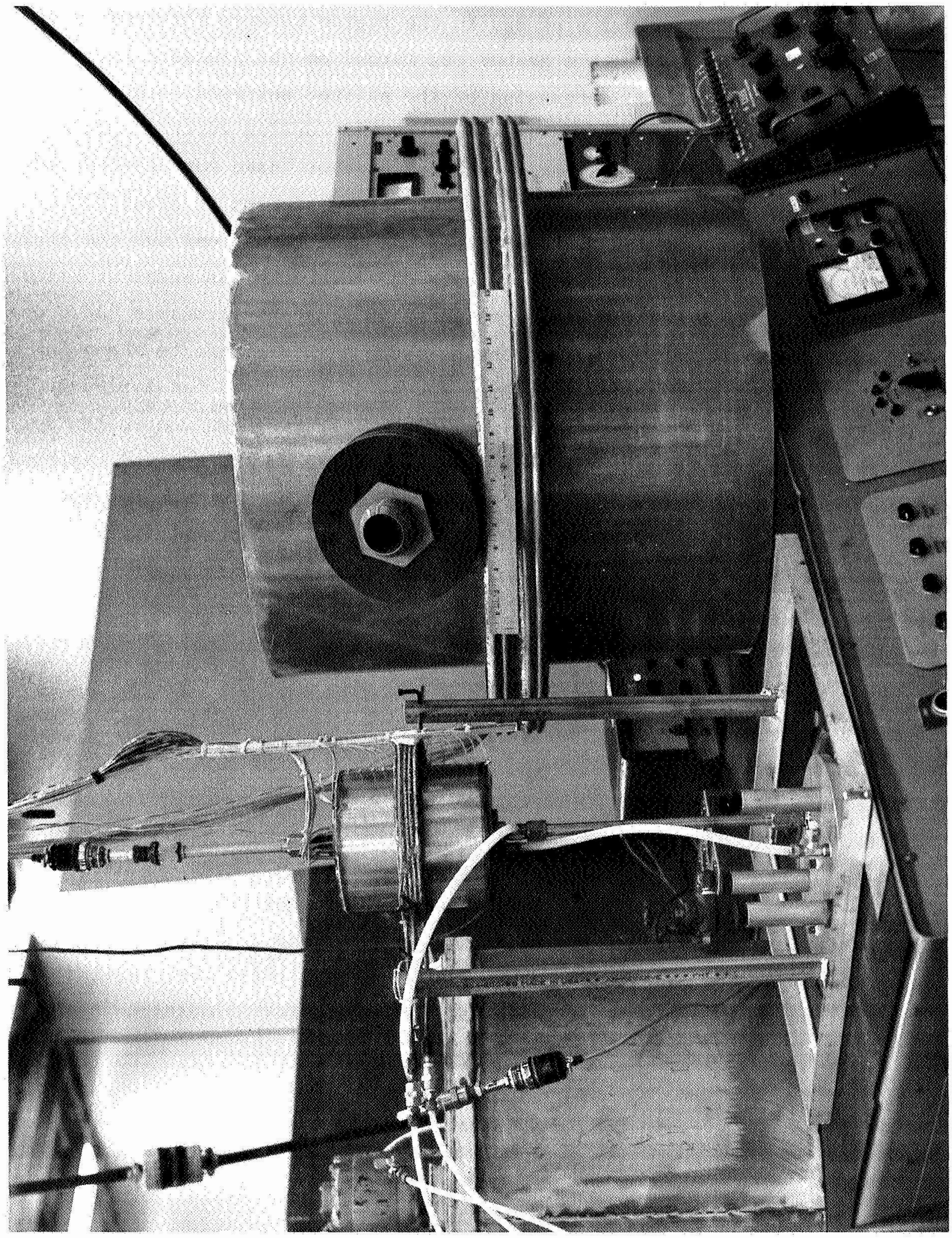

FIGURE II–36 FULL SCALE AND ¼ SCALE MODELS

After insulating the model with polyurethane foam (as shown in Figure II-32) it was re-installed in the test set up. The vacuum system was turned on and the model evacuated to about 0.2 μ of Hg. in the region between the inner and outer cylinders. However, when the heater was turned on the pressure increased to about 1 μ of Hg. due to the outgassing of the painted surfaces. In order to reduce the outgassing the heater was left on with the cooling water off in an attempt to "bake out" the system. After several days of "bake out" the pressure appeared to stabilize at 0.85 μ of Hg. with the heater section at about 200°F and the outer wall at about 150°F. The heater was then turned off and the cooling water turned on to find the minimum attainable pressure with the model at below room temperature. The model had cooled to about 45°F and the pressure had dropped to 0.3 μ of Hg. when a leak opened and the pressure abruptly rose to about 5 μ of Hg. Since all attempts at achieving a high vacuum in the model had failed it became necessary to run the tests under conditions where the gas conduction is significant. This meant that the effect of gas pressure on the thermal response of the model had to be determined. The pressure must be high enough for the gas heat conduction mechanism to be described by the thermal conductivity of the gas (as opposed to molecular or slip flow considerations); however, the pressure must also be low enough to eliminate any free convection effects. Also the increased pressure in the model necessitated expansion of the thermal math model to account for the gaseous condition process.

II.5.6.1.2 Initial Test Series

The initial test series consisted of 17 runs including five runs made during the "bake out" of the system. These runs during the system "bake out" were primarily made to monitor the model temperatures and to checkout the repeatability of the measurements. The remaining runs were made to determine the pressure effects on the model temperatures and to generate the data required for upgrading the thermal math model. Table II-7 gives the test conditions for these runs.

The power input was determined by measuring the voltage and current (by means of a calibrated shunt) with a null volt meter. The D.C. power supply regulated

TABLE II-7 INITIAL TEST SERIES

Run No.	Date	Time	Pressure Inner Cylinder	Pressure Outer Cylinder	Power Input Voltage	Power Input **Current	Power Input Watts	Cooling Water
1	10/4/69	-	4 μ	0.44 μ	15.3	-		Off
2	10/6/69	-	16 μ	0.9 μ	24.0	-		
3	10/6/69	1400	28 μ	0.85 μ	24.14	-		
4	10/6/69	1700	28 μ	0.85 μ	24.10	-		Off
5	10/8/69	1700	8 μ	6.0 μ	0	0	0	On
6	10/10/69	1800	24 μ	5.0 μ	42.60	.3260	13.87	
7	10/14/69	1130	1 mm	1 mm	42.63	.3272	13.93	
8	10/15/69	1100	2 mm	2 mm	42.66	.3275	13.96	
9	10/15/69	2230	1 ATM	1 ATM	42.70	.3283	14.00	
*10	10/16/69	1500	1 ATM	2 mm	42.64	.3277	13.96	
11	10/17/69	1630	1 mm	1 mm	48.87	.3742	18.27	
12	10/21/69	-	1 ATM	1 ATM	48.85	.3749	18.30	
13	10/22/69	1630	Cooling Water Problems					
*14	10/24/69	1400	1 ATM	1 mm	48.85	.3746	18.28	
*15	10/27/69	1800	1 ATM	1 mm	39.00	.2999	11.68	
*16	10/28/69	1800	1 ATM	750 μ	33.685	.2595	8.733	
*17	10/29/69	1730	1 ATM	900 μ	27.43	.2117	5.801	On

* Runs used for upgrading thermal math model

** Voltage read across 1.001 OHM shunt resistor the voltage to within about ± 0.01 volts. The pressure was controlled by throttling the flow to the vacuum system and bleeding in air between the model and the throttling valve. Generally, several sets of data were taken to establish that steady state conditions had been achieved, however only one run number was recorded. The stability and repeatability of the experimental conditions proved to be excellent. After taking a set of data the thermocouple output that was measured first was remeasured and if it had changed more than 1 μ volt (0.03°F) the test run was continued and another set of data taken at a later time. The following table gives the maximum temperature change and time elapsed between the last two sets of data taken for the runs.

Run No.	Elapsed Time (hours)	Maximum Temperature Change μVolts
1-6	Not available	8.0
7	3.0	8.0
8	19.0	7.0
9	7.0	42.0
10	6.0	5.0
11-13	Not available	
14	5.0	5.0
15	4.0	15.0
16	4.5	7.0
17	3.5	4.0

Runs 6-14 were made to determine the effect of gas pressure on the thermal response of the model. Runs 6-10 were made at one heating rate and 11-14 at a different heating rate. Run 6 was made at the lowest pressure that could be attained in the model. After taking the data for this run, the pressure in both the inner and outer cylinders was slowly increased while the temperature at the heater section (TC 6) was monitored. It was expected that as the pressure increased and the heat transfer mechanism for the gas changed from the molecular or slip flow process to the continuum process, the heater section temperature would decrease because of the increased conductive losses. Figure II-37 shows the unexpected results of this test. Instead of decreasing, the temperature increased for about 20 minutes before it began to drop. This indicates that the thermal conductance between the heater core and the cylinder wall is a strong function of pressure (as would be the case if a gap existed between the heater and the wall). At the lower pressure the thermal conductance

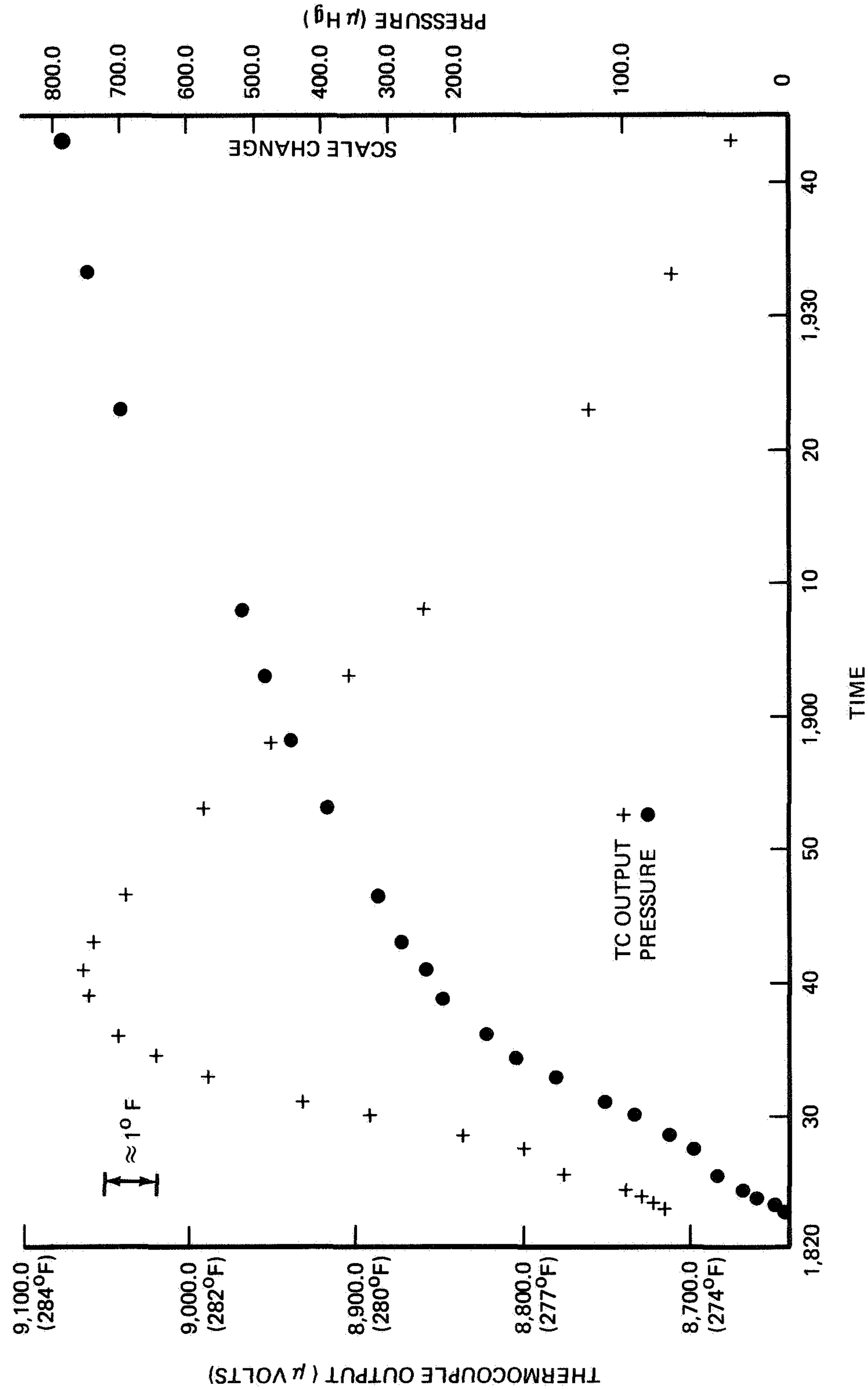

Figure II-37: TRANSIENT RESPONSE OF HEATER SECTION DUE TO CHANGING GAS PRESSURE is small and the temperature of the heater core is considerably higher than the equilibrium wall temperature and as the pressure (and thermal conductance) is increased the excess thermal energy stored in the heater core is transferred to the wall giving an increase in wall temperature while this excess heat is being dissipated.

Figure II-38 shows the temperature distribution for runs 6-10. These data show the effect of gas pressure on the thermal response of the model. The following observations can be made of the data.

- Free convection effects are readily apparent in run 9 where the outer cylinder was at atmospheric pressure.

- The data for runs 7, 8 and 10 group together with the exception of TCs 7 and 19.

- The low pressure case (run 6) shows a significant difference from runs 7, 8 and 10.

Figure II-39 shows the temperature differences between runs 6, 7, and 8 and run 10. The temperature for run 6 is significantly higher for the inner cylinder and is somewhat lower for the outer cylinder. This indicates that there is less heat transfer by gas conduction and the pressure (5 μ of Hg.) is low enough for the gas conduction to take place by molecular or slip flow phenomena. The temperature for runs 7 and 8 are slightly higher at the heater section and slightly lower for the rest of the model than those for run 10. The difference in temperatures for the inner cylinder can be explained by the higher gas pressure in the inner cylinder for run 10. This higher pressure gives increased thermal conductance through the microquartz insulation in the inner cylinder and lowers the heater section temperature while increasing the temperature in the surrounding regions. The generally lower temperatures for runs 7 and 8 might be explained by a combination of the increased heat leak from the heater section through the heater leads, the very slightly larger heat input for run 10, the differences in the ambient temperature and the differences in cooling water temperature. For purposes of upgrading the radiation-conduction aspects of the thermal math model, the temperature gradients are of greater importance

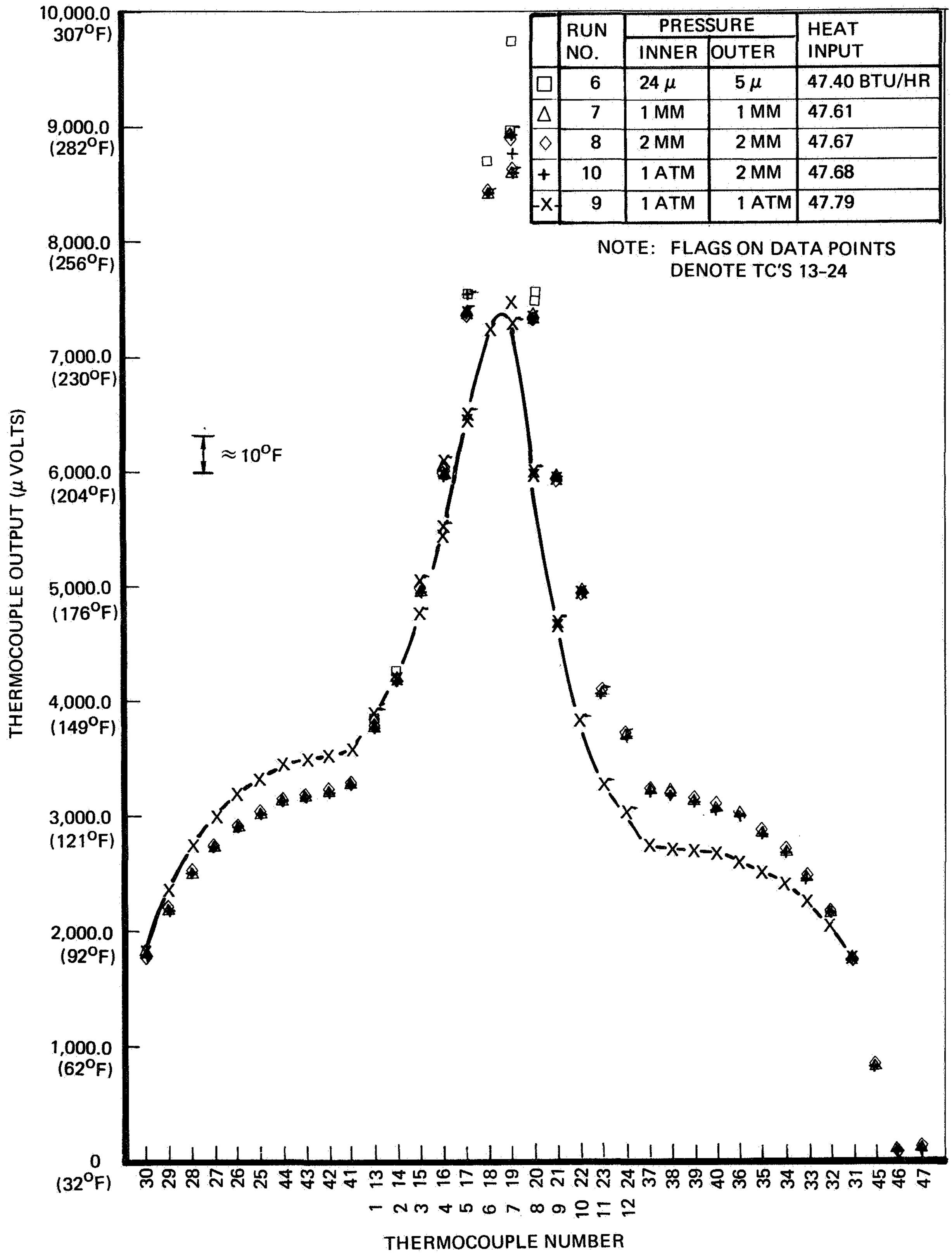

Figure II-38: EFFECT OF GAS PRESSURE ON THERMAL RESPONSE OF 1/4 SCALE MODEL

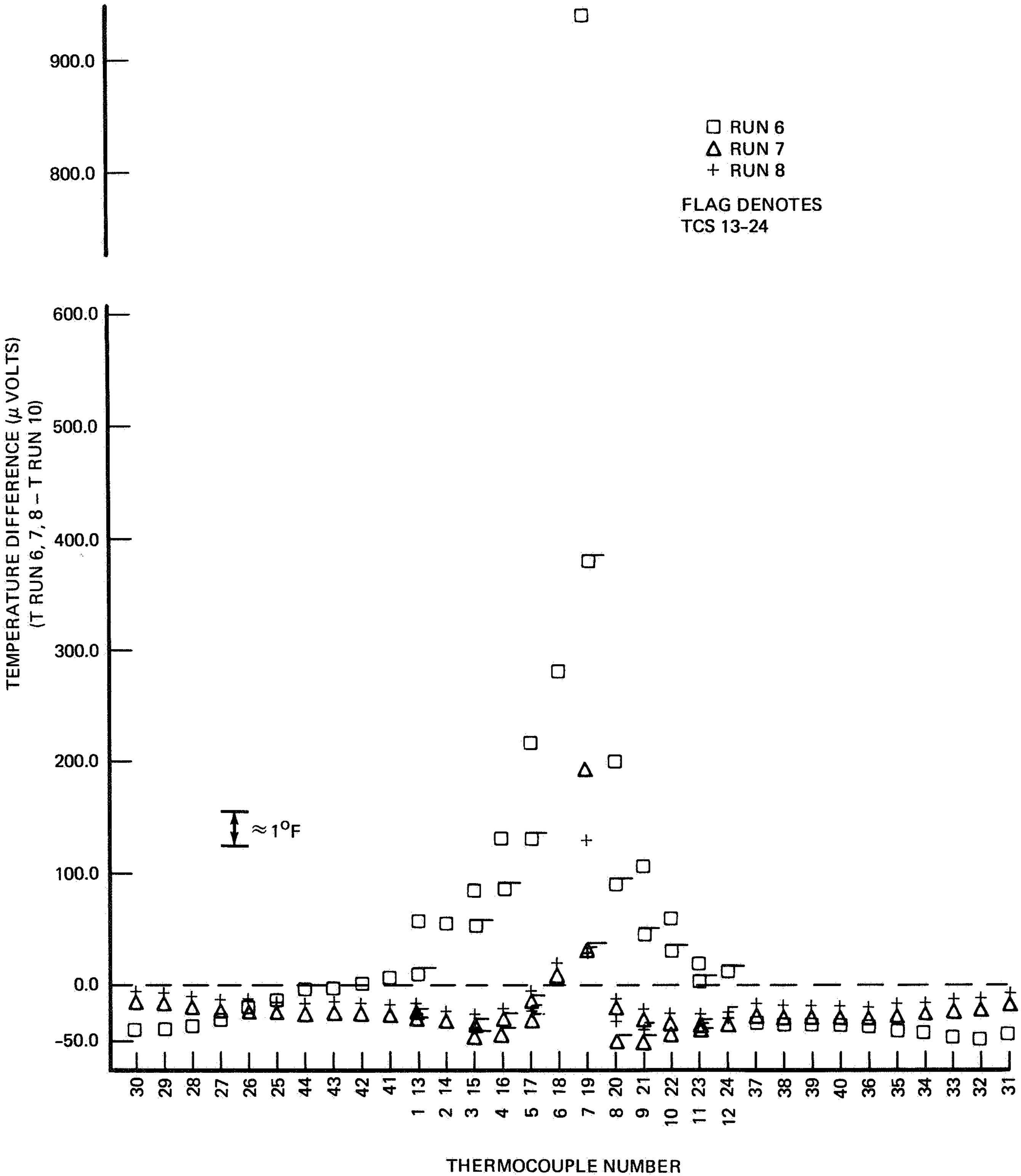

Figure II-39: TEMPERATURE DIFFERENCES BETWEEN RUNS 6, 7 & 8 VS RUN 10 than the absolute values of the temperature. Table II-8 gives a comparison of the temperature gradients for runs 6, 7, 8 and 10. With the exception of the gradients that involve TCs 7 and 19, the agreement is quite good. It should be noted that the thermocouple outputs were measured to the nearest microvolt, except for TCs 37-44 where the temperature gradients are small. The outputs for these TCs were measured and read to the nearest 0.1 microvolts with an approximate accuracy of ± 0.1 microvolts.

The results of runs 6-10 show that a pressure in the outer cylinder region on the order of 1 mm of Hg. will result in gaseous heat transfer by thermal conduction. The results also show the temperature distribution for the inner cylinder to be dependent to some extent on the pressure inside the inner cylinder.

Runs 11-14 were made at an increased heating rate over runs 6-10 and represent a further investigation of the pressure effects. Run 11 was made at a pressure of 1 mm of Hg. in both inner and outer cylinders and run 14 was made at a pressure of 1 mm of Hg. in the outer cylinder and at atmospheric pressure in the inner cylinder. The temperature comparision between runs 11 and 14 is very similar to that between runs 7 and 8 and run 10. Run 12 was made with both inner and outer cylinders at atmospheric pressure. The free convection effects were easily seen in this run. Run 13 was an attempt to run with the inner cylinder evacuated to about 1 mm of Hg. while the outer cylinder was at atmospheric pressure, however, the small pumping line to the inner cylinder and a leak between the inner and outer cylinders limited the pressure to about 3-5 mm of Hg. Aside from the pump down problems, refrigerator problems during this run gave rise to variations in the inlet cooling water temperature of about 1°F which invalidated the data taken.

Since it was apparent that a reduced pressure could not be maintained in the inner cylinder for the cases to be run with the outer cylinder pressurized, it was decided to run the radiation-conduction test series with atmospheric pressure in the inner cylinder while maintaining a pressure about 1 mm of Hg. in the outer cylinder. Runs 10 and 14 constitute part of this test series and runs 15-17 make up the rest of the test series.

TABLE II-8

TEMPERATURE GRADIENT COMPARISON

THERMOCOUPLES	TEMPERATURE GRADIENT (μ volts)*			
	Run 6	Run 7	Run 8	Run 10
1-2	391.	385.	388.	393.
13-14	TC # 14 NOT READING			
2-3	841.	782.	784.	785.
14-15	TC # 14 NOT READING			
3-4	1057.	1012.	1013.	1010.
15-16	1041.	1010.	1011.	1007.
4-5	1445.	1376.	1373.	1359.
16-17	1415.	1381.	1384.	1371.
5-6	1140	1097	1098.	1083.
17-18	TC # 18 NOT READING			
6-7	1025	516	447.	329.
18-19	TC # 18 NOT READING			
7-8	2197.	1631.	1563.	1420.
19-20	1524.	1312.	1290.	1230.
8-9	1480.	1401.	1399.	1388.
20-21	1455.	1416.	1420.	1417.
9-10	1072.	1026.	1027.	1022.
21-22	1044.	1022	1025	1027.
10-11	840.	802.	801.	801.
22-23	834.	805.	808.	809.
11-12	TC # 12 READS ERRONEOUSLY			
23-24	373.	374	376.	381.
25-26	143.	135.	135.	138.
26-27	228.	220.	220.	223.
27-28	228.	220.	220.	223.
28-29	323.	317.	317.	319.
29-30	443.	441.	442.	445.
30-31	5.	8.	7.	9.
31-32	425.	427.	428.	431.

* 35 μv $\approx$ 1°F

TABLE II-8 (CONT.)

THERMOCOUPLES	TEMPERATURE GRADIENT (μ volts)			
	Run 6	Run 7	Run 8	Run 10
32-33	321.	318.	319.	320.
33-34	226.	222.	221.	224.
34-35	168.	164.	165.	165.
35-36	120.	128.	129.	130.
37-38	46.	45.6	46.0	46.5
38-39	34.	34.6	34.5	34.3
39-40	28.	27.2	26.9	27.2
41-42	64.	59.5	58.5	59.1
42-43	45.	41.2	41.0	41.1
43-44	32.	30.4	30.6	30.8
45-46,47	778.	787.	790.	794.

As a point of interest, the systematic variation of the temperature around the inner cylinder is shown in Figure II-40 for various pressures and in Figure II-41 for various power inputs. The difference in temperature from one side of the inner cylinder to the other is larger than expected. An adequate explanation of these differences has not been developed, however, they appear to be connected to the heater installation and the heater lead routing. The most perplexing phenomena is the reversal of the temperature differences for the low pressure cases (run 6 in the data presented, runs 1 and 2 also show this reversal). The effect of power input is much greater for the end of the inner cylinder (TCs 1-6 and 13-18) through which the heater leads are routed than for the other end. The effect of these anomalies will be minimized by using an average temperature in the upgrading of the thermal math model.

II.5.6.1.3 Free Convection Test Series

After completing the initial test series the 1/4 scale model was set up for the free convection test series. The test setup for these runs is shown in Figure II-42. The test setup was changed between the 1/2 and 1 atmosphere pressure runs and the 2, 4 and 8 atmosphere pressure runs. A photograph of the free convection test set up is shown in Figure II-43.

Some difficulty was encountered in running the 1/2 atmosphere pressure cases. The pressure was set by adjusting the bleed and throttling valves shown in Figure II-42. The pressure was very sensitive to small adjustments of these values. After setting the valves to obtain the proper pressure the system was allowed to come to thermal equilibrium, however; during the time between setting the valves and taking the data the pressure would change slightly.

During the first attempt to run at 8 atmospheres an air leak between the inner and outer cylinder was discovered. The 8 atmosphere pressure probably increased the size of a small leak between the two regions. In order to continue the tests of the model a bracket was constructed to retain the air distribution plugs in the inner cylinder and the inner cylinder was pressurized to the same pressure as the outer cylinder. This support bracket may be seen in Figure II-43. After

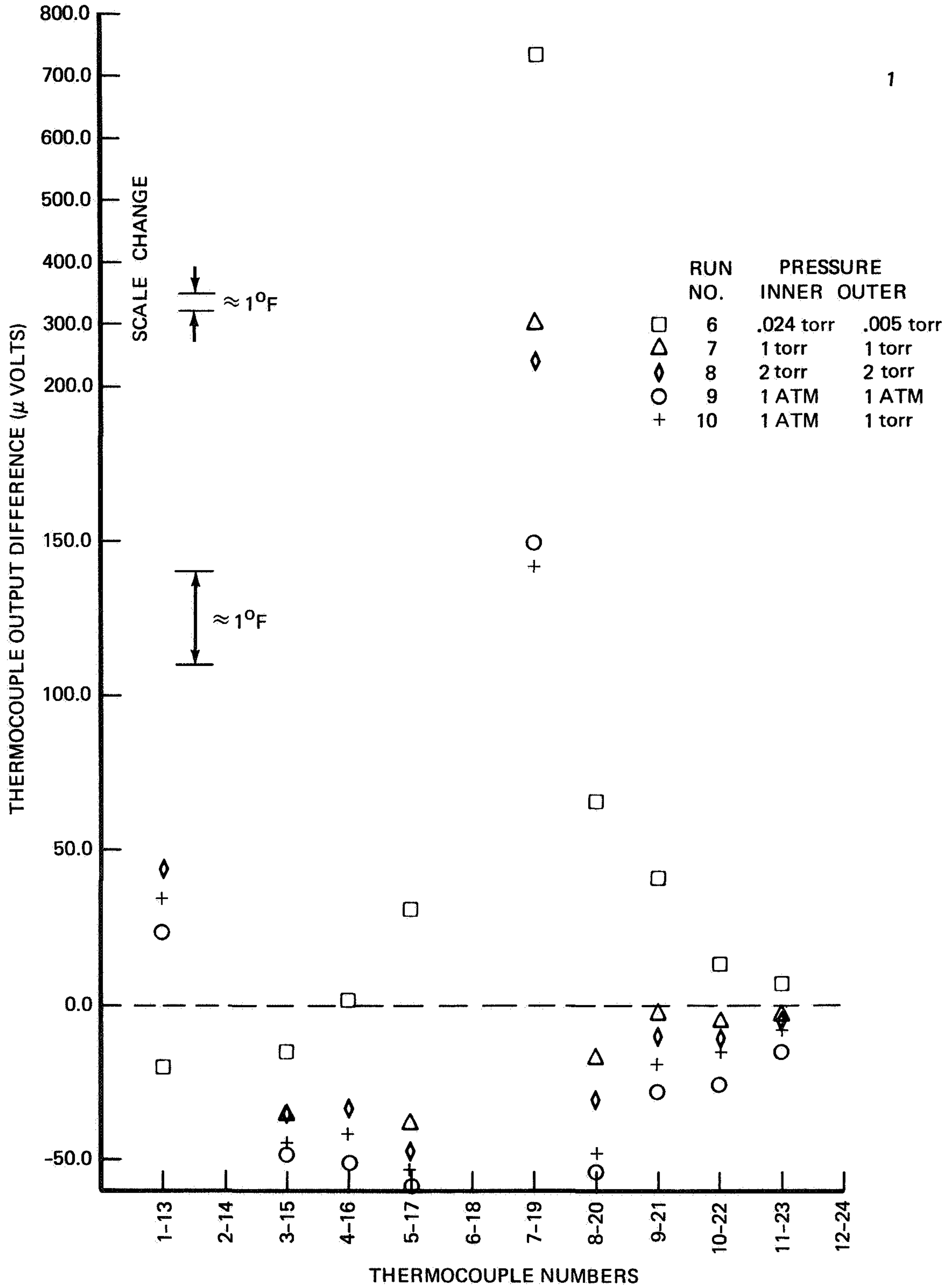

Figure II-40: *TEMPERATURE DIFFERENCE ACROSS INNER CYLINDER FOR VARIOUS PRESSURES*

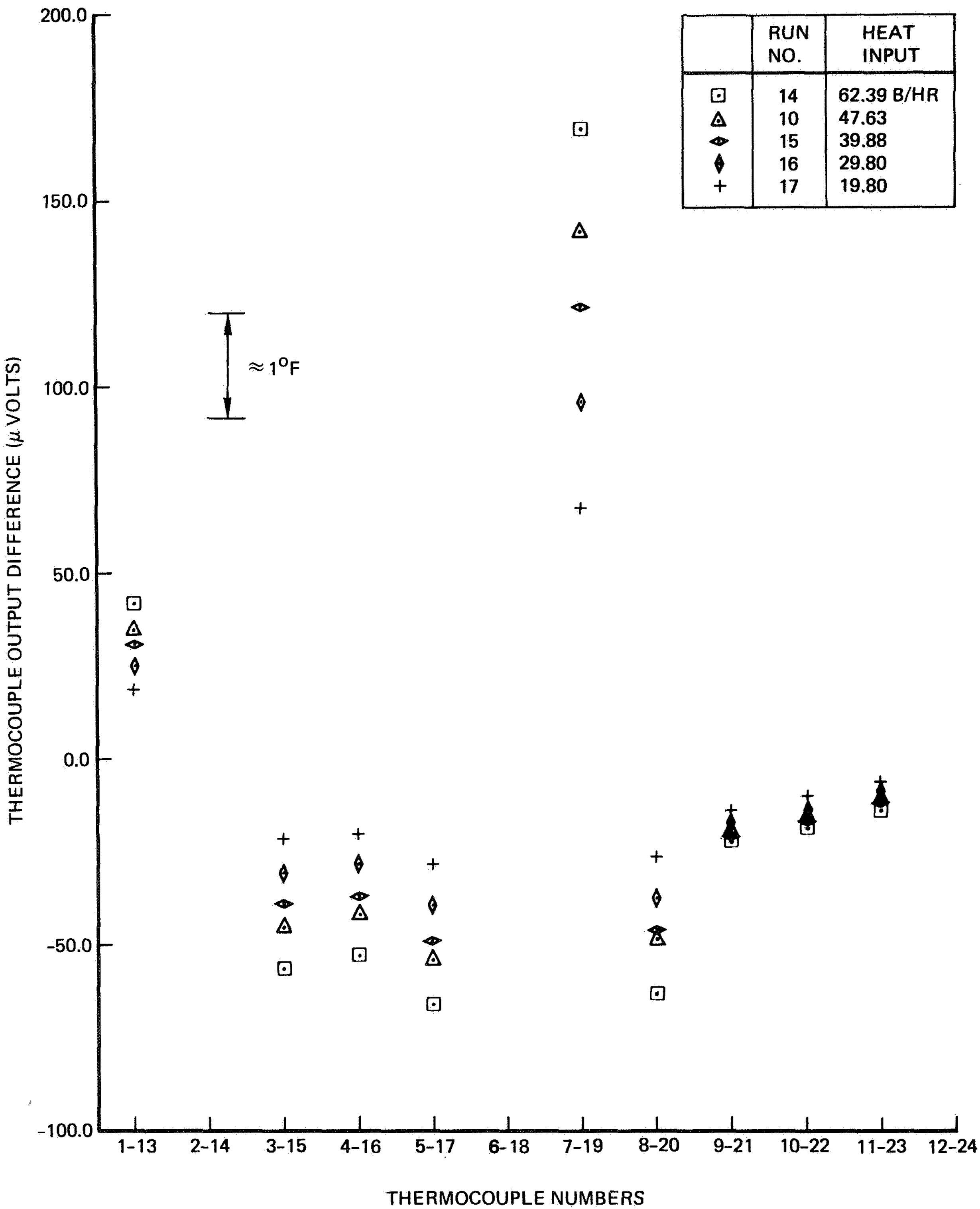

Figure II-41: TEMPERATURE DIFFERENCE ACROSS INNER CYLINDER FOR VARIOUS HEATING RATES

1/2 & 1 ATM CASES

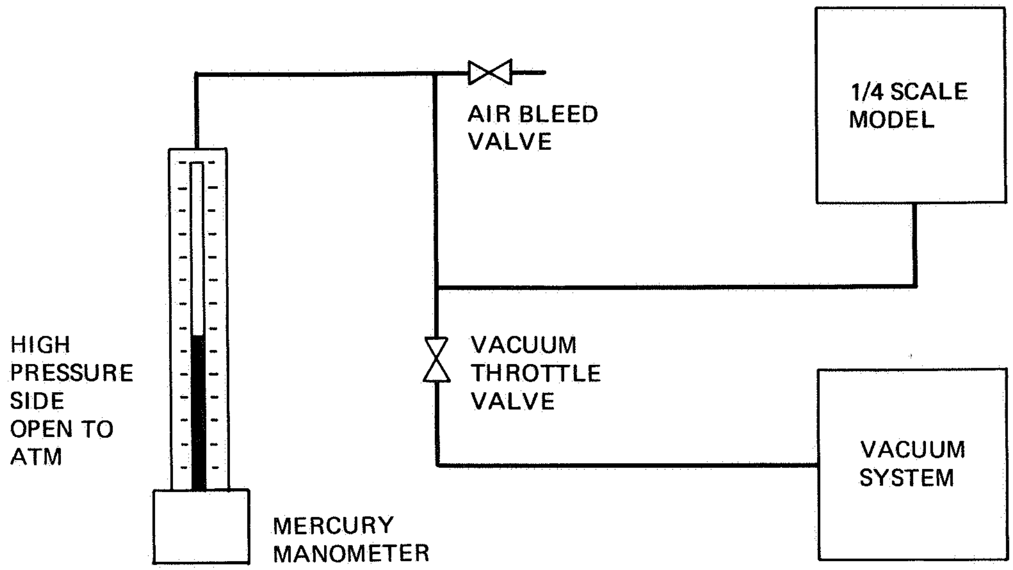

2, 4 & 8 ATM CASES

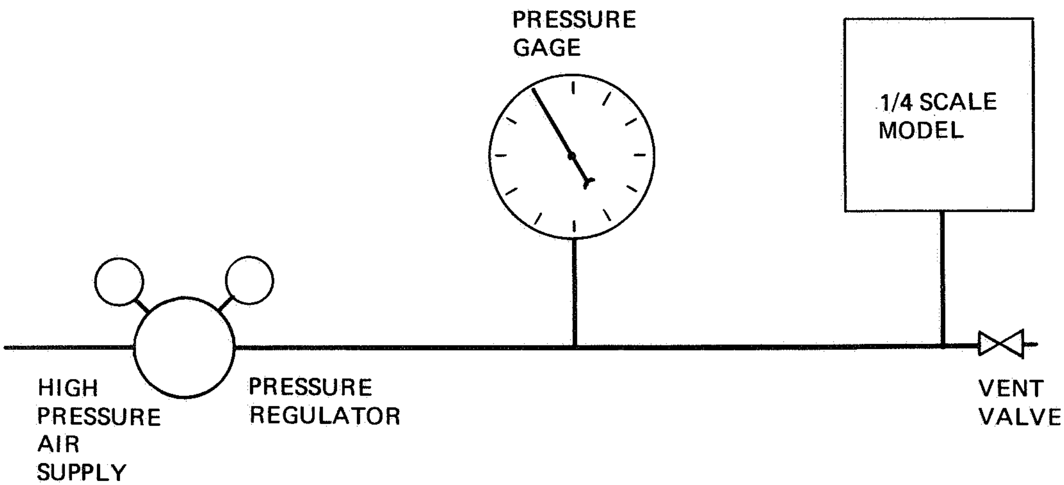

Figure II-42: 1/4 SCALE MODEL FREE CONVECTION TEST SETUP SCHEMATIC

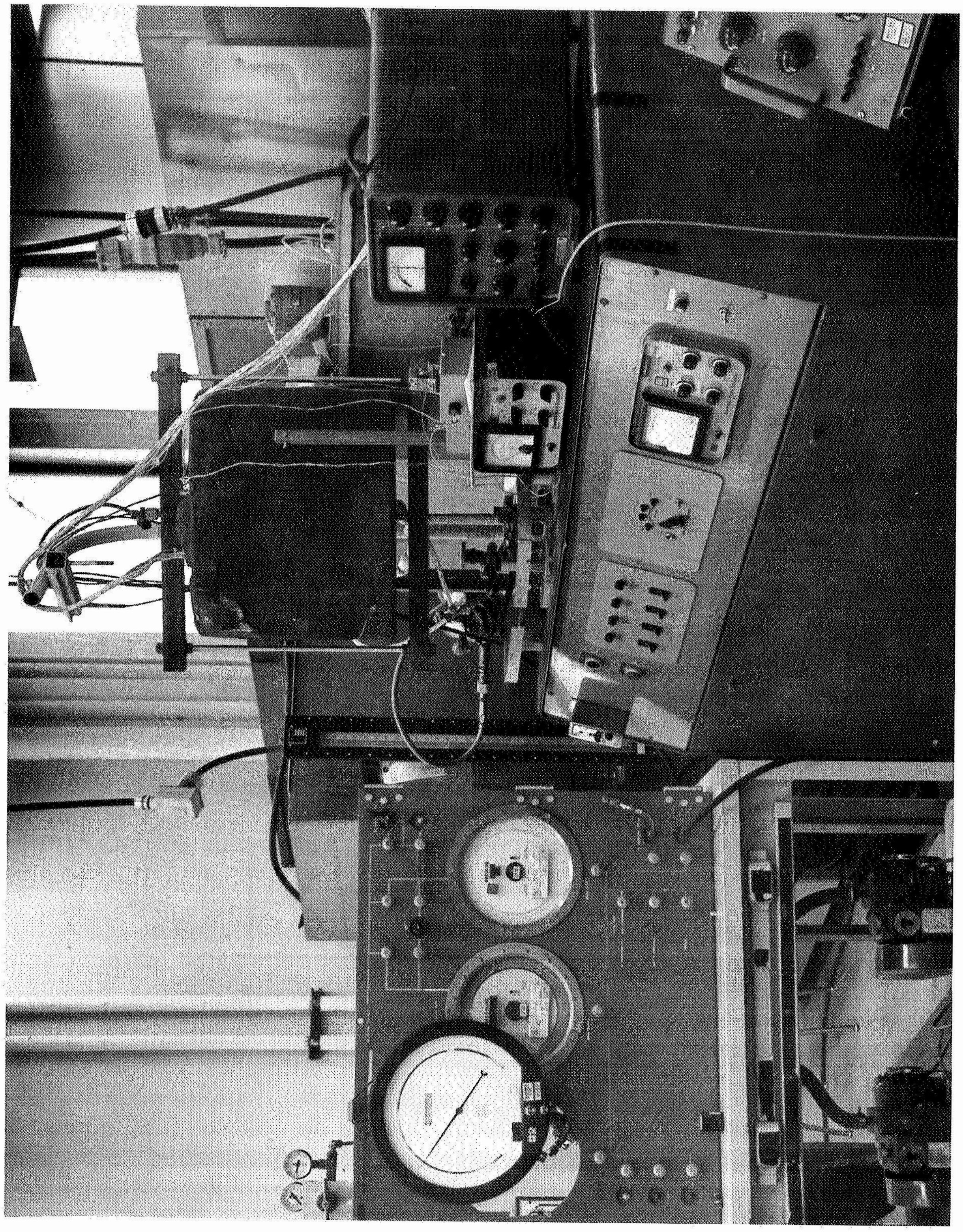

FIGURE II–43 ¼ SCALE MODEL FREE CONVECTION TEST SETUP making the first run at 8 atmospheres pressure (run 30) a repeat run was made for a 4 atmosphere pressure case. Figure II-44 shows the differences between runs 29 and 29.1, without and with the inner cylinder pressurized, respectively. This figure indicates that the air leak was removing some heat from the system since run 29 has a lower average model temperature than run 29.1. The depression in temperature in the heater section region of the model for run 29.1 is due primarily to the increased free convection (run 29.1 had a pressure of 4.22 atm whereas run 29 had 4.01 atm pressure). All of the 4 atmosphere pressures cases were rerun with the inner cylinder pressurized. A check of the 2 atmosphere pressure cases (runs 31.3 and 37.2) showed no significant difference between inner cylinder being pressurized and not pressurized. The free convection test series conditions are given in Table II-9.

II.5.6.1.4 Forced Convection Test Series

The Forced Convection Test Series test setup for the 1/4 scale model is shown in Figure II-45. Figure II-46 shows a photograph of the test setup. Calibrated "rotometers" were used to measure the air flow rate through the model. The air pressure at the rotometer was regulated to a value P_o. The system pressure P_s and the air flow rate were set by adjusting the "flow rate control valve" and the "system pressure control valve." A mercury manometer was used to measure the pressure drop ΔP through the model. This pressure drop was significant for the high flow rate cases. Thermocouples were installed in the air stream at the ends of the air inlet and air outlet tubes. For the 1/2 atmosphere pressure runs the vent line was attached to a vacuum system (the "roughing" pump for Boeing's Space Simulation Chamber A). The vent line and "system pressure control valve" were removed for the 1 atmosphere pressure runs. The operating conditions for the 1/4 Scale Model Forced Convection Test Services are given in Table II-10.

The thermocouple output stability obtained in the "Radiation-Conduction" and "Free Convection Test Series" was not matched in the "Forced Convection Test Series." Temperature oscillations of up to about $\pm 0.5°F$ were present for some regions of the inner cylinder and for the air outlet temperature. The air inlet temperature variation during a recording of the test data was generally less than about $\pm 0.1°F$. The outer cylinder and end plate temperatures were quite steady

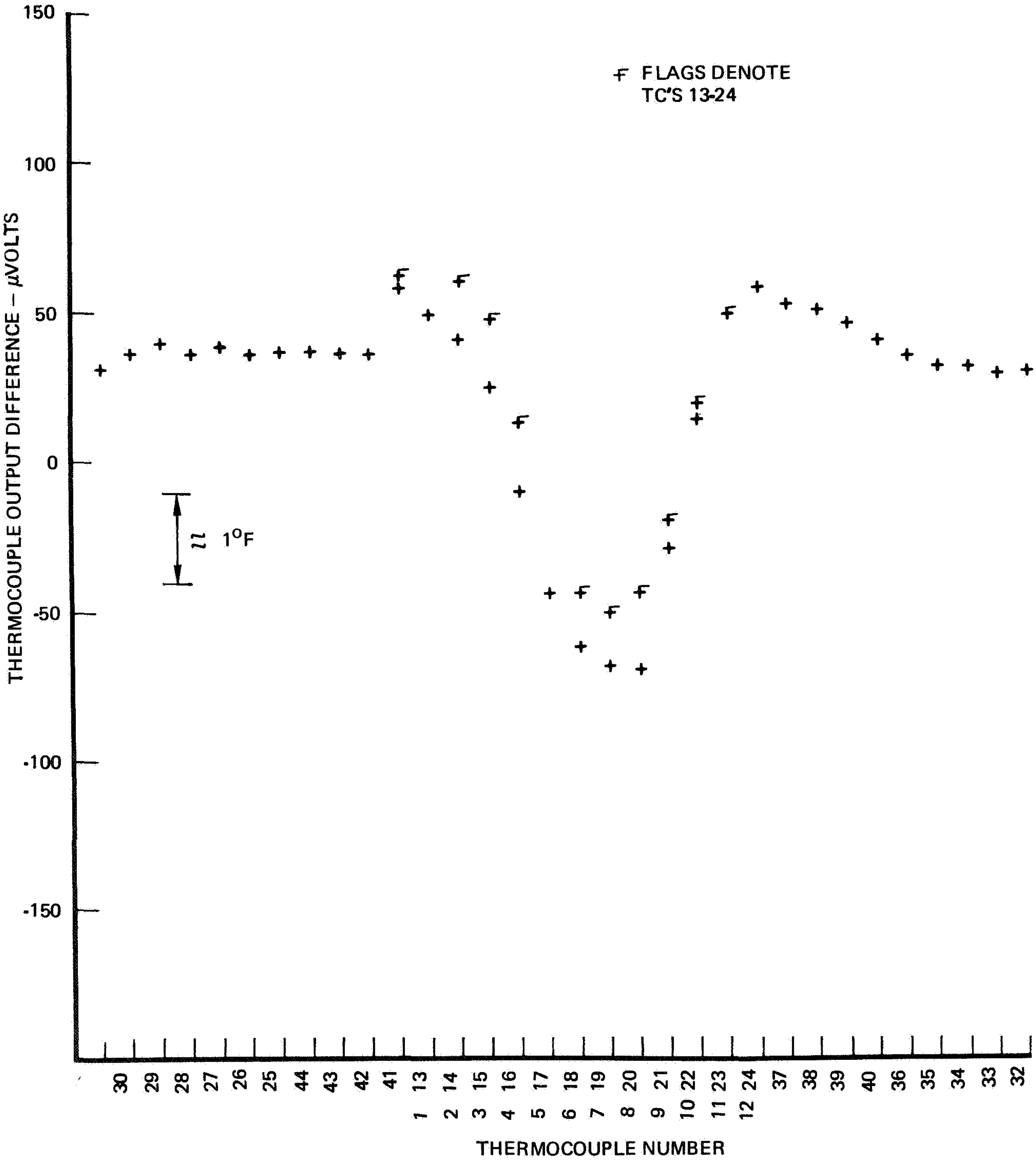

Figure II-44: TEMPERATURE DIFFERENCE WITH INNER CYLINDER PRESSURIZED (DIFFERENCE BETWEEN RUN 29.1 AND RUN 29)

TABLE II-9

FREE CONVECTION TEST SERIES

Run No.	Date	Time		PRESSURE Barometric in.Hg.	Outer Cylinder *Reading	Outer Cylinder ATM	POWER Voltage Volts	Current 1.001 x Amps	Watts
18	11/18/69	0930		30.45	15.1	0.513	27.46	.2119	5.813
19	11/24/69	1515		30.37	0	1.015	27.49	.2122	5.828
20	11/25/69	1730		30.34	0	1.014	Variation		
20.1	11/26/69	1730		30.39	0	1.016	33.76	.2602	8.776
21	12/1/69	1130		30.03	15.4	0.489	33.69	.2597	8.741
22	12/3/69	1430		29.90	16.4	0.451	39.06	.3007	11.73
23	12/4/69	1100		30.27	0	1.012	39.03	.3005	11.72
24	12/5/69	1800		30.16	0	1.008	42.61	.3277	13.95
25	12/8/69	1800		29.73	15.4	0.479	42.61	.3277	13.95
26	12/9/69	1800			15.7		Variation		
26.1	12/10/69	1430		29.64	16.4	0.443	48.65	.3732	18.14
27	12/11/69	1630		29.37	0	0.982	48.64	.3707	18.01
27.1	12/12/69	1030		29.83	0	0.997	48.59	.3730	18.11
28	12/15/69	1500		29.85	15.6	2.06	48.57	.3730	18.10
31	12/17/69	1130		30.00	15.6	2.06	42.61	.3279	13.96
31.1	12/17/69	1830		29.94	15.54	2.06	42.64	.3282	13.98
34	12/18/69	1030		30.14	15.05	2.03	38.97	.3002	11.69
37	12/19/69	1600		29.67	15.1	2.02	33.68	.2600	8.748
38	12/20/69	1830		29.76	42.8	3.91	33.67	.2600	8.745
35	12/21/69	1800		29.75	44.2	4.00	38.98	.3006	11.71
32	12/22/69	1530		29.36	44.2	3.99	42.63	.3283	13.98
29	12/23/69	1530		29.81	44.2	4.00	48.83	.3753	18.31
**30	12/31/69	1445	102.8 psig	30.47	102.8	8.01	48.87	.3760	18.36
29.1	1/2/70	1615		30.31	47.2	4.22	48.80	.3752	18.29
32.1	1/5/70	-		30.28	44.1	4.01	42.68	0.3289	14.02
33	1/6/70	-		30.36	101.9	7.94	42.68	0.3290	14.03
36	1/7/70	1445		29.95	101.5	7.90	38.98	0.3008	11.71
35.1	1/8/70	1800		29.71	44.6	4.03	39.00	0.3010	11.73
38.1	1/10/70	1430		29.99	44.2	4.01	33.67	0.2598	8.739
39	1/12/70	1000		29.77	102.0	7.93	33.675	0.2600	8.747

TABLE II-9 (CONT.)

31.2	1/14/70	1030	29.58	14.7	1.99	42.665	0.3282	13.99
37.1	1/15/70	1600	29.94	14.75	2.00	33.665	0.2597	8.734

* Reading in inches of Hg for runs 18-27 and in psig for other runs

** Leak between inner and outer cylinder required inner cylinder to be maintained at outer cylinder pressure for run 30 and the following runs. The earlier runs had the inner cylinder open to the atmosphere.

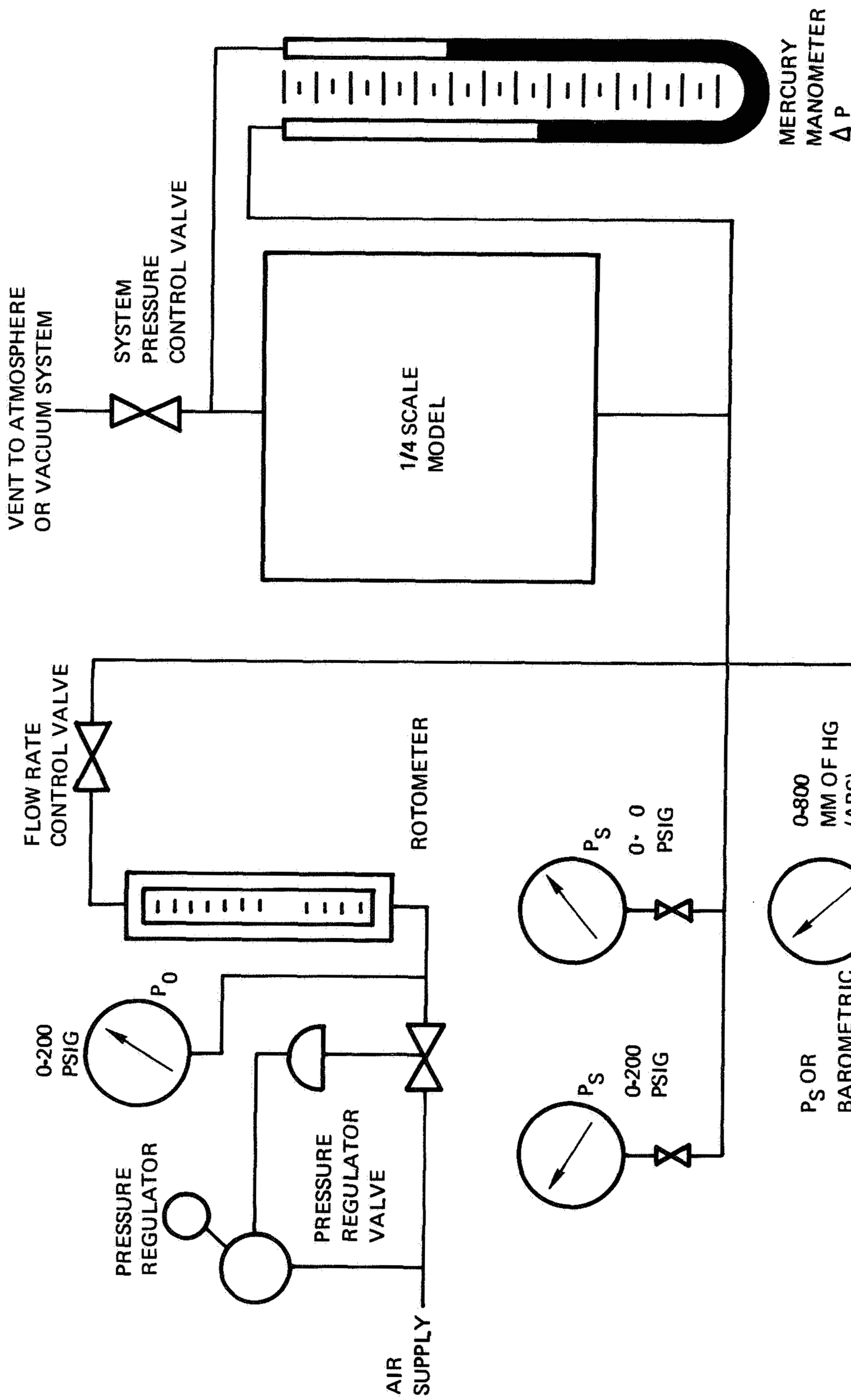

Figure II-45: FORCED CONVECTION TEST SETUP SCHEMATIC

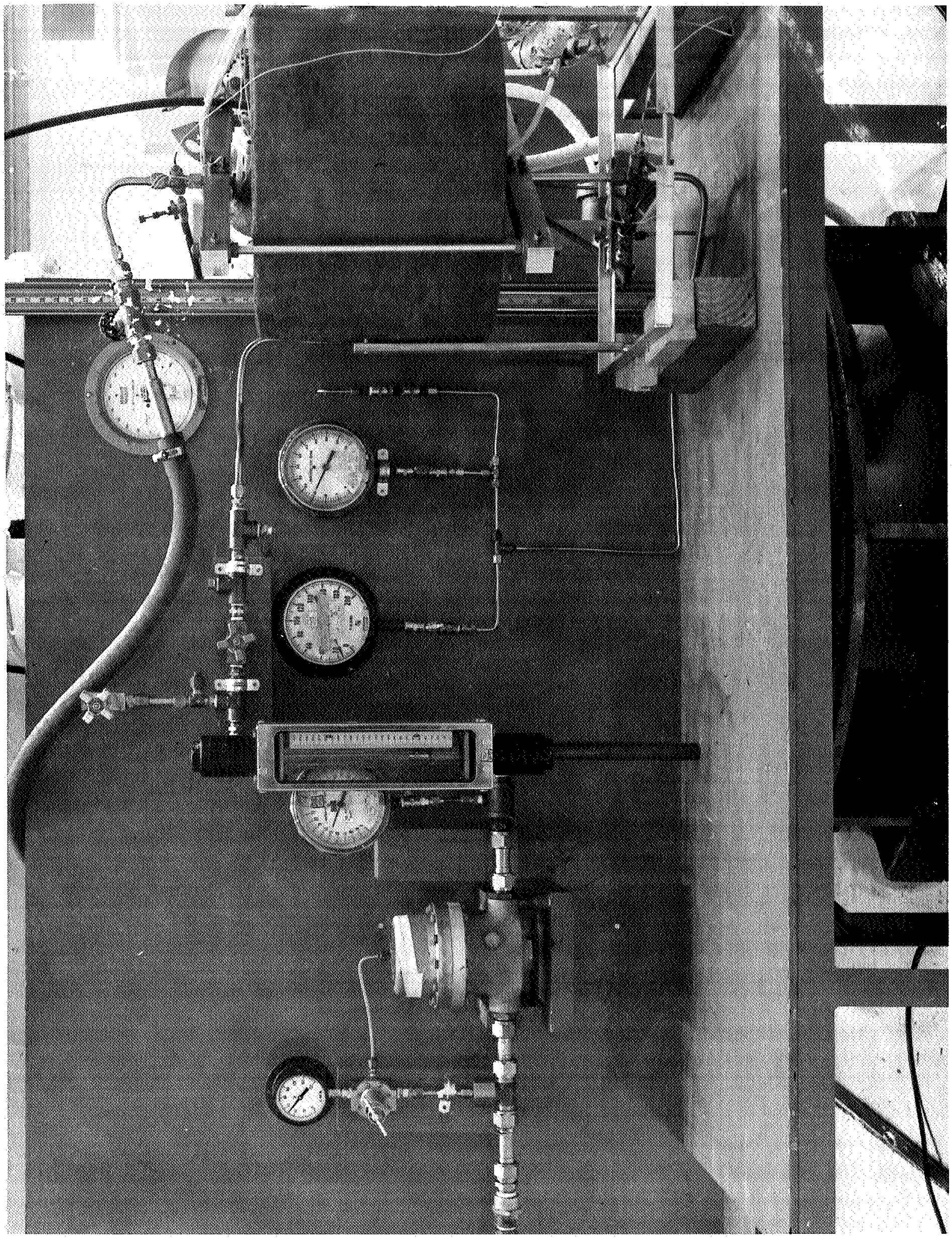

FIGURE II–46 FORCED CONVECTION TEST SETUP

TABLE II-10 1/4 SCALE MODEL FORCED CONVECTION TEST SERIES

RUN NO.	DATE	TIME	AIR FLOW RATE: ROTOMETER SERIAL NO.	AIR FLOW RATE: ROTOMETER P_0, PSIG	AIR FLOW RATE: ROTOMETER READING	AIR FLOW RATE: MASS FLOW RATE LB/MIN	PRESSURE: BAROMETRIC MM OF HG (IN OF HG)	PRESSURE: P_S PSIG (MM OF HG)	PRESSURE: ΔP IN OF HG	PRESSURE: SYSTEM PRESSURE ATM	POWER INPUT: VOLTAGE VOLTS	POWER INPUT: CURRENT 1.001 x AMPS (0.09986) x AMPS	POWER INPUT: POWER WATTS
a. 42	2/4/70	1800	BAC 505967	51.0	56.5	1.25	759	15.0	2.8	1.97	0	0	0
a. 43	2/5/70	1030		50.0	56.0	1.24	N/A	15.3	2.75	1.99	48.85	0.3767	18.38
43.1		1500		50.5	56.2	1.24	758	15.3	2.75	1.99	48.87	0.3767	18.39
44		1800		50.5	55.8	1.24	N/A	15.3	2.75	1.99	60.38	0.4642	28.00
45		2300		50.2	55.8	1.24	N/A	2.9	5.05	1.11	60.34	0.4639	27.96
46	2/6/70	1100		50.8	56.0	1.24	N/A	42.5	1.45	3.87	60.41	0.4644	28.03
b. 46.1		1600		109.0	39.6	1.26	762	42.2	1.45	3.85	60.63	0.4661	28.23
47		2300		109.2	39.2	1.26	760	102.5	0.65	7.96	60.58	0.4658	28.19
48	2/9/70	2100	BCX 176102	108.5	12.0	0.290	N/A	102.5	0.05	7.97	48.87	0.3765	18.38
49	2/10/70	1415		110.0	12.0	0.292	757	1.25	0.35	1.075	48.87	0.3765	18.38
50		1800		110.0	11.7	0.285	759	1.25	0.35	1.078	48.87	0.3765	18.38
51		2330		110.0	11.8	0.287	760	14.3	0.20	1.97	48.854	0.3760	18.35
52	2/11/70	1730		110.0	12.0	0.292	760	44.2	0.15	4.00	48.861	0.3761	18.36
53		2345		110.0	12.0	0.292	759	103.0	0.05	8.00	60.25	0.4625	27.84
54	2/12/70	0900		112.0	12.0	0.294	N/A	1.25	0.35	1.07	60.22	0.4620	27.79
55		1650		110.5	11.7	0.285	750	14.2	0.20	1.95	60.275	0.4624	27.84
c. 56	2/13/70	1100											
56.1		1330		110.0	12.0	0.292	756	44.2	0.10	4.00	60.25	0.4623	27.83
57		1830		110.5	12.0	0.292	757	44.5	0.10	4.02	42.628	0.3285	13.99
58		2130		111.0	12.0	0.293	757	1.25	0.30	1.076	42.636	0.3286	14.00
59	2/16/70	0930	BAC 148522-3	109.5	18.85	0.0734	749	101.5	$\le$ 0.05	7.89	48.93	0.3766	18.41
60		1430		109.3	19.02	0.0743	747	45.2		4.06	48.926	0.3764	18.40
61		1915		109.0	19.05	0.0743	746	14.7		1.98	48.925	0.3762	18.39
62		2330		108.5	19.20	0.0749	748	0.2		0.997	48.933	0.3761	18.39
63	2/17/70	0900		108.5	19.25	0.0750	757	0.2		1.01	42.60	0.3281	13.96
64		1430		108.2	19.11	0.0744	761	14.6		1.99	42.607	0.3282	13.97
65		1845		108.5	19.00	0.0739	762	44.3		4.02	42.592	0.3282	13.96
66	2/18/70	0915		108.5	19.25	0.0750	771	103.5		8.05	42.60	0.3284	13.98
67		1430		108.8	19.30	0.0755	772	103.0		8.02	38.97	0.3008	11.71
68		2300		108.0	19.33	0.0752	775	0		1.02	39.003	0.3007	11.72
69	2/19/70	0830		108.5	19.30	0.0752	774	14.6		2.01	38.977	0.3007	11.71
70		1300		108.8	19.45	0.0761	772	44.8	$\le$ 0.05	4.06	38.984	0.3006	11.71
71		2030	BAC 505967	50.8	55.8	1.24	771	15.8	2.75	2.04	0	0	0
72		2145		50.8	56.0	1.24	771	43.5	1.45	3.95	0	0	0
73		2330		51.0	56.2	1.24	770	3.0	5.25	1.13	0	0	0
74	2/20/70	1000		51.0	56.2	1.24	767	3.0	5.25	1.12	48.98	0.3755	18.47
75		1500		50.5	56.5	1.24	762	16.1	2.75	2.05	48.99	0.3777	18.49
76		1750		50.5	56.5	1.24	762	44.2	1.45	3.99	49.00	0.3777	18.49

TABLE II-10 1/4 SCALE MODEL FORCED CONVECTION TEST SERIES (continued)

RUN NO.	DATE	TIME	AIR FLOW RATE: ROTOMETER SERIAL NO.	AIR FLOW RATE: ROTOMETER P_0,PSIG	AIR FLOW RATE: ROTOMETER READING	AIR FLOW RATE: MASS FLOW RATE LB/MIN	PRESSURE: BAROMETRIC MM OF HG (IN OF HG)	PRESSURE: P_S PSIG (MM OF HG)	PRESSURE: ΔP IN OF HG	PRESSURE: SYSTEM PRESSURE ATM	POWER INPUT: VOLTAGE VOLTS	POWER INPUT: CURRENT 1.001 x AMPS (.09986) x AMPS	POWER INPUT: POWER WATTS
77	2/24/70	0830	BAC 148522-3	109.5	19.50	0.0767	N/A	(381)	N/A	0.501	39.00	0.3005	11.71
78		1710		109.3	19.45	0.0765	N/A	(381)		0.501	42.677	0.3285	14.01
79	2/25/70	0845		109.0	19.45	0.0765	N/A	(383)		0.504	48.83	0.3754	18.31
80		1720		0.0	5.85	0.00483	30.30	(389)		0.512	48.87	0.3750	18.31
81		2230		0.0	5.80	0.00477	30.30	(382)		0.503	42.65	0.3279	13.97
82	2/26/70	0900		0.0	5.75	0.00471	30.22	(386)		0.508	38.99	0.3001	11.69
83		1730		0.0	15.9	0.01812	30.08	(381)		0.501	48.92	0.3756	18.36
84	2/27/70	0045		0.0	16.0	0.0182	29.93	(384)		0.505	42.59	0.3276	13.94
d.85		0900		0.0	15.9	0.0181	N/A	(382)		0.503	38.99	0.3003	11.70
85.1		1510		0.0	15.8	0.0179	29.84	(378)		0.497	39.00	0.3004	11.70
86	3/19/70	1400	BAC 505967	50.5	56.0	1.24	(766)	2.9	N/A	1.13	48.99	(0.03772)	18.50
87		1830		51.0	56.0	1.24	(764)	44.5	0.85	4.02	48.94	(0.03772)	18.49
88	3/20/70	1000	BCX 176102	110.0	12.0	0.293	(762)	43.2	0.1	3.92	48.90	(0.03766)	18.44
89		1730		110.0	12.05	0.294	(762)	0.3	0.3	1.018	48.921	(0.03790)	18.57
90		2345		109.8	12.05	0.294	(765)	102.0	≤ 0.05	7.95	48.955	(0.03785)	18.56
91	3/23/70	0900		109.8	12.0	0.293	(765)	0.3	0.27	1.022	0	0	0
92		1400		110.0	54.0	1.28	(764)	3.2	4.7	1.14	0	0	0
93	3/24/70	0015	BAC 148522-3	109.5	18.95	0.0740	(766)	101.0	≤ 0.05	7.88	48.897	(0.03775)	18.48
94		0845		111.0	19.05	0.0750	(770)	44.3		4.03	48.867	(0.03768)	18.44
95		1530		110.0	19.0	0.0744	(772)	0		1.016	48.884	(0.03780)	18.50
96		2345		110.0	19.0	0.0744	(772)	15.0	≤ 0.05	2.04	48.839	(0.03775)	18.46
97	3/25/70	1030		110.0	19.0	0.0744	N/A	(379)	N/A	0.499	48.835	(0.03777)	18.47
98		2230		0.0	16.0	0.0183	30.26	(386)	N/A	0.508	48.851	(0.03771)	18.45
99	3/26/70	0900		0.1	5.8	0.00480	30.37	(377)	N/A	0.496	48.831	(0.03773)	18.45

a. Checkout
b. Repeat run with different rotometer setting
c. Notat equilibrium
d. Equilibrium upset by opening of building roll up door

Note: Runs 86-99 have air flow direction reversed (flow downward) with no measurable temperature oscillations present. At the lower heating rate cases the temperature oscillations were much less than for the higher heating rate cases.

II.5.6.2 Full Scale Model Tests

Prior to testing the full scale model, the thermocouples were checked for continuity. Several broken leads were discovered. These were all repaired with the exception of thermocouple number 13. Thermocouple numbers 48 and 49 were installed in the air distribution plugs for measurement of inlet and outlet gas temperatures and the model was insulated with polyurethane foam (as shown in Figure II-31).

The 1/4 scale model test setup, without the pressure control equipment, was used for the full scale model tests. A photograph of the full scale model and the test setup is shown in Figure II-47.

The "Free Convection Test Series" operating conditions are given in Table II-11. These tests were made with the bottom air supply tube blocked off to prevent gas flow through the model. The top tube was left partially open to keep the model at atmospheric pressure.

The "Forced Convection Test Series" operating conditions are given in Table II-12. It is interesting to note that the small temperature oscillations present in the 1/4 scale model forced convection tests were also apparent in the full scale model tests.

II.5.7 Data Analysis and Correlation

II.5.7.1 Thermal Math Model Expansion and Upgrading

The basic thermal math model for the 1/4 scale model was expanded to correspond to the actual test configuration of the model. The nodal model expansion included the following:

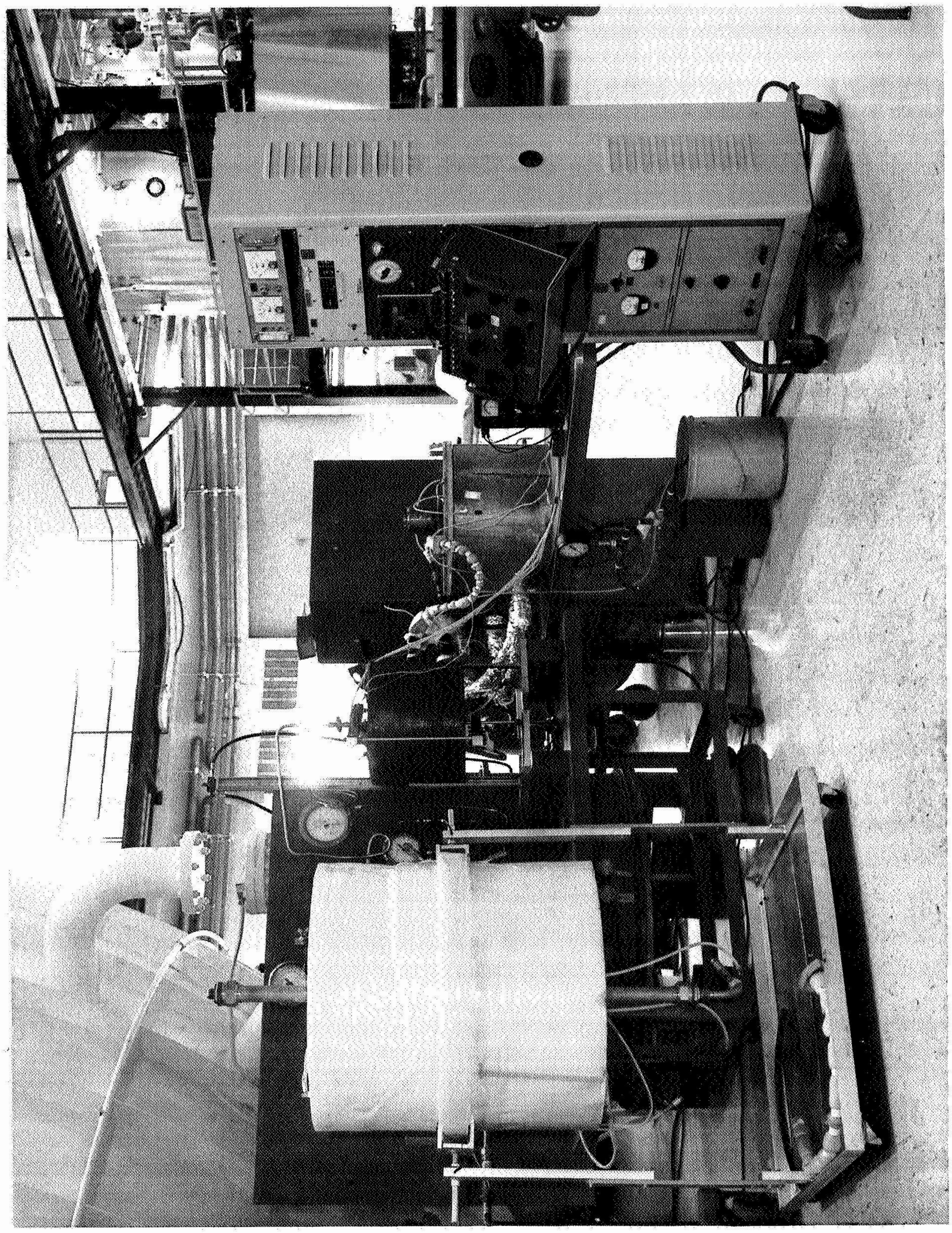

FIGURE II–47 FULL SCALE MODEL WITH FREE CONVECTION TEST SETUP

TABLE II-11 FULL SCALE MODEL FREE CONVECTION TEST SERIES

RUN NO.	DATE	TIME	PRESSURE mm of Hg	PRESSURE ATM	POWER INPUT VOLTAGE VOLTS	POWER INPUT CURRENT .09986 x AMPS	POWER WATTS
a. 100A	3/3/70	0900	N/A	1.0	88.45	0.2117	187.5
a. 100B	3/3/70	1500	N/A	1.0	88.48	0.2120	187.8
101	3/3/70	1800	757.	0.996	88.52	0.2120	187.9
102	3/4/70	0900	755.	0.993	96.69	0.2312	223.9
103	3/4/70	2300	760.	1.000	111.0	0.2646	294.1
b. 104A	3/5/70	0900	760.	1.000	76.60	0.1838	141.0
c. 104B	3/5/70	1330	758.	0.997	76.65	0.1838	141.1
104	3/5/70	2000	756.	0.995	76.60	0.1838	141.0
105	3/6/70	0830	756.	0.995	62.25	0.1496	93.26

a. Checkout
b. Not at equilibrium
c. Not at equilibrium (loss of power to cooling water mixer)

TABLE II-12 FULL SCALE MODEL FORCED CONVECTION TEST SERIES

RUN NO.	DATE	TIME	AIR FLOW RATE: ROTOMETER SERIAL NO.	AIR FLOW RATE: ROTOMETER P_o PSIG	AIR FLOW RATE: ROTOMETER READING	AIR FLOW RATE: MASS FLOW RATE LB/MIN	PRESSURE: BAROMETRIC MM OF HG.	PRESSURE: SYSTEM PRESSURE ATM	POWER INPUT: VOLTAGE VOLTS	POWER INPUT: CURRENT .09986 x AMPS	POWER INPUT: POWER WATTS
[a] 106A	3/9/70	1200	BAC 505697	50.0	240.5	5.04	756	1.002	110.91	.2653	294.6
106		1430		50.0	239.5	5.02	755	1.000	100.90	.2653	294.6
107		2330		50.0	240.5	5.04	755	1.000	96.65	.2316	224.2
108	3/10/70	0845		50.0	240.5	5.04	756	1.002	88.48	.2123	188.1
109		2230		50.0	53.0	1.173	753	0.994	111.06	.2653	295.1
110	3/11/70	1030		50.0	52.5	1.167	752	0.992	96.72	.2315	224.2
111		1830		50.0	53.0	1.174	758	1.000	88.36	.2118	187.4
112	3/12/70	1130		15.2	24.9	0.295	755	0.993	88.45	.2119	187.7
113		2130		15.2	25.0	0.296	760	1.000	96.75	.2313	224.1
114	3/13/70	1030		15.5	25.3	0.301	764	1.005	110.60	.2640	292.4
115	3/16/70	1130		14.9	24.8	0.293	763	1.004	111.04	.2647	294.3
[b] 116A	3/17/70	0900		50.8	53.0	1.181	770	1.016	111.0	.2647	294.2
116	3/18/70	0840		50.8	53.0	1.182	773	1.020	110.85	.2645	293.6
117		1615		50.5	241.5	5.10	770	1.020	110.93	.2650	294.4

a. Not at equilibrium
b. Cooling water problems

Note: Runs 115-117 have air flow direction reversed (flow is downward)

- Foam insulation (polyurethane foam)
- Insulation inside inner cylinder (microquartz)
- Support rod (phenolic)
- Air distribution plug (phenolic)
- Heater leads (copper)
- Air flow tubes (stainless steel)
- Gas inside of model (air)

Figure II-48 shows the nodal network for the expanded thermal math model. The inner cylinder assembly is represented by 26 nodes exclusive of the inner cylinder wall nodes of the basic math model. The air inside the model is represented by 28 nodes and the foam insulation by 49 nodes. The external temperature (ambient) is represented by a single boundary node. The basic model structure is represented by 12 nodes for the inner cylinder, 8 nodes for the end plates, 12 nodes for the outer cylinder and 2 nodes for the cooling fin (the basic math model consisted of these nodes).

The experimental data from test runs 10, 14, 15, 16 and 17 were used in conjunction with the expanded thermal math model to determine the upgrading necessary to develop a valid thermal math model. The temperatures for these runs are presented in Appendix II-A.1.1. These temperatures were calculated from the experimental data using the thermocouple calibration correction. The temperatures for the inner cylinder were taken as the average of the two thermocouple (where available) measurements with the exception of node 307. Since the thermocouples (numbers 7 and 19) used to measure the temperature at node 307 apparently are reading high and since the radiation-conduction tests give a symmetrical temperature distribution, a temperature correction term was developed for thermocouple number 19. This term corrects the temperature measured with thermocouple 19 to that measured by thermocouple 6 for the radiation-conduction tests. Figure II-49 shows the correction term as a function of heater power. This correction was applied to all of the 1/4 scale model test results listed in Appendix II-A. The temperature distributions for test runs 10, 14, 15, 16, and 17 are shown in Figure II-50.

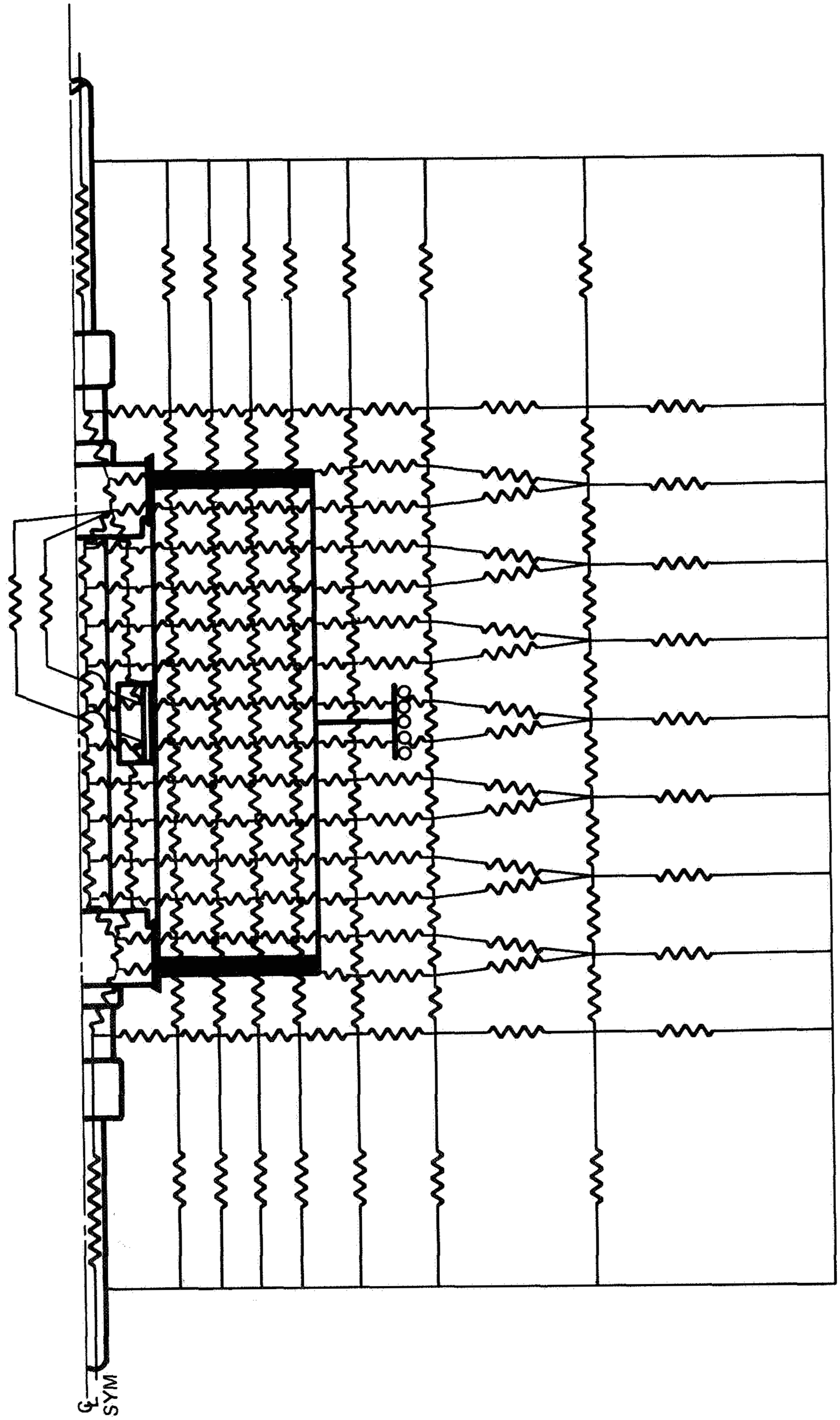

Figure II-48: EXPANDED NODAL NETWORK FOR THERMAL MATH MODEL OF 1/4 SCALE THERMAL MODEL

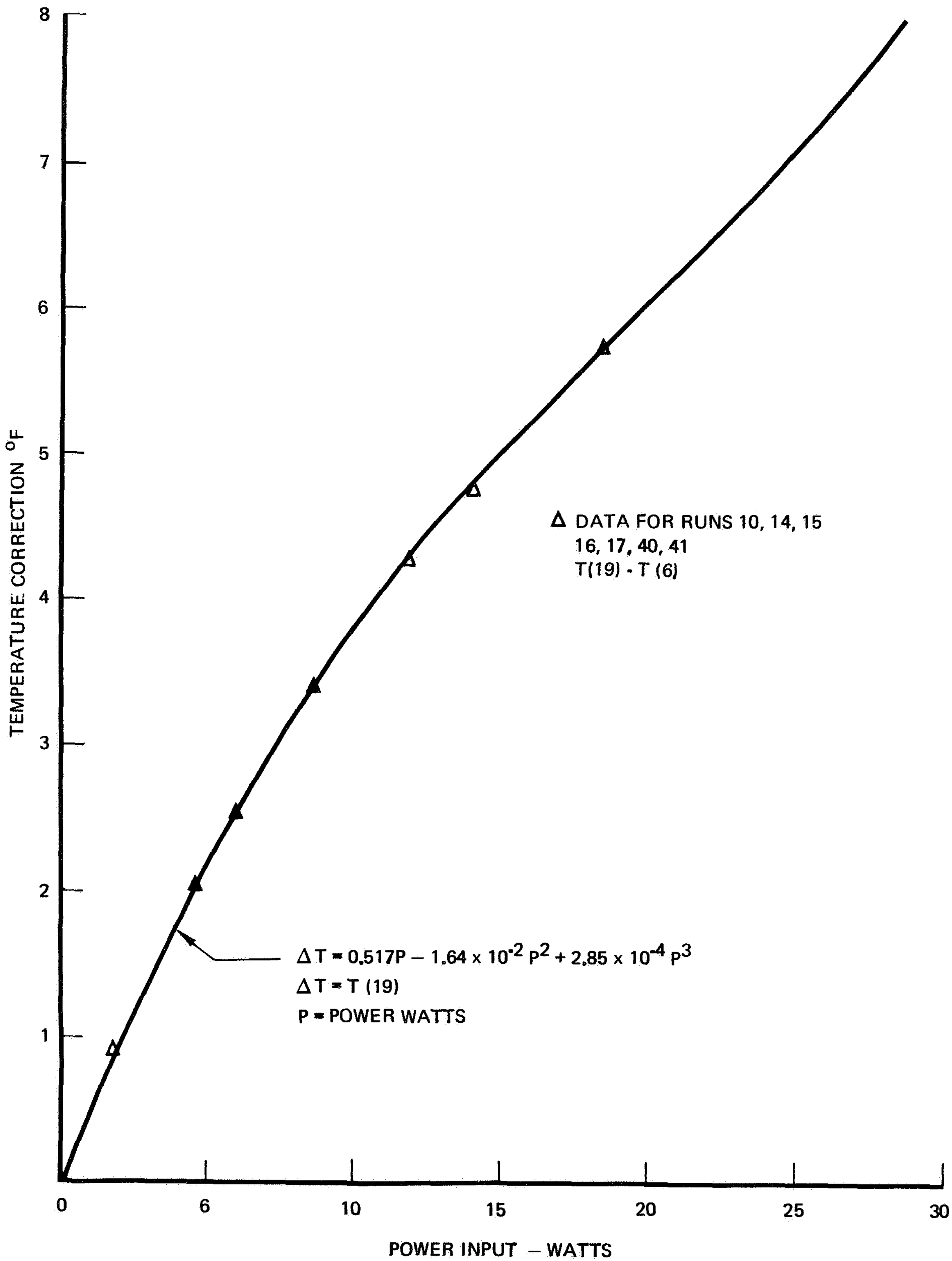

Figure II-49: TEMPERATURE CORRECTION FOR TC NO. 19 AT NODE 307

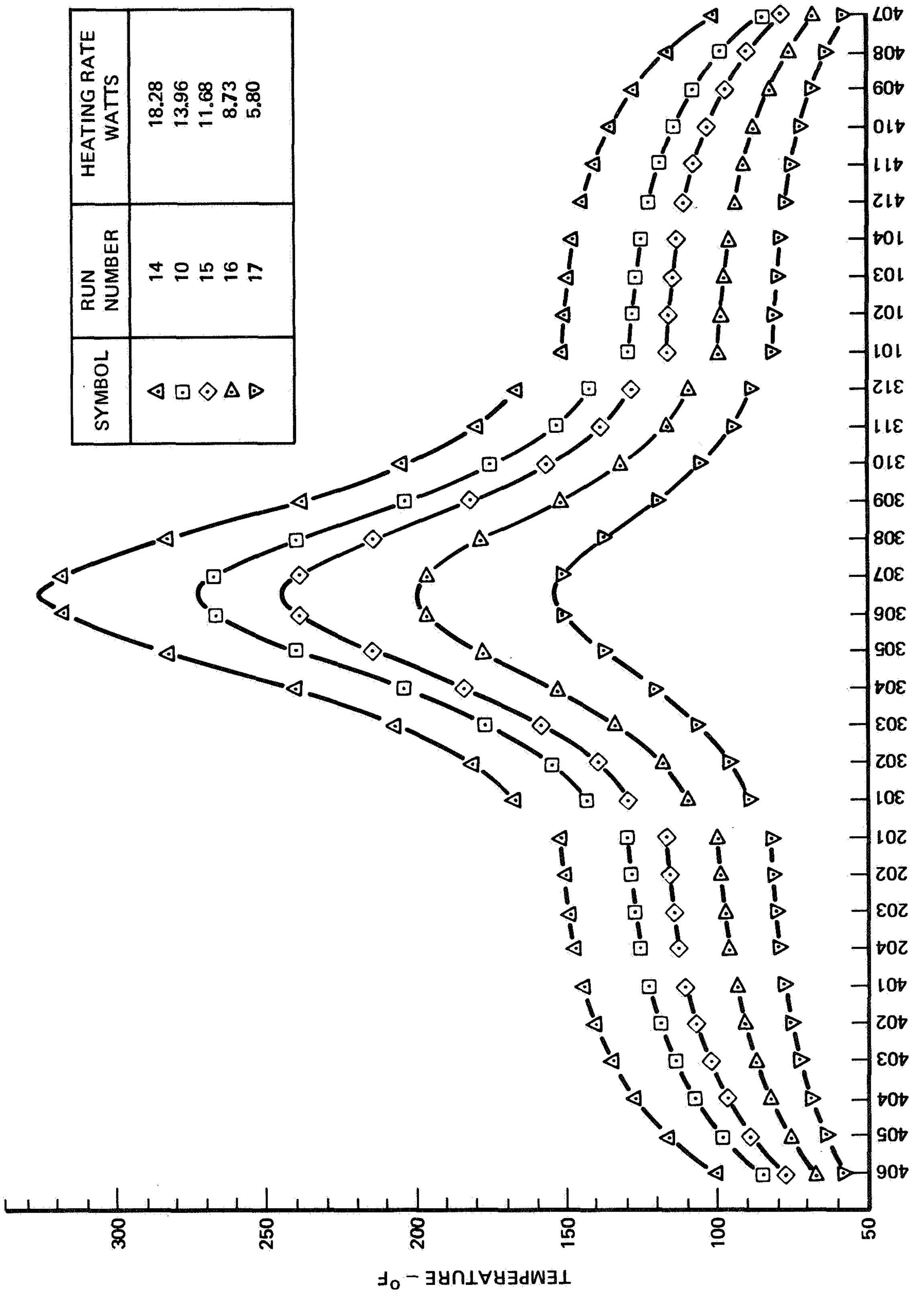

Figure II-50: 1/4 SCALE MODEL RADIATION–CONDUCTION TESTS

Two additional 1/4 scale model radiation-conduction test runs were made (runs 40 and 41, listed in Appendix II-A.1.1) without water cooling in an attempt to obtain a better definition of the model heat leak paths. The results of these runs were used in most of the thermal math model upgrading runs. However, these results were of limited value and the upgrading effort concentrated on the results from test runs 10, 14, 15, 16 and 17.

The required upgrading was determined by comparing the basic math model thermal conductances calculated from the geometry and thermal conductivity (input conductances) with those calculated from the experimental data (upgraded conductances). The method of obtaining the upgraded conductances and comparing them to the input conductances is as follows:

1. The expanded thermal math model nodal network is input to the BETA program.

2. A subroutine takes the thermocouple output data from the test run, applies the themocouple calibration correction and determines the temperature at each node of the basic math model and the ambient temperature. These temperatures are then made boundary temperatures for the expanded thermal math model.

3. The BETA program then calculates the nodal temperatures for the expanded thermal math model using the boundary temperatures obtained in the subroutine and the measured power input to the heater.

4. A subroutine than takes the calculated temperatures and makes the following determinations for each node of the basic math model.

   a. Radiative heat transfer to the node.

   b. Conductive heat transfer from the air inside the model to the node.

   c. Conductive heat transfer to the node from one (two for two nodes) of the following sources, the heater, the insulation inside the inner cylinder, the air distribution plugs and the foam insulation.

5. The subroutine then makes a thermal balance at each node of the basic math model and determines the thermal conductances between adjacent nodes. The method of this determination can be explained by referring to Figure II-51 which shows the nodal network detail near the heater. The power input is divided equally between nodes 526 and 527 which represent the heater. The conductors connected to these nodes represent the various heat flow paths from the heater. The paths of interest for the basic math model are those between nodes 526 and 306 and nodes 527 and 307. By assuming negligible thermal conduction between nodes 306 and 307 the thermal conductances may be determined stepwise around each half of the model starting at nodes 306 and 307. The radiative heat transfer to node 306 is given by

$$QRAD(306) = \sum_j \sigma A_{306} \mathcal{F}_{306,j} \left[T_j^4 - T^4(306) \right]$$

the heat transfer to node 306 from the air is given by

$$QGAS(306) = K(306) \; [\; T(606) - T(306) \;]$$

and the heat transfer from the heater is given by

$$QINS(306) = K(106) \; [\; T(526) - T(306) \;]$$

The heat conducted between node 306 and node 305 is then given by (QRAD(306) + QGAS(306) + QINS(306)) and the upgraded conductance between nodes 306 and 305 is given by

$$K'(5) = \frac{QRAD(306) + QGAS(306) + QINS(306)}{T(306) - T(305)}$$

The conductance between node 305 and node 304 can now be calculated from

$$K'(4) = \frac{QRAD(305) + QGAS(305) + QINS(305) + K'(5)\,[T(306) - T(305)]}{T(305) - T(304)}$$

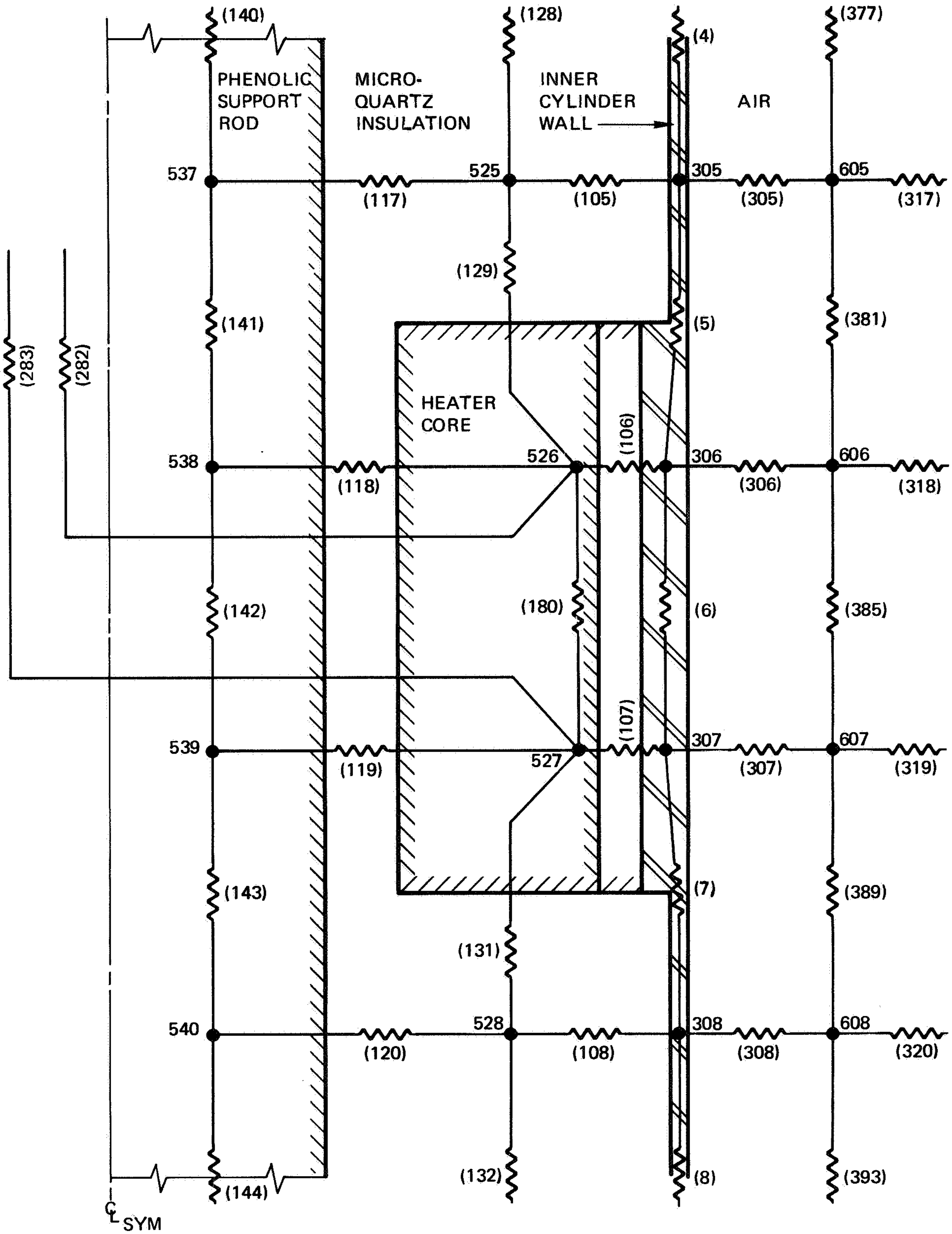

Figure II-51: THERMAL MATH MODEL NODAL NETWORK DETAIL NEAR HEATER where

$$QRAD(305) = \sum_{j} \sigma A_{305} \mathcal{F}_{305,j} \left[T_j^4 - T^4(305) \right]$$

$$QGAS(305) = K(305) \; [\; T(605) - T(305) \;]$$

and

$$QINS(305) = K(105) \; [\; T(525) - T(305) \;]$$

In a similar fashion the conductances are determined around the model to the cooling fin for nodes 304, 303, 302, 301, 201, 202, 203, 204, 401, 402, 403, 404, 405, 406, 413. Likewise the conductances are determined for the other half of the model, nodes 307, 308, 309, 310, 311, 312, 101, 102, 103, 104, 412, 411, 410, 409, 408, 407, 413. Finally the conductance between nodes 413 and 414 is determined.

6. The program then makes a comparison of the upgraded and input conductances by calculating the ratios K'(i)/K(i) where

   K'(i) = upgraded conductance determined using experimental data

   K(i) = input conductance determined from kA /Δx

Figure II-52 shows the first comparison of the upgraded conductances with the input values for the five test runs. This comparison was used to gain the insight needed to upgrade the expanded thermal math model. Several observations can be made from Figure II-52:

1. The conductance ratio is low for the conductors between

   a. The inner cylinder and the end plates, nodes 312 to 101 and 301 to 201.

      This discrepancy is explained by the comparison of the input to the actual geometry of the end plate to inner cylinder connection.

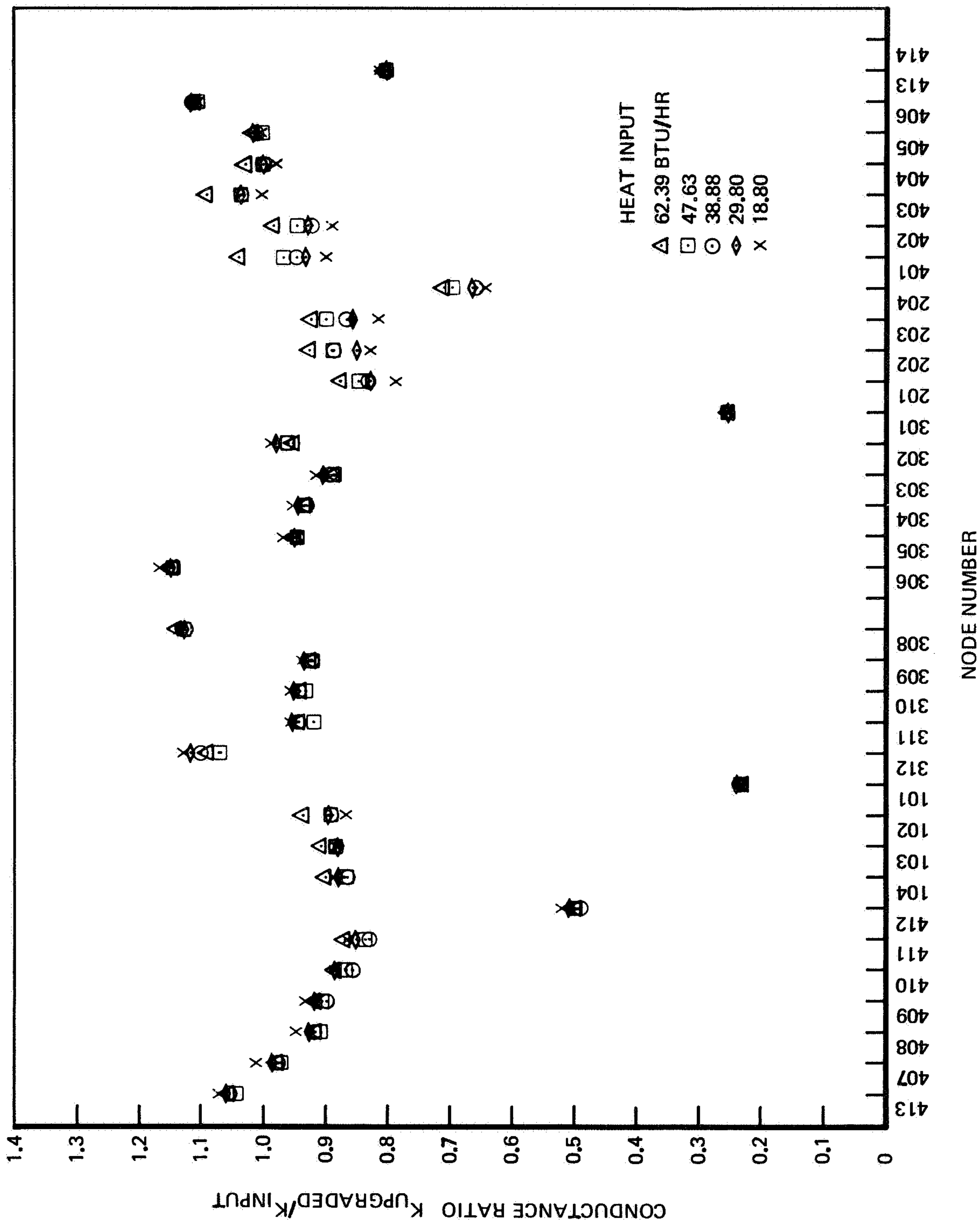

Figure II-52: INITIAL UPGRADING RUN RESULTS

Figure II-53 shows this comparison along with an approximate calculation of the expected conductance ratio. This ratio is in agreement with that calculated from the experimental data.

b. The end plates and the outer cylinder, nodes 104 to 412 and 204 to 401.

This discrepancy is also explained by the difference in the input and actual geometry of this connection. Figure II-54 shows a comparison of the input and actual geometry along with an approximate calculation of the conductance ratio. This ratio is in fair agreement with that calculated from the experimental data.

c. The cooling fin and the cooling water coils, nodes 413 to 414.

This discrepancy is apparently due to the input value assuming an infinite conductance from the end of the fin to the cooling coils. A more reasonable approach, see Figure II-55, gives a conductance ratio in agreement to that calculated from the experimental data.

2. The conductance ratio is high for the conductors between

a. The heater section and adjacent nodes, nodes 306 to 305 and 307 to 308.

The discrepancy is partially explained by using ($\frac{kA}{\Delta x}$) to calculate the input conductance for the heated section. The conduction of the heater core may also contribute to the discrepancy.

b. The inner cylinder nodes 311 and 312

This difference is probably due to the temperature difference around the inner cylinder since only one thermocouple is available at node 312 and the temperature at node 311 is taken as the average of the two thermocouple readings at that position.

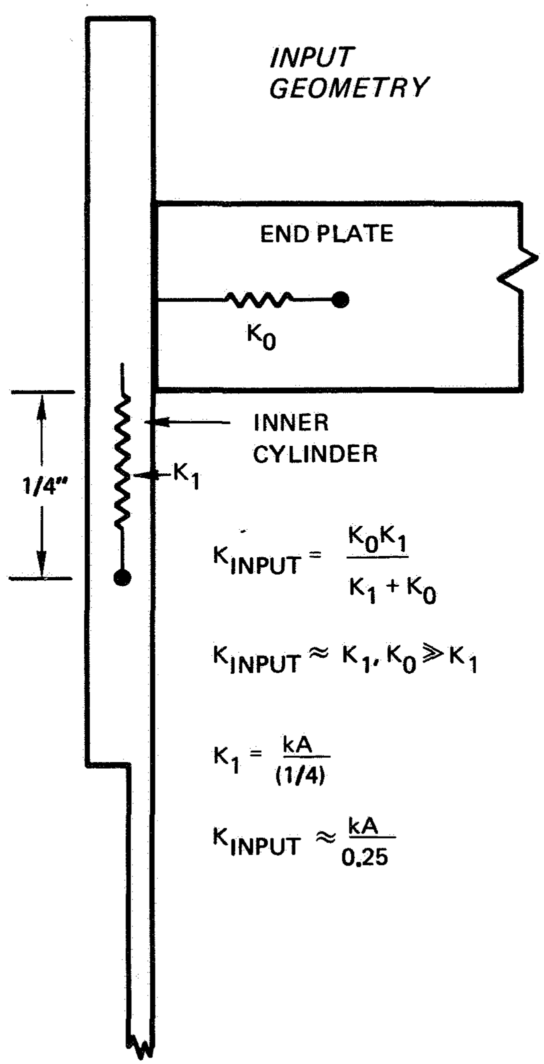

$$K_{INPUT} = \frac{K_0 K_1}{K_1 + K_0}$$

$$K_{INPUT} \approx K_1,\ K_0 \gg K_1$$

$$K_1 = \frac{kA}{(1/4)}$$

$$K_{INPUT} \approx \frac{kA}{0.25}$$

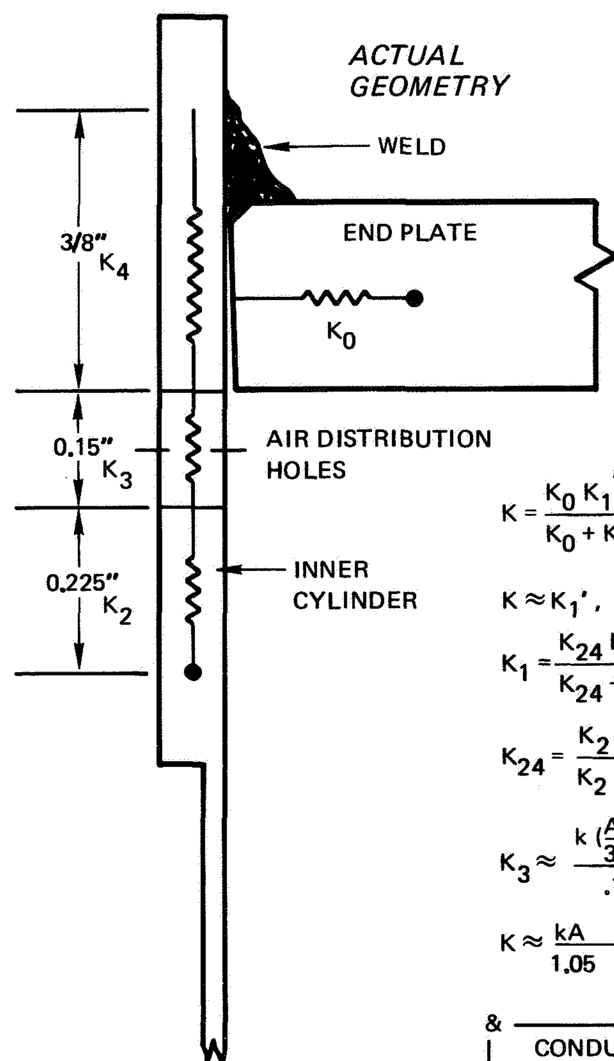

$$K = \frac{K_0 K_1'}{K_0 + K_1'}, \quad K_1' = \frac{1}{1/K_2 + 1/K_3 + 1/K_4}$$

$$K \approx K_1',\ K_0 \gg K_1'$$

$$K_1 = \frac{K_{24} K_3}{K_{24} + K_3}$$

$$K_{24} = \frac{K_2 K_4}{K_2 + K_4} = \frac{kA}{0.6}$$

$$K_3 \approx \frac{k\left(\frac{A}{3}\right)}{.15} = \frac{kA}{0.45}$$

$$K \approx \frac{kA}{1.05}$$

& CONDUCTANCE RATIO

$$\frac{K}{K_{INPUT}} \approx 0.25$$

Figure II-53: END PLATE TO INNER CYLINDER CONNECTION

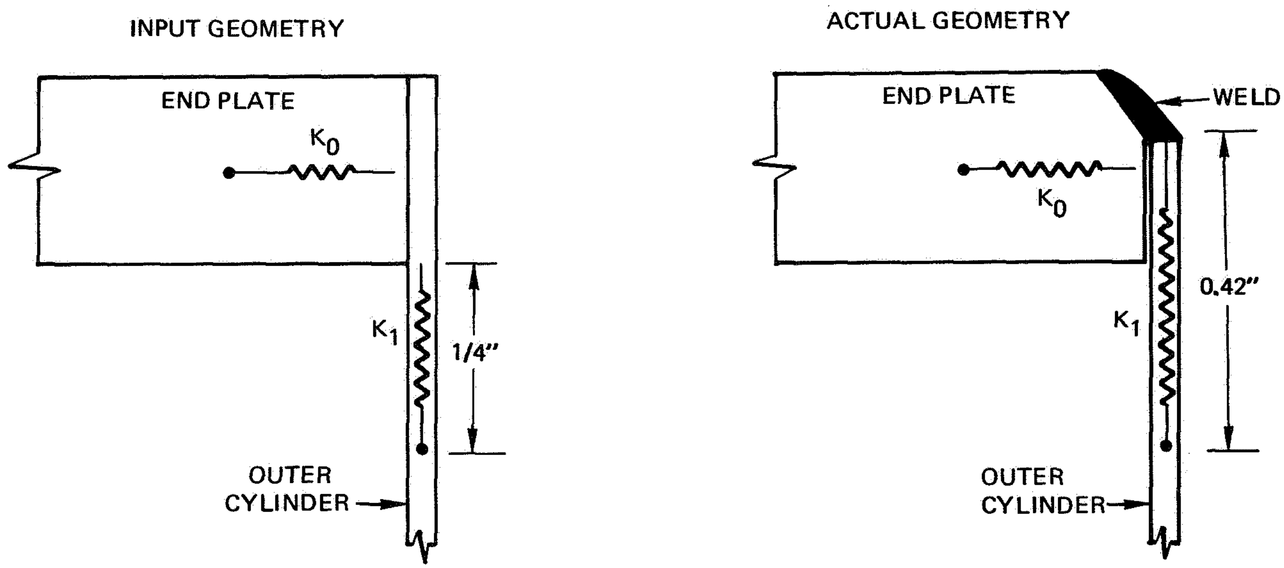

$$K_{INPUT} = \frac{K_0 K_1}{K_1 + K_0}$$

$$\approx K_1;\ K_0 \gg K_1$$

$$\approx \frac{kA}{.25}$$

$$K = \frac{K_0 K_1}{K_0 + K_1}$$

$$\approx K_1;\quad K_0 \gg K_1$$

$$\approx \frac{kA}{0.42}$$

CONDUCTANCE RATIO

$$\frac{K}{K_{INPUT}} \approx 0.6$$

Figure II-54: END PLATE TO OUTER CYLINDER CONNECTION

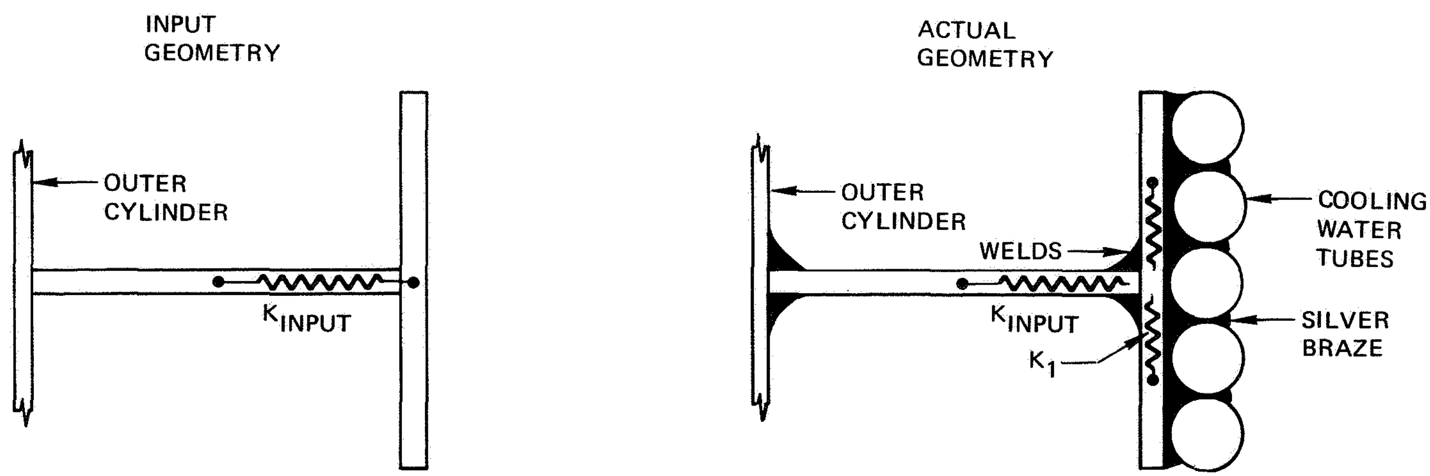

$$K = \frac{K_{INPUT}\,(2\,K_1)}{2\,K_1 + K_{INPUT}}$$

$$K_1 \approx 2\,K_{INPUT}$$

$$K \approx \frac{4}{5}\,K_{INPUT}$$

CONDUCTANCE RATIO

$$\frac{K}{K_{INPUT}} \approx 0.8$$

Figure II-55: COOLING FIN GEOMETRY

3. There is greater scatter in the data on one half of the model than the other half.

   The side with the larger scatter has the thermocouple and heater leads routed through it and the scatter is probably related to the heat leak not being calculated properly.

4. There is a tendency for the conductance ratio to increase along the outer cylinder from the end plate to the fin especially for nodes 412 to 407.

   This may be caused by too much radiation heat transfer in the thermal math model. The script F values were calculated for an emissivity of 0.88 whereas the measured sample value was 0.85 before baking at 400°F and 0.88 after baking.

5. The conductance ratio is generally less than unity.

   Possibly the input value of thermal conductivity for the stainless steel is somewhat larger.

6. The data scatter appears to be systematic with heat input, especially for nodes 201 to 204 and 401 to 405.

   This is probably due to the heat leak not being calculated properly.

7. The scatter in the data is largest in regions away from the heater section and cooling fin.

   These are the regions in which the conductive heat transfer is small and minor error elsewhere are amplified in these regions.

Table II-13 outlines the 25 thermal math model upgrading runs. These runs investigated the effects of changes in the following aspects of the math model:

- Radiation exchange factors (emissivity)
- Air supply and return tube effective conductance to ambient
- Heater lead routing and conductance
- Foam insulation conductance
- Heat leak due to vacuum line penetrations into foam
- Thermal conductivity of phenolic air distribution plugs
- Conductance between heater and inner cylinder wall
- Conductivity of stainless steel

The second upgrading run reduced the emissivity from 0.88 to about 0.865 (assuming $F/F_o = (\varepsilon/\varepsilon_o)^2$). The results of this run are shown in Figure II-56. The emissivity change corrected the tendency of the conductance ratio to increase along the outer cylinder toward the fin. However, the data scatter increased for the end plates and outer cylinder. A more detailed evaluation was then made of the heat leaks and the conductances of several heat flow paths were changed for run 3. The results of this run, shown in Figure II-57, show some reduction in the data scatter. Runs 4-9 investigate the effects of changes in thermal conductivity of stainless steel and phenolic, heater lead routing and increased conductance of the air lines. The changes for the phenolic had little effect on the results. The increase in thermal conductivity for steel slightly increased the scatter. The routing of the heater leads to the outer air distribution plug and the increase of the air tube conductances somewhat reduced the data scatter.

Runs 10 and 11 compared the extreme cases of the heater leads having no interaction with the model between the heater and ambient and of the heater leads having no direct interaction with ambient. Connecting the heat leads directly to ambient, run 10, resulted in reduced data scatter for the top end plate, nodes 201-204, and upper half of the inner cylinder, nodes 401-406. However, the resulting conductance values for the top end plate appeared unrealistically low ($k_{upgraded}/k_{input} \approx 0.7$). Disconnecting the heater leads from ambient and connecting them directly to node 520, run 11, increased the conductance values, but also increased the data scatter. Run 12 was made in an attempt to reduce

TABLE II-13 THERMAL MATH MODEL UPGRADING RUNS

Run Number	Changes Made to Thermal Math Model
1	Original expanded math model
2	Script F's changed by factor of 0.966 from original values
3	Added effect of heater leads through insulation, K(284) = 0.0048; increased air tube conductances, K(280) & K(281) = 0.0011 k_{ss}; increased conductance of heater leads to air distribution plug, K(282) = 0.0048, K(283) = 0.00295; foam insulation conductance reduced to 0.9 of original value.
4	Increased thermal conductivity of stainless steel k_{ss} to 8.5 B/FT-HR-°F at 32°F data point
5	Heater leads connected to outer node (520) of air distribution plug with K(282) = 0.0038 and K(283) = 0.0026.
6	Decreased thermal conductivity of phenolic (air distribution plugs) from 0.11 to 0.09 B/FT-HR-°F
7	Increased thermal conductivity of phenolic to 0.3 B/FT-HR-°F
8	Reset phenolic conductivity to 0.11; increased conductance of air tubes to 0.0022 k_{ss}
9	Reset k_{ss} to 8.0 B/FT-HR-°F at 32°F
10	Connected heater leads directly to ambient with no connection to air distribution plugs
11	Heater leads connected to air distribution plug (node 520) and no connection to ambient, K(282) = 0.0038, K(283) = 0.0026
12	Script F's changed by factor of 0.977 from original values
13	Minor revisions made to Script F values to achieve symmetry
14	Script F's changed by factor of 0.933 from original values

15	Heater leads reconnected to ambient K(284) = 0.010; added conductance of vacuum lines to insulation, K(285) = 0.010.
16	Increased heater lead conductance to ambient, K(284) = 0.015; decreased vacuum line conductance, K(285) = 0.005
17	Conductance between heater and cylinder, K(106) & K(107), reduced from 0.23 to 0.12.
18	Script F's changed by factor of 0.955 from original values
19	Increased heater lead conductance to ambient, K(284) = 0.020; Increased vacuum line conductance to insulation, K(285) = 0.010; reset conductance from heater to cylinder, K(106) & K(107), to 0.23; set foam insulation conductivity equal to that of air.
20	Reset foam conductance to 0.9 of its original value; reset heater lead conductance to ambient to K(284) = 0.015; set vacuum line conductances to foam K(285) = 0.005
21	Increased conductance from heater to cylinder, K(106) & K(107), to 0.46
22	Set foam insulation conductivity equal to that of air
23	Script F's changed to 0.940 of original values; reset insulation conductance, K(106) & K(107), to 0.23.
24	Script F's changed to 0.946 of original values
25	Changed heater to cylinder conductance, K(106) & K(107), to 0.20

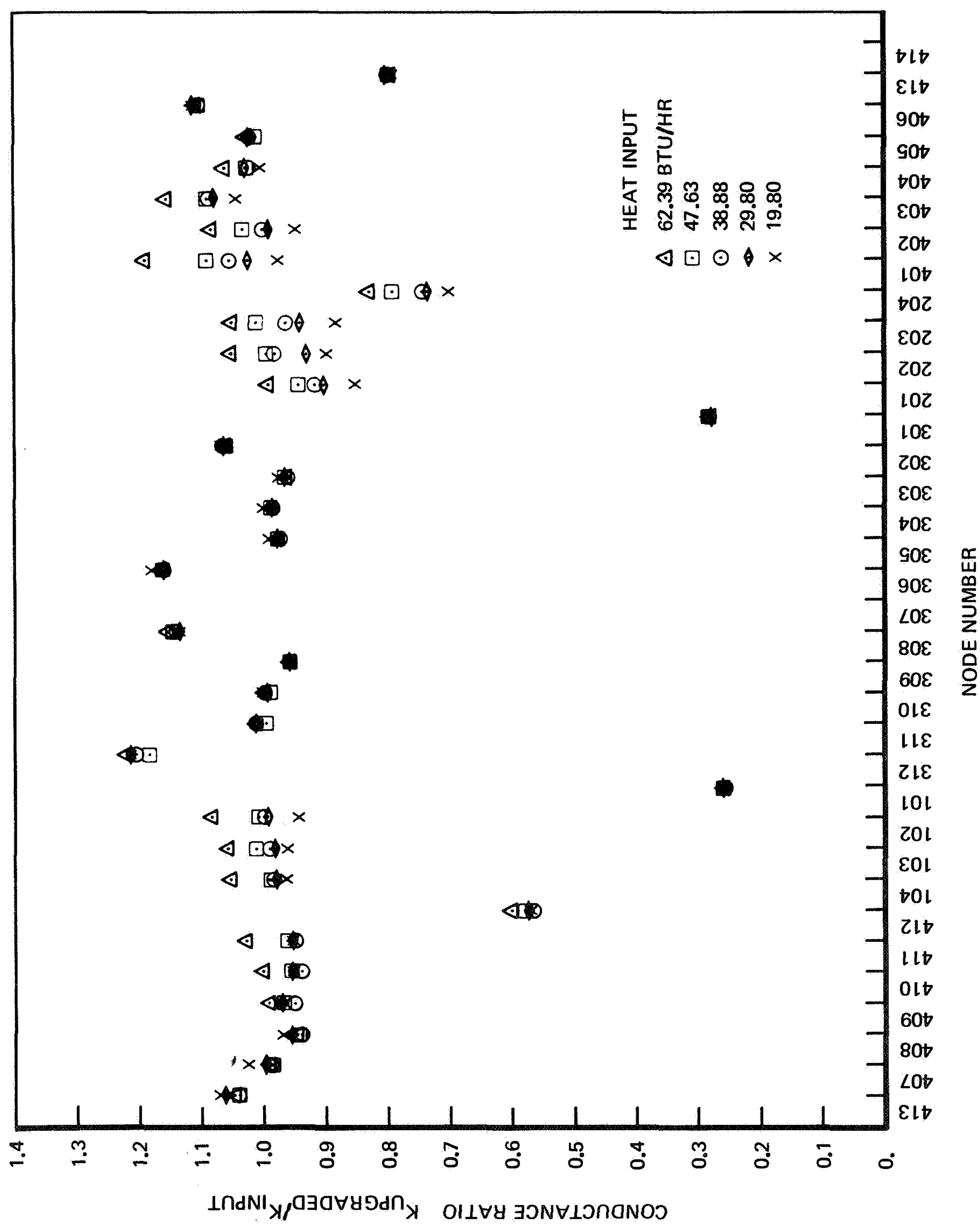

Figure II-56: UPGRADING RESULTS WITH REDUCED EMISSIVITY

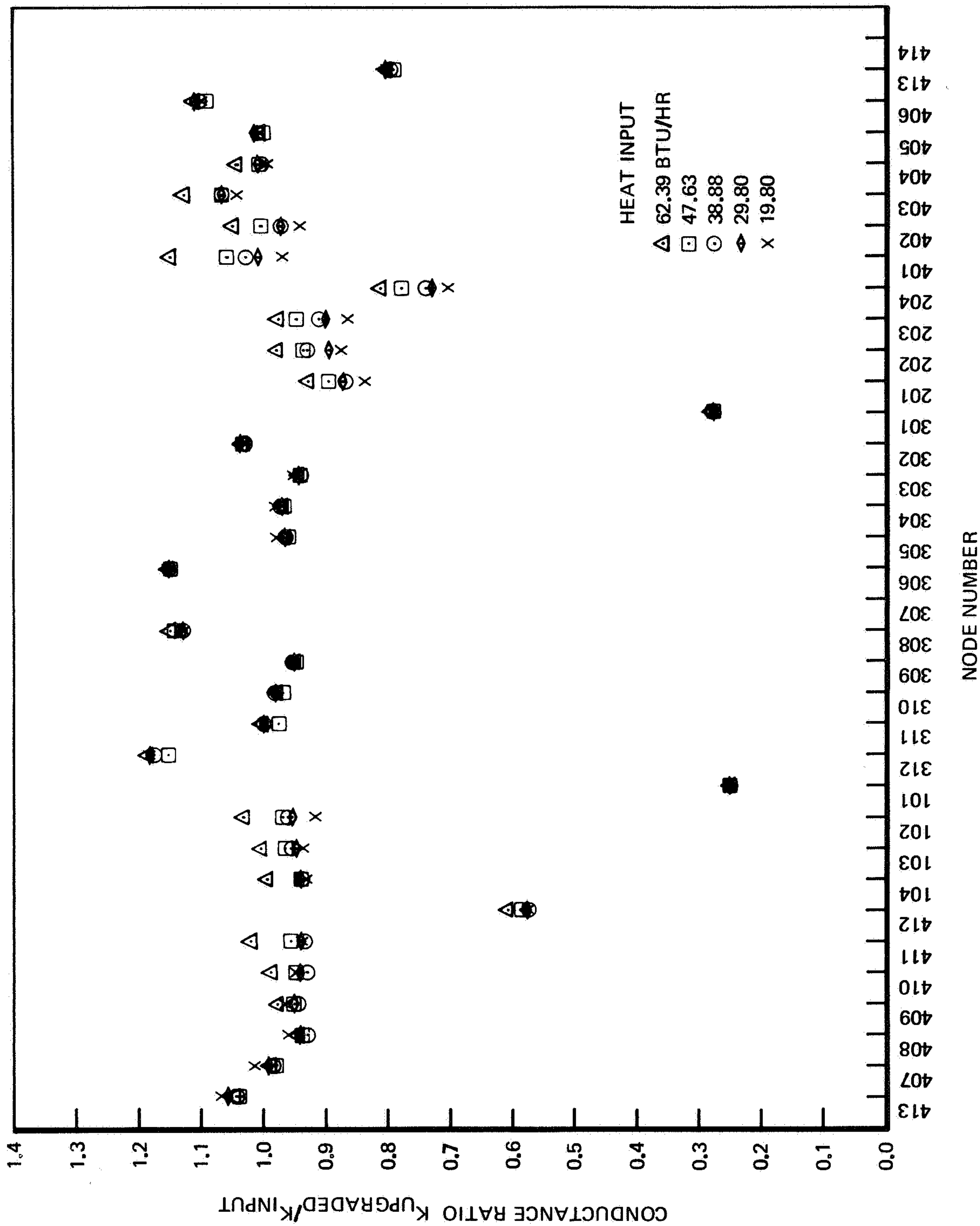

Figure II-57: UPGRADING RESULTS WITH REVISED HEAT LEAK PATHS the scatter by increasing the emissivity. This attempt was only partially successful and the results inconclusive.

At this point a complete check was made of the TMM to see if any errors were present. It was discovered that the radiation exchange factors (F's) were not quite symmetric. This occurred due to some redundant calculations being made for these factors with the results not being quite equal, i.e., the calculated values for A_iF_{ij} were not quite equal to those for A_jF_{ji}. Subsequently these radiation exchange factors were changed to be symmetric with the AF value taken as the average of the two calculated values. The results of run 13, a repeat of run 12 with the revisions to the radiator cards, showed the effects of these changes to be very minor.

The results for most of these remaining runs are shown in Figure II-58 and II-59 which give the average conductance ratio, $k_{upgraded}/k_{input}$, and the range of variation for this ratio, the difference between maximum and minimum divided by the average value.

Figure II-58 shows the effects of changing the penetration conductors K(284) (heater leads) and K(285) (vacuum lines), the conductors between the heater and the wall K(106, 107) and one case of emissivity change. The conductance of the insulating foam remained at its original input value.

Figure II-59 shows the effects of changing the emissivity, the foam conductance and the conductors between the heater and the wall.

Inspection of Figures II-58 and II-59 indicates that the upgraded conductance ratio is quite sensitive to changes in the TMM which are within the range of uncertainty. The range of variation in the conductance ratio is not so sensitive to these changes, however; the individual test run deviation from the average ratio is strongly affected by some of the changes in the TMM and different test runs give the extremum variations for a given conductor.

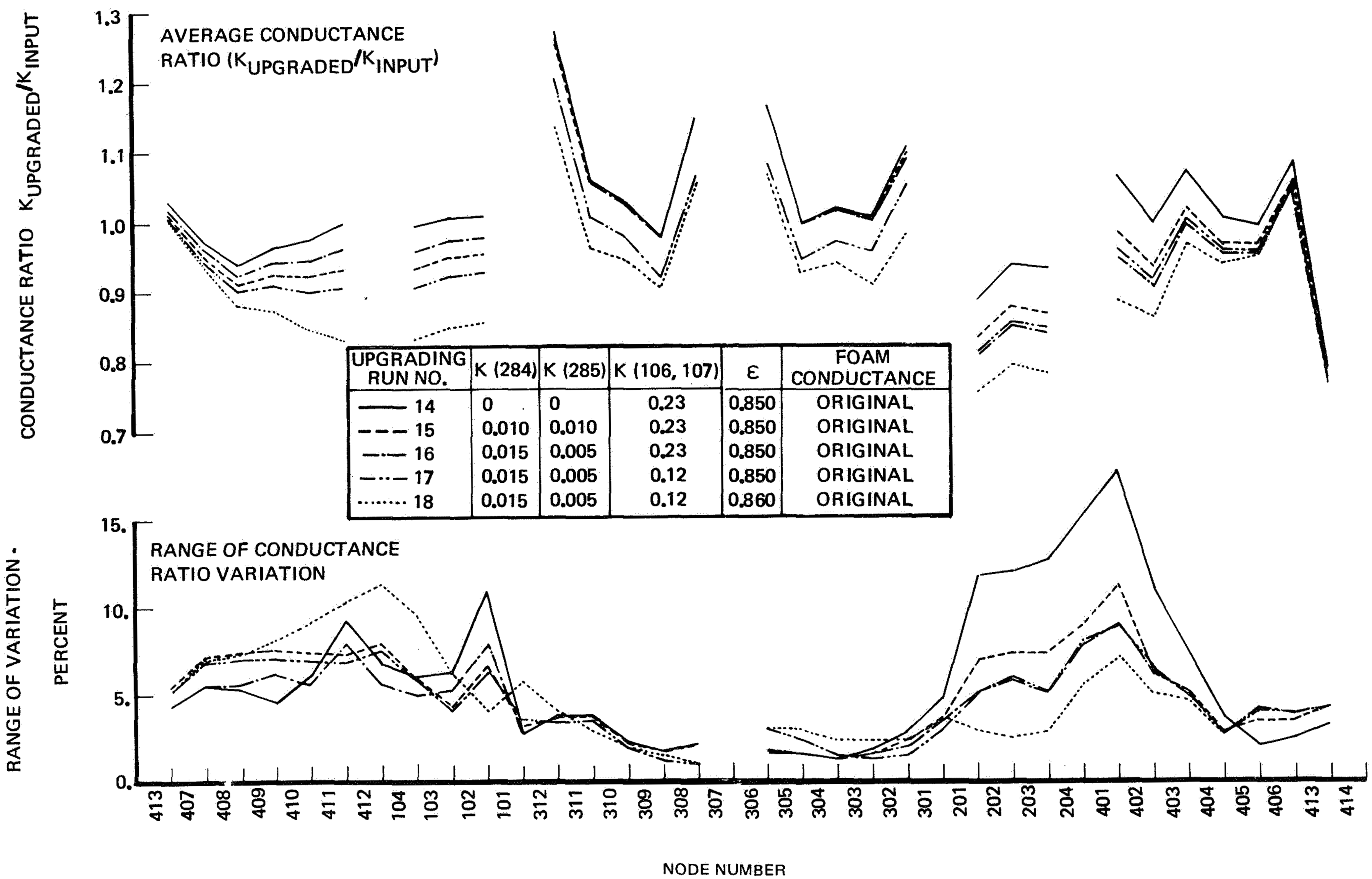

UPGRADING RUN NO.	K (284)	K (285)	K (106, 107)	ε	FOAM CONDUCTANCE
—— 14	0	0	0.23	0.850	ORIGINAL
– – – 15	0.010	0.010	0.23	0.850	ORIGINAL
–·– 16	0.015	0.005	0.23	0.850	ORIGINAL
–··– 17	0.015	0.005	0.12	0.850	ORIGINAL
······ 18	0.015	0.005	0.12	0.860	ORIGINAL

Figure II-58: UPGRADING RESULTS FOR TEST RUNS 10, 14, 15, 16, AND 17

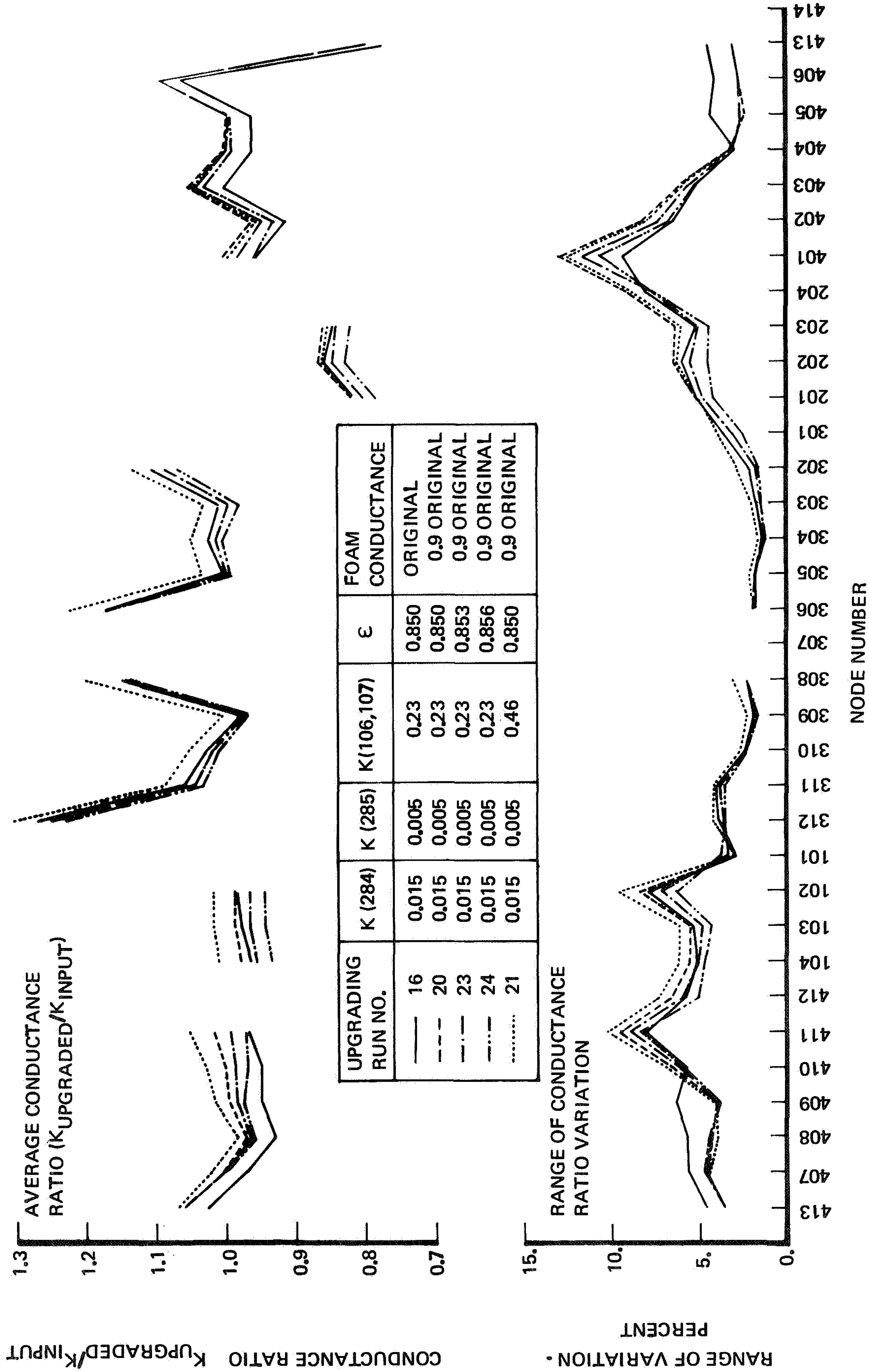

UPGRADING RUN NO.	K (284)	K (285)	K(106,107)	ε	FOAM CONDUCTANCE
16	0.015	0.005	0.23	0.850	ORIGINAL
20	0.015	0.005	0.23	0.850	0.9 ORIGINAL
23	0.015	0.005	0.23	0.853	0.9 ORIGINAL
24	0.015	0.005	0.23	0.856	0.9 ORIGINAL
21	0.015	0.005	0.46	0.850	0.9 ORIGINAL

Figure II-59: UPGRADING RESULTS FOR TEST RUNS 10, 14, 15, 16, AND 17

Consideration was given to the detailed results of the upgrading runs in an attempt to discover cause and effect relationships between the results. In many cases apparent cause and effect relationships for the scatter at the top end of the model have the opposite effect at the bottom end of the model.

The following aspects of the model may be responsible for limiting the degree to which the thermal math model could be upgraded:

- Paint emissivity - The emissivity of the paint may be temperature dependent or the paint may not be uniform over the surfaces.
- Foam Insulation - The foam insulation may not be uniform in properties. (The insulation was formed by pouring several batches of foam.)
- Conductance between heater and cylinder - The conductance between the heater and cylinder may be nonuniform and is probably influenced by the "joint conductance" between the RTV and cylinder wall. The "joint conductance" is strongly dependent on the pressure at the joint and consequently strongly dependent on the heater temperature.

II.5.7.2 Free Convection Test Series Correlations

II.5.7.2.1 1/4 Scale Model Nusselt Number Correlation

The 1/4 scale model data for the free convection test series are listed in Appendix II-A.1.2. Typical temperature distributions are shown in Figure II-60 for different pressures at a given heating rate.

Application of the Nusselt number preservation scaling technique to the free convection tests requires the Nusselt number to be correlated with the Grashof number. Appropriate definitions of the Nusselt and Grashof numbers must be made in order to achieve a correlation between them.

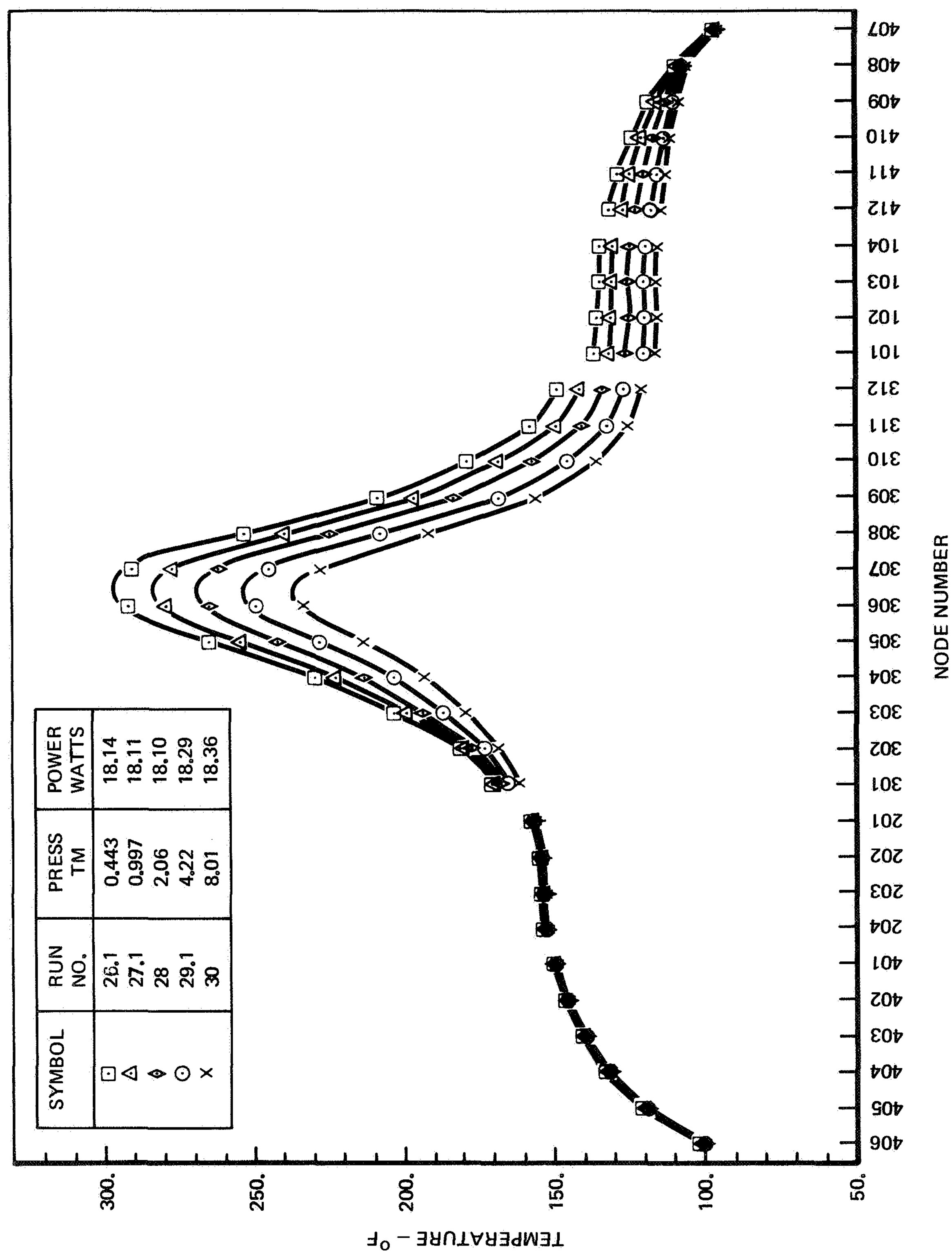

Figure II-60: TYPICAL FREE CONVECTION TEST TEMPERATURE DISTRIBUTIONS 1/4 SCALE MODEL – HIGH HEATING RATE

The critical factor in these definitions is the temperature differences that are used. The Grashof number is generally based on the characteristic temperature difference between the wall and the gas and the local Nusselt number is generally based on the local temperature difference between the wall and the gas. In the model tests there were no measurements of the gas temperature distribution, consequently either the gas temperature must be calculated in some manner or other temperature differences must be used. It should be noted that measurement of the gas temperature distribution would add a large amount of instrumentation and would probably result in complicating the problem.

Two subroutines were developed for the expanded thermal math model to analyze the 1/4 Scale Model "Free Convection Test Series" data. One subroutine was used to input the upgraded conductance values and the other used to analyze the convective heat transfer in the model. The upgraded conductances and other pertinent parameters from upgrading run number 20 were used in the data analysis. The data analysis subroutine makes a thermal balance at each node and determines the convective heat transfer rate. The Nusselt number for each node and the Grashof number for the test run are then calculated. Several definitions for the Nusselt and Grashof numbers were tried before an adequate correlation was achieved.

The first correlation attempt based the Nusselt number on the difference between the node and average gas temperature, i.e.,

$$Nu_i = \left(\frac{L Q_g^i}{k_g^i A_i}\right)\left(T_i - \bar{T}_g\right)$$

where

Nu_i = Nusselt number at node i

k_g^i = gas thermal conductivity at T

A_i = area of node i

Q_g^i = heat transfer to gas from node i

T_i = temperature of node i

$\bar{T}_g$ = average gas temperatures

L = characteristic length (taken as 6 inches for the 1/4 scale model)

Using this definition of the Nusselt number and noting that the net heat transfer to the gas must be zero, the average gas temperature can be written as

$$\bar{T}_g = \frac{\sum_i k_g^i A_i Nu_i T_i}{\sum_i k_g^i A_i Nu_i}$$

The subroutine used an iterative process to solve these equations for the average gas temperature and the local Nusselt numbers. The Grashof number was based on the rms temperature difference between the wall and the gas with an area weighting factor, i.e.,

$$Gr = \left(\frac{\rho^2 g \beta L^3}{\mu^2}\right) \frac{\sum_i A_i \sqrt{(T_i - \bar{T}_g)^2}}{\sum_i A_i}$$

The results of this analysis, using the average gas temperature, failed to produce a correlation between the Nusselt and Grashof numbers. The calculated thermal balances, however, were useful in further correlation attempts.

The calculated overall thermal balance, using the upgraded conductance values from upgrading run No. 20, is shown in Table II-14 for each of the "Free Convection Test Series" runs. An overall thermal balance is achieved to within 3.5 percent of the heat input for all of the runs. There is, however, a calculated net heat transfer to the gas for all of the runs which is about 8 percent of the heat input for the worse case. This indicates further upgrading of the TMM may be required. It is interesting to note that up to 70 percent of the heat input is transferred to the gas.

Since the use of the average gas temperature did not allow a correlation of the data the detailed computer results were used to search for a new analysis scheme. The proper gas temperature to use in the calculation of convective heat transfer from the common equation $Q = hA\,(T_w - T_g)$ is known at the two locations on the model where the heat transfer to the gas is zero. At these points $T_w = T_g$. Having these two gas temperatures it is possible to calculated the gas temperature variations around the model from the calculated heat transfer to

TABLE II-14 CALCULATED THERMAL BALANCE FOR 1/4 SCALE MODEL FREE CONVECTION RUNS

Test Run No.	Press. ATM	Heat Input Btu/Hr	Heat Loss Thru Fin Btu/Hr	Heat Loss Thru Insulation Btu/Hr	Heat Into Gas Btu/Hr	Heat Out of Gas Btu/Hr	Net Heat to Gas Btu/Hr	Total Heat Loss Btu/Hr	Heat in Minus Heat Out Btu/Hr
18	1/2	19.84	16.81	2.34	6.77	6.11	0.66	19.81	+ 0.03
19	1	19.89	17.02	2.12	8.57	7.71	0.86	20.00	- 0.11
21	1/2	29.83	24.24	5.18	9.66	9.17	0.49	29.91	- 0.08
20.1	1	29.95	24.53	4.97	12.03	11.41	0.62	30.12	- 0.17
37.1	2	29.81	23.76	4.50	14.80	14.18	0.62	28.88	+ 0.93
38.1	4	29.83	24.63	4.35	17.59	16.18	1.41	30.39	- 0.56
39	8	29.85	24.57	3.90	20.61	18.20	2.41	30.88	- 1.03
22	1/2	40.05	31.60	7.80	12.04	11.33	0.71	40.11	- 0.06
23	1	39.98	31.64	7.51	15.64	14.78	0.86	40.01	- 0.03
34	2	39.89	31.49	7.37	19.00	17.89	1.11	39.97	- 0.08
35.1	4	40.03	32.13	6.84	23.23	21.60	1.63	40.60	- 0.57
36	8	39.98	32.12	6.47	27.09	24.43	2.66	41.25	- 1.27
25	1/2	47.61	36.82	9.66	14.19	13.37	0.82	47.30	+ 0.31
24	1	47.61	37.11	9.54	18.19	17.44	0.75	47.40	+ 0.21
31.2	2	47.74	37.62	8.97	22.50	20.94	1.56	48.15	- 0.41
32.1	4	47.86	37.72	8.85	27.22	25.33	1.89	48.46	- 0.60
33	8	47.88	38.06	8.30	31.91	29.03	2.88	49.24	- 1.36
26.1	1/2	61.91	47.08	13.28	17.09	16.05	1.04	61.40	+ 0.51
27.1	1	61.80	46.88	12.94	22.84	21.50	1.34	61.16	+ 0.64
28	2	61.77	47.20	12.60	28.59	26.69	1.90	61.70	+ 0.07
29.1	4	62.43	48.40	12.57	34.67	32.50	2.17	63.14	- 0.71
30	8	62.65	48.87	12.05	40.22	37.55	2.67	63.59	- 0.94

the gas, assuming a uniform gas circulation, by integrating the heat transfer to the gas between the two positions, i.e.,

$$T_g(x) = T_g(x_0) + \left[T_g(x_1) - T_g(x_0)\right] \frac{\int_{x_0}^{x} Q_g\,dx}{\int_{x_0}^{x_1} Q_g\,dx}$$

A hand calculation was made for test run 20.1, using the calculated thermal balance, to determine the gas temperature variation around the model. Figure II-61 shows the model and calculated gas temperature as well as the heat transfer to the gas at each affected node. The Nusselt number, based on the local temperature difference between the gas and the wall, could probably be correlated with the Grashof number. However, it would be difficult to use this correlation in the full scale model analysis. Consequently a simpler correlation technique was sought.

If the temperature profiles for all of the test runs are similar to those shown in Figure II-61, then the Nusselt number could be based on a characteristic temperature difference and a correlation with the Grashof number should be obtained. For similar temperature profiles the temperature crossover points should remain at the same position. A calculation of these crossover points showed that their positions were nearly the same for all of the test runs. Table II-15 lists these positions for each run. The slight variations of position may be due to inaccuracies in the TMM.

A direct correlation of the local heat transfer to the gas as a function of Grashof number was tried but was not successful. However, the heat transfer to the gas divided by a characteristic temperature difference showed promise of correlating with the Grashof number based on this temperature difference.

Consequently the data analysis scheme was revised to base both the Nusselt and Grashof numbers on a characteristic temperature difference, i.e.,

$$Nu_i = \frac{\dot{Q}_g^{\,i} L}{k_g^{\,i} A_i \Delta T_0}$$

and

$$Gr = \frac{\rho^2 g \beta L^3 \Delta T_0}{\mu^2}$$

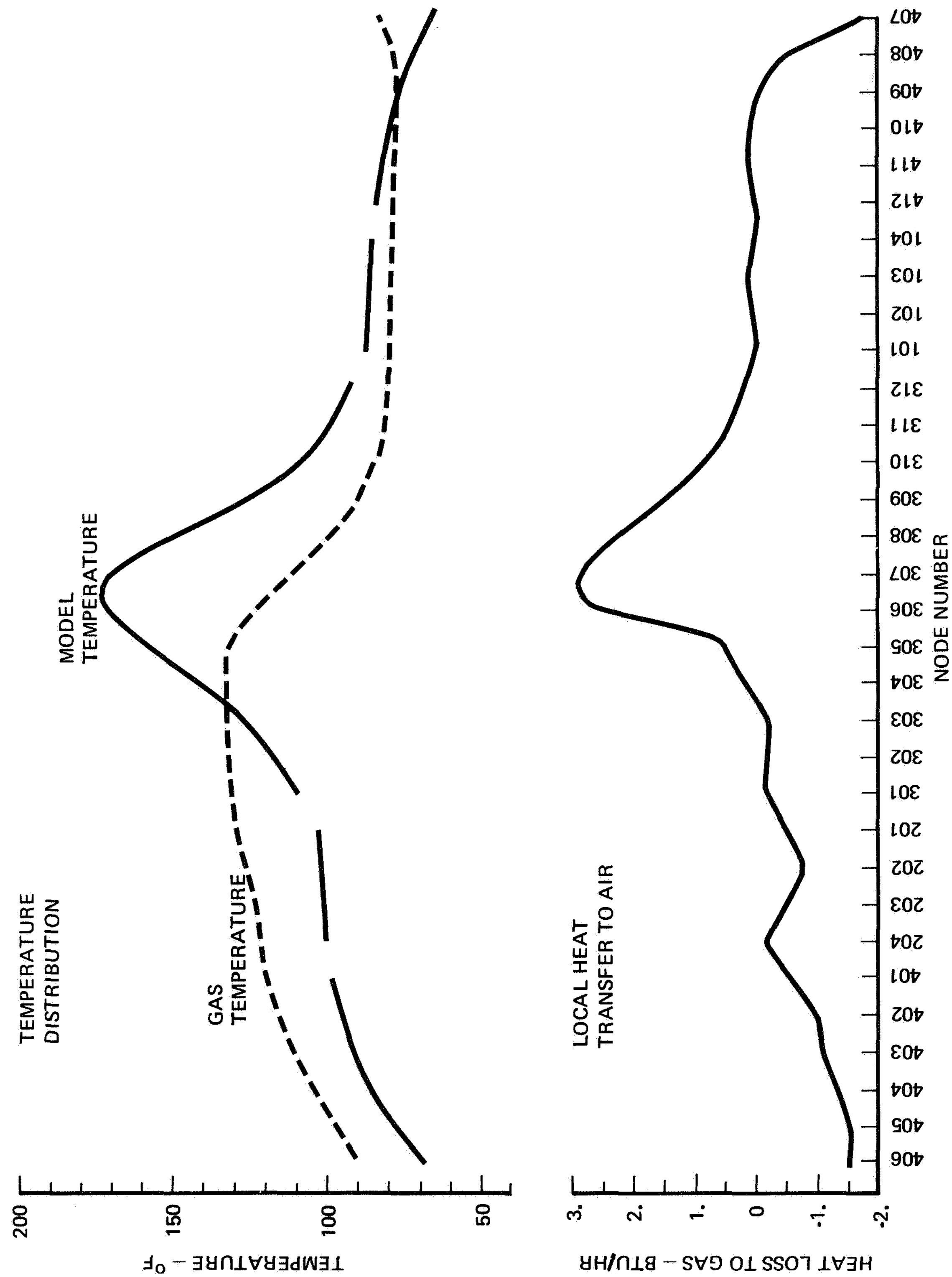

Figure II-61: DATA ANALYSES RESULTS FOR TEST RUN 20.1

TABLE II-15

CALCULATED POSITIONS WHERE HEAT TRANSFER TO GAS IS ZERO

Run Number	Outer Cylinder Wall - Inches From Top	Inner Cylinder Wall - Inches From Top
18	4.15	1.48
19	4.20	1.45
21	4.15	1.50
20.1	4.35	1.46
37.1	4.24	1.42
38.1	4.43	1.37
39	4.42	1.31
22	4.22	1.51
23	4.34	1.48
34	4.40	1.38
35.1	4.46	1.40
36	4.45	1.32
25	4.49	1.51
24	4.46	1.49
31.2	4.37	1.46
32.1	4.48	1.42
33	4.44	1.34
26.1	4.51	1.57
27.1	4.44	1.54
28	4.42	1.50
29.1	4.48	1.44
30	4.51	1.40

The characteristic temperature difference was defined as one half of the difference between the average inner and outer cylinder temperatures,

$$\Delta T_o = \frac{1}{2}\left(\bar{T}_{inner} - \bar{T}_{outer} \right)$$

The results of this analysis produced a correlation between the Nusselt and Grashof numbers. These results are listed in Appendix II-B. Since the Nusselt number is based on a characteristic temperature difference negative values are calculated for nodes which are heated by the gas and positive values for those cooled by the gas. The results were correlated by plotting the Nusselt number versus the Grashof number for each inner cylinder node, pairs of outer cylinder nodes and the four nodes (area averaged) of each end plate. As expected the data scatter for the nodes having large convective heat transfer was much less than that for those having a small convective heat transfer. Figure II-62 shows typical results for nodes having relatively large convection effects. The curves for the nodes are quite linear, however, their slopes differ. Figure II-63 shows typical results for nodes having small convection effects. The data scatter is relatively large and the correlation is marginal.

Since the variation of the heating rate at a given pressure does not produce large variations in the Grashof number the data were averaged at each pressure and the results plotted for all the nodes. Figure II-64 shows the correlation for the inner cylinder nodes and Figure II-65 shows the correlation for the outer cylinder and end plate nodes.

The Nusselt number variation around the model is shown for three Grashof numbers in Figure II-66. From this Figure it is apparent that the regions where the data scatter is large have negligible convection effects. Consequently the data correlation should be adequate for predicting the full scale model performance.

The Nusselt number preservation scaling technique investigation was terminated at this point. There was not adequate time to pursue this investigation to its completion. However, the work completed does allow an assessment of this scaling technique.

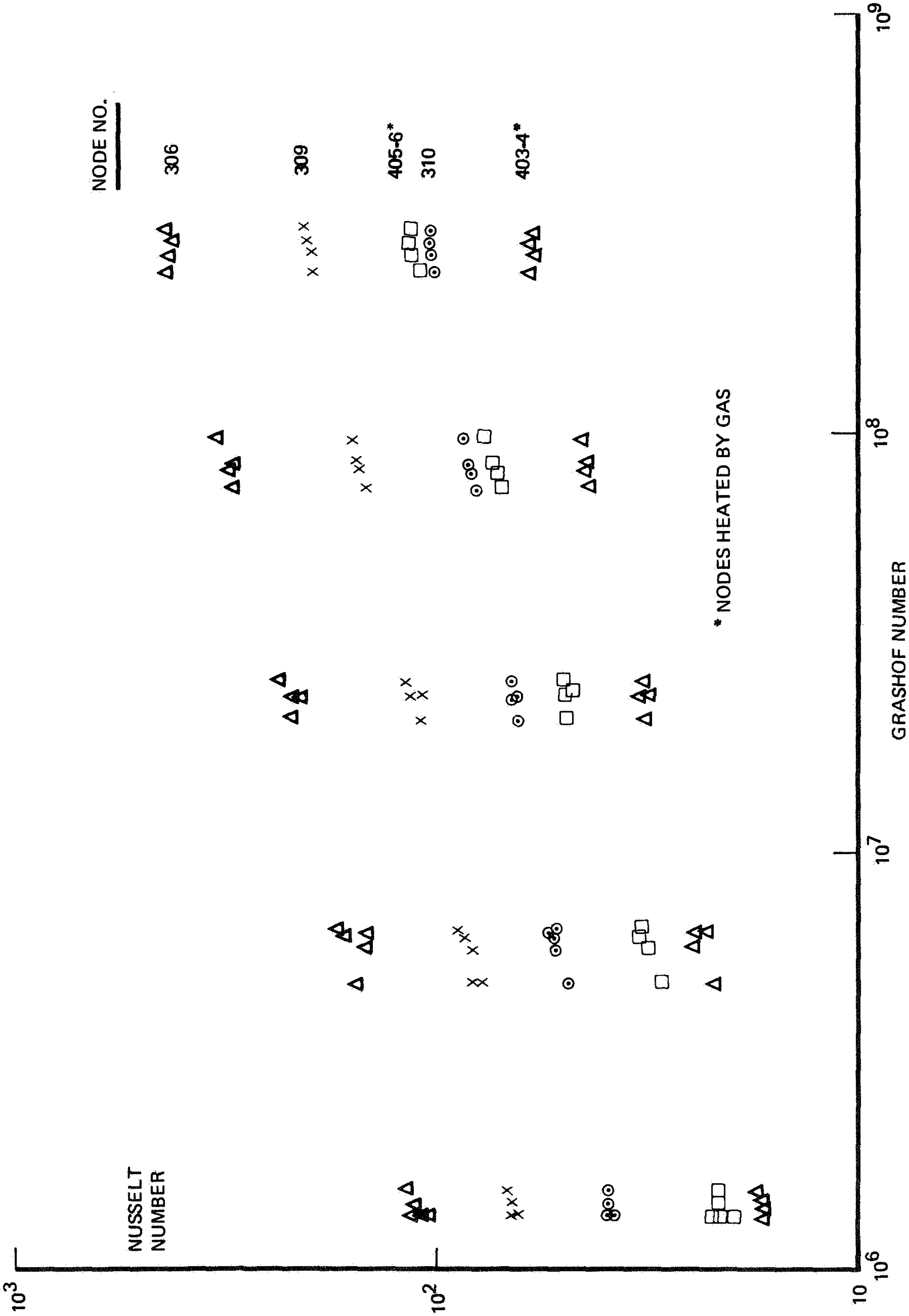

Figure II-62: TYPICAL NUSSELT NUMBER CORRELATIONS FOR REGIONS WITH LARGE CONVECTION EFFECTS

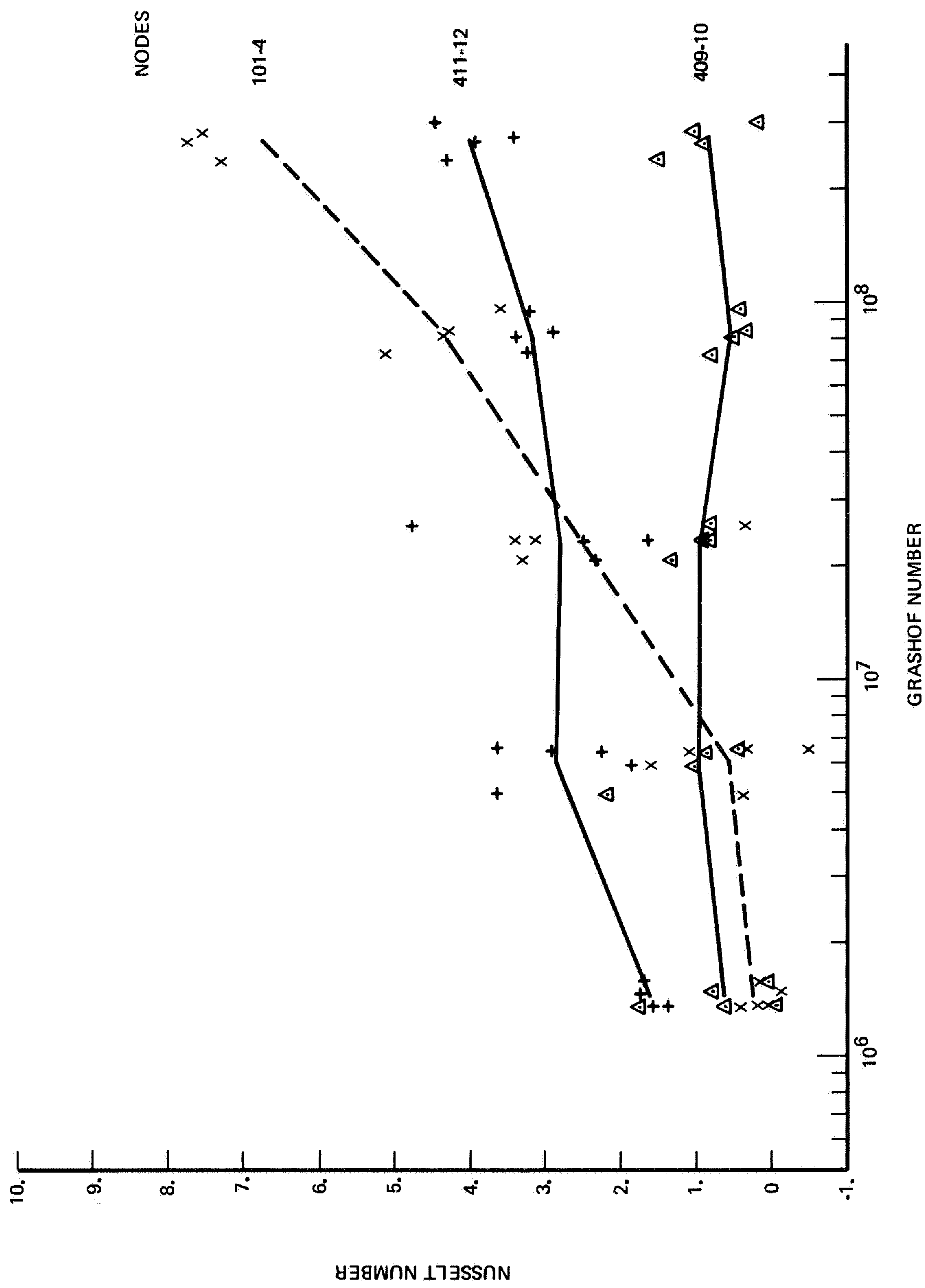

Figure II-63: TYPICAL NUSSELT NUMBER CORRELATIONS FOR REGIONS WITH SMALL CONVECTION EFFECTS

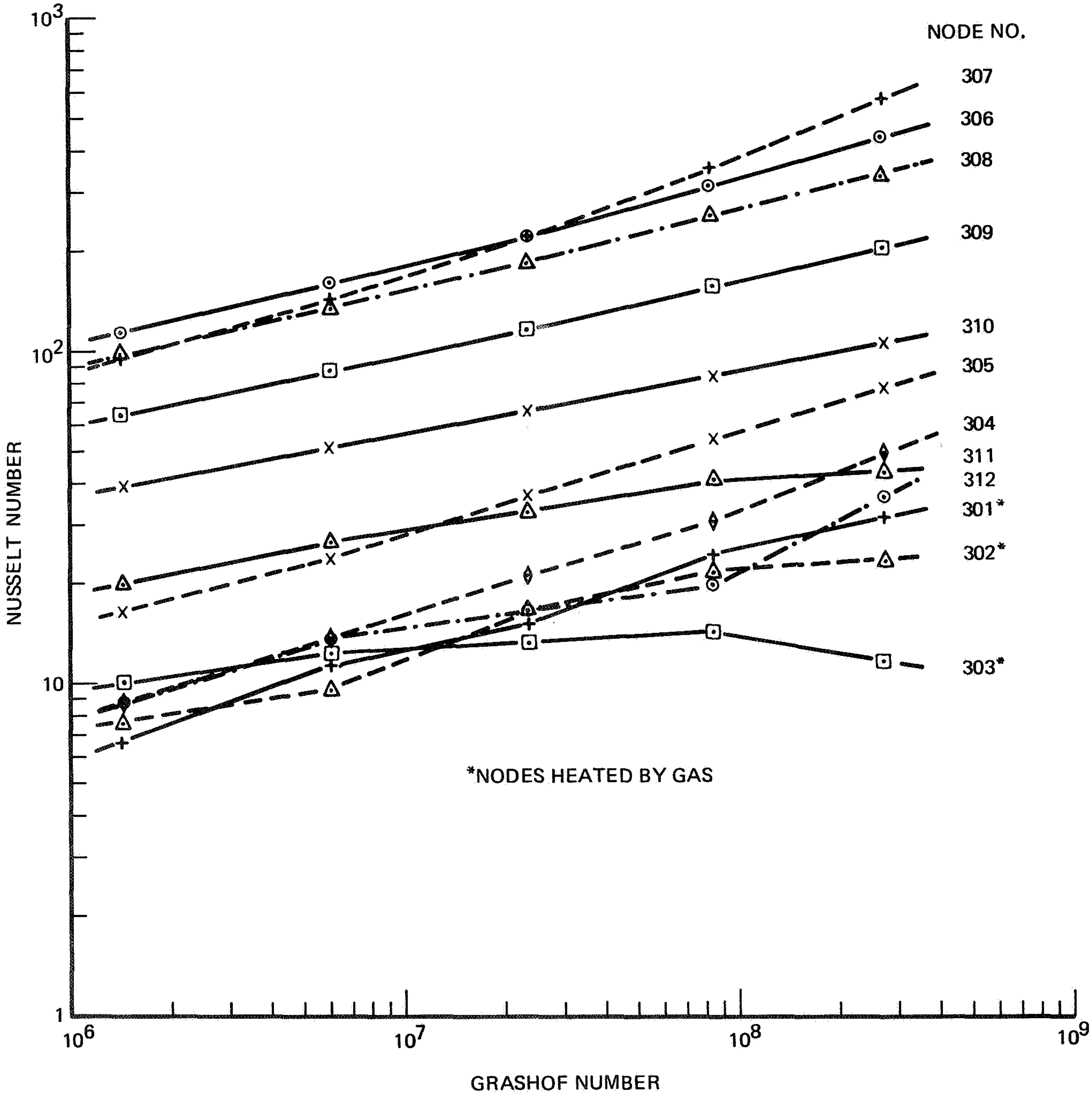

Figure II-64: NUSSELT NUMBER CORRELATION FOR INNER CYLINDER NODES

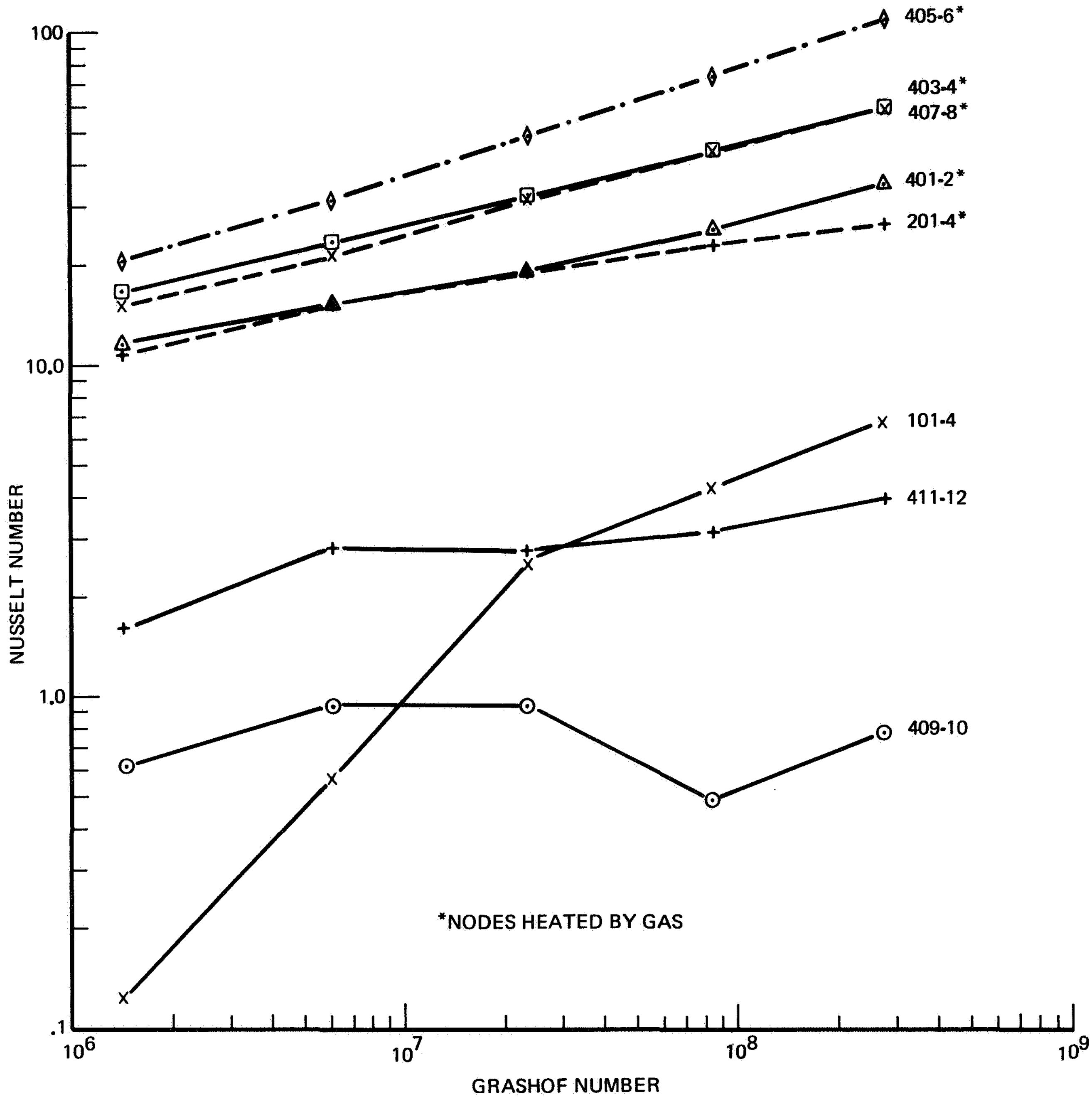

Figure II-65: NUSSELT NUMBER CORRELATION FOR OUTER CYLINDER AND END PLATE NODES

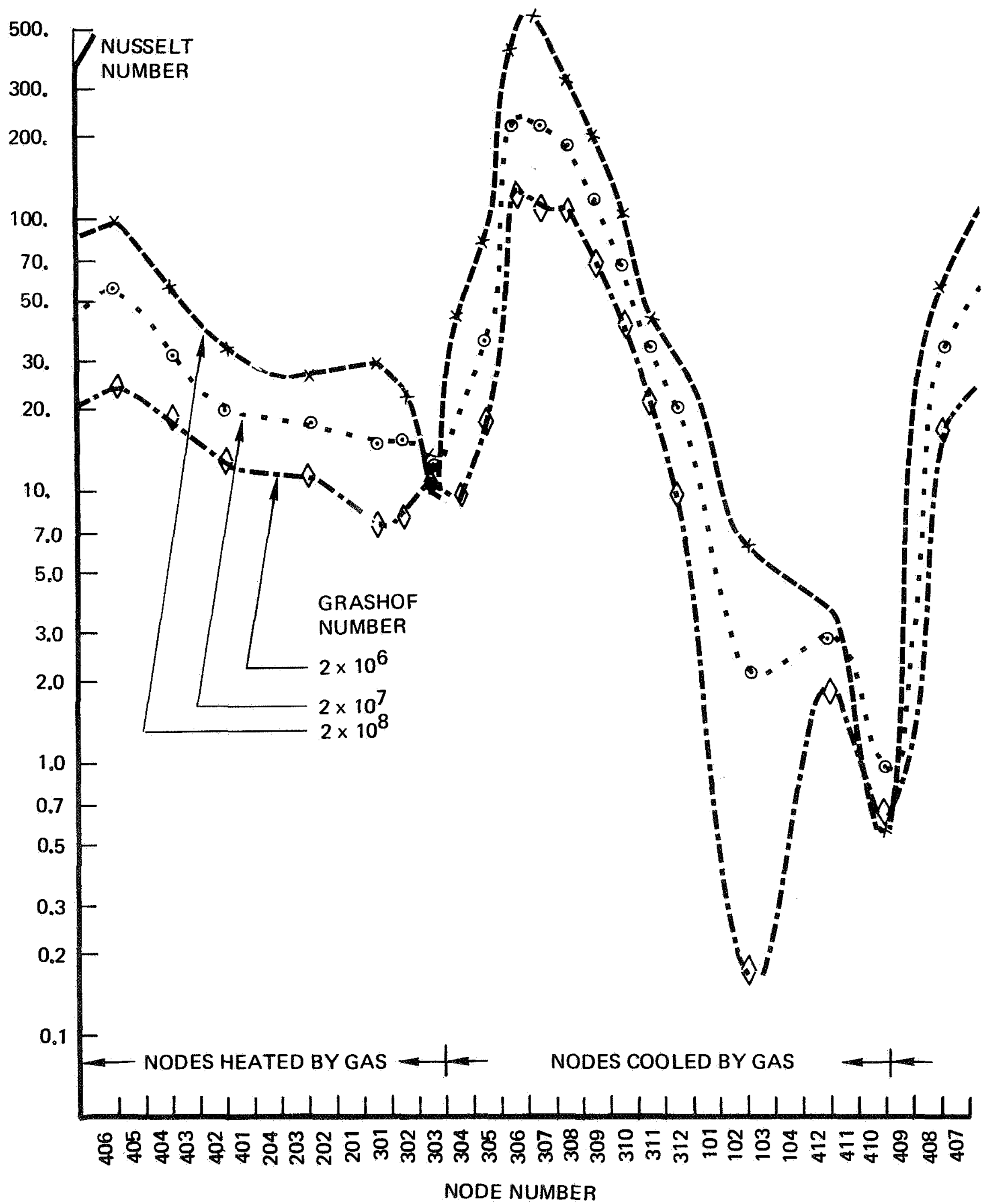

Figure II-66: NUSSELT NUMBER VARIATION AROUND MODEL

The Nusselt number correlation developed for the free convection test series using the 1/4 scale model can be used with an expanded thermal math model of the full scale model to predict its thermal performance. This expanded math model would make use of the information gained from upgrading the thermal math model for the 1/4 scale model. In particular the conductances at the weld joints would be reevaluated.

It should be possible to develop a Nusselt number correlation for the forced convection test series using the 1/4 scale model data. This correlation is expected to be more complex and more difficult to develop than that for free convection. The amount of time and effort required to develop this correlation cannot be accurately predicted.

II.5.7.2.2 Correlation Between Full Scale and 1/4 Scale Models

The results of the 1/4 scale model free convection tests made at a pressure of 1/2 atmosphere were compared directly with the full scale model free convection tests (the full scale model free convection test series data are listed in Appendix II-A.2.1). This comparision is shown in Figure II-67. The full scale model temperatures are somewhat greater than those for the 1/4 scale model. This temperature difference is greater at the higher heating rates. The temperature difference between the full scale and 1/4 scale models is shown for the highest and lowest heating rate cases in Figure II-68.

The temperature measurements for the full scale model heater section (nodes 306 and 307) appear to be somewhat erroneous. This was expected because of the earlier problems with these thermocouple installations. Apart from these nodes the maximum temperature difference for the highest heating rate is about 13°F and that for the lowest heating rate 3.5°F. These temperature differences are probably caused by slightly different emissivities in 1/4 scale and full scale model. The paint sample measurements taken after "baking" gave an emissivity of 0.83 for the aluminum base and 0.88 for the stainless steel base. It is estimated that this difference could result in a higher full scale model temperature by as much as 20°F at the heater section for the highest heating rate case. Other differences between the 1/4 scale and full scale models do not explain the measured temperature differences. The differences in conduction between the models tends to lower the full scale model temperatures relative to those of the 1/4 scale model. This is the reverse of what is observed.

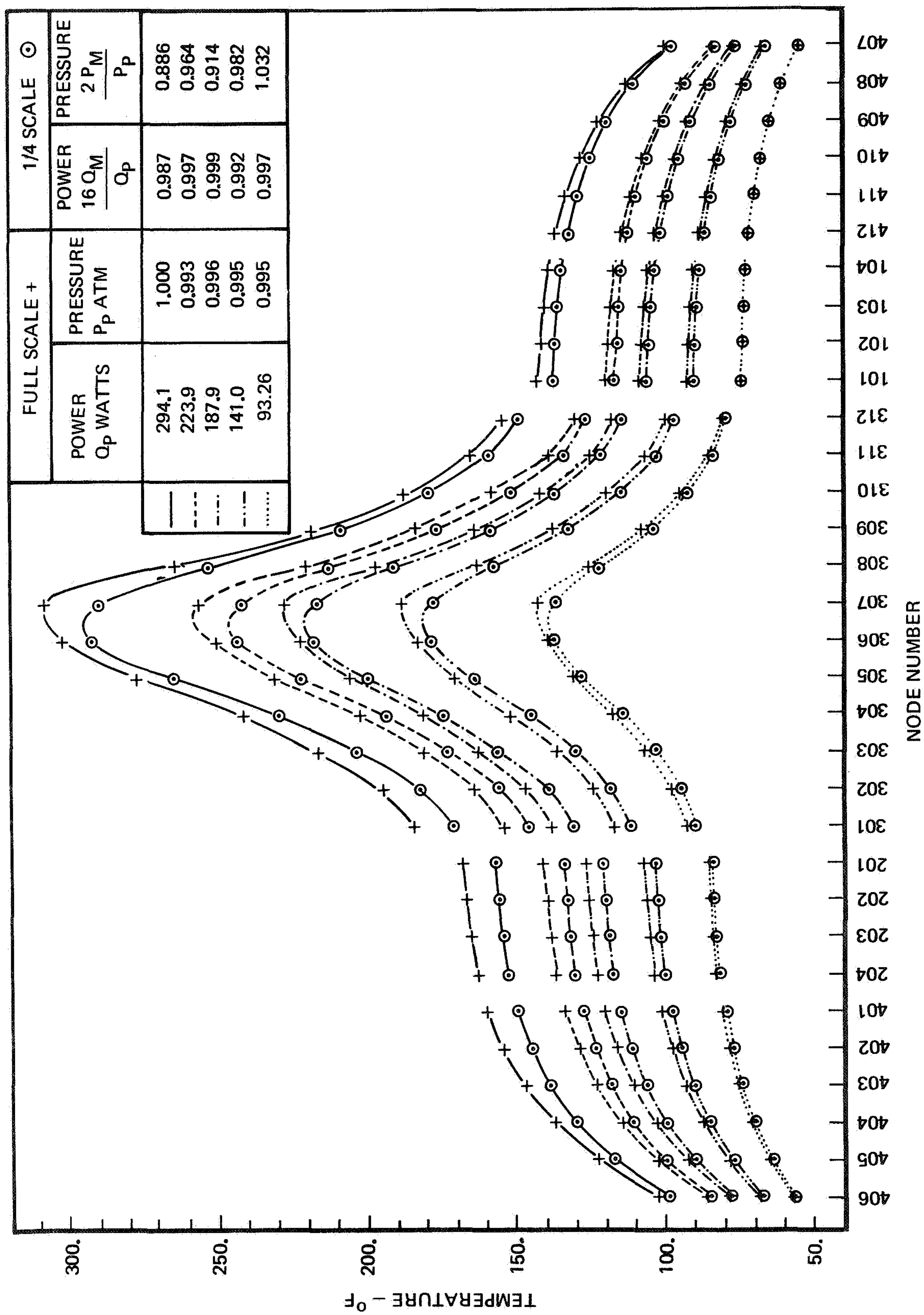

Figure II-67: THERMAL SCALE MODELING CORRELATION BETWEEN 1/4 SCALE AND FULL SCALE MODELS – FREE CONVECTION TESTS

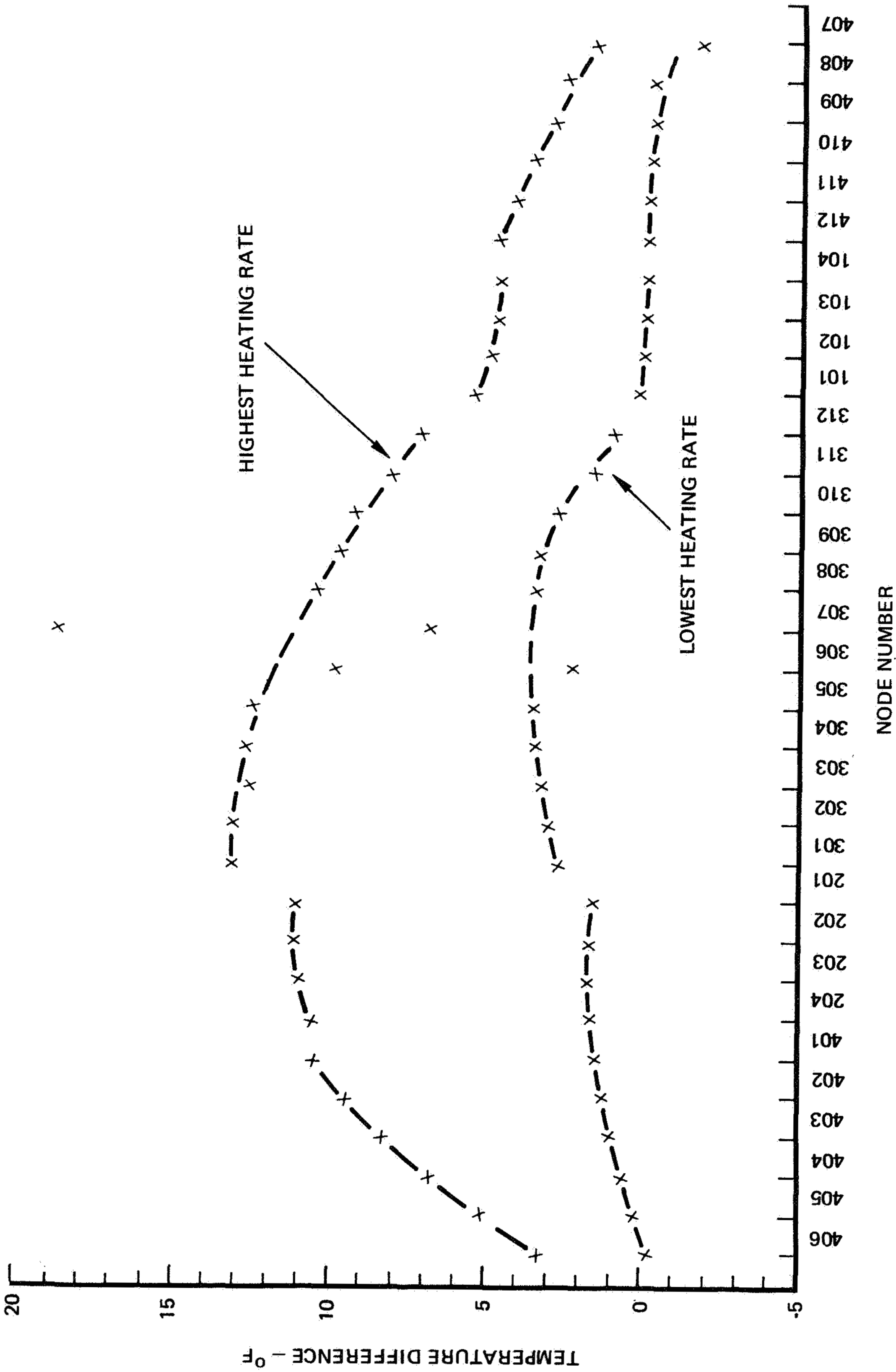

Figure II-68: TEMPERATURE DIFFERENCE BETWEEN FULL SCALE AND 1/4 SCALE MODELS — FREE CONVECTION TESTS

The excess heat leak (due to the heater leads) of the 1/4 scale model is not large enough to account for the temperature differences. The maximum effect of this heat leak is estimated to be 2-3°F. The temperature differences between the models does not appear to be caused by differences in the free convection heat transfer. Based on the Nusselt number versus Grashof number correlation, the average convective heat transfer in the full scale model should be about 4 percent greater than that in the 1/4 scale model.

The correlation between the models shows that the radiation and conduction as well as the free convection heat transfer processes can be preserved in a thermal scale model.

II.5.7.3 Forced Convection Test Series Correlations

The 1/4 scale model data for the forced convection tests are listed in Appendix II-A.2.* The full scale model tests were made at atmospheric pressure for nominal Reynolds numbers of 300, 1200 and 4800 and nominal heating rates of 187, 224 and 294 watts. The high heating rate case was repeated for the three flow rates with the flow direction reversed. The 1/4 scale model was tested at various pressures and heating rates for Reynolds numbers equal to those of the full scale model. These tests were to be used to develop a Nusselt number correlation for the Nusselt number preservation scaling technique. However, as discussed previously no correlation was attempted since adequate time to accomplish this task was unavailable. The 1/4 scale model was also tested under mass flux and heat transfer coefficient preservation conditions. These tests were used for direct correlations between the 1/4 scale and full scale models.

The correlations between the 1/4 scale and full scale models, at the high heating rate, are shown in Figures II-69, II-70 and II-71 for the high, intermediate and low flow rate cases respectively. The 1/4 scale model data

* The gas outlet temperature measurements for the 1/4 scale model are inaccurate especially at the low flow rates.

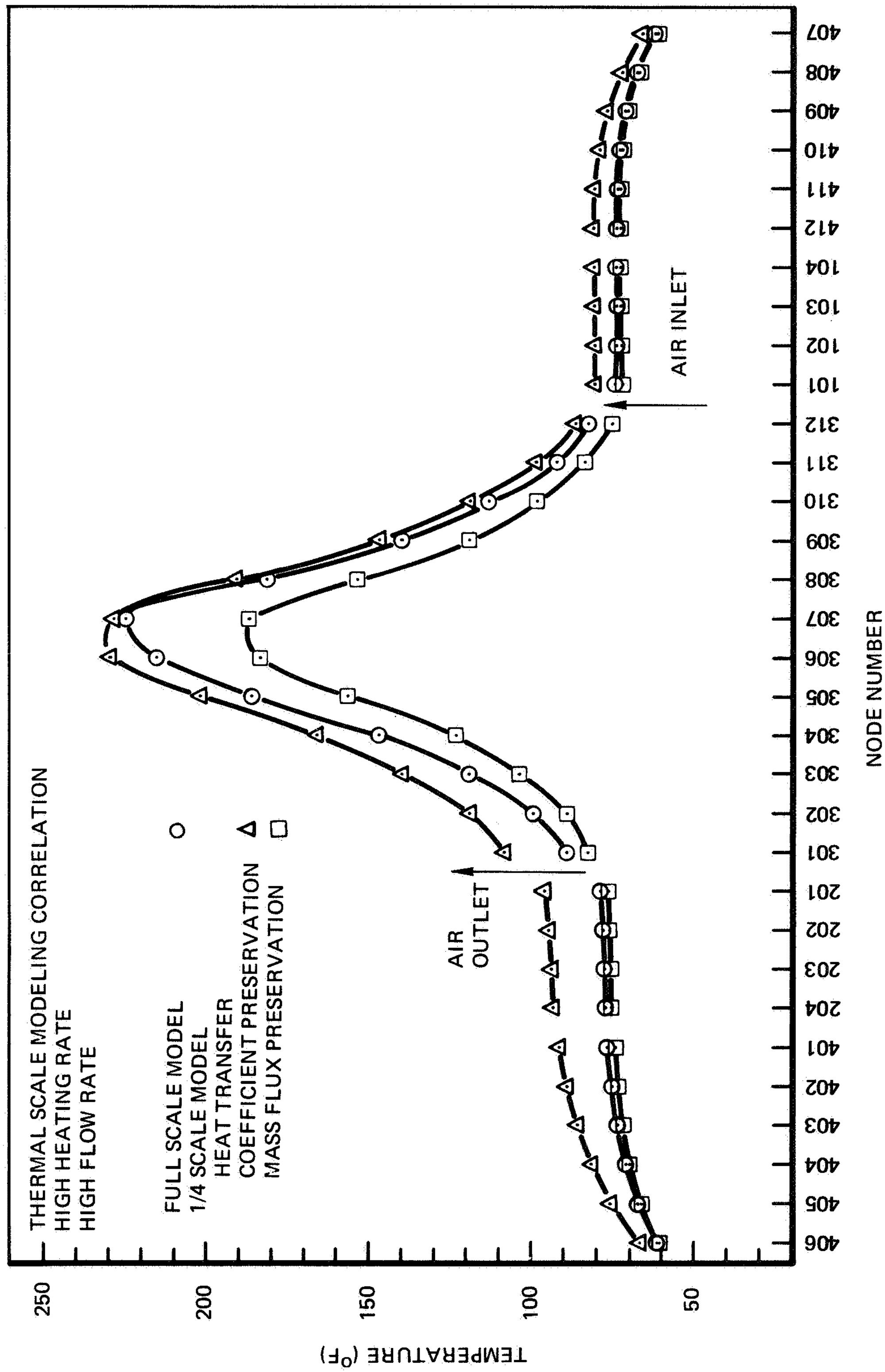
THERMAL SCALE MODELING CORRELATION
HIGH HEATING RATE
HIGH FLOW RATE
FULL SCALE MODEL
1/4 SCALE MODEL
HEAT TRANSFER
COEFFICIENT PRESERVATION
MASS FLUX PRESERVATION
AIR
OUTLET
AIR INLET
TEMPERATURE (oF)
250
200
150
100
50
NODE NUMBER
406
405
404
403
402
401
204
203
202
201
301
302
303
304
305
306
307
308
309
310
311
312
101
102
103
104
412
411
410
409
408
407

Figure II-69:

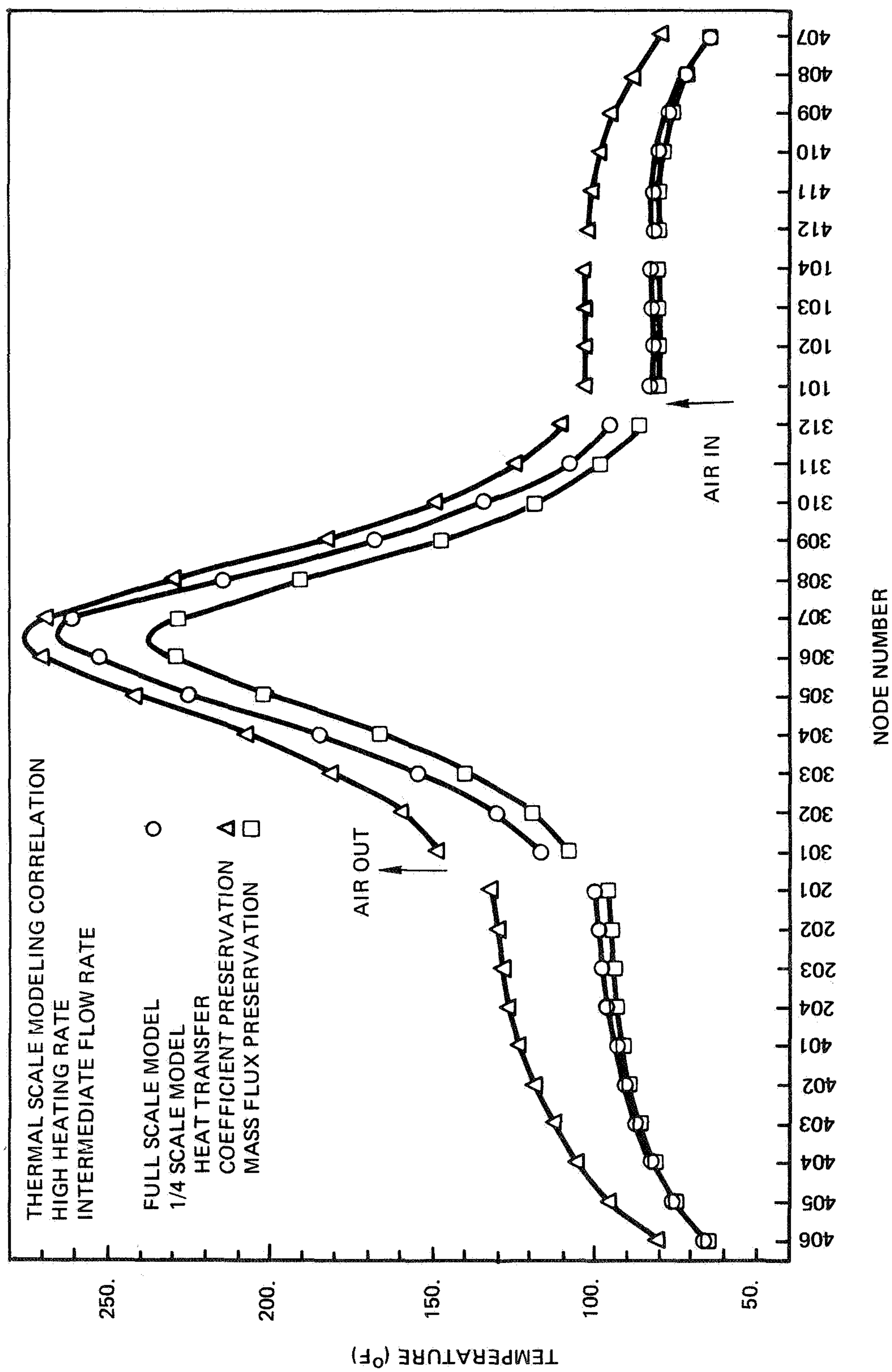
THERMAL SCALE MODELING CORRELATION
HIGH HEATING RATE
INTERMEDIATE FLOW RATE
FULL SCALE MODEL
1/4 SCALE MODEL
HEAT TRANSFER
COEFFICIENT PRESERVATION
MASS FLUX PRESERVATION
AIR OUT
AIR IN
TEMPERATURE (°F)
50.
100.
150.
200.
250.
NODE NUMBER
406
405
404
403
402
401
204
203
202
201
301
302
303
304
305
306
307
308
309
310
311
312
101
102
103
104
412
411
410
409
408
407

Figure II-70:

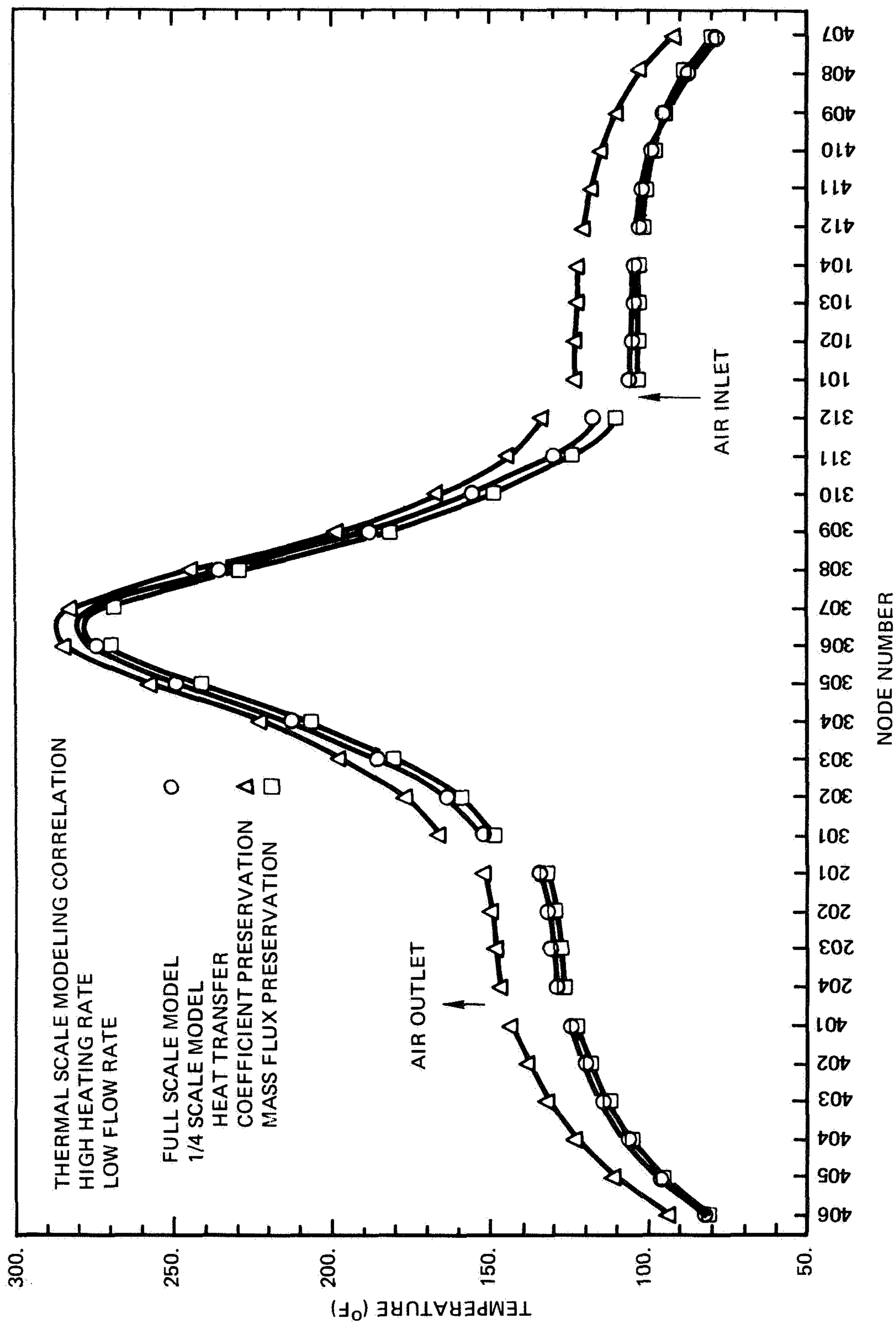
THERMAL SCALE MODELING CORRELATION
HIGH HEATING RATE
LOW FLOW RATE
FULL SCALE MODEL
1/4 SCALE MODEL
HEAT TRANSFER
COEFFICIENT PRESERVATION
MASS FLUX PRESERVATION
AIR OUTLET
AIR INLET
TEMPERATURE (°F)
NODE NUMBER
300.
250.
200.
150.
100.
50.
406
405
404
403
402
401
204
203
202
201
301
302
303
304
305
306
307
308
309
310
311
312
101
102
103
104
412
411
410
409
408
407

Figure II-71:

are shown for both the mass flux and the heat transfer coefficient preservation techniques. Figures II-72, II-73 and II-74 show the same correlations with the flow direction through the model reversed (the flow is from top to bottom instead of bottom to top). These correlations show that the preservation of mass flux results in 1/4 scale model temperatures generally lower than the full scale model while preservation of the heat transfer coefficient results in higher model temperatures. These results are in qualitative agreement with the approximate analysis presented in Section II.4.3. Figure II-75 shows the results of this analysis using parameters applicable to the model configuration. Since the inlet gas temperature is less than the reference temperature (temperature without gas flow) these results show that preservation of mass flux results in lower 1/4 scale model temperatures and heat transfer coefficient preservation results in higher temperatures.

The temperature distribution correlation between the 1/4 scale and full scale models, shown in Figures II-69 through II-74, can be qualitatively explained as follows:

> At the high flow rate forced convection dominates and the temperature correlation for the heat transfer coefficient preservation is directly related to the air temperature change through the model. The largest temperatures differences occur in the air outlet region and these differences closely correspond to the air outlet temperature differences between the 1/4 scale and full scale model. At the low flow rate free convection dominates and the temperature differences are related to the differences in the air cooling rate. The average air temperature in the models is fixed primarily by the free convection effects and should be nearly equal in 1/4 scale and full scale models. Consequently the relatively smaller mass flow rate in the 1/4 scale model results in less air cooling and more heat conduction to the cooling fin. This results in generally higher temperatures in the 1/4 scale model. At the intermediate flow rate combined convection is important and the correlation is not as good as that at the high and low flow rates.

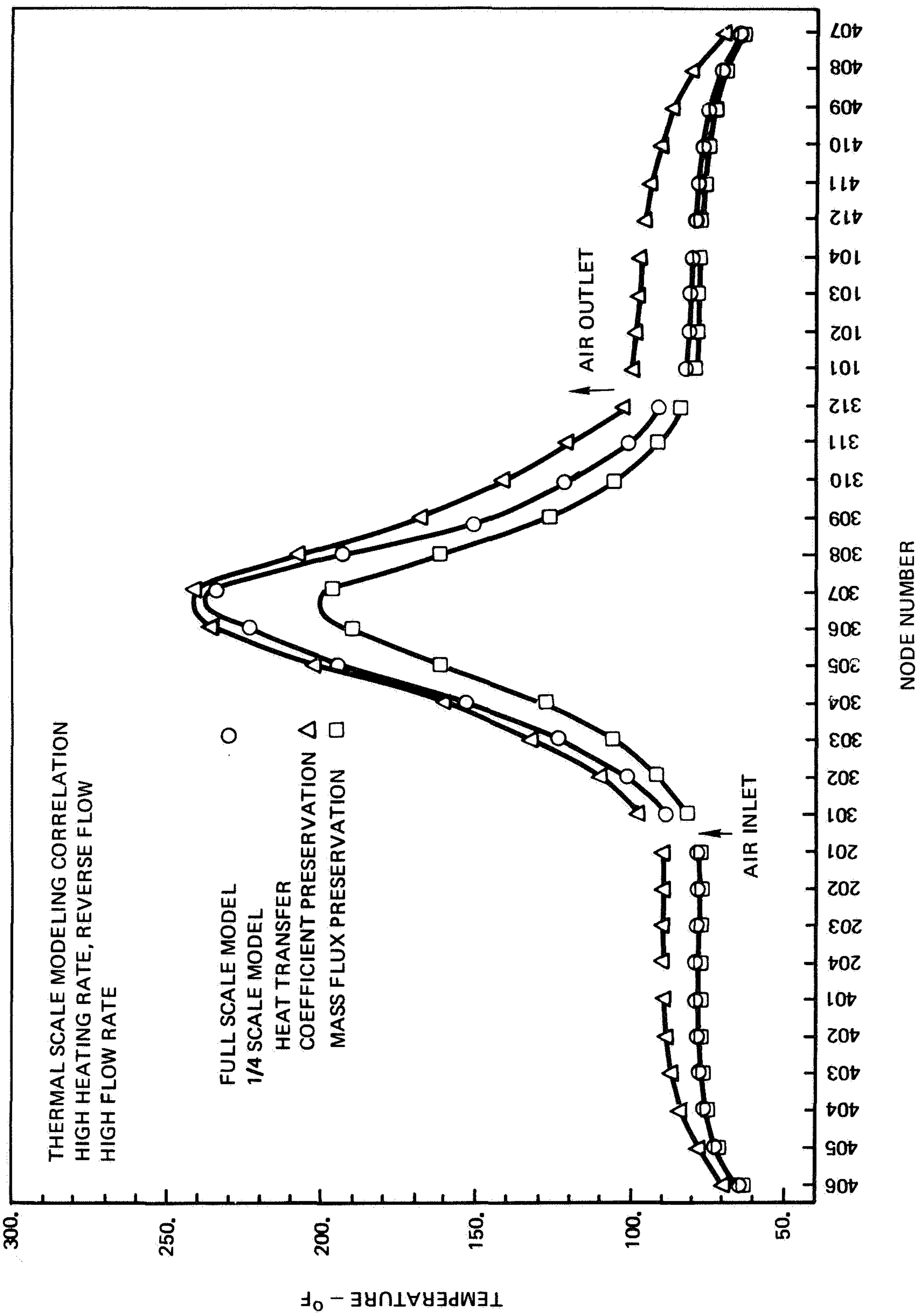
THERMAL SCALE MODELING CORRELATION
HIGH HEATING RATE, REVERSE FLOW
HIGH FLOW RATE
FULL SCALE MODEL
1/4 SCALE MODEL
HEAT TRANSFER
COEFFICIENT PRESERVATION
MASS FLUX PRESERVATION
AIR OUTLET
AIR INLET
TEMPERATURE – °F
300.
250.
200.
150.
100.
50.
NODE NUMBER
406
405
404
403
402
401
204
203
202
201
301
302
303
304
305
306
307
308
309
310
311
312
101
102
103
104
412
411
410
409
408
407

Figure II-72:

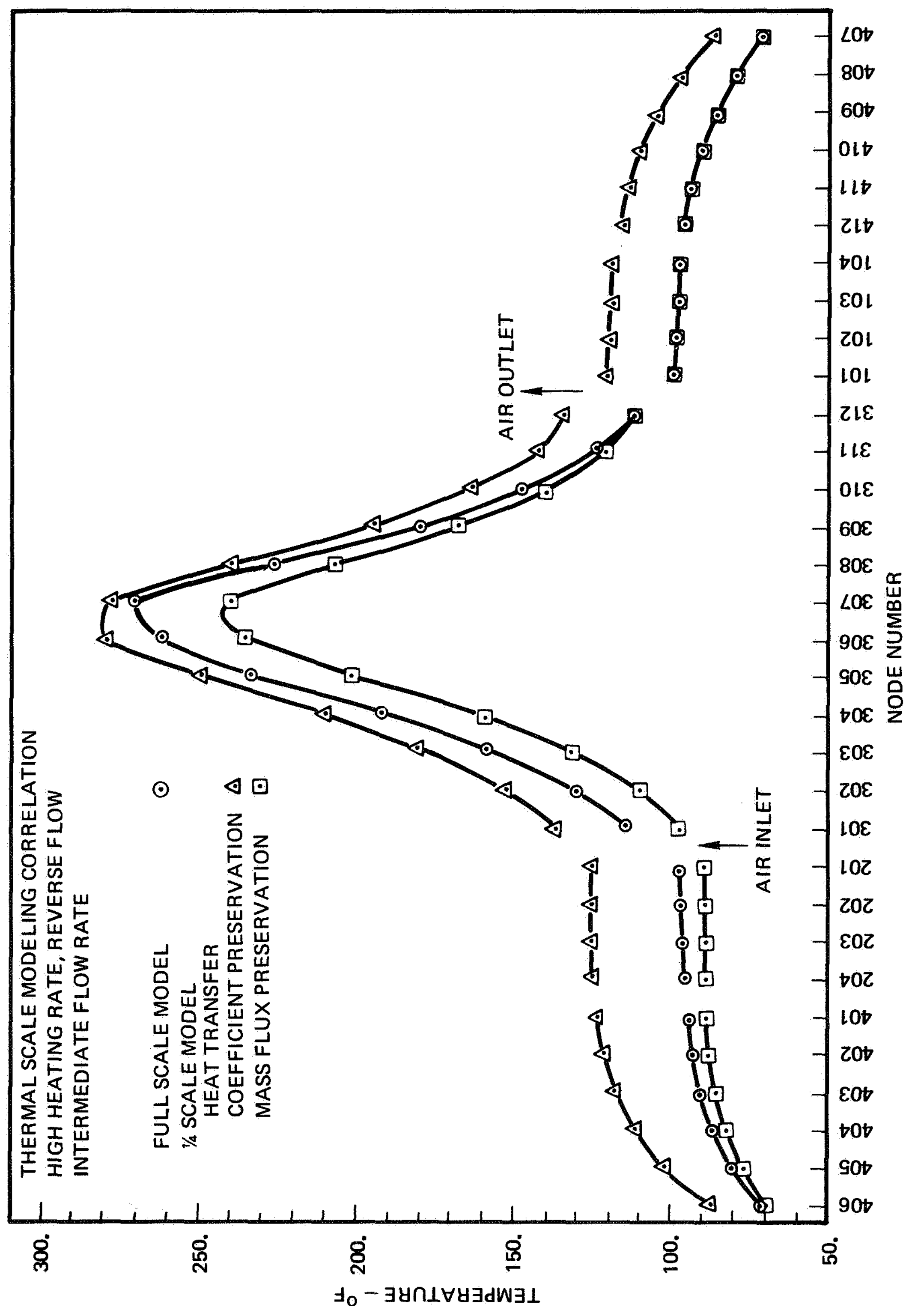
THERMAL SCALE MODELING CORRELATION
HIGH HEATING RATE, REVERSE FLOW
INTERMEDIATE FLOW RATE
FULL SCALE MODEL
¼ SCALE MODEL
HEAT TRANSFER
COEFFICIENT PRESERVATION
MASS FLUX PRESERVATION
AIR OUTLET
AIR INLET
TEMPERATURE — °F
300.
250.
200.
150.
100.
50.
NODE NUMBER
406
405
404
403
402
401
204
203
202
201
301
302
303
304
305
306
307
308
309
310
311
312
101
102
103
104
412
411
410
409
408
407

Figure II-73:

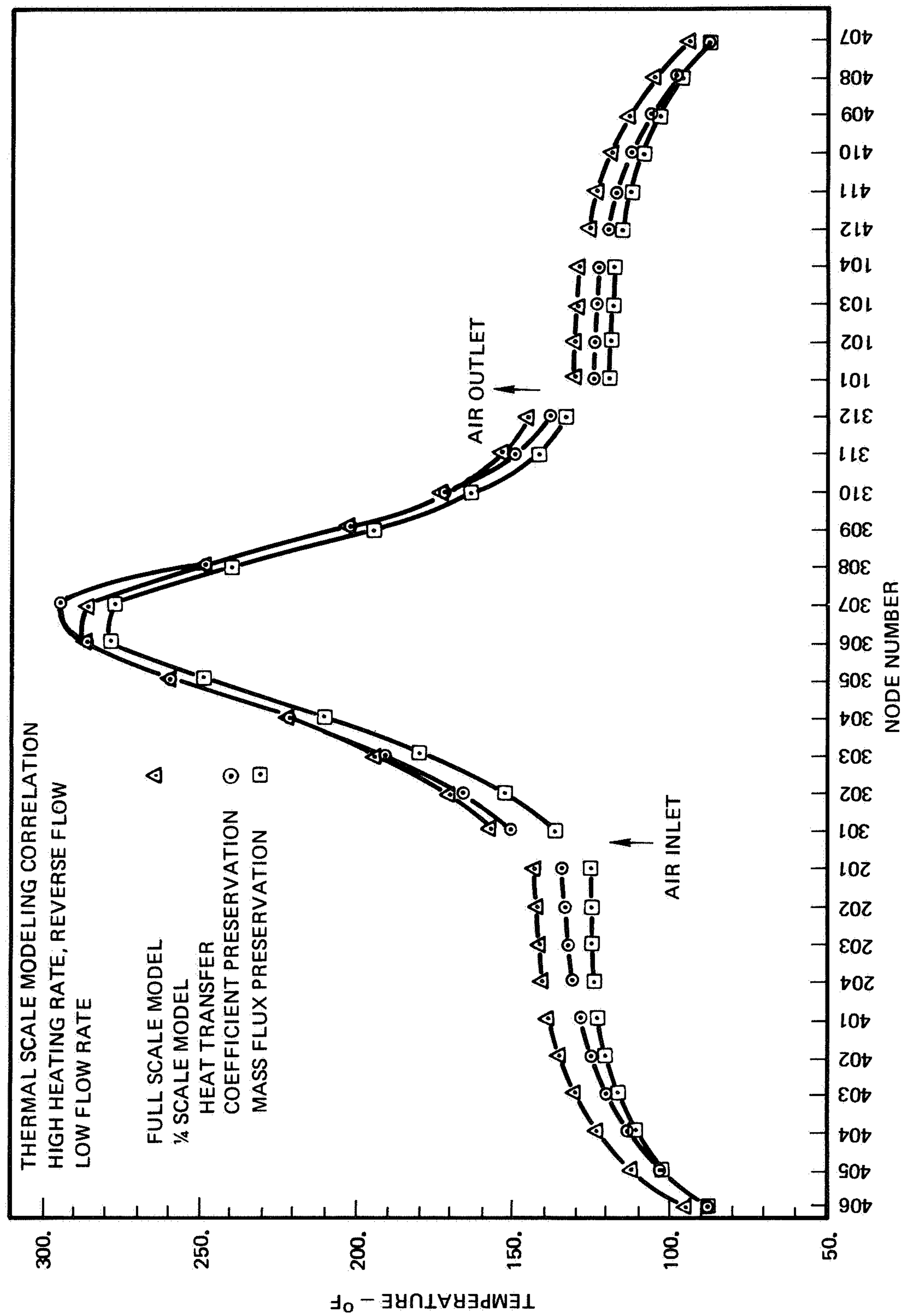
THERMAL SCALE MODELING CORRELATION
HIGH HEATING RATE, REVERSE FLOW
LOW FLOW RATE
FULL SCALE MODEL
¼ SCALE MODEL
HEAT TRANSFER
COEFFICIENT PRESERVATION
MASS FLUX PRESERVATION
AIR INLET
AIR OUTLET
TEMPERATURE – °F
300.
250.
200.
150.
100.
50.
NODE NUMBER
406
405
404
403
402
401
204
203
202
201
301
302
303
304
305
306
307
308
309
310
311
312
101
102
103
104
412
411
410
409
408
407

Figure II-74:

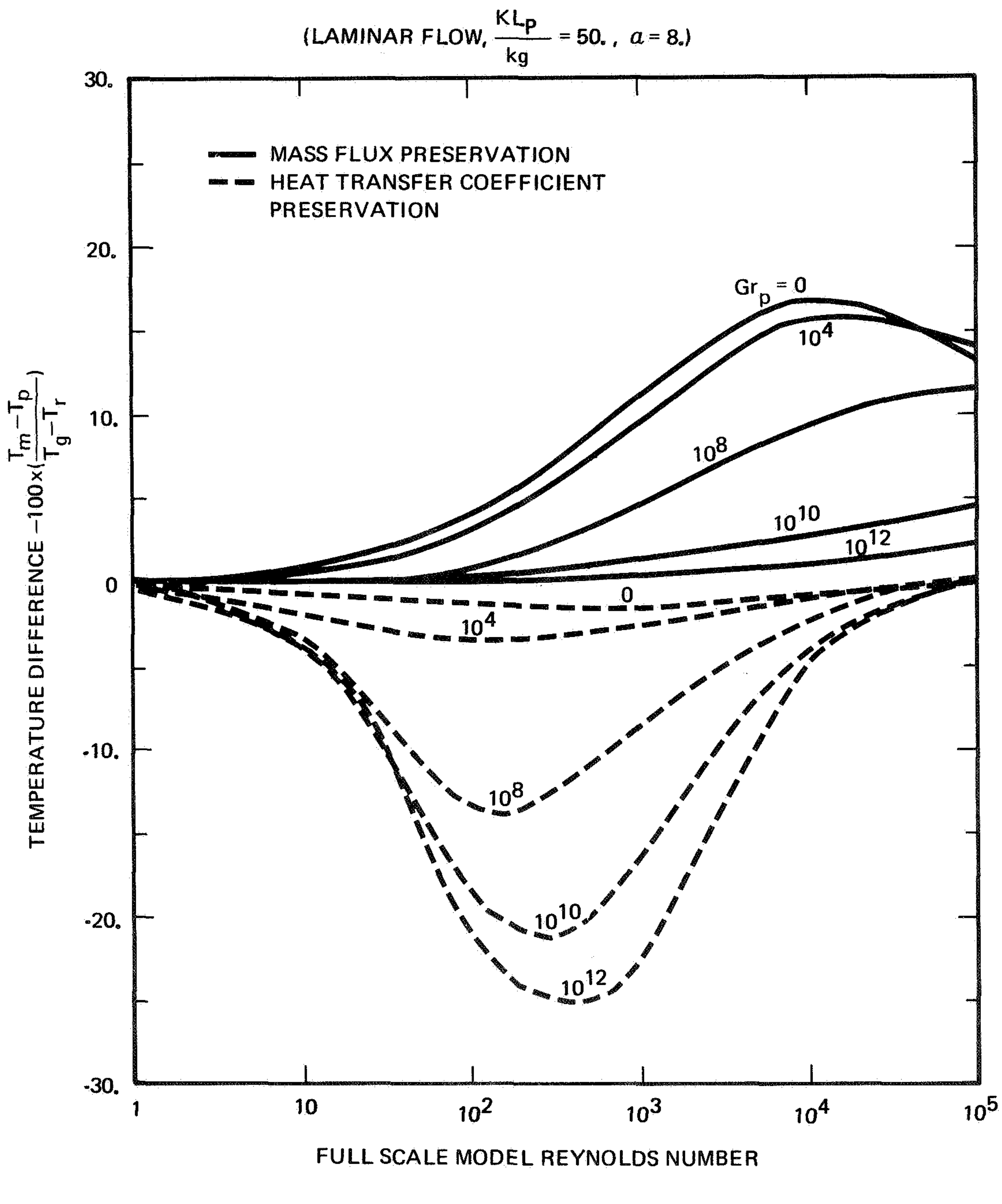

Figure: CALCULATED EFFECTS OF SCALING COMPROMISES FOR ¼ SCALE MODEL

Figure II-75:

Preservation of mass flux results in good correlation for the end plates and outer cylinder temperatures. Since the full scale model end plates and outer cylinder temperatures are not far different from the air temperature at the higher flow rates, the increased convective heat transfer in these regions tends to bring these temperatures even closer to the air temperature. This tendency is offset somewhat by the increased air cooling of the inner cylinder which results in less heat transfer from the inner to outer cylinder. The net effect then is for the mass flux preservation technique to result in good correlation for the end plates and outer cylinder and poorer correlation for the inner cylinder which excessivley cooled by the air. As expected the correlation is best for the low flow rate case where free convection dominates. The correlation for the inner cylinder improves as the flow rate is decreased.

The correlations between the 1/4 scale and full scale models for the intermediate heating rate and presented in Figure II-76 which shows the temperature differences between the 1/4 scale and full scale model at each of the flow rates for both scaling techniques. This Figure shows that the two techniques do not quite bound the full scale model temperatures. The higher convective heat transfer coefficient for mass flux preservation keeps the outer cylinder warmer in the regions near the cooling fin.

The forced convection test series data were compared with the approximate analysis presented in Section II.4.3 by averaging the end plate, outer cylinder and inner cylinder node temperature. This comparison was made for the three flow rates and the three heating rates. The reference temperature for a particular heating rate was taken as the average temperature of the full scale model under free convection conditions at the same heating rate. Figure II-77 shows the nondimensional temperature difference between model and prototype as a function of Reynolds number for the three heating rate cases. Also shown in Figure II-77 are the results, calculated for a prototype Grashof number of 10^8, for a 1/5 scale spacecraft (see Section II.4.3) as well as those for the 1/4 scale model. Even though the analysis is a poor representation of the model the

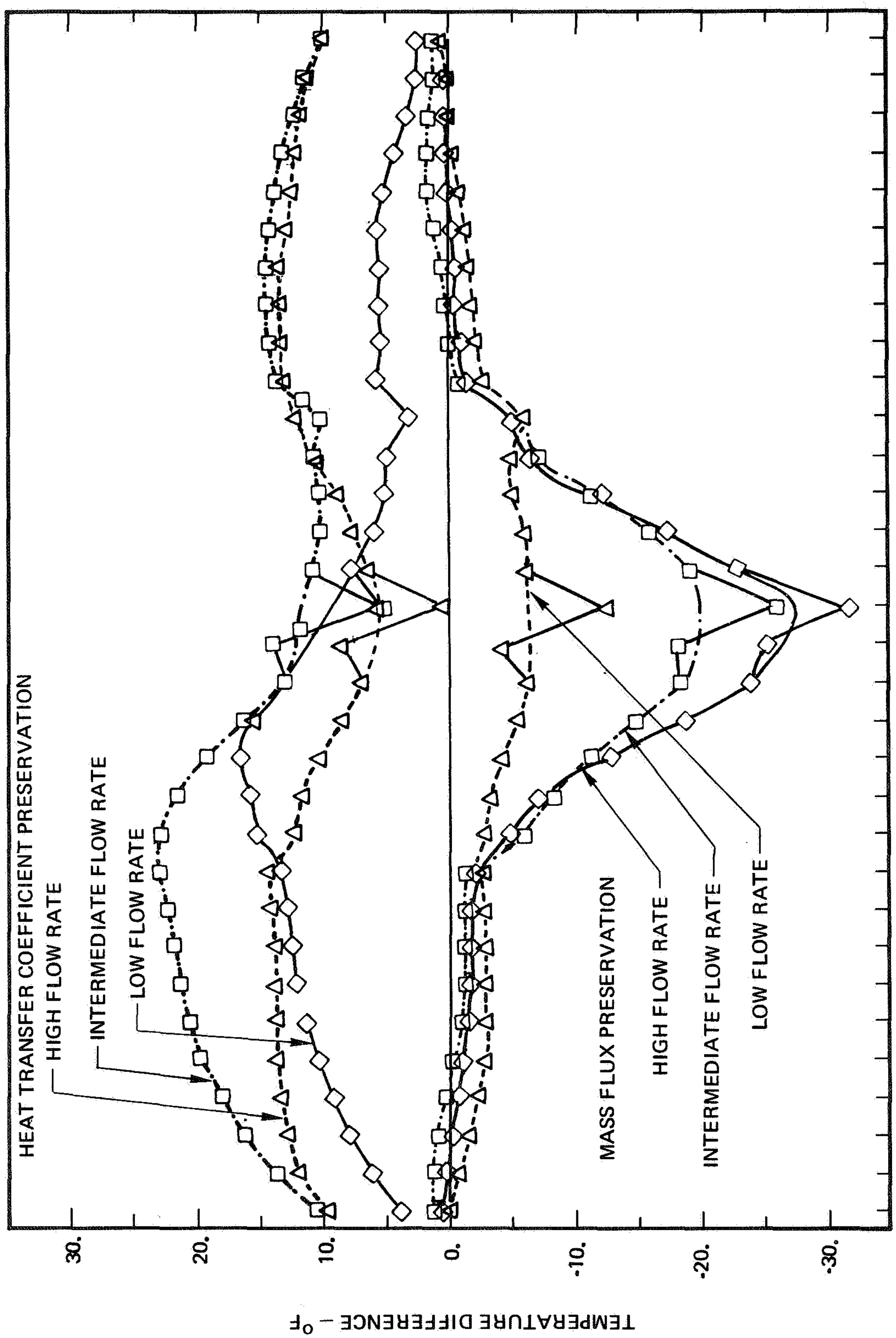

Figure II-76: CORRELATION BETWEEN 1/4 SCALE AND FULL SCALE MODELS FORCED CONVECTION TEST SERIES — INTERMEDIATE HEATING RATE

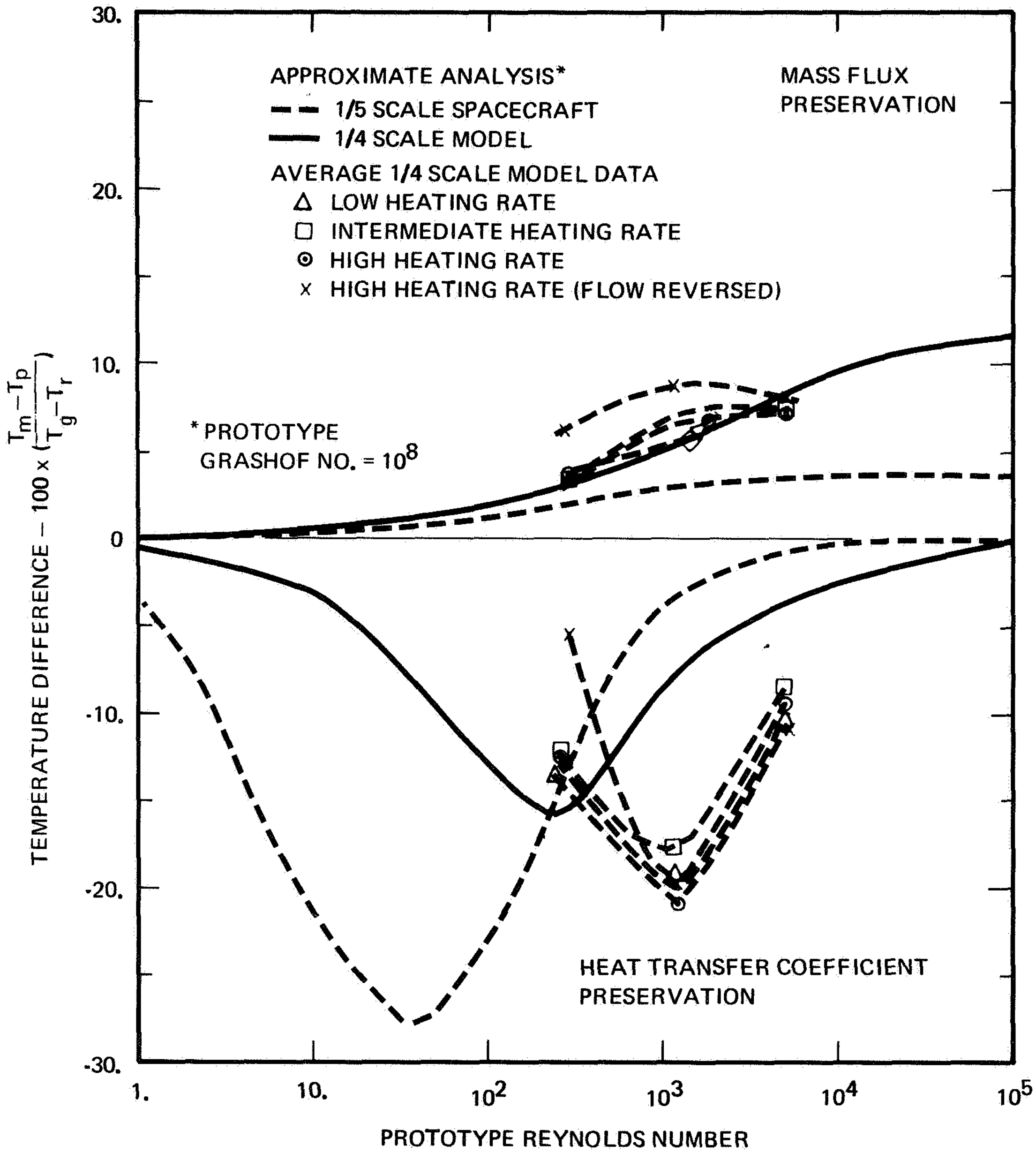

Figure II-77: TEMPERATURE DIFFERENCES BETWEEN MODEL AND PROTOTYPE DUE TO SCALING COMPROMISES calculated results are in fair agreement with the data, however, the maximum temperature differences for heat transfer coefficient preservation do not coincide. Since the approximate analysis is more representative of a manned spacecraft configuration than of the model configuration the calculated results should give a good indication of the temperature differences to be expected in thermal scale modeling a manned spacecraft. The results shown in Figure II-77 indicate that, at a typical manned spacecraft Reynolds number of 10^4, better thermal similitude would be achieved in a 1/5 scale spacecraft than that achieved in the 1/4 scale model.

II.6 CONCLUSIONS

Adequate thermal similitude may be achieved in thermal scale modeling of radiation-conduction-convection systems by using the compromised scaling techniques of either mass flux or heat transfer coefficient preservation. The best thermal similitude is achieved with mass flux preservation when free convection effects dominate and with heat transfer coefficient preservation when forced convection effects dominate. The degree of thermal similitude achieved with either technique depends on the system being modeled. This is illustrated by the approximate analysis presented in Section II.4.3 and was verified in the experimental investigation.

The heat transfer coefficient preservation scaling technique should give better thermal similitude than mass flux preservation in thermal scale modeling applications for manned spacecraft. The approximate analysis of Section II.4.3 indicates that very good thermal similitude (both transient and steady state) can be achieved with a 1/5 scale model spacecraft using heat transfer coefficient preservation. This analysis indicates that, for a typical manned spacecraft Reynolds number of 10^4, the temperature agreement between 1/5 scale model and prototype spacecraft will be within about 5°F and that the transient response time will be scaled to within about 5 percent.

The major problem involved in using heat transfer coefficient preservation is determining the proper relationship between the Nusselt and Reynolds number. Transitions between laminar and turbulent flow may also cause problems. However, in the experimental investigation flat plate laminar flow theory was used for the relationship between Nusselt and Reynolds numbers with good results even through the inlet flow was highly turbulent and the flow through the model was in the laminar flow regime. The experimental investigation represents a more severe test of thermal scale modeling involving convection than does thermal scale modeling of a manned spacecraft. These more severe test conditions were large conduction and radiation effects and the high inlet gas velocities. Consequently the use of heat transfer coefficient preservation should not present any major problems in thermal scale modeling of manned spacecraft.

The Nusselt number preservation scaling technique is a workable technique that, if carried out properly, will allow prototype performance to be predicted using the Nusselt number correlations developed from the thermal scale model tests. Much of the detailed work reported in this document indicates the methods required to implement this scaling technique. Thermal scale modeling using this technique must be approached as an experimental research program rather than as an engineering test program. As is the case with most research investigations involving convective heat transfer great care is required throughout the investigation to achieve an accurate determination of the heat transfer coefficients. Once the heat transfer coefficients are accurately determined, the use of this techinque assumes that a valid correlation for the Nusselt number can be found. This correlation of the Nusselt number with the system parameters requires the investigator to be thoroughly versed in convective heat transfer. The experimental investigation carried the Nusselt number preservation scaling technique to the point of achieving a correlation for the 1/4 scale model free convection data. There was insufficient time to carry this investigation to its completion. It is estimated that at least an order of magnitude greater effort is required to use the Nusselt number preservation technique than the other techniques. For some critical problem areas it may be necessary to use Nusselt number preservation to accurately determine the convection effects. However, before such a task is undertaken the requirements of using this technique should be well understood since any attempts to do a "quick and dirty" job will result in a wasted effort.

REFERENCES

1. Adkins, D. L., "Scaling of Transient Temperature Distributions of Simple Bodies in a Space Chamber," AIAA Paper 65-660, AIAA Thermophysics Conference, Monterey, September 1965.

2. Rolling, R. E., "Results of Transient Thermal Modeling in a Simulated Space Environment," AIAA Paper 65-659, AIAA Thermophysics Conference, Monterey, September 1965.

3. Rolling, R. E., "Thermal Modeling of a Truncated Cone in a Simulated Space Environment," AIAA Space Simulation Conference, Houston, September 1966.

4. Thompson, R. K., Klockzien, V. G. and Dufoe, G. E., "Analyses and Tests of Thermal Scale Models of a Simulated Spacecraft," J. Spacecraft and Rockets, Volume 4, No. 4, pp. 486-491, 1967.

5. Gabron, F. and Johnson, R. W., "Thermal Scale Modeling of the Mariner IV Spacecraft," Final Report to J.P.L., August 20, 1965.

6. Katzoff, S., "Similitude in Thermal Models of Spacecraft," NASA TND-1631, April 1963.

7. Pasczewski, K. I. and Renzi, P. N., "Scale Model Studies of Temperature Distributions in Internally Heated Enclosures," ASHRAE 70th Annual Meeting, Milwaukee, June 1963,

8. MacGregor, R. K., Lester, A. B. and Drake, R. L., "Thermal Radioactive Interchange Factor Program (An Engineer's Guide to AS2814-360/67 Version)," The Boeing Company, D2-114470-1, May 1970.

9. Bullock, R. H., Brossard, J. J. and MacGregor, R. K., "Boeing Engineering Thermal Analyzer (AS1917)," Volume I (Program User's Guide - System 360 Version), The Boeing Company, D180-10016-1, August 8, 1970.

10. Adams, R. K. and Davisson, E. G., "Smoothed Thermocouple Tables of Extended Significance," ORNL-3649 Volume 2, UC-37-Instruments TID-4500 (37th Edition), Oak Ridge National Laboratory.

APPENDIX II-A

TEST DATA

II-A.1 1/4 SCALE MODEL DATA

II-A.1.1 RADIATION-CONDUCTION TEST SERIES

D180-15048-1

1/4 SCALE MODEL TEMPERATURES DEG F RADIATION-CONDUCTION TEST SERIES

RUN NUMBER 14.0 VOLTAGE 48.85 VOLTS CURRENT 0.3742 AMPS POWER 18.281 WATTS PRESSURE 1.000 TORR FLOW 0.0 LB/MIN

NODE 101	151.42	NODE 102	149.97	NODE 103	148.83	NODE 104	148.03
NODE 201	152.33	~~NODE 202~~	~~150.46~~	~~NODE 203~~	~~147.16~~	~~NODE 204~~	~~148.14~~
NODE 301	167.86	NODE 302	181.19	NODE 303	207.45	NODE 304	240.01
NODE 305	284.02	NODE 306	317.86	NODE 307	317.88	NODE 308	233.39
NODE 309	237.95	NODE 310	205.00	NODE 311	179.27	~~NODE 312~~	~~157.11~~
NODE 401	144.86	NODE 402	140.58	NODE 403	134.76	NODE 404	127.37
NODE 405	116.23	NODE 406	100.05	NODE 407	100.39	NODE 408	116.10
NODE 409	127.39	~~NODE 410~~	~~135.01~~	~~NODE 411~~	~~140.39~~	~~NODE 412~~	~~144.42~~
NODE 413	64.97	NODE 414	34.02				

RUN NUMBER 10.0 VOLTAGE 42.64 VOLTS CURRENT 0.3274 AMPS POWER 13.959 WATTS PRESSURE 2.000 TORR FLOW 0.0 LB/MIN

NODE 101	128.82	NODE 102	127.48	NODE 103	126.51	NODE 104	125.74
NODE 201	129.87	NODE 202	128.19	NODE 203	127.02	~~NODE 204~~	~~126.13~~
NODE 301	143.28	NODE 302	154.74	NODE 303	176.97	NODE 304	204.25
NODE 305	240.43	NODE 306	267.73	NODE 307	267.66	NODE 308	239.96
NODE 309	202.79	~~NODE 310~~	~~175.02~~	~~NODE 311~~	~~152.82~~	~~NODE 312~~	~~142.28~~
NODE 401	123.18	NODE 402	119.24	NODE 403	114.14	NODE 404	107.75
NODE 405	98.51	NODE 406	85.50	NODE 407	85.76	NODE 408	98.36
NODE 409	107.63	NODE 410	114.08	NODE 411	118.80	~~NODE 412~~	~~122.51~~
NODE 413	57.91	NODE 414	33.68				

RUN NUMBER 15.0 VOLTAGE 39.00 VOLTS CURRENT 0.2996 AMPS POWER 11.684 WATTS PRESSURE 1.000 TORR FLOW 0.0 LB/MIN

NODE 101	116.12	NODE 102	114.88	NODE 103	113.98	NODE 104	113.28
NODE 201	116.98	~~NODE 202~~	~~115.43~~	~~NODE 203~~	~~114.36~~	~~NODE 204~~	~~113.53~~
NODE 301	129.20	NODE 302	139.37	NODE 303	159.16	NODE 304	183.15
NODE 305	214.72	NODE 306	238.18	NODE 307	238.20	NODE 308	214.12
NODE 309	181.45	NODE 310	157.09	NODE 311	137.59	~~NODE 312~~	~~128.30~~
NODE 401	110.71	NODE 402	107.04	NODE 403	102.33	NODE 404	96.63
NODE 405	88.58	NODE 406	77.47	NODE 407	77.67	NODE 408	88.52
NODE 409	96.64	~~NODE 410~~	~~102.43~~	~~NODE 411~~	~~106.77~~	~~NODE 412~~	~~110.23~~
NODE 413	54.13	NODE 414	33.70				

1/4 SCALE MODEL TEMPERATURES DEG F RADIATION-CONDUCTION TEST SERIES

RUN NUMBER 16.0 VOLTAGE 33.68 VOLTS CURRENT 0.2592 AMPS POWER 8.733 WATTS PRESSURE 0.750 TORR FLOW 0.0 LB/MIN

NODE 101	93.85	~~NODE 202~~	~~98.42~~	NODE 103	97.03	NODE 104	95.44
NODE 201	99.74	NODE 302	118.03	~~NODE 203~~	~~97.49~~	~~NODE 204~~	~~96.70~~
NODE 301	109.75	NODE 306	196.53	NODE 303	134.01	NODE 304	153.26
NODE 305	178.23	NODE 310	132.12	NODE 307	196.45	NODE 308	177.64
NODE 309	151.71	NODE 402	91.12	NODE 311	116.32	~~NODE 312~~	~~108.75~~
NODE 401	94.34	NODE 406	67.20	NODE 403	87.13	NODE 404	82.43
NODE 405	75.92	~~NODE 410~~	~~87.11~~	NODE 407	57.34	NODE 408	75.33
NODE 409	82.34	NODE 414	33.64	NODE 411	99.78	~~NODE 412~~	~~93.79~~
NODE 413	49.30						

RUN NUMBER 17.0 VOLTAGE 27.43 VOLTS CURRENT 0.2115 AMPS POWER 5.901 WATTS PRESSURE 0.900 TORR FLOW 0.0 LB/MIN

NODE 101	80.93	NODE 102	80.11	NODE 103	79.52	NODE 104	79.06
NODE 201	81.91	NODE 202	80.88	NODE 203	80.17	~~NODE 204~~	~~79.62~~
NODE 301	89.30	NODE 302	95.31	NODE 303	106.78	NODE 304	120.54
NODE 305	138.16	NODE 306	150.87	NODE 307	150.77	NODE 308	137.61
NODE 309	119.19	~~NODE 310~~	~~105.10~~	~~NODE 311~~	~~93.67~~	~~NODE 312~~	~~88.20~~
NODE 401	77.67	NODE 402	75.08	NODE 403	71.93	NODE 404	68.33
NODE 405	63.48	NODE 406	57.19	NODE 407	57.28	NODE 408	63.30
NODE 409	69.06	NODE 410	71.67	NODE 411	74.56	~~NODE 412~~	~~75.95~~
NODE 413	44.61	NODE 414	33.65				

RUN NUMBER 40.0 VOLTAGE 24.03 VOLTS CURRENT 0.1851 AMPS POWER 4.448 WATTS PRESSURE 1.000 TORR FLOW 0.0 LB/MIN

NODE 101	150.13	NODE 102	149.95	NODE 103	149.77	NODE 104	149.58
NODE 201	149.63	~~NODE 202~~	~~149.37~~	~~NODE 203~~	~~149.19~~	~~NODE 204~~	~~149.02~~
NODE 301	154.27	NODE 302	158.59	NODE 303	165.77	NODE 304	175.51
NODE 305	189.48	NODE 306	199.06	NODE 307	199.06	NODE 308	189.52
NODE 309	176.50	NODE 310	166.64	NODE 311	158.67	~~NODE 312~~	~~154.73~~
NODE 401	148.87	NODE 402	148.99	NODE 403	149.05	NODE 404	143.90
NODE 405	143.41	NODE 406	147.15	NODE 407	147.25	NODE 408	148.79
NODE 409	149.56	~~NODE 410~~	~~145.60~~	~~NODE 411~~	~~149.79~~	~~NODE 412~~	~~149.65~~
NODE 413	143.53	NODE 414	129.50				

1/4 SCALE MODEL TEMPERATURES DEG F RADIATION-CONDUCTION TEST SERIES

RUN NUMBER 41.0 VOLTAGE 14.98 VOLTS CURRENT 0.1158 AMPS POWER 1.734 WATTS PRESSURE 1.000 TORR FLOW 0.0 LB/MIN

NODE 101	103.06	NODE 102	102.91	NODE 103	102.83	NODE 104	102.73
NODE 201	102.81	NODE 202	102.68	NODE 203	102.57	NODE 204	102.49
NODE 301	104.96	NODE 302	107.00	NODE 303	110.90	NODE 304	115.23
NODE 305	120.95	NODE 306	125.04	NODE 307	125.10	NODE 308	120.99
NODE 309	115.25	NODE 310	110.75	NODE 311	107.03	NODE 312	105.14
NODE 401	102.28	NODE 402	102.27	NODE 403	102.21	NODE 404	102.11
NODE 405	101.82	NODE 406	101.31	NODE 407	101.37	NODE 408	102.01
NODE 409	102.40	NODE 410	102.58	NODE 411	102.66	NODE 412	102.73
NODE 413	99.85	NODE 414	94.09				

II-A.1.2 FREE CONVECTION TEST SERIES

1/4 SCALE ~~MODEL TEMPERATURES~~ DEG F FREE CONVECTION TEST SERIES

RUN NUMBER 18.0 VOLTAGE 27.46 VOLTS CURRENT 0.2117 AMPS POWER 5.313 WATTS PRESSURE 0.513 ATM FLOW 0.0 LB/MIN

NODE 101	74.00	NODE 102	73.44	NODE 103	73.02	NODE 104	72.71
NODE 201	83.65	~~NODE 202~~	~~82.77~~	~~NODE 203~~	~~82.12~~	~~NODE 204~~	~~81.60~~
NODE 301	89.65	NODE 302	94.43	NODE 303	103.35	NODE 304	113.64
NODE 305	127.17	NODE 306	137.01	NODE 307	136.04	NODE 308	121.93
NODE 309	104.09	~~NODE 310~~	~~91.90~~	~~NODE 311~~	~~82.97~~	~~NODE 312~~	~~79.03~~
NODE 401	79.80	NODE 402	77.31	NODE 403	73.93	NODE 404	70.00
NODE 405	64.53	NODE 406	57.25	NODE 407	56.31	NODE 408	60.86
NODE 409	64.38	~~NODE 410~~	~~67.05~~	~~NODE 411~~	~~69.23~~	~~NODE 412~~	~~71.05~~
NODE 413	44.35	NODE 414	33.58				

RUN NUMBER 19.0 VOLTAGE 27.47 VOLTS CURRENT 0.2120 AMPS POWER 5.828 WATTS PRESSURE 1.015 ATM FLOW 0.0 LB/MIN

NODE 101	72.30	NODE 102	71.73	NODE 103	71.45	NODE 104	71.18
NODE 201	83.83	NODE 202	83.04	~~NODE 203~~	~~82.42~~	~~NODE 204~~	~~81.91~~
NODE 301	89.21	NODE 302	93.41	NODE 303	101.37	NODE 304	110.52
NODE 305	122.93	NODE 306	131.99	NODE 307	130.85	NODE 308	116.76
NODE 309	99.51	NODE 310	88.08	~~NODE 311~~	~~80.01~~	~~NODE 312~~	~~76.54~~
NODE 401	80.21	NODE 402	77.84	NODE 403	74.58	NODE 404	70.63
NODE 405	65.13	NODE 406	57.67	NODE 407	56.46	NODE 408	60.65
NODE 409	63.79	NODE 410	66.12	NODE 411	63.03	~~NODE 412~~	~~69.65~~
NODE 413	44.53	NODE 414	33.68				

RUN NUMBER 20.1 VOLTAGE 33.76 VOLTS CURRENT 0.2599 AMPS POWER 8.775 WATTS PRESSURE 1.016 ATM FLOW 0.0 LB/MIN

NODE 101	87.04	NODE 102	86.42	NODE 103	85.96	NODE 104	85.61
NODE 201	103.14	NODE 202	102.13	~~NODE 203~~	~~101.31~~	~~NODE 204~~	~~130.64~~
NODE 301	110.64	NODE 302	116.71	NODE 303	127.84	NODE 304	140.77
NODE 305	158.35	NODE 306	171.60	NODE 307	169.92	NODE 308	149.70
NODE 309	125.19	NODE 310	109.13	NODE 311	97.91	~~NODE 312~~	~~93.08~~
NODE 401	98.50	NODE 402	95.53	NODE 403	91.32	NODE 404	86.05
NODE 405	78.47	NODE 406	68.06	NODE 407	66.33	NODE 408	72.18
NODE 409	76.40	NODE 410	79.42	NODE 411	81.81	~~NODE 412~~	~~83.82~~
NODE 413	49.27	NODE 414	33.59				

1/4 SCALE MODEL TEMPERATURES DEG F FREE CONVECTION TEST SERIES

RUN NUMBER 21.0 VOLTAGE 33.69 VOLTS CURRENT 0.2594 AMPS POWER 8.741 WATTS PRESSURE 0.489 ATM FLOW 0.0 LB/MIN

NODE 101	89.68	NODE 102	88.96	NODE 103	83.43	NODE 104	88.02
NODE 201	102.84	~~NODE 202~~	~~101.75~~	~~NODE 203~~	~~100.89~~	~~NODE 204~~	~~100.18~~
NODE 301	111.07	NODE 302	117.80	NODE 303	130.37	NODE 304	144.92
NODE 305	164.24	NODE 306	178.52	NODE 307	177.22	NODE 308	157.01
NODE 309	131.71	NODE 310	114.56	NODE 311	102.10	~~NODE 312~~	~~96.58~~
NODE 401	97.89	NODE 402	94.77	NODE 403	90.44	NODE 404	85.14
NODE 405	77.73	NODE 406	67.61	NODE 407	66.30	NODE 408	72.71
NODE 409	77.43	~~NODE 410~~	~~80.96~~	~~NODE 411~~	~~83.67~~	~~NODE 412~~	~~85.94~~
NODE 413	49.18	NODE 414	33.68				

RUN NUMBER 22.0 VOLTAGE 39.06 VOLTS CURRENT 0.3004 AMPS POWER 11.734 WATTS PRESSURE 0.451 ATM FLOW 0.0 LB/MIN

NODE 101	105.27	NODE 102	104.40	NODE 103	103.77	NODE 104	103.28
NODE 201	120.91	NODE 202	119.57	~~NODE 203~~	~~118.53~~	~~NODE 204~~	~~117.69~~
NODE 301	131.31	NODE 302	139.77	NODE 303	155.75	NODE 304	174.38
NODE 305	199.37	NODE 306	218.04	NODE 307	215.67	NODE 308	190.65
NODE 309	158.48	NODE 310	136.76	~~NODE 311~~	~~121.06~~	~~NODE 312~~	~~114.10~~
NODE 401	115.04	NODE 402	111.36	NODE 403	106.23	NODE 404	99.76
NODE 405	90.54	NODE 406	77.76	NODE 407	75.22	NODE 408	84.52
NODE 409	90.54	NODE 410	94.87	NODE 411	98.16	~~NODE 412~~	~~100.83~~
NODE 413	53.91	NODE 414	33.76				

RUN NUMBER 23.0 VOLTAGE 39.02 VOLTS CURRENT 0.3001 AMPS POWER 11.713 WATTS PRESSURE 1.012 ATM FLOW 0.0 LB/MIN

NODE 101	101.42	NODE 102	100.71	NODE 103	100.19	NODE 104	99.77
NODE 201	121.13	NODE 202	119.97	NODE 203	118.99	~~NODE 204~~	~~118.17~~
NODE 301	130.44	NODE 302	137.94	NODE 303	152.02	NODE 304	168.38
NODE 305	190.85	NODE 306	207.88	NODE 307	206.12	NODE 308	130.00
NODE 309	148.91	NODE 310	128.74	NODE 311	114.76	NODE 312	108.78
NODE 401	115.70	NODE 402	112.19	NODE 403	107.12	NODE 404	100.75
NODE 405	91.39	NODE 406	78.24	NODE 407	76.10	NODE 408	83.58
NODE 409	88.84	NODE 410	92.53	NODE 411	95.37	~~NODE 412~~	~~97.64~~
NODE 413	54.03	NODE 414	33.86				

1/4 SCALE MODEL TEMPERATURES DEG F FREE CONVECTION TEST SERIES

RUN NUMBER 24.0 VOLTAGE 42.61 VOLTS CURRENT 0.3274 AMPS POWER 13.949 WATTS PRESSURE 1.003 ATM FLOW 0.0 LB/MIN

NODE 101	112.23	NODE 102	111.44	NODE 103	110.38	NODE 104	110.41
NODE 201	134.37	NODE 202	133.05	NODE 203	131.95	NODE 204	131.05
NODE 301	144.95	NODE 302	153.49	NODE 303	169.51	NODE 304	188.26
NODE 305	214.21	NODE 306	234.16	NODE 307	232.16	NODE 308	201.38
NODE 309	166.15	NODE 310	143.17	NODE 311	127.32	NODE 312	120.57
NODE 401	128.30	NODE 402	124.51	NODE 403	113.90	NODE 404	111.66
NODE 405	100.98	NODE 406	85.70	NODE 407	83.31	NODE 408	92.06
NODE 409	98.19	NODE 410	102.34	NODE 411	105.50	NODE 412	107.98
NODE 413	57.31	NODE 414	33.69				

RUN NUMBER 25.0 VOLTAGE 42.61 VOLTS CURRENT 0.3274 AMPS POWER 13.949 WATTS PRESSURE 0.479 ATM FLOW 0.0 LB/MIN

NODE 101	116.28	NODE 102	115.36	NODE 103	114.67	NODE 104	114.13
NODE 201	133.97	NODE 202	132.56	NODE 203	131.38	NODE 204	130.44
NODE 301	145.55	NODE 302	155.04	NODE 303	173.00	NODE 304	194.06
NODE 305	222.62	NODE 306	244.26	NODE 307	242.73	NODE 308	212.68
NODE 309	175.95	NODE 310	151.43	NODE 311	133.80	NODE 312	126.39
NODE 401	127.56	NODE 402	123.57	NODE 403	117.84	NODE 404	110.60
NODE 405	100.02	NODE 406	85.20	NODE 407	83.40	NODE 408	93.08
NODE 409	100.04	NODE 410	104.89	NODE 411	108.53	NODE 412	111.44
NODE 413	57.25	NODE 414	33.82				

RUN NUMBER 26.1 VOLTAGE 48.65 VOLTS CURRENT 0.3728 AMPS POWER 18.138 WATTS PRESSURE 0.443 ATM FLOW 0.0 LB/MIN

NODE 101	137.16	NODE 102	136.11	NODE 103	135.35	NODE 104	134.71
NODE 201	157.02	NODE 202	155.39	NODE 203	154.08	NODE 204	153.01
NODE 301	170.67	NODE 302	182.09	NODE 303	203.76	NODE 304	229.52
NODE 305	264.57	NODE 306	292.39	NODE 307	290.63	NODE 308	253.58
NODE 309	208.79	NODE 310	179.15	NODE 311	158.04	NODE 312	148.80
NODE 401	149.74	NODE 402	145.26	NODE 403	138.70	NODE 404	130.18
NODE 405	117.46	NODE 406	99.21	NODE 407	97.14	NODE 408	109.50
NODE 409	118.19	NODE 410	124.05	NODE 411	123.34	NODE 412	131.62
NODE 413	63.30	NODE 414	33.92				

1/4-SCALE MODEL TEMPERATURES DEG F FREE CONVECTION TEST SERIES

RUN NUMBER 27.1 VOLTAGE 48.59 VOLTS CURRENT 0.3726 AMPS POWER 13.107 WATTS PRESSURE 0.997 ATM FLOW 0.0 LB/MIN

NODE 101	131.91	NODE 102	131.09	NODE 103	130.45	NODE 104	129.96
NODE 201	157.51	~~NODE 202~~	~~155.99~~	~~NODE 203~~	~~154.71~~	~~NODE 204~~	~~153.65~~
NODE 301	170.04	NODE 302	180.18	NODE 303	199.63	NODE 304	222.48
NODE 305	254.59	NODE 306	279.73	NODE 307	277.44	NODE 308	240.00
NODE 309	196.39	~~NODE 310~~	168.59	~~NODE 311~~	143.56	~~NODE 312~~	~~141.56~~
NODE 401	150.52	NODE 402	146.24	NODE 403	139.77	NODE 404	131.25
NODE 405	119.37	NODE 406	99.58	NODE 407	96.73	NODE 408	107.83
NODE 409	115.50	~~NODE 410~~	~~120.57~~	~~NODE 411~~	~~124.28~~	~~NODE 412~~	~~127.09~~
NODE 413	63.83	NODE 414	34.09				

RUN NUMBER 28.0 VOLTAGE 48.57 VOLTS CURRENT 0.3726 AMPS POWER 13.099 WATTS PRESSURE 2.060 ATM FLOW 0.0 LB/MIN

NODE 101	125.99	NODE 102	125.36	NODE 103	124.90	NODE 104	124.51
NODE 201	156.77	NODE 202	155.41	~~NODE 203~~	154.19	~~NODE 204~~	~~153.20~~
NODE 301	168.06	NODE 302	176.94	NODE 303	193.87	NODE 304	213.71
NODE 305	242.34	NODE 306	265.17	NODE 307	262.22	NODE 308	224.74
NODE 309	182.91	~~NODE 310~~	~~157.45~~	~~NODE 311~~	~~140.72~~	~~NODE 312~~	~~133.35~~
NODE 401	150.33	NODE 402	146.35	NODE 403	140.13	NODE 404	131.35
NODE 405	119.03	NODE 406	99.90	NODE 407	96.21	NODE 408	106.06
NODE 409	112.52	NODE 410	116.71	NODE 411	119.77	NODE 412	122.06
NODE 413	63.89	NODE 414	33.94				

RUN NUMBER 29.1 VOLTAGE 48.80 VOLTS CURRENT 0.3748 AMPS POWER 13.291 WATTS PRESSURE 4.220 ATM FLOW 0.0 LB/MIN

NODE 101	120.35	NODE 102	119.88	NODE 103	119.50	NODE 104	119.17
NODE 201	155.52	NODE 202	154.36	NODE 203	153.24	~~NODE 204~~	~~152.39~~
NODE 301	165.38	NODE 302	173.08	NODE 303	187.09	NODE 304	203.51
NODE 305	228.33	NODE 306	248.95	NODE 307	244.78	NODE 308	207.67
NODE 309	168.31	NODE 310	145.80	NODE 311	131.94	NODE 312	126.51
NODE 401	149.88	NODE 402	146.41	NODE 403	140.64	NODE 404	132.78
NODE 405	120.31	NODE 406	100.92	NODE 407	95.41	NODE 408	104.68
NODE 409	110.13	NODE 410	113.36	NODE 411	115.71	~~NODE 412~~	~~117.49~~
NODE 413	64.16	NODE 414	32.45				

1/4 SCALE MODEL TEMPERATURES DEG F FREE CONVECTION TEST SERIES

RUN NUMBER 30.0 VOLTAGE 48.87 VOLTS CURRENT 0.3756 AMPS POWER 18.357 WATTS PRESSURE 8.010 ATM FLOW 0.0 LB/MIN

NODE 101	116.03	NODE 102	115.74	NODE 103	115.49	NODE 104	115.26
NODE 201	153.76	~~NODE 202~~	~~152.75~~	~~NODE 203~~	~~151.82~~	~~NODE 204~~	~~151.04~~
NODE 301	161.95	NODE 302	168.25	NODE 303	179.50	NODE 304	192.94
NODE 305	214.29	NODE 306	232.82	NODE 307	227.70	NODE 308	192.03
NODE 309	155.64	~~NODE 310~~	~~136.19~~	~~NODE 311~~	~~124.85~~	~~NODE 312~~	~~120.54~~
NODE 401	148.93	NODE 402	145.91	NODE 403	140.72	NODE 404	133.37
NODE 405	121.34	NODE 406	101.91	NODE 407	96.67	NODE 408	104.01
NODE 409	108.29	~~NODE 410~~	~~110.80~~	~~NODE 411~~	~~112.59~~	~~NODE 412~~	~~113.93~~
NODE 413	64.61	NODE 414	33.61				

RUN NUMBER 31.2 VOLTAGE 42.66 VOLTS CURRENT 0.3279 AMPS POWER 13.989 WATTS PRESSURE 1.990 ATM FLOW 0.0 LB/MIN

NODE 101	107.67	NODE 102	107.05	NODE 103	106.58	NODE 104	106.23
NODE 201	133.66	~~NODE 202~~	~~132.47~~	~~NODE 203~~	~~131.45~~	~~NODE 204~~	~~130.59~~
NODE 301	143.21	NODE 302	150.79	NODE 303	164.67	NODE 304	180.96
NODE 305	204.17	NODE 306	222.39	NODE 307	213.71	NODE 308	189.72
NODE 309	155.45	~~NODE 310~~	~~134.34~~	~~NODE 311~~	~~120.29~~	~~NODE 312~~	~~114.56~~
NODE 401	128.01	NODE 402	124.51	NODE 403	119.15	NODE 404	112.15
NODE 405	101.59	NODE 406	86.11	NODE 407	83.11	NODE 408	90.95
NODE 409	96.15	NODE 410	99.67	NODE 411	102.28	~~NODE 412~~	~~104.34~~
NODE 413	57.48	NODE 414	33.53				

RUN NUMBER 32.1 VOLTAGE 42.68 VOLTS CURRENT 0.3286 AMPS POWER 14.023 WATTS PRESSURE 4.010 ATM FLOW 0.0 LB/MIN

NODE 101	102.55	NODE 102	102.09	NODE 103	101.74	NODE 104	101.48
NODE 201	132.09	NODE 202	131.07	~~NODE 203~~	~~130.15~~	~~NODE 204~~	~~129.39~~
NODE 301	140.20	NODE 302	146.52	NODE 303	157.94	NODE 304	171.41
NODE 305	191.44	NODE 306	207.69	NODE 307	204.23	NODE 308	174.64
NODE 309	142.56	NODE 310	123.97	NODE 311	112.33	~~NODE 312~~	~~107.77~~
NODE 401	127.13	NODE 402	124.03	NODE 403	119.07	NODE 404	112.44
NODE 405	102.05	NODE 406	86.35	NODE 407	82.64	NODE 408	89.37
NODE 409	93.64	NODE 410	96.38	~~NODE 411~~	~~98.42~~	~~NODE 412~~	~~100.02~~
NODE 413	57.41	NODE 414	33.39				

1/4 SCALE MODEL TEMPERATURES DEG F FREE CONVECTION TEST SERIES

RUN NUMBER 33.0 VOLTAGE 42.68 VOLTS CURRENT 0.3287 AMPS POWER 14.028 WATTS PRESSURE 7.940 ATM FLOW 0.0 LB/MIN

NODE 101	97.09	NODE 102	96.87	NODE 103	96.68	NODE 104	96.53
NODE 201	129.21	~~NODE 202~~	~~128.32~~	~~NODE 203~~	~~127.54~~	~~NODE 204~~	~~125.94~~
NODE 301	135.68	NODE 302	140.69	NODE 303	149.47	NODE 304	160.16
NODE 305	177.14	NODE 306	191.72	NODE 307	137.36	NODE 308	159.38
NODE 309	130.10	~~NODE 310~~	~~114.13~~	NODE 311	104.59	~~NODE 312~~	~~110.83~~
NODE 401	125.29	NODE 402	122.75	NODE 403	113.35	NODE 404	112.27
NODE 405	102.51	NODE 406	86.73	NODE 407	82.19	NODE 408	87.72
NODE 409	90.98	~~NODE 410~~	~~92.97~~	~~NODE 411~~	~~94.43~~	~~NODE 412~~	~~95.54~~
NODE 413	57.66	NODE 414	33.44				

RUN NUMBER 34.0 VOLTAGE 38.97 VOLTS CURRENT 0.2999 AMPS POWER 11.687 WATTS PRESSURE 2.030 ATM FLOW 0.0 LB/MIN

NODE 101	97.09	NODE 102	96.52	NODE 103	95.10	NODE 104	95.77
NODE 201	119.38	~~NODE 202~~	~~118.85~~	~~NODE 203~~	~~117.93~~	~~NODE 204~~	~~117.13~~
NODE 301	127.74	NODE 302	134.42	NODE 303	146.31	NODE 304	160.45
NODE 305	180.64	NODE 306	196.55	NODE 307	194.12	NODE 308	168.75
NODE 309	139.35	~~NODE 310~~	~~120.91~~	~~NODE 311~~	~~103.52~~	~~NODE 312~~	~~103.35~~
NODE 401	114.90	NODE 402	111.73	NODE 403	106.95	NODE 404	100.77
NODE 405	91.54	NODE 406	78.18	NODE 407	75.54	NODE 408	82.22
NODE 409	86.73	NODE 410	89.81	NODE 411	92.18	~~NODE 412~~	~~94.08~~
NODE 413	53.85	NODE 414	33.78				

RUN NUMBER 35.1 VOLTAGE 39.00 VOLTS CURRENT 0.3007 AMPS POWER 11.727 WATTS PRESSURE 4.030 ATM FLOW 0.0 LB/MIN

NODE 101	92.91	NODE 102	92.49	NODE 103	92.18	NODE 104	91.94
NODE 201	118.96	NODE 202	118.04	~~NODE 203~~	~~117.22~~	~~NODE 204~~	~~116.55~~
NODE 301	126.09	NODE 302	131.54	NODE 303	141.35	NODE 304	152.95
NODE 305	170.08	NODE 306	183.86	NODE 307	180.78	NODE 308	155.50
NODE 309	127.86	NODE 310	111.73	NODE 311	101.59	~~NODE 312~~	~~97.55~~
NODE 401	114.55	NODE 402	111.70	NODE 403	107.24	NODE 404	101.33
NODE 405	92.21	NODE 406	78.56	NODE 407	75.33	NODE 408	81.10
NODE 409	84.82	NODE 410	87.26	NODE 411	89.11	~~NODE 412~~	~~90.57~~
NODE 413	53.82	NODE 414	33.33				

1/4 SCALE MODEL TEMPERATURES DEG F FREE CONVECTION TEST SERIES

RUN NUMBER 36.0 VOLTAGE 38.98 VOLTS CURRENT 0.3005 AMPS POWER 11.713 WATTS PRESSURE 7.900 ATM FLOW 0.0 LB/MIN

NODE 101	87.44	NODE 102	87.23	NODE 103	87.07	NODE 104	86.93
NODE 201	115.70	NODE 202	114.91	NODE 203	114.24	~~NODE 204~~	~~113.71~~
NODE 301	121.41	NODE 302	125.64	NODE 303	133.17	NODE 304	142.37
NODE 305	156.90	NODE 306	169.13	NODE 307	165.42	NODE 308	141.35
NODE 309	116.11	NODE 310	102.26	NODE 311	94.03	~~NODE 312~~	~~90.69~~
NODE 401	112.26	NODE 402	109.95	NODE 403	105.03	NODE 404	100.63
NODE 405	92.12	NODE 406	78.47	NODE 407	74.50	NODE 408	79.18
NODE 409	81.99	NODE 410	83.73	NODE 411	95.03	~~NODE 412~~	~~36.03~~
NODE 413	53.85	NODE 414	33.37				

RUN NUMBER 37.1 VOLTAGE 33.66 VOLTS CURRENT 0.2594 AMPS POWER 8.734 WATTS PRESSURE 2.000 ATM FLOW 0.0 LB/MIN

NODE 101	83.24	NODE 102	82.75	NODE 103	82.38	NODE 104	82.12
NODE 201	101.82	NODE 202	100.92	NODE 203	100.17	~~NODE 204~~	~~99.56~~
NODE 301	108.42	NODE 302	113.62	NODE 303	123.12	NODE 304	134.20
NODE 305	149.73	NODE 306	161.61	NODE 307	159.62	NODE 308	139.68
NODE 309	116.45	NODE 310	101.89	~~NODE 311~~	92.12	~~NODE 312~~	~~88.08~~
NODE 401	97.51	NODE 402	94.80	NODE 403	90.32	NODE 404	85.73
NODE 405	78.30	NODE 406	67.76	NODE 407	65.70	NODE 408	70.89
NODE 409	74.47	NODE 410	77.02	NODE 411	79.01	~~NODE 412~~	~~30.66~~
NODE 413	48.57	NODE 414	33.38				

RUN NUMBER 38.1 VOLTAGE 33.67 VOLTS CURRENT 0.2595 AMPS POWER 8.739 WATTS PRESSURE 4.010 ATM FLOW 0.0 LB/MIN

NODE 101	79.85	NODE 102	79.46	NODE 103	79.18	NODE 104	73.98
NODE 201	100.70	NODE 202	99.92	~~NODE 203~~	99.25	~~NODE 204~~	~~98.72~~
NODE 301	106.30	NODE 302	110.57	NODE 303	118.24	NODE 304	127.34
NODE 305	140.68	NODE 306	151.21	NODE 307	143.76	NODE 308	129.23
NODE 309	107.58	NODE 310	94.88	NODE 311	95.81	~~NODE 312~~	~~93.61~~
NODE 401	96.99	NODE 402	94.56	NODE 403	93.82	NODE 404	96.05
NODE 405	78.77	NODE 406	68.03	NODE 407	65.46	NODE 408	69.94
NODE 409	72.92	NODE 410	74.94	~~NODE 411~~	76.52	~~NODE 412~~	~~77.42~~
NODE 413	49.01	NODE 414	33.27				

1/4 SCALE MODEL TEMPERATURES DEG F FREE CONVECTION TEST SERIES

RUN NUMBER 39.0 VOLTAGE 33.67 VOLTS CURRENT 0.2597 AMPS POWER 8.747 WATTS PRESSURE 7.930 ATM FLOW 0.0 LB/MIN

NODE 101	75.91	NODE 102	75.67	NODE 103	75.49	NODE 104	75.36
NODE 201	98.24	NODE 202	97.57	NODE 203	97.00	NODE 204	96.57
NODE 301	102.67	NODE 302	105.82	NODE 303	111.68	NODE 304	118.75
NODE 305	129.92	NODE 306	139.18	NODE 307	136.35	NODE 308	117.69
NODE 309	98.05	NODE 310	87.28	NODE 311	80.86	NODE 312	78.35
NODE 401	95.30	NODE 402	93.28	NODE 403	90.03	NODE 404	85.61
NODE 405	78.74	NODE 406	68.03	NODE 407	64.95	NODE 408	68.63
NODE 409	70.93	NODE 410	72.42	NODE 411	73.59	NODE 412	74.53
NODE 413	49.12	NODE 414	33.42				

II-A.1.3 FORCED CONVECTION TEST SERIES

1/4 SCALE MODEL TEMPERATURES DEG F FORCED CONVECTION TEST SERIES

RUN NUMBER 44.0 VOLTAGE 60.38 VOLTS CURRENT 0.4637 AMPS POWER 28.000 WATTS PRESSURE 1.990 ATM FLOW 1.24000 LB/MIN

NODE 101	68.08	NODE 102	68.47	NODE 103	69.67	NODE 104	68.76
NODE 201	69.86	NODE 202	69.69	NODE 203	69.60	NODE 204	69.51
NODE 301	71.94	NODE 302	74.53	NODE 303	81.86	NODE 304	95.71
NODE 305	127.79	NODE 306	164.34	NODE 307	168.00	NODE 308	131.31
NODE 309	98.50	NODE 310	83.64	NODE 311	74.60	NODE 312	69.85
NODE 401	69.24	NODE 402	68.86	NODE 403	68.34	NODE 404	67.44
NODE 405	65.56	NODE 406	61.46	NODE 407	62.15	NODE 408	66.91
NODE 409	68.73	NODE 410	69.19	NODE 411	69.18	NODE 412	69.36
NODE 413	46.89	NODE 414	33.30	AIR TOP	69.07	AIR BOTTOM	64.97

RUN NUMBER 45.0 VOLTAGE 60.34 VOLTS CURRENT 0.4634 AMPS POWER 27.964 WATTS PRESSURE 1.110 ATM FLOW 1.24000 LB/MIN

NODE 101	67.84	NODE 102	68.21	NODE 103	69.42	NODE 104	68.52
NODE 201	69.54	NODE 202	69.41	NODE 203	69.32	NODE 204	69.28
NODE 301	71.43	NODE 302	74.00	NODE 303	91.34	NODE 304	95.13
NODE 305	127.28	NODE 306	164.04	NODE 307	167.43	NODE 308	130.71
NODE 309	98.37	NODE 310	83.43	NODE 311	74.52	NODE 312	69.55
NODE 401	68.93	NODE 402	68.65	NODE 403	68.14	NODE 404	67.24
NODE 405	65.37	NODE 406	61.26	NODE 407	61.96	NODE 408	66.70
NODE 409	68.54	NODE 410	69.01	NODE 411	69.02	NODE 412	68.86
NODE 413	46.65	NODE 414	32.94	AIR TOP	67.03	AIR BOTTOM	63.65

RUN NUMBER 46.1 VOLTAGE 60.63 VOLTS CURRENT 0.4656 AMPS POWER 28.231 WATTS PRESSURE 3.850 ATM FLOW 1.26000 LB/MIN

NODE 101	67.95	NODE 102	68.33	NODE 103	68.54	NODE 104	68.63
NODE 201	69.65	NODE 202	69.47	NODE 203	69.39	NODE 204	69.31
NODE 301	71.69	NODE 302	74.20	NODE 303	81.75	NODE 304	94.39
NODE 305	126.74	NODE 306	163.26	NODE 307	166.29	NODE 308	129.61
NODE 309	97.59	NODE 310	82.81	NODE 311	74.08	NODE 312	69.53
NODE 401	69.01	NODE 402	68.73	NODE 403	68.19	NODE 404	67.29
NODE 405	65.40	NODE 406	61.29	NODE 407	61.92	NODE 408	66.59
NODE 409	68.39	NODE 410	68.85	NODE 411	68.92	NODE 412	68.75
NODE 413	46.62	NODE 414	32.97	AIR TOP	69.45	AIR BOTTOM	65.36

1/4 SCALE MODEL TEMPERATURES DEG F FORCED CONVECTION TEST SERIES

RUN NUMBER 47.0 VOLTAGE 60.58 VOLTS CURRENT 0.4653 AMPS POWER 28.190 WATTS PRESSURE 7.960 ATM FLOW 1.26000 LB/MIN

NODE 101	70.20	NODE 102	70.55	NODE 103	70.76	NODE 104	70.85
NODE 201	71.90	NODE 202	71.69	NODE 203	71.57	NODE 204	71.49
NODE 301	74.50	NODE 302	76.67	NODE 303	84.26	NODE 304	97.28
NODE 305	128.31	NODE 306	164.62	NODE 307	166.55	NODE 308	130.28
NODE 309	98.72	NODE 310	84.48	NODE 311	75.08	NODE 312	71.76
NODE 401	71.18	NODE 402	70.93	NODE 403	70.43	NODE 404	69.50
NODE 405	67.51	NODE 406	63.06	NODE 407	63.55	NODE 408	68.52
NODE 409	70.46	NODE 410	71.02	NODE 411	71.02	NODE 412	70.93
NODE 413	47.69	NODE 414	33.07	AIR TOP	71.81	AIR BOTTOM	67.87

RUN NUMBER 48.0 VOLTAGE 48.87 VOLTS CURRENT 0.3761 AMPS POWER 18.381 WATTS PRESSURE 7.970 ATM FLOW 0.29000 LB/MIN

NODE 101	70.57	NODE 102	70.57	NODE 103	70.58	NODE 104	70.57
NODE 201	77.99	NODE 202	77.13	NODE 203	75.62	NODE 204	76.30
NODE 301	85.19	NODE 302	93.15	NODE 303	106.94	NODE 304	123.54
NODE 305	150.16	NODE 306	172.67	NODE 307	171.89	NODE 308	138.68
NODE 309	106.05	NODE 310	89.10	NODE 311	78.51	NODE 312	73.63
NODE 401	75.31	NODE 402	73.97	NODE 403	72.22	NODE 404	69.89
NODE 405	66.18	NODE 406	59.78	NODE 407	59.01	NODE 408	63.75
NODE 409	66.98	NODE 410	68.93	NODE 411	69.89	NODE 412	70.27
NODE 413	45.59	NODE 414	33.07	AIR TOP	78.13	AIR BOTTOM	68.74

RUN NUMBER 49.0 VOLTAGE 48.87 VOLTS CURRENT 0.3760 AMPS POWER 18.375 WATTS PRESSURE 1.075 ATM FLOW 0.29200 LB/MIN

NODE 101	72.08	NODE 102	72.31	NODE 103	72.43	NODE 104	72.47
NODE 201	76.31	NODE 202	75.75	NODE 203	75.39	NODE 204	75.15
NODE 301	82.37	NODE 302	89.17	NODE 303	103.47	NODE 304	123.63
NODE 305	156.29	NODE 306	182.96	NODE 307	186.20	NODE 308	153.15
NODE 309	118.67	NODE 310	98.36	NODE 311	83.72	NODE 312	75.89
NODE 401	74.21	NODE 402	73.11	NODE 403	71.56	NODE 404	69.47
NODE 405	66.09	NODE 406	60.56	NODE 407	60.89	NODE 408	66.70
NODE 409	70.24	NODE 410	71.96	NODE 411	72.55	NODE 412	72.66
NODE 413	46.50	NODE 414	33.79	AIR TOP	76.06	AIR BOTTOM	66.64

1/4 SCALE MODEL TEMPERATURES DEG F FORCED CONVECTION TEST SERIES

RUN NUMBER 50.0 VOLTAGE 48.87 VOLTS CURRENT 0.3760 AMPS POWER 18.376 WATTS PRESSURE 1.078 ATM FLOW 0.28500 LB/MIN

NODE 101	72.05	NODE 102	72.28	NODE 103	72.41	NODE 104	72.44
NODE 201	76.52	NODE 202	75.96	NODE 203	75.60	NODE 204	75.35
NODE 301	82.71	NODE 302	89.34	NODE 303	104.21	NODE 304	124.58
NODE 305	157.60	NODE 306	184.18	NODE 307	187.44	NODE 308	154.12
NODE 309	119.31	NODE 310	98.72	NODE 311	83.90	NODE 312	75.95
NODE 401	74.44	NODE 402	73.30	NODE 403	71.69	NODE 404	69.57
NODE 405	66.14	NODE 406	60.53	NODE 407	60.86	NODE 408	66.75
NODE 409	70.30	NODE 410	71.99	NODE 411	72.59	NODE 412	72.70
NODE 413	46.22	NODE 414	33.21	AIR TOP	76.18	AIR BOTTOM	66.47

RUN NUMBER 51.0 VOLTAGE 48.85 VOLTS CURRENT 0.3756 AMPS POWER 18.351 WATTS PRESSURE 1.970 ATM FLOW 0.28700 LB/MIN

NODE 101	72.33	NODE 102	72.52	NODE 103	72.62	NODE 104	72.65
NODE 201	76.97	NODE 202	76.40	NODE 203	76.03	NODE 204	75.77
NODE 301	83.42	NODE 302	90.05	NODE 303	104.99	NODE 304	125.09
NODE 305	157.20	NODE 306	183.29	NODE 307	185.80	NODE 308	152.65
NODE 309	118.22	NODE 310	98.17	NODE 311	83.78	NODE 312	76.16
NODE 401	74.86	NODE 402	73.67	NODE 403	72.04	NODE 404	69.82
NODE 405	66.32	NODE 406	60.65	NODE 407	60.88	NODE 408	66.70
NODE 409	70.29	NODE 410	71.99	NODE 411	72.66	NODE 412	72.79
NODE 413	46.32	NODE 414	33.33	AIR TOP	76.80	AIR BOTTOM	67.30

RUN NUMBER 52.0 VOLTAGE 48.86 VOLTS CURRENT 0.3757 AMPS POWER 18.358 WATTS PRESSURE 4.000 ATM FLOW 0.29200 LB/MIN

NODE 101	70.93	NODE 102	71.05	NODE 103	71.13	NODE 104	71.15
NODE 201	76.77	NODE 202	76.13	NODE 203	75.76	NODE 204	75.47
NODE 301	98.50	NODE 302	90.52	NODE 303	105.59	NODE 304	124.75
NODE 305	155.32	NODE 306	180.32	NODE 307	181.17	NODE 308	147.31
NODE 309	113.54	NODE 310	94.37	NODE 311	80.86	NODE 312	74.65
NODE 401	74.55	NODE 402	73.32	NODE 403	71.58	NODE 404	69.30
NODE 405	65.62	NODE 406	59.74	NODE 407	59.59	NODE 408	64.90
NODE 409	68.24	NODE 410	69.92	NODE 411	70.62	NODE 412	70.84
NODE 413	45.78	NODE 414	33.34	AIR TOP	76.68	AIR BOTTOM	67.03

1/4 SCALE MODEL TEMPERATURES DEG F FORCED CONVECTION TEST SERIES

RUN NUMBER 53.0 VOLTAGE 60.25 VOLTS CURRENT 0.4620 AMPS POWER 27.338 WATTS PRESSURE 8.000 ATM FLOW 0.29200 LB/MIN

NODE 101	72.33	NODE 102	72.40	NODE 103	72.47	NODE 104	72.49
NODE 201	85.59	NODE 202	84.40	NODE 203	83.74	NODE 204	83.31
NODE 301	97.29	NODE 302	107.23	NODE 303	127.64	NODE 304	151.77
NODE 305	190.44	NODE 306	223.32	NODE 307	221.15	NODE 308	172.25
NODE 309	124.35	NODE 310	99.32	NODE 311	83.83	NODE 312	76.49
NODE 401	81.94	NODE 402	79.99	NODE 403	77.71	NODE 404	74.93
NODE 405	70.73	NODE 406	63.44	NODE 407	62.46	NODE 408	67.39
NODE 409	70.40	NODE 410	71.89	NODE 411	72.36	NODE 412	72.48
NODE 413	47.52	NODE 414	33.45	AIR TOP	85.48	AIR BOTTOM	69.21

RUN NUMBER 54.0 VOLTAGE 60.22 VOLTS CURRENT 0.4615 AMPS POWER 27.794 WATTS PRESSURE 1.070 ATM FLOW 0.29400 LB/MIN

NODE 101	75.45	NODE 102	75.88	NODE 103	76.15	NODE 104	76.25
NODE 201	83.76	NODE 202	83.07	NODE 203	82.65	NODE 204	82.38
NODE 301	92.30	NODE 302	101.68	NODE 303	123.29	NODE 304	152.71
NODE 305	199.91	NODE 306	239.31	NODE 307	242.85	NODE 308	194.81
NODE 309	144.55	NODE 310	114.51	NODE 311	92.75	NODE 312	80.84
NODE 401	81.44	NODE 402	80.31	NODE 403	78.68	NODE 404	76.34
NODE 405	72.34	NODE 406	65.64	NODE 407	65.75	NODE 408	72.10
NODE 409	75.54	NODE 410	76.82	NODE 411	76.99	NODE 412	76.78
NODE 413	48.75	NODE 414	33.49	AIR TOP	82.56	AIR BOTTOM	66.76

RUN NUMBER 55.0 VOLTAGE 60.27 VOLTS CURRENT 0.4615 AMPS POWER 27.343 WATTS PRESSURE 1.950 ATM FLOW 0.23500 LB/MIN

NODE 101	73.55	NODE 102	73.94	NODE 103	74.13	NODE 104	74.20
NODE 201	83.03	NODE 202	82.30	NODE 203	81.89	NODE 204	81.58
NODE 301	92.22	NODE 302	101.97	NODE 303	124.28	NODE 304	153.07
NODE 305	200.62	NODE 306	239.02	NODE 307	242.01	NODE 308	193.11
NODE 309	142.16	NODE 310	112.13	NODE 311	90.58	NODE 312	78.97
NODE 401	80.62	NODE 402	79.42	NODE 403	77.69	NODE 404	75.26
NODE 405	71.23	NODE 406	64.55	NODE 407	64.52	NODE 408	70.43
NODE 409	73.74	NODE 410	74.94	NODE 411	75.11	NODE 412	74.87
NODE 413	48.19	NODE 414	33.49	AIR TOP	81.91	AIR BOTTOM	65.57

1/4 SCALE MODEL TEMPERATURES DEG F FORCED CONVECTION TEST SERIES

RUN NUMBER 56.1 VOLTAGE 60.25 VOLTS CURRENT 0.4618 AMPS POWER 27.826 WATTS PRESSURE 4.000 ATM FLOW 0.29200 LB/MIN

NODE 101	73.47	NODE 102	73.73	NODE 103	73.89	NODE 104	73.96
NODE 201	84.04	NODE 202	83.12	NODE 203	82.61	NODE 204	82.26
NODE 301	94.79	NODE 302	104.60	NODE 303	127.11	NODE 304	155.16
NODE 305	199.22	NODE 306	235.37	NODE 307	236.53	NODE 308	186.45
NODE 309	136.04	NODE 310	107.76	NODE 311	83.33	NODE 312	78.68
NODE 401	81.11	NODE 402	79.71	NODE 403	77.84	NODE 404	75.29
NODE 405	71.02	NODE 406	63.99	NODE 407	63.58	NODE 408	69.28
NODE 409	72.49	NODE 410	73.77	NODE 411	74.03	NODE 412	73.91
NODE 413	47.64	NODE 414	33.11	AIR TOP	83.45	AIR BOTTOM	67.57

RUN NUMBER 57.0 VOLTAGE 42.63 VOLTS CURRENT 0.3282 AMPS POWER 13.989 WATTS PRESSURE 4.020 ATM FLOW 0.29200 LB/MIN

NODE 101	70.05	NODE 102	70.11	NODE 103	70.13	NODE 104	70.14
NODE 201	73.43	NODE 202	72.91	NODE 203	72.57	NODE 204	72.33
NODE 301	78.74	NODE 302	83.76	NODE 303	95.13	NODE 304	109.89
NODE 305	133.75	NODE 306	153.16	NODE 307	154.16	NODE 308	128.70
NODE 309	102.41	NODE 310	87.71	NODE 311	77.74	NODE 312	71.91
NODE 401	71.48	NODE 402	70.32	NODE 403	68.71	NODE 404	66.59
NODE 405	63.23	NODE 406	57.88	NODE 407	57.97	NODE 408	63.28
NODE 409	66.82	NODE 410	68.71	NODE 411	69.59	NODE 412	69.92
NODE 413	44.85	NODE 414	33.06	AIR TOP	73.59	AIR BOTTOM	67.27

RUN NUMBER 58.0 VOLTAGE 42.64 VOLTS CURRENT 0.3283 AMPS POWER 13.996 WATTS PRESSURE 1.076 ATM FLOW 0.29300 LB/MIN

NODE 101	70.64	NODE 102	70.77	NODE 103	70.85	NODE 104	70.85
NODE 201	73.03	NODE 202	72.54	NODE 203	72.25	NODE 204	72.01
NODE 301	77.72	NODE 302	82.79	NODE 303	93.89	NODE 304	109.33
NODE 305	134.81	NODE 306	155.57	NODE 307	158.11	NODE 308	132.81
NODE 309	106.24	NODE 310	90.52	NODE 311	79.46	NODE 312	73.61
NODE 401	71.13	NODE 402	70.04	NODE 403	68.54	NODE 404	66.57
NODE 405	63.48	NODE 406	58.42	NODE 407	58.92	NODE 408	64.66
NODE 409	68.30	NODE 410	70.12	NODE 411	70.96	NODE 412	71.16
NODE 413	45.19	NODE 414	33.07	AIR TOP	73.09	AIR BOTTOM	66.67

1/4 SCALE MODEL TEMPERATURES DEG F FORCED CONVECTION TEST SERIES

RUN NUMBER 59.0 VOLTAGE 48.93 VOLTS CURRENT 0.3762 AMPS POWER 18.409 WATTS PRESSURE 7.990 ATM FLOW 0.07340 LB/MIN

NODE 101	74.00	NODE 102	73.93	NODE 103	73.91	NODE 104	73.89
NODE 201	100.68	~~NODE 202~~	~~99.14~~	~~NODE 203~~	~~98.17~~	~~NODE 204~~	~~97.43~~
NODE 301	110.08	NODE 302	116.74	NODE 303	129.20	NODE 304	144.53
NODE 305	168.42	NODE 306	188.77	NODE 307	185.36	NODE 308	149.08
NODE 309	113.18	NODE 310	94.14	~~NODE 311~~	92.41	~~NODE 312~~	~~77.40~~
NODE 401	95.45	NODE 402	92.11	NODE 403	87.36	NODE 404	81.75
NODE 405	74.53	NODE 406	64.73	NODE 407	62.61	NODE 408	66.93
NODE 409	69.72	~~NODE 410~~	~~71.53~~	~~NODE 411~~	~~72.67~~	~~NODE 412~~	~~73.31~~
NODE 413	47.84	NODE 414	33.40	AIR TOP	101.94	AIR BOTTOM	70.02

RUN NUMBER 60.0 VOLTAGE 48.93 VOLTS CURRENT 0.3760 AMPS POWER 18.397 WATTS PRESSURE 4.060 ATM FLOW 0.07430 LB/MIN

NODE 101	74.87	NODE 102	74.86	NODE 103	74.87	NODE 104	74.86
NODE 201	98.25	NODE 202	96.55	NODE 203	95.42	~~NODE 204~~	~~94.53~~
NODE 301	110.02	NODE 302	118.69	NODE 303	134.64	NODE 304	153.60
NODE 305	181.73	NODE 306	204.61	NODE 307	201.92	NODE 308	164.44
NODE 309	124.85	~~NODE 310~~	~~101.97~~	~~NODE 311~~	~~85.67~~	~~NODE 312~~	~~79.51~~
NODE 401	91.80	NODE 402	88.11	NODE 403	83.59	NODE 404	78.71
NODE 405	72.35	NODE 406	63.72	NODE 407	62.35	NODE 408	67.30
NODE 409	70.57	NODE 410	72.60	NODE 411	73.73	~~NODE 412~~	~~74.29~~
NODE 413	47.35	NODE 414	33.44	AIR TOP	100.17	AIR BOTTOM	68.20

RUN NUMBER 61.0 VOLTAGE 48.92 VOLTS CURRENT 0.3758 AMPS POWER 18.387 WATTS PRESSURE 1.930 ATM FLOW 0.07430 LB/MIN

NODE 101	78.40	NODE 102	78.41	NODE 103	78.44	NODE 104	78.43
NODE 201	97.74	~~NODE 202~~	~~96.09~~	~~NODE 203~~	~~95.03~~	~~NODE 204~~	~~94.27~~
NODE 301	110.81	NODE 302	120.74	NODE 303	139.71	NODE 304	162.11
NODE 305	193.94	NODE 306	219.13	NODE 307	217.11	NODE 308	179.18
NODE 309	137.28	NODE 310	111.59	NODE 311	93.32	NODE 312	~~83.93~~
NODE 401	91.72	NODE 402	88.61	NODE 403	84.79	NODE 404	80.44
NODE 405	74.31	NODE 406	65.52	NODE 407	64.37	NODE 408	70.09
NODE 409	73.89	~~NODE 410~~	~~76.23~~	NODE 411	~~77.45~~	~~NODE 412~~	~~77.99~~
NODE 413	48.27	NODE 414	33.52	AIR TOP	99.04	AIR BOTTOM	69.12

1/4 SCALE MODEL TEMPERATURES DEG F FORCED CONVECTION TEST SERIES

RUN NUMBER 62.0 VOLTAGE 48.93 VOLTS CURRENT 0.3757 AMPS POWER 18.385 WATTS PRESSURE 0.997 ATM FLOW 0.07490 LB/MIN

NODE 101	80.99	NODE 102	81.09	NODE 103	81.15	NODE 104	81.13
NODE 201	97.76	~~NODE 202~~	~~96.33~~	~~NODE 203~~	~~95.41~~	~~NODE 204~~	~~94.74~~
NODE 301	110.60	NODE 302	121.06	NODE 303	141.62	NODE 304	166.06
NODE 305	200.59	NODE 306	227.34	NODE 307	225.14	NODE 308	188.27
NODE 309	145.21	~~NODE 310~~	~~117.99~~	~~NODE 311~~	~~97.80~~	~~NODE 312~~	~~86.87~~
NODE 401	92.58	NODE 402	89.91	NODE 403	86.52	NODE 404	82.34
NODE 405	76.13	NODE 406	67.06	NODE 407	66.02	NODE 408	72.33
NODE 409	76.59	~~NODE 410~~	~~79.13~~	~~NODE 411~~	~~80.42~~	~~NODE 412~~	~~80.93~~
NODE 413	49.00	NODE 414	33.45	AIR TOP	97.85	AIR BOTTOM	69.33

RUN NUMBER 63.0 VOLTAGE 42.60 VOLTS CURRENT 0.3278 AMPS POWER 13.963 WATTS PRESSURE 1.010 ATM FLOW 0.07500 LB/MIN

NODE 101	76.94	NODE 102	76.90	NODE 103	76.86	NODE 104	76.81
NODE 201	88.31	~~NODE 202~~	~~87.13~~	~~NODE 203~~	~~86.35~~	~~NODE 204~~	~~85.79~~
NODE 301	98.62	NODE 302	106.80	NODE 303	123.26	NODE 304	142.58
NODE 305	169.84	NODE 306	190.77	NODE 307	189.75	NODE 308	160.29
NODE 309	126.64	~~NODE 310~~	~~105.50~~	~~NODE 311~~	~~93.04~~	~~NODE 312~~	~~81.87~~
NODE 401	83.93	NODE 402	81.57	NODE 403	78.56	NODE 404	74.93
NODE 405	69.62	NODE 406	61.92	NODE 407	61.20	NODE 408	66.91
NODE 409	71.05	~~NODE 410~~	~~73.84~~	~~NODE 411~~	~~75.53~~	~~NODE 412~~	~~76.37~~
NODE 413	46.64	NODE 414	33.49	AIR TOP	89.06	AIR BOTTOM	69.24

RUN NUMBER 64.0 VOLTAGE 42.61 VOLTS CURRENT 0.3279 AMPS POWER 13.970 WATTS PRESSURE 1.990 ATM FLOW 0.07440 LB/MIN

NODE 101	75.49	NODE 102	75.41	NODE 103	75.34	NODE 104	75.27
NODE 201	88.61	~~NODE 202~~	~~87.28~~	~~NODE 203~~	~~86.39~~	~~NODE 204~~	~~85.79~~
NODE 301	99.12	NODE 302	107.09	NODE 303	122.22	NODE 304	139.97
NODE 305	165.12	NODE 306	184.81	NODE 307	183.29	NODE 308	153.91
NODE 309	121.13	NODE 310	101.12	~~NODE 311~~	~~87.11~~	~~NODE 312~~	~~80.16~~
NODE 401	83.69	NODE 402	81.12	NODE 403	77.92	NODE 404	74.22
NODE 405	68.93	NODE 406	61.35	NODE 407	60.46	NODE 408	65.71
NODE 409	69.47	NODE 410	72.08	~~NODE 411~~	~~73.73~~	~~NODE 412~~	~~74.64~~
NODE 413	46.32	NODE 414	33.45	AIR TOP	90.20	AIR BOTTOM	69.51

1/4 SCALE MODEL TEMPERATURES DEG F   FORCED CONVECTION TEST SERIES

RUN NUMBER 65.0   VOLTAGE 42.59 VOLTS   CURRENT 0.3279 AMPS   POWER 13.965 WATTS   PRESSURE 4.020 ATM   FLOW 0.07390 LB/MIN

NODE 101	73.02	NODE 102	72.86	NODE 103	72.77	NODE 104	72.68
NODE 201	89.09	NODE 202	87.70	~~NODE 203~~	~~86.79~~	~~NODE 204~~	~~86.12~~
NODE 301	98.57	NODE 302	105.67	NODE 303	113.51	NODE 304	133.85
NODE 305	156.26	NODE 306	174.23	NODE 307	171.89	NODE 308	142.93
NODE 309	111.90	NODE 310	94.05	NODE 311	82.30	~~NODE 312~~	~~77.05~~
NODE 401	83.84	NODE 402	80.80	NODE 403	77.13	NODE 404	73.12
NODE 405	67.75	NODE 406	60.31	NODE 407	59.22	NODE 408	63.87
NODE 409	67.15	NODE 410	69.45	~~NODE 411~~	~~71.02~~	~~NODE 412~~	~~71.95~~
NODE 413	45.87	NODE 414	33.48	AIR TOP	91.05	AIR BOTTOM	69.21

RUN NUMBER 66.0   VOLTAGE 42.60 VOLTS   CURRENT 0.3281 AMPS   POWER 13.975 WATTS   PRESSURE 8.050 ATM   FLOW 0.07500 LB/MIN

NODE 101	71.55	NODE 102	71.37	NODE 103	71.26	NODE 104	71.16
NODE 201	90.24	NODE 202	89.05	NODE 203	88.26	~~NODE 204~~	~~87.72~~
NODE 301	97.61	NODE 302	102.95	NODE 303	113.16	NODE 304	125.62
NODE 305	144.67	NODE 306	160.56	NODE 307	157.81	NODE 308	129.80
NODE 309	101.80	~~NODE 310~~	~~86.98~~	~~NODE 311~~	~~78.10~~	~~NODE 312~~	~~74.59~~
NODE 401	85.99	NODE 402	83.26	NODE 403	79.42	NODE 404	74.88
NODE 405	69.02	NODE 406	60.87	NODE 407	53.25	NODE 408	63.27
NODE 409	66.01	~~NODE 410~~	67.97	~~NODE 411~~	69.45	~~NODE 412~~	~~70.42~~
NODE 413	46.16	NODE 414	33.48	AIR TOP	91.66	AIR BOTTOM	70.05

RUN NUMBER 67.0   VOLTAGE 38.97 VOLTS   CURRENT 0.3005 AMPS   POWER 11.710 WATTS   PRESSURE 8.020 ATM   FLOW 0.07550 LB/MIN

NODE 101	69.65	NODE 102	69.46	NODE 103	69.31	NODE 104	69.20
NODE 201	84.73	~~NODE 202~~	~~83.70~~	~~NODE 203~~	~~83.03~~	~~NODE 204~~	~~92.55~~
NODE 301	91.22	NODE 302	96.01	NODE 303	104.86	NODE 304	115.58
NODE 305	132.04	NODE 306	145.63	NODE 307	143.16	NODE 308	119.52
NODE 309	95.52	NODE 310	82.96	NODE 311	75.37	~~NODE 312~~	~~72.47~~
NODE 401	81.02	NODE 402	78.55	NODE 403	73.14	NODE 404	71.17
NODE 405	65.96	NODE 406	58.64	NODE 407	57.23	NODE 408	61.06
NODE 409	53.75	~~NODE 410~~	~~65.73~~	~~NODE 411~~	~~67.30~~	~~NODE 412~~	~~69.39~~
NODE 413	45.11	NODE 414	33.43	AIR TOP	35.21	AIR BOTTOM	68.93

1/4 SCALE MODEL TEMPERATURES DEG F FORCED CONVECTION TEST SERIES

RUN NUMBER 68.0 VOLTAGE 39.00 VOLTS CURRENT 0.3004 AMPS POWER 11.715 WATTS PRESSURE 1.020 ATM FLOW 0.07520 LB/MIN

NODE 101	74.90	NODE 102	74.79	NODE 103	74.70	NODE 104	74.61
NODE 201	83.51	NODE 202	82.45	~~NODE 203~~	~~81.75~~	~~NODE 204~~	~~81.24~~
NODE 301	92.47	NODE 302	99.56	NODE 303	113.53	NODE 304	130.16
NODE 305	153.50	NODE 306	171.27	NODE 307	170.35	NODE 308	145.40
NODE 309	116.84	NODE 310	98.96	NODE 311	85.99	~~NODE 312~~	~~79.33~~
NODE 401	79.53	NODE 402	77.37	NODE 403	74.58	NODE 404	71.22
NODE 405	66.35	NODE 406	59.37	NODE 407	53.80	NODE 408	64.18
NODE 409	68.25	NODE 410	71.18	NODE 411	73.06	~~NODE 412~~	~~74.03~~
NODE 413	45.43	NODE 414	33.42	AIR TOP	84.62	AIR BOTTOM	69.18

RUN NUMBER 69.0 VOLTAGE 39.00 VOLTS CURRENT 0.3004 AMPS POWER 11.715 WATTS PRESSURE 2.010 ATM FLOW 0.07520 LB/MIN

NODE 101	73.32	NODE 102	73.17	NODE 103	73.05	NODE 104	72.95
NODE 201	83.20	NODE 202	82.04	NODE 203	81.30	~~NODE 204~~	~~80.75~~
NODE 301	92.30	NODE 302	99.18	NODE 303	112.19	NODE 304	127.46
NODE 305	149.07	NODE 306	165.91	NODE 307	154.51	NODE 308	139.62
NODE 309	111.76	~~NODE 310~~	~~94.89~~	~~NODE 311~~	~~83.12~~	~~NODE 312~~	~~77.49~~
NODE 401	78.89	NODE 402	76.62	NODE 403	73.79	NODE 404	70.45
NODE 405	65.66	NODE 406	58.84	NODE 407	58.09	NODE 408	63.03
NODE 409	66.69	NODE 410	69.39	NODE 411	71.19	~~NODE 412~~	~~72.23~~
NODE 413	45.19	NODE 414	33.44	AIR TOP	84.36	AIR BOTTOM	69.15

RUN NUMBER 70.0 VOLTAGE 38.98 VOLTS CURRENT 0.3003 AMPS POWER 11.707 WATTS PRESSURE 4.060 ATM FLOW 0.07610 LB/MIN

NODE 101	70.78	NODE 102	70.59	NODE 103	70.43	NODE 104	70.35
NODE 201	83.20	~~NODE 202~~	~~82.01~~	~~NODE 203~~	~~81.20~~	~~NODE 204~~	~~80.34~~
NODE 301	91.45	NODE 302	97.04	NODE 303	103.75	NODE 304	121.93
NODE 305	141.20	NODE 306	156.57	NODE 307	154.45	NODE 308	129.92
NODE 309	103.61	NODE 310	88.56	~~NODE 311~~	~~73.68~~	~~NODE 312~~	~~74.38~~
NODE 401	78.62	NODE 402	76.05	NODE 403	72.87	NODE 404	69.38
NODE 405	64.62	NODE 406	57.90	NODE 407	56.97	NODE 408	61.33
NODE 409	64.47	~~NODE 410~~	~~66.81~~	~~NODE 411~~	~~49.50~~	~~NODE 412~~	~~69.54~~
NODE 413	44.70	NODE 414	33.40	AIR TOP	85.09	AIR BOTTOM	68.35

1/4 SCALE MODEL TEMPERATURES DEG F FORCED CONVECTION TEST SERIES

RUN NUMBER 74.0 VOLTAGE 48.98 VOLTS CURRENT 0.3771 AMPS POWER 18.471 WATTS PRESSURE 1.120 ATM FLOW 1.24000 LB/MIN

NODE 101	66.76	NODE 102	66.97	NODE 103	67.11	NODE 104	67.18
NODE 201	67.42	~~NODE 202~~	~~67.32~~	~~NODE 203~~	~~67.23~~	~~NODE 204~~	~~67.17~~
NODE 301	68.76	NODE 302	70.45	NODE 303	75.06	NODE 304	84.01
NODE 305	105.06	NODE 306	129.70	NODE 307	131.62	NODE 308	107.58
NODE 309	86.32	NODE 310	76.69	~~NODE 311~~	~~70.86~~	~~NODE 312~~	~~67.83~~
NODE 401	66.90	NODE 402	66.56	NODE 403	66.00	NODE 404	65.11
NODE 405	63.33	NODE 406	59.50	NODE 407	60.16	NODE 408	64.69
NODE 409	66.54	~~NODE 410~~	~~67.10~~	~~NODE 411~~	~~67.22~~	~~NODE 412~~	~~67.20~~
NODE 413	45.83	NODE 414	33.05	AIR TOP	64.91	AIR BOTTOM	63.44

RUN NUMBER 75.0 VOLTAGE 48.99 VOLTS CURRENT 0.3773 AMPS POWER 18.485 WATTS PRESSURE 2.050 ATM FLOW 1.24000 LB/MIN

NODE 101	67.18	NODE 102	67.41	NODE 103	67.55	NODE 104	67.62
NODE 201	67.89	NODE 202	67.75	NODE 203	67.67	~~NODE 204~~	~~67.59~~
NODE 301	69.21	NODE 302	70.87	NODE 303	75.46	NODE 304	84.35
NODE 305	105.42	NODE 306	130.21	NODE 307	131.89	NODE 308	107.91
NODE 309	86.55	~~NODE 310~~	~~76.96~~	~~NODE 311~~	~~71.19~~	~~NODE 312~~	~~68.36~~
NODE 401	67.27	NODE 402	66.93	NODE 403	66.35	NODE 404	65.46
NODE 405	63.64	NODE 406	59.81	NODE 407	60.47	NODE 408	65.05
NODE 409	66.92	~~NODE 410~~	67.45	~~NODE 411~~	67.56	~~NODE 412~~	~~67.56~~
NODE 413	45.98	NODE 414	33.05	AIR TOP	67.24	AIR BOTTOM	65.00

RUN NUMBER 76.0 VOLTAGE 49.00 VOLTS CURRENT 0.3773 AMPS POWER 18.489 WATTS PRESSURE 3.990 ATM FLOW 1.24000 LB/MIN

NODE 101	67.83	NODE 102	68.06	NODE 103	68.20	NODE 104	68.24
NODE 201	68.54	~~NODE 202~~	~~68.40~~	~~NODE 203~~	~~63.31~~	~~NODE 204~~	~~68.23~~
NODE 301	69.96	NODE 302	71.61	NODE 303	76.22	NODE 304	84.95
NODE 305	105.84	NODE 306	130.24	NODE 307	131.92	NODE 308	108.14
NODE 309	86.90	NODE 310	77.45	~~NODE 311~~	~~71.77~~	~~NODE 312~~	~~69.05~~
NODE 401	67.94	NODE 402	67.60	NODE 403	67.02	NODE 404	66.10
NODE 405	64.25	NODE 406	60.30	NODE 407	60.97	NODE 408	65.62
NODE 409	67.51	~~NODE 410~~	~~68.06~~	~~NODE 411~~	~~68.20~~	~~NODE 412~~	~~63.16~~
NODE 413	46.24	NODE 414	33.05	AIR TOP	63.50	AIR BOTTOM	66.17

1/4 SCALE MODEL TEMPERATURES DEG F FORCED CONVECTION TEST SERIES

RUN NUMBER 77.0 VOLTAGE 39.00 VOLTS CURRENT 0.3002 AMPS POWER 11.703 WATTS PRESSURE 0.501 ATM FLOW 0.07670 LB/MIN

NODE 101	74.66	NODE 102	74.57	NODE 103	74.49	NODE 104	74.41
NODE 201	82.53	~~NODE 202~~	~~81.55~~	~~NODE 203~~	~~80.90~~	~~NODE 204~~	~~80.42~~
NODE 301	91.19	NODE 302	98.34	NODE 303	112.94	NODE 304	130.35
NODE 305	154.57	NODE 306	172.94	NODE 307	172.40	NODE 308	147.35
NODE 309	118.51	~~NODE 310~~	~~100.06~~	~~NODE 311~~	~~86.46~~	~~NODE 312~~	~~79.09~~
NODE 401	78.81	NODE 402	76.71	NODE 403	74.00	NODE 404	70.69
NODE 405	65.85	NODE 406	58.94	NODE 407	58.49	NODE 408	64.14
NODE 409	68.42	~~NODE 410~~	~~71.41~~	~~NODE 411~~	~~73.25~~	~~NODE 412~~	~~74.23~~
NODE 413	45.02	NODE 414	32.98	AIR TOP	83.24	AIR BOTTOM	68.14

RUN NUMBER 78.0 VOLTAGE 42.68 VOLTS CURRENT 0.3232 AMPS POWER 14.305 WATTS PRESSURE 0.501 ATM FLOW 0.07650 LB/MIN

NODE 101	77.05	NODE 102	77.05	NODE 103	77.03	NODE 104	77.00
NODE 201	87.64	NODE 202	86.56	NODE 203	85.83	~~NODE 204~~	~~85.31~~
NODE 301	97.79	NODE 302	106.19	NODE 303	123.26	NODE 304	143.53
NODE 305	171.87	NODE 306	193.48	NODE 307	192.81	NODE 308	163.34
NODE 309	129.26	NODE 310	107.32	NODE 311	91.02	~~NODE 312~~	~~32.02~~
NODE 401	83.59	NODE 402	81.31	NODE 403	78.38	NODE 404	74.77
NODE 405	69.44	NODE 406	61.76	NODE 407	61.16	NODE 408	67.19
NODE 409	71.57	NODE 410	74.46	NODE 411	76.12	~~NODE 412~~	~~76.92~~
NODE 413	46.33	NODE 414	33.04	AIR TOP	83.03	AIR BOTTOM	68.29

RUN NUMBER 79.0 VOLTAGE 48.83 VOLTS CURRENT 0.3750 AMPS POWER 18.312 WATTS PRESSURE 0.504 ATM FLOW 0.07650 LB/MIN

NODE 101	80.44	NODE 102	80.58	NODE 103	30.69	NODE 104	30.73
NODE 201	95.91	~~NODE 202~~	94.61	~~NODE 203~~	~~33.78~~	~~NODE 204~~	~~93.19~~
NODE 301	108.38	NODE 302	118.92	NODE 303	140.32	NODE 304	165.89
NODE 305	201.55	NODE 306	229.26	NODE 307	228.26	NODE 308	190.60
NODE 309	147.22	NODE 310	119.22	NODE 311	98.20	NODE 312	~~86.23~~
NODE 401	91.22	NODE 402	88.76	NODE 403	35.53	NODE 404	31.50
NODE 405	75.42	NODE 406	66.48	NODE 407	65.61	NODE 408	72.14
NODE 409	76.55	~~NODE 410~~	79.15	~~NODE 411~~	~~30.44~~	~~NODE 412~~	~~30.87~~
NODE 413	48.52	NODE 414	33.07	AIR TOP	95.49	AIR BOTTOM	67.63

1/4 SCALE MODEL TEMPERATURES FEG-F ~~FORCED CONVECTION TEST SERIES~~

RUN NUMBER 80.0 VOLTAGE 48.87 VOLTS CURRENT 0.3746 AMPS POWER 18.303 WATTS PRESSURE 0.512 ATM FLOW 0.00483 LB/MIN

NODE 101	123.29	NODE 102	122.84	NODE 103	122.48	NODE 104	122.12
NODE 201	151.15	~~NODE 202~~	~~149.06~~	~~NODE 203~~	~~147.44~~	~~NODE 204~~	~~146.19~~
NODE 301	155.53	NODE 302	176.42	NODE 303	197.08	NODE 304	222.12
NODE 305	257.09	NODE 306	284.21	NODE 307	282.38	NODE 308	244.16
NODE 309	197.87	~~NODE 310~~	~~166.64~~	~~NODE 311~~	~~143.88~~	~~NODE 312~~	~~133.22~~
NODE 401	142.39	NODE 402	137.52	NODE 403	130.89	NODE 404	122.45
NODE 405	110.48	NODE 406	93.35	NODE 407	91.15	NODE 408	102.04
NODE 409	109.47	~~NODE 410~~	~~114.33~~	~~NODE 411~~	~~117.66~~	~~NODE 412~~	~~120.00~~
NODE 413	60.95	NODE 414	33.30	AIR TOP	103.71	AIR BOTTOM	69.18

RUN NUMBER 81.0 VOLTAGE 42.65 VOLTS CURRENT 0.3276 AMPS POWER 13.971 WATTS PRESSURE 0.503 ATM FLOW 0.00477 LB/MIN

NODE 101	107.11	NODE 102	106.56	NODE 103	106.15	NODE 104	105.78
NODE 201	129.51	NODE 202	127.73	~~NODE 203~~	~~126.35~~	~~NODE 204~~	~~125.28~~
NODE 301	141.78	NODE 302	150.93	NODE 303	168.04	NODE 304	188.64
NODE 305	216.95	NODE 306	238.39	NODE 307	236.89	NODE 308	206.30
NODE 309	168.76	~~NODE 310~~	~~143.24~~	~~NODE 311~~	~~124.52~~	~~NODE 312~~	~~115.99~~
NODE 401	121.96	NODE 402	117.64	NODE 403	111.84	NODE 404	104.76
NODE 405	94.67	NODE 406	80.78	NODE 407	78.97	NODE 408	87.80
NODE 409	93.98	NODE 410	98.24	~~NODE 411~~	~~101.35~~	~~NODE 412~~	~~103.70~~
NODE 413	55.05	NODE 414	33.19	AIR TOP	92.25	AIR BOTTOM	69.18

RUN NUMBER 82.0 VOLTAGE 38.99 VOLTS CURRENT 0.2998 AMPS POWER 11.639 WATTS PRESSURE 0.508 ATM FLOW 0.00471 LB/MIN

NODE 101	96.49	NODE 102	95.97	NODE 103	95.57	NODE 104	95.21
NODE 201	115.96	NODE 202	114.33	~~NODE 203~~	~~113.11~~	~~NODE 204~~	~~112.16~~
NODE 301	126.72	NODE 302	134.81	NODE 303	149.91	NODE 304	167.85
NODE 305	192.36	NODE 306	210.74	NODE 307	209.37	NODE 308	183.07
NODE 309	150.49	NODE 310	128.24	NODE 311	111.89	~~NODE 312~~	~~104.59~~
NODE 401	109.09	NODE 402	105.16	NODE 403	100.01	NODE 404	93.80
NODE 405	85.07	NODE 406	73.18	NODE 407	71.61	NODE 408	79.10
NODE 409	84.43	NODE 410	88.19	~~NODE 411~~	~~91.61~~	~~NODE 412~~	~~93.21~~
NODE 413	51.49	NODE 414	33.11	AIR TOP	87.33	AIR BOTTOM	68.47

~~1/4~~ SCALE ~~MODEL~~ ~~TEMPERATURES~~ DEG F ~~FORCED~~ CONVECTION TEST ~~SERIES~~

RUN NUMBER 83.0 VOLTAGE 48.92 VOLTS CURRENT 0.3752 AMPS POWER 18.356 WATTS PRESSURE 0.501 ATM FLOW 0.01812 LB/MIN

NODE 101	102.72	NODE 102	102.72	NODE 103	102.73	NODE 104	102.63
~~NODE 201~~	~~131.80~~	~~NODE 202~~	~~129.41~~	~~NODE 203~~	~~127.77~~	~~NODE 204~~	~~126.58~~
NODE 301	148.16	NODE 302	159.09	NODE 303	180.69	NODE 304	206.52
NODE 305	241.03	NODE 306	265.79	NODE 307	268.42	NODE 308	229.28
NODE 309	181.82	~~NODE 310~~	~~149.08~~	~~NODE 311~~	~~123.94~~	~~NODE 312~~	~~110.16~~
NODE 401	122.83	NODE 402	118.08	NODE 403	112.05	NODE 404	104.89
NODE 405	94.77	NODE 406	80.96	NODE 407	79.31	NODE 408	88.34
NODE 409	94.47	~~NODE 410~~	~~98.26~~	~~NODE 411~~	~~100.43~~	~~NODE 412~~	~~101.62~~
NODE 413	55.16	NODE 414	33.18	AIR TOP	123.62	AIR BOTTOM	69.01

RUN NUMBER 84.0 VOLTAGE 42.59 VOLTS CURRENT 0.3273 AMPS POWER 13.939 WATTS PRESSURE 0.505 ATM FLOW 0.01820 LB/MIN

NODE 101	91.32	NODE 102	91.18	NODE 103	91.06	NODE 104	90.91
NODE 201	112.98	NODE 202	110.99	NODE 203	109.61	~~NODE 204~~	~~108.50~~
NODE 301	126.66	NODE 302	136.03	NODE 303	153.65	NODE 304	174.77
NODE 305	203.63	NODE 306	225.56	NODE 307	223.95	NODE 308	193.25
NODE 309	155.24	NODE 310	128.87	~~NODE 311~~	~~108.68~~	~~NODE 312~~	~~98.10~~
NODE 401	105.36	NODE 402	101.22	NODE 403	95.09	NODE 404	90.09
NODE 405	81.97	NODE 406	70.84	NODE 407	69.61	NODE 408	77.00
NODE 409	82.28	NODE 410	85.80	NODE 411	88.11	~~NODE 412~~	~~89.58~~
NODE 413	50.43	NODE 414	33.02	AIR TOP	107.98	AIR BOTTOM	58.65

RUN NUMBER 85.1 VOLTAGE 39.00 VOLTS CURRENT 0.3001 AMPS POWER 11.704 WATTS PRESSURE 0.497 ATM FLOW 0.01790 LB/MIN

NODE 101	84.93	NODE 102	84.70	NODE 103	84.52	NODE 104	84.34
NODE 201	102.62	NODE 202	100.88	~~NODE 203~~	~~99.66~~	~~NODE 204~~	~~98.76~~
NODE 301	114.72	NODE 302	123.02	NODE 303	138.60	NODE 304	157.14
NODE 305	182.25	NODE 306	201.18	NODE 307	199.73	NODE 308	173.43
NODE 309	140.59	NODE 310	117.72	NODE 311	100.26	NODE 312	~~91.24~~
NODE 401	95.85	NODE 402	92.11	NODE 403	87.53	NODE 404	82.26
NODE 405	75.08	NODE 406	65.53	NODE 407	64.54	NODE 408	71.09
NODE 409	75.86	NODE 410	79.20	NODE 411	81.50	~~NODE 412~~	~~83.01~~
NODE 413	47.93	NODE 414	33.00	AIR TOP	99.36	AIR BOTTOM	67.45

1/4 SCALE MODEL TEMPERATURES DEG F FORCED CONVECTION TEST SERIES

RUN NUMBER 86.0 VOLTAGE 48.99 VOLTS CURRENT 0.3777 AMPS POWER 18.505 WATTS PRESSURE 1.130 ATM FLOW 1.24000 LB/MIN

NODE 101	70.33	NODE 102	70.28	NODE 103	70.26	NODE 104	70.24
NODE 201	70.12	NODE 202	70.30	NODE 203	70.42	NODE 204	70.47
NODE 301	71.88	NODE 302	76.28	NODE 303	82.62	NODE 304	93.10
NODE 305	114.68	NODE 306	137.80	NODE 307	139.43	NODE 308	111.95
NODE 309	88.40	NODE 310	78.31	NODE 311	73.31	NODE 312	72.03
NODE 401	70.34	NODE 402	70.34	NODE 403	70.17	NODE 404	69.60
NODE 405	67.73	NODE 406	62.74	NODE 407	62.19	NODE 408	66.35
NODE 409	68.38	NODE 410	69.30	NODE 411	69.74	NODE 412	69.98
NODE 413	47.15	NODE 414	33.25	AIR TOP	65.72	AIR BOTTOM	68.26

RUN NUMBER 87.0 VOLTAGE 48.94 VOLTS CURRENT 0.3777 AMPS POWER 18.485 WATTS PRESSURE 4.020 ATM FLOW 1.24000 LB/MIN

NODE 101	70.29	NODE 102	70.21	NODE 103	70.18	NODE 104	70.15
NODE 201	69.87	NODE 202	70.04	NODE 203	70.16	NODE 204	70.20
NODE 301	71.70	NODE 302	76.43	NODE 303	83.40	NODE 304	94.53
NODE 305	116.87	NODE 306	135.88	NODE 307	142.57	NODE 308	114.19
NODE 309	89.67	NODE 310	78.90	NODE 311	73.50	NODE 312	72.06
NODE 401	70.25	NODE 402	70.26	NODE 403	70.09	NODE 404	69.45
NODE 405	67.52	NODE 406	62.41	NODE 407	61.90	NODE 408	66.03
NODE 409	68.08	NODE 410	69.06	NODE 411	69.55	NODE 412	69.83
NODE 413	47.05	NODE 414	33.45	AIR TOP	67.39	AIR BOTTOM	70.11

RUN NUMBER 88.0 VOLTAGE 48.90 VOLTS CURRENT 0.3771 AMPS POWER 18.442 WATTS PRESSURE 3.920 ATM FLOW 0.29300 LB/MIN

NODE 101	78.02	NODE 102	77.71	NODE 103	77.51	NODE 104	77.37
NODE 201	76.93	NODE 202	77.25	NODE 203	77.44	NODE 204	77.53
NODE 301	82.20	NODE 302	92.56	NODE 303	109.68	NODE 304	130.84
NODE 305	163.73	NODE 306	185.12	NODE 307	192.28	NODE 308	157.12
NODE 309	121.39	NODE 310	101.15	NODE 311	83.41	NODE 312	83.67
NODE 401	77.77	NODE 402	77.77	NODE 403	74.98	NODE 404	75.29
NODE 405	71.54	NODE 406	64.40	NODE 407	63.69	NODE 408	69.21
NODE 409	72.55	NODE 410	74.55	NODE 411	75.82	NODE 412	76.67
NODE 413	47.60	NODE 414	33.17	AIR TOP	68.41	AIR BOTTOM	77.01

1/4 SCALE MODEL TEMPERATURES DEG F FORCED CONVECTION TEST SERIES

RUN NUMBER 89.0 VOLTAGE 48.92 VOLTS CURRENT 0.3795 AMPS POWER 18.567 WATTS PRESSURE 1.018 ATM FLOW 0.29400 LB/MIN

NODE 101	78.74	NODE 102	78.38	NODE 103	78.18	NODE 104	78.03
~~NODE 201~~	~~76.39~~	~~NODE 202~~	~~76.70~~	~~NODE 203~~	~~76.88~~	~~NODE 204~~	~~76.97~~
NODE 301	80.85	NODE 302	91.01	NODE 303	105.90	NODE 304	127.17
NODE 305	161.59	NODE 306	190.21	NODE 307	196.13	NODE 308	161.87
~~NODE 309~~	~~126.24~~	~~NODE 310~~	~~164.90~~	~~NODE 311~~	~~90.76~~	~~NODE 312~~	~~33.96~~
NODE 401	77.21	NODE 402	77.13	NODE 403	76.43	NODE 404	74.75
NODE 405	70.98	NODE 406	63.81	NODE 407	63.40	NODE 408	69.08
~~NODE 409~~	~~72.57~~	~~NODE 410~~	~~74.68~~	~~NODE 411~~	~~76.03~~	~~NODE 412~~	~~76.96~~
NODE 413	47.46	NODE 414	33.24	AIR TOP	68.83	AIR BOTTOM	77.33

RUN NUMBER 90.0 VOLTAGE 48.95 VOLTS CURRENT 0.3790 AMPS POWER 18.555 WATTS PRESSURE 7.950 ATM FLOW 0.29400 LB/MIN

NODE 101	80.89	NODE 102	80.61	NODE 103	80.41	NODE 104	80.27
~~NODE 201~~	~~82.04~~	~~NODE 202~~	~~82.17~~	~~NODE 203~~	~~82.26~~	~~NODE 204~~	~~82.26~~
NODE 301	89.14	NODE 302	100.69	NODE 303	119.35	NODE 304	138.84
NODE 305	166.65	NODE 306	188.69	NODE 307	188.19	NODE 308	152.97
~~NODE 309~~	~~118.55~~	~~NODE 310~~	~~106.26~~	~~NODE 311~~	~~83.34~~	~~NODE 312~~	~~85.29~~
NODE 401	82.12	NODE 402	82.10	NODE 403	81.38	NODE 404	79.76
NODE 405	75.93	NODE 406	68.13	NODE 407	67.03	NODE 408	72.59
~~NODE 409~~	~~75.90~~	~~NODE 410~~	~~77.82~~	~~NODE 411~~	~~78.99~~	~~NODE 412~~	~~79.78~~
NODE 413	49.64	NODE 414	33.35	AIR TOP	72.28	AIR BOTTOM	80.11

RUN NUMBER 93.0 VOLTAGE 48.90 VOLTS CURRENT 0.3780 AMPS POWER 18.484 WATTS PRESSURE 7.880 ATM FLOW 0.07400 LB/MIN

NODE 101	95.20	NODE 102	94.82	NODE 103	94.54	NODE 104	94.31
~~NODE 201~~	~~102.57~~	~~NODE 202~~	~~102.82~~	~~NODE 203~~	~~102.73~~	~~NODE 204~~	~~102.57~~
NODE 301	111.27	NODE 302	125.10	NODE 303	145.62	NODE 304	164.69
NODE 305	190.36	NODE 306	211.03	NODE 307	207.75	NODE 308	171.81
NODE 309	135.58	NODE 310	116.11	~~NODE 311~~	~~104.52~~	~~NODE 312~~	~~100.65~~
NODE 401	102.03	NODE 402	101.34	NODE 403	95.58	NODE 404	96.56
NODE 405	90.78	NODE 406	79.63	NODE 407	77.70	NODE 408	84.58
~~NODE 409~~	~~88.69~~	~~NODE 410~~	~~91.07~~	~~NODE 411~~	~~92.59~~	~~NODE 412~~	~~93.60~~
NODE 413	55.07	NODE 414	33.32	AIR TOP	72.34	AIR BOTTOM	90.82

1/4 SCALE MODEL TEMPERATURES DEG F FORCED CONVECTION TEST SERIES

RUN NUMBER 94.0 VOLTAGE 48.87 VOLTS CURRENT 0.3773 AMPS POWER 18.439 WATTS PRESSURE 4.030 ATM FLOW 0.07500 LB/MIN

NODE 101	95.95	NODE 102	95.46	NODE 103	95.10	NODE 104	94.82
NODE 201	~~100.71~~	~~NODE 202~~	~~100.79~~	~~NODE 203~~	~~100.68~~	~~NODE 204~~	~~100.50~~
NODE 301	110.86	NODE 302	125.70	NODE 303	149.49	NODE 304	172.19
NODE 305	202.37	NODE 306	225.54	NODE 307	223.34	NODE 308	186.26
NODE 309	146.50	~~NODE 310~~	~~123.29~~	~~NODE 311~~	~~108.43~~	~~NODE 312~~	~~103.35~~
NODE 401	99.74	NODE 402	98.77	NODE 403	96.55	NODE 404	93.00
NODE 405	86.67	NODE 406	76.22	NODE 407	75.02	NODE 408	82.53
NODE 409	~~87.27~~	~~NODE 410~~	~~90.19~~	~~NODE 411~~	~~92.13~~	~~NODE 412~~	~~93.53~~
NODE 413	53.29	NODE 414	33.42	AIR TOP	72.19	AIR BOTTOM	91.40

RUN NUMBER 95.0 VOLTAGE 48.88 VOLTS CURRENT 0.3785 AMPS POWER 18.504 WATTS PRESSURE 1.016 ATM FLOW 0.07440 LB/MIN

NODE 101	98.72	NODE 102	97.95	NODE 103	97.44	NODE 104	97.06
NODE 201	93.98	~~NODE 202~~	~~94.29~~	~~NODE 203~~	~~94.46~~	~~NODE 204~~	~~94.48~~
NODE 301	102.22	NODE 302	116.46	NODE 303	140.69	NODE 304	169.63
NODE 305	210.22	NODE 306	241.35	NODE 307	242.75	NODE 308	207.26
NODE 309	~~165.28~~	~~NODE 310~~	~~137.59~~	~~NODE 311~~	~~117.71~~	~~NODE 312~~	~~110.02~~
NODE 401	94.21	NODE 402	93.43	NODE 403	91.35	NODE 404	87.73
NODE 405	81.47	NODE 406	72.00	NODE 407	71.92	NODE 408	80.54
NODE 409	~~86.54~~	~~NODE 410~~	~~90.47~~	~~NODE 411~~	~~93.25~~	~~NODE 412~~	~~95.31~~
NODE 413	51.35	NODE 414	33.30	AIR TOP	71.09	AIR BOTTOM	93.65

RUN NUMBER 96.0 VOLTAGE 48.84 VOLTS CURRENT 0.3780 AMPS POWER 18.463 WATTS PRESSURE 2.040 ATM FLOW 0.07440 LB/MIN

NODE 101	96.52	NODE 102	95.92	NODE 103	95.51	NODE 104	95.20
NODE 201	~~97.54~~	~~NODE 202~~	~~97.78~~	~~NODE 203~~	~~97.78~~	~~NODE 204~~	~~97.71~~
NODE 301	107.34	NODE 302	122.65	NODE 303	148.16	NODE 304	175.00
NODE 305	210.13	NODE 306	236.61	NODE 307	235.66	NODE 308	198.42
NODE 309	156.34	~~NODE 310~~	~~130.10~~	NODE 311	112.23	~~NODE 312~~	~~105.78~~
NODE 401	97.29	NODE 402	96.34	NODE 403	94.15	NODE 404	90.46
NODE 405	84.05	NODE 406	73.95	NODE 407	73.19	NODE 408	81.14
NODE 409	86.36	~~NODE 410~~	~~85.72~~	~~NODE 411~~	~~92.02~~	~~NODE 412~~	~~93.72~~
NODE 413	52.17	NODE 414	33.37	AIR TOP	69.99	AIR BOTTOM	91.08

1/4 SCALE MODEL TEMPERATURES DEG F ~~FORCED CONVECTION~~ TEST SERIES

RUN NUMBER 97.0 VOLTAGE 48.83 VOLTS CURRENT 0.3782 AMPS POWER 18.471 WATTS PRESSURE 0.499 ATM FLOW 0.07440 LB/MIN

NODE 101	98.72	NODE 102	97.82	NODE 103	97.24	NODE 104	96.82
~~NODE 201~~	~~88.70~~	~~NODE 202~~	~~88.79~~	~~NODE 203~~	~~88.86~~	~~NODE 204~~	~~88.86~~
NODE 301	96.54	NODE 302	109.16	NODE 303	131.35	NODE 304	159.97
NODE 305	201.96	NODE 306	235.16	NODE 307	240.39	NODE 308	207.05
~~NODE 309~~	~~167.49~~	~~NODE 310~~	~~140.36~~	~~NODE 311~~	~~119.96~~	~~NODE 312~~	~~111.66~~
NODE 401	88.49	NODE 402	87.78	NODE 403	83.99	NODE 404	82.77
NODE 405	77.28	NODE 406	69.11	NODE 407	69.88	NODE 408	79.07
~~NODE 409~~	~~85.50~~	~~NODE 410~~	~~85.75~~	~~NODE 411~~	~~92.67~~	~~NODE 412~~	~~94.82~~
NODE 413	50.20	NODE 414	33.25	AIR TOP	70.79	AIR BOTTOM	93.77

RUN NUMBER 98.0 VOLTAGE 48.85 VOLTS CURRENT 0.3776 AMPS POWER 18.448 WATTS PRESSURE 0.508 ATM FLOW 0.01830 LB/MIN

NODE 101	120.58	NODE 102	119.63	NODE 103	118.96	NODE 104	118.43
~~NODE 201~~	~~125.42~~	~~NODE 202~~	~~125.45~~	~~NODE 203~~	~~125.20~~	~~NODE 204~~	~~124.84~~
NODE 301	136.51	NODE 302	152.57	NODE 303	180.23	NODE 304	210.41
NODE 305	249.40	NODE 306	278.58	NODE 307	277.47	NODE 308	240.07
~~NODE 309~~	~~194.45~~	~~NODE 310~~	~~163.80~~	~~NODE 311~~	~~141.76~~	~~NODE 312~~	~~133.96~~
NODE 401	123.50	NODE 402	121.45	NODE 403	117.27	NODE 404	111.12
NODE 405	101.50	NODE 406	87.30	NODE 407	86.21	NODE 408	97.05
~~NODE 409~~	~~104.54~~	~~NODE 410~~	~~109.53~~	~~NODE 411~~	~~113.14~~	~~NODE 412~~	~~115.88~~
NODE 413	58.39	NODE 414	33.43	AIR TOP	71.57	AIR BOTTOM	104.78

RUN NUMBER 99.0 VOLTAGE 48.83 VOLTS CURRENT 0.3778 AMPS POWER 18.450 WATTS PRESSURE 0.495 ATM FLOW 0.00480 LB/MIN

NODE 101	131.91	NODE 102	130.85	NODE 103	130.11	NODE 104	129.49
~~NODE 201~~	~~143.62~~	~~NODE 202~~	~~142.78~~	~~NODE 203~~	~~142.00~~	~~NODE 204~~	~~141.29~~
NODE 301	156.54	NODE 302	170.26	NODE 303	194.59	NODE 304	222.37
NODE 305	259.30	NODE 306	287.47	NODE 307	285.89	NODE 308	248.61
~~NODE 309~~	~~203.51~~	~~NODE 310~~	~~173.71~~	~~NODE 311~~	~~152.66~~	~~NODE 312~~	~~145.78~~
NODE 401	138.95	NODE 402	135.80	NODE 403	130.58	NODE 404	123.32
NODE 405	112.05	NODE 406	95.44	NODE 407	93.83	NODE 408	105.79
~~NODE 409~~	~~114.00~~	~~NODE 410~~	~~119.53~~	~~NODE 411~~	~~123.55~~	~~NODE 412~~	~~126.38~~
NODE 413	62.13	NODE 414	33.44	AIR TOP	71.00	AIR BOTTOM	81.03

II-A.2 FULL SCALE MODEL DATA

II-A.2.1 FREE CONVECTION TEST SERIES

FULL SCALE MODEL TEMPERATURES DEG F FREE CONVECTION TEST SERIES

RUN NUMBER 101.0 VOLTAGE 88.52 VOLTS CURRENT 2.1230 AMPS POWER 187.925 WATTS PRESSURE 0.995 ATM FLOW 0.0 LB/MIN

NODE 101	107.38	NODE 102	106.23	NODE 103	105.46	NODE 104	104.85
NODE 201	126.74	~~NODE 202~~	~~125.35~~	~~NODE 203~~	~~124.36~~	~~NODE 204~~	~~123.40~~
NODE 301	138.56	NODE 302	146.94	NODE 303	162.47	NODE 304	131.11
NODE 305	205.60	NODE 306	221.98	NODE 307	227.35	NODE 308	195.92
NODE 309	163.77	NODE 310	141.49	NODE 311	124.39	~~NODE 312~~	~~116.96~~
NODE 401	120.42	NODE 402	115.98	NODE 403	110.29	NODE 404	102.77
NODE 405	92.64	NODE 406	78.71	NODE 407	76.07	NODE 408	84.93
NODE 409	91.23	NODE 410	95.88	NODE 411	99.55	~~NODE 412~~	~~102.48~~
NODE 413	51.43	NODE 414	33.87	AIR TOP	112.40	AIR BOTTOM	108.45

RUN NUMBER 102.0 VOLTAGE 96.69 VOLTS CURRENT 2.3152 AMPS POWER 223.861 WATTS PRESSURE 0.993 ATM FLOW 0.0 LB/MIN

NODE 101	119.25	NODE 102	118.00	NODE 103	117.14	NODE 104	116.46
NODE 201	141.03	NODE 202	139.49	NODE 203	138.28	~~NODE 204~~	~~137.34~~
NODE 301	154.37	NODE 302	163.84	NODE 303	181.42	NODE 304	202.73
NODE 305	231.06	NODE 306	25C.33	NODE 307	256.27	NODE 308	219.93
NODE 309	~~183.04~~	~~NODE 310~~	~~157.69~~	~~NODE 311~~	~~138.41~~	~~NODE 312~~	~~130.04~~
NODE 401	134.10	NODE 402	129.19	NODE 403	122.80	NODE 404	114.35
NODE 405	102.75	NODE 406	86.64	NODE 407	93.64	NODE 408	93.97
NODE 409	101.22	NODE 410	106.51	~~NODE 411~~	~~110.59~~	~~NODE 412~~	~~113.87~~
NODE 413	54.73	NODE 414	34.C7	AIR TOP	119.56	AIR BOTTOM	118.37

RUN NUMBER 103.0 VOLTAGE 111.00 VOLTS CURRENT 2.6497 AMPS POWER 294.118 WATTS PRESSURE 1.000 ATM FLOW 0.0 LB/MIN

NODE 101	142.45	NODE 102	141.00	NODE 103	140.01	NODE 104	139.21
NODE 201	~~168.26~~	~~NODE 202~~	~~166.45~~	~~NODE 203~~	~~165.30~~	~~NODE 204~~	~~163.51~~
NODE 301	183.88	NODE 302	195.12	NODE 303	216.27	NODE 304	242.15
NODE 305	277.45	NODE 306	302.27	NODE 307	309.37	NODE 308	263.96
NODE 309	~~218.50~~	~~NODE 310~~	~~187.82~~	~~NODE 311~~	~~164.93~~	~~NODE 312~~	~~154.90~~
NODE 401	160.24	NODE 402	154.57	NODE 403	147.08	NODE 404	136.89
NODE 405	122.63	NODE 406	102.36	NODE 407	98.74	NODE 408	112.00
NODE 409	~~121.09~~	~~NODE 410~~	~~127.56~~	~~NODE 411~~	~~132.40~~	~~NODE 412~~	~~136.24~~
NODE 413	61.37	NODE 414	34.57	AIR TOP	137.14	AIR BOTTOM	139.04

FULL SCALE MODEL TEMPERATURES DEG F FREE CONVECTION TEST SERIES

RUN NUMBER 104.0 VOLTAGE 76.60 VOLTS CURRENT 1.8406 AMPS POWER 140.939 WATTS PRESSURE 0.995 ATM FLOW 0.0 LB/MIN

NODE 101	91.08	NODE 102	90.10	NODE 103	83.49	NODE 104	88.97
NODE 201	~~106.76~~	~~NODE 202~~	~~105.60~~	~~NODE 203~~	~~104.68~~	~~NODE 204~~	~~103.84~~
NODE 301	116.57	NODE 302	123.41	NODE 303	136.01	NODE 304	150.93
NODE 305	170.30	NODE 306	182.73	NODE 307	133.06	NODE 308	152.59
NODE 309	137.07	NODE 310	119.10	~~NODE~~ 311	105.23	~~NODE 312~~	~~99.05~~
NODE 401	101.49	NODE 402	97.77	NODE 403	93.07	NODE 404	86.99
NODE 405	78.91	NODE 406	68.00	NODE 407	65.94	NODE 408	72.77
NODE 409	~~77.75~~	~~NODE 410~~	~~81.51~~	~~NODE 411~~	~~94.52~~	~~NODE 412~~	~~86.99~~
NODE 413	46.96	NODE 414	33.53	AIR TOP	97.95	AIR BOTTOM	93.02

RUN NUMBER 105.0 VOLTAGE 62.25 VOLTS CURRENT 1.4981 AMPS POWER 93.257 WATTS PRESSURE 0.995 ATM FLOW 0.0 LB/MIN

NODE 101	74.15	NODE 102	73.40	NODE 103	72.95	NODE 104	72.55
NODE 201	85.29	NODE 202	84.45	NODE 203	83.79	~~NODE 204~~	~~83.21~~
NODE 301	92.47	NODE 302	97.38	NODE 303	106.47	NODE 304	117.12
NODE 305	130.66	NODE 306	139.18	NODE 307	142.81	NODE 308	125.32
NODE 309	~~107.38~~	~~NODE 310~~	~~94.56~~	~~NODE 311~~	~~84.51~~	~~NODE 312~~	~~80.01~~
NODE 401	81.33	NODE 402	78.53	NODE 403	75.03	NODE 404	70.54
NODE 405	64.75	NODE 406	57.10	NODE 407	54.44	NODE 408	60.47
NODE 409	64.08	NODE 410	66.86	NODE 411	69.14	~~NODE 412~~	~~71.01~~
NODE 413	42.58	NODE 414	33.35	AIR TOP	83.31	AIR BOTTOM	77.46

II-A.2.2 FORCED CONVECTION TEST SERIES

FULL SCALE MODEL TEMPERATURES DEG F FORCED CONVECTION TEST SERIES

RUN NUMBER 106.0 VOLTAGE 110.90 VOLTS CURRENT 2.6567 AMPS POWER 294.630 WATTS PRESSURE 1.000 ATM FLOW 5.02000 LB/MIN

NODE 101	74.06	NODE 102	73.79	NODE 103	73.73	NODE 104	73.67
NODE 201	~~78.70~~	~~NODE 202~~	~~78.07~~	~~NODE 203~~	~~77.65~~	~~NODE 204~~	~~77.32~~
NODE 301	88.90	NODE 302	98.83	NODE 303	119.25	NODE 304	146.76
NODE 305	185.99	NODE 306	214.65	NODE 307	224.74	NODE 308	181.44
NODE 309	~~140.10~~	~~NODE 310~~	112.71	~~NODE 311~~	~~92.13~~	~~NODE 312~~	~~32.72~~
NODE 401	76.50	NODE 402	75.10	NODE 403	73.29	NODE 404	70.70
NODE 405	66.71	NODE 406	60.52	NODE 407	60.94	NODE 408	67.34
~~NODE 409~~	~~70.93~~	~~NODE 410~~	72.69	~~NODE 411~~	~~73.36~~	~~NODE 412~~	~~73.52~~
NODE 413	44.30	NODE 414	33.23	AIR TOP	75.56	AIR BOTTOM	66.20

RUN NUMBER 107.0 VOLTAGE 96.65 VOLTS CURRENT 2.3192 AMPS POWER 224.155 WATTS PRESSURE 1.000 ATM FLOW 5.04000 LB/MIN

NODE 101	71.78	NODE 102	71.53	NODE 103	71.45	NODE 104	71.39
NODE 201	74.31	NODE 202	73.77	NODE 203	73.41	~~NODE 204~~	~~73.14~~
NODE 301	82.55	NODE 302	90.40	NODE 303	105.55	NODE 304	127.94
NODE 305	158.50	NODE 306	130.86	NODE 307	189.90	NODE 308	155.59
NODE 309	123.31	NODE 310	101.99	NODE 311	36.01	~~NODE 312~~	~~78.65~~
NODE 401	72.26	NODE 402	70.93	NODE 403	69.23	NODE 404	66.85
NODE 405	63.28	NODE 406	57.82	NODE 407	58.39	NODE 408	64.51
NODE 409	68.10	NODE 410	69.99	NODE 411	70.85	NODE 412	71.15
NODE 413	43.28	NODE 414	33.26	AIR TOP	72.47	AIR BOTTOM	66.05

RUN NUMBER 108.0 VOLTAGE 88.48 VOLTS CURRENT 2.1260 AMPS POWER 188.105 WATTS PRESSURE 1.002 ATM FLOW 5.04000 LB/MIN

NODE 101	70.12	NODE 102	69.87	NODE 103	69.81	NODE 104	69.75
NODE 201	~~71.63~~	NODE 202	71.16	~~NODE~~ 203	~~70.81~~	~~NODE 204~~	~~70.55~~
NODE 301	78.77	NODE 302	85.41	NODE 303	99.09	NODE 304	117.46
NODE 305	143.62	NODE 306	162.47	NODE 307	170.53	NODE 308	141.15
NODE 309	113.93	NODE 310	95.66	~~NODE~~ 311	32.21	NODE 312	~~76.06~~
NODE 401	69.66	NODE 402	68.39	NODE 403	66.77	NODE 404	64.52
NODE 405	61.21	NODE 406	56.16	NODE 407	55.82	NODE 408	62.71
~~NODE 409~~	~~66.26~~	~~NODE 410~~	~~68.15~~	~~NODE 411~~	~~69.07~~	~~NODE 412~~	~~69.43~~
NODE 413	42.59	NODE 414	33.20	AIR TOP	70.27	AIR BOTTOM	65.57

FULL SCALE MODEL TEMPERATURES DEG F FORCED CONVECTION TEST SERIES

RUN NUMBER 109.0 VOLTAGE 111.06 VOLTS CURRENT 2.6567 AMPS POWER 295.055 WATTS PRESSURE 0.994 ATM FLOW 1.17300 LB/MIN

NODE 101	83.11	NODE 102	82.42	NODE 103	82.04	NODE 104	81.75
~~NODE 201~~	~~100.17~~	~~NODE 202~~	~~98.74~~	~~NODE 203~~	~~97.75~~	~~NODE 204~~	~~96.89~~
NODE 301	116.91	NODE 302	129.84	NODE 303	154.45	NODE 304	184.68
NODE 305	224.70	NODE 306	252.34	NODE 307	260.54	NODE 308	214.47
~~NODE 309~~	~~167.29~~	~~NODE 310~~	~~134.17~~	~~NODE 311~~	~~107.86~~	~~NODE 312~~	~~95.47~~
NODE 401	94.14	NODE 402	90.50	NODE 403	86.42	NODE 404	81.46
NODE 405	74.82	NODE 406	65.58	NODE 407	64.51	NODE 408	71.48
~~NODE 409~~	~~75.89~~	~~NODE 410~~	~~78.45~~	~~NODE 411~~	~~79.86~~	~~NODE 412~~	~~80.83~~
NODE 413	46.09	NODE 414	33.36	AIR TOP	99.43	AIR BOTTOM	65.51

RUN NUMBER 110.0 VOLTAGE 96.72 VOLTS CURRENT 2.3182 AMPS POWER 224.221 WATTS PRESSURE 0.992 ATM FLOW 1.16700 LB/MIN

NODE 101	77.77	NODE 102	77.11	NODE 103	76.75	NODE 104	76.45
NODE 201	89.81	NODE 202	88.57	~~NODE 203~~	~~87.74~~	~~NODE 204~~	~~87.05~~
NODE 301	103.64	NODE 302	114.28	NODE 303	134.31	NODE 304	158.46
NODE 305	190.19	NODE 306	211.56	NODE 307	218.74	NODE 308	182.25
~~NODE 309~~	~~144.92~~	~~NODE 310~~	~~118.53~~	~~NODE 311~~	~~97.60~~	~~NODE 312~~	~~87.78~~
NODE 401	84.71	NODE 402	81.55	NODE 403	78.06	NODE 404	73.80
NODE 405	68.14	NODE 406	60.37	NODE 407	59.63	NODE 408	65.79
NODE 409	69.98	NODE 410	72.67	~~NODE 411~~	~~74.32~~	~~NODE 412~~	~~75.40~~
NODE 413	44.05	NODE 414	33.35	AIR TOP	89.57	AIR BOTTOM	65.27

RUN NUMBER 111.0 VOLTAGE 88.36 VOLTS CURRENT 2.1210 AMPS POWER 187.409 WATTS PRESSURE 1.000 ATM FLOW 1.17400 LB/MIN

NODE 101	74.71	NODE 102	74.07	NODE 103	73.74	NODE 104	73.47
NODE 201	83.97	~~NODE 202~~	82.87	~~NODE 203~~	~~82.14~~	~~NODE 204~~	~~81.53~~
NODE 301	96.21	NODE 302	105.43	NODE 303	122.73	NODE 304	143.60
NODE 305	170.66	NODE 306	188.78	NODE 307	195.44	NODE 308	163.97
NODE 309	132.15	NODE 310	109.72	~~NODE 311~~	~~91.78~~	~~NODE 312~~	~~83.41~~
NODE 401	79.47	NODE 402	76.64	NODE 403	73.48	NODE 404	69.61
NODE 405	64.52	NODE 406	57.58	NODE 407	57.00	NODE 408	62.73
~~NODE 409~~	~~66.76~~	~~NODE 410~~	~~69.49~~	~~NODE 411~~	~~71.25~~	~~NODE 412~~	~~72.44~~
NODE 413	42.93	NODE 414	33.32	AIR TOP	34.25	AIR BOTTOM	65.03

FULL SCALE MODEL TEMPERATURES DEG F FORCED CONVECTION TEST SERIES

RUN NUMBER 112.0 VOLTAGE 88.45 VOLTS CURRENT 2.1220 AMPS POWER 187.688 WATTS PRESSURE 0.993 ATM FLOW 0.29500 LB/MIN

NODE 101	87.66	NODE 102	86.94	NODE 103	86.50	NODE 104	86.11
NODE 201	105.16	~~NODE 202~~	~~103.72~~	~~NODE 203~~	~~102.67~~	~~NODE 204~~	~~101.78~~
NODE 301	117.51	NODE 302	126.14	NODE 303	142.39	NODE 304	162.06
NODE 305	187.74	NODE 306	204.58	NODE 307	211.05	NODE 308	178.73
NODE 309	145.96	~~NODE 310~~	~~122.90~~	~~NODE 311~~	~~104.81~~	~~NODE 312~~	~~96.52~~
NODE 401	98.94	NODE 402	94.97	NODE 403	90.15	NODE 404	33.93
NODE 405	76.23	NODE 406	66.02	NODE 407	64.38	NODE 408	71.23
NODE 409	76.21	~~NODE 410~~	~~79.86~~	~~NODE 411~~	~~82.50~~	~~NODE 412~~	~~84.50~~
NODE 413	46.29	NODE 414	33.61	AIR TOP	114.41	AIR BOTTOM	69.04

RUN NUMBER 113.0 VOLTAGE 96.75 VOLTS CURRENT 2.3162 AMPS POWER 224.097 WATTS PRESSURE 1.000 ATM FLOW 0.29600 LB/MIN

NODE 101	93.99	NODE 102	93.25	NODE 103	92.80	NODE 104	92.40
NODE 201	115.26	~~NODE 202~~	~~113.63~~	~~NODE 203~~	~~112.45~~	~~NODE 204~~	~~111.42~~
NODE 301	129.53	NODE 302	139.24	NODE 303	157.72	NODE 304	180.14
NODE 305	209.83	NODE 306	229.66	NODE 307	236.42	NODE 308	199.13
NODE 309	161.17	~~NODE 310~~	~~134.45~~	~~NODE 311~~	~~113.54~~	~~NODE 312~~	~~103.95~~
NODE 401	108.27	NODE 402	103.87	NODE 403	98.42	NODE 404	91.54
NODE 405	82.60	NODE 406	70.85	NODE 407	68.90	NODE 408	76.63
NODE 409	82.10	NODE 410	86.02	~~NODE 411~~	~~88.73~~	~~NODE 412~~	~~90.73~~
NODE 413	48.22	NODE 414	33.61	AIR TOP	125.77	AIR BOTTOM	69.55

RUN NUMBER 114.0 VOLTAGE 110.60 VOLTS CURRENT 2.6437 AMPS POWER 292.393 WATTS PRESSURE 1.005 ATM FLOW 0.30100 LB/MIN

NODE 101	105.86	NODE 102	105.12	NODE 103	104.68	NODE 104	104.29
NODE 201	134.21	NODE 202	132.19	~~NODE 203~~	~~130.78~~	~~NODE 204~~	~~129.50~~
NODE 301	151.29	NODE 302	162.99	NODE 303	185.23	NODE 304	212.44
NODE 305	248.92	NODE 306	274.03	NODE 307	281.71	NODE 308	235.27
NODE 309	188.02	NODE 310	155.04	NODE 311	129.32	~~NODE 312~~	~~117.52~~
NODE 401	125.84	NODE 402	120.69	NODE 403	114.23	NODE 404	105.91
NODE 405	94.99	NODE 406	80.44	NODE 407	77.94	NODE 408	87.28
NODE 409	93.69	~~NODE 410~~	~~97.96~~	~~NODE 411~~	~~100.71~~	~~NODE 412~~	~~102.67~~
NODE 413	52.25	NODE 414	34.01	AIR TOP	147.29	AIR BOTTOM	69.79

FULL SCALE MODEL TEMPERATURES DEG F FORCED CONVECTION TEST SERIES

RUN NUMBER 115.0 VOLTAGE 111.04 VOLTS CURRENT 2.6507 AMPS POWER 294.335 WATTS PRESSURE 1.004 ATM FLOW 0.29300 LB/MIN

NODE 101	125.65	NODE 102	124.32	NODE 103	123.44	NODE 104	122.74
~~NODE 201~~	~~134.80~~	~~NODE 202~~	~~133.62~~	~~NODE 203~~	~~133.66~~	~~NODE 204~~	~~131.67~~
NODE 301	151.26	NODE 302	165.86	NODE 303	192.34	NODE 304	222.36
NODE 305	260.92	NODE 306	287.14	NODE 307	294.97	NODE 308	249.63
~~NODE 309~~	~~203.56~~	~~NODE 310~~	~~172.36~~	~~NODE 311~~	~~148.57~~	~~NODE 312~~	~~137.85~~
NODE 401	128.85	NODE 402	125.05	NODE 403	120.09	NODE 404	113.15
NODE 405	103.02	NODE 406	88.19	NODE 407	84.68	NODE 408	98.59
~~NODE 409~~	~~106.82~~	~~NODE 410~~	~~112.68~~	~~NODE 411~~	~~116.95~~	~~NODE 412~~	~~120.22~~
NODE 413	55.73	NODE 414	34.21	AIR TOP	71.52	AIR BOTTOM	123.12

RUN NUMBER 116.0 VOLTAGE 110.85 VOLTS CURRENT 2.6487 AMPS POWER 293.600 WATTS PRESSURE 1.020 ATM FLOW 1.18200 LB/MIN

NODE 101	99.89	NODE 102	98.83	NODE 103	98.20	NODE 104	97.69
NODE 201	~~97.24~~	NODE 202	96.45	~~NODE 203~~	~~95.93~~	~~NODE 204~~	~~95.45~~
NODE 301	113.99	NODE 302	129.89	NODE 303	158.86	NODE 304	191.64
NODE 305	233.80	NODE 306	261.99	NODE 307	270.66	NODE 308	225.61
~~NODE 309~~	~~179.34~~	~~NODE 310~~	~~147.46~~	~~NODE 311~~	~~122.73~~	~~NODE 312~~	~~111.44~~
NODE 401	94.15	NODE 402	92.50	NODE 403	90.24	NODE 404	86.53
NODE 405	80.46	NODE 406	71.13	NODE 407	70.92	NODE 408	79.87
NODE 409	86.13	NODE 410	90.51	~~NODE 411~~	~~93.62~~	~~NODE 412~~	~~95.90~~
NODE 413	49.27	NODE 414	34.57	AIR TOP	65.34	AIR BOTTOM	93.13

RUN NUMBER 117.0 VOLTAGE 110.93 VOLTS CURRENT 2.6537 AMPS POWER 294.375 WATTS PRESSURE 1.020 ATM FLOW 5.10000 LB/MIN

NODE 101	81.79	NODE 102	81.14	NODE 103	80.82	NODE 104	80.56
NODE 201	77.58	NODE 202	77.33	~~NODE 203~~	77.19	~~NODE 204~~	~~77.13~~
NODE 301	88.37	NODE 302	100.32	NODE 303	122.94	NODE 304	152.81
NODE 305	194.49	NODE 306	223.29	NODE 307	234.49	NODE 308	192.55
NODE 309	150.70	NODE 310	122.20	NODE 311	100.48	~~NODE 312~~	~~90.63~~
NODE 401	77.25	NODE 402	76.88	NODE 403	75.05	NODE 404	74.09
NODE 405	70.19	NODE 406	63.28	NODE 407	63.01	NODE 408	69.49
NODE 409	73.67	~~NODE 410~~	76.44	~~NODE 411~~	~~73.29~~	~~NODE 412~~	~~73.55~~
NODE 413	45.92	NODE 414	34.28	AIR TOP	68.09	AIR BOTTOM	76.92

APPENDIX II-B

NUSSELT NUMBER CORRELATIONS FOR FREE CONVECTION TESTS

NUSSELT NUMBER VERSUS GRASHOF NUMBER

NUSSELT NUMBER NODE 101	NODE 102	NODE 103	NODE 104	GRASHOF NUMBER	RUN NUMBER
-1.125	0.455	5.528	-3.801	0.1363974E 07	18.0
-9.061	12.603	3.286	-5.569	0.4926023E 07	19.0
0.344	3.428	4.565	-1.445	0.5901717E 07	20.1
-3.272	2.376	2.948	-2.886	0.1473230E 07	21.0
0.860	1.213	3.187	-2.608	0.1372414E 07	22.0
3.335	2.398	2.563	-2.037	0.6368430E 07	23.0
2.040	4.567	0.211	-2.953	0.6536687E 07	24.0
3.515	-0.189	2.020	-2.619	0.1583025E 07	25.0
3.852	1.618	-1.519	-1.456	0.1371040E 07	26.1
7.044	0.065	3.297	-7.489	0.6498184E 07	27.1
10.796	4.719	1.514	-8.170	0.2558674E 08	28.0
11.236	3.539	2.012	1.435	0.9565482E 08	29.1
16.959	2.171	6.232	-1.369	0.3015027E 09	30.0
7.826	3.538	5.782	-1.527	0.2338917E 08	31.2
7.599	5.108	9.088	-1.835	0.8418930E 08	32.1
28.541	3.988	8.456	-0.616	0.2829284E 09	33.0
9.250	3.175	4.793	-0.378	0.2339274E 08	34.0
10.165	6.259	7.586	-2.190	0.8135189E 08	35.1
28.015	6.833	8.625	-1.705	0.2668704E 09	36.0
4.631	3.794	9.597	-2.789	0.2071602E 08	37.1
5.021	8.158	9.699	-0.561	0.7298242E 08	38.1
12.377	9.609	10.572	-0.707	0.2398449E 09	39.0

NUSSELT NUMBER VERSUS GRASHOF NUMBER

NUSSELT NUMBER NODE 201	NODE 202	NODE 203	NODE 204	GRASHOF NUMBER	RUN NUMBER
-22.098	-15.091	-9.600	-3.289	0.1363074E 07	18.0
-24.056	-23.703	-11.732	-3.513	0.4926023E 07	19.0
-23.602	-25.023	-13.684	-3.889	0.5901717E 07	20.1
-17.417	-20.871	-12.342	-2.619	0.1473230E 07	21.0
-16.294	-20.352	-9.074	-2.621	0.1372414E 07	22.0
-22.078	-27.714	-14.970	-1.542	0.6368430E 07	23.0
-19.622	-29.585	-13.704	-3.641	0.6536687E 07	24.0
-13.043	-25.569	-9.690	-1.125	0.1583025E 07	25.0
-12.667	-21.930	-11.024	-2.134	0.1371040E 07	26.1
-18.938	-29.892	-14.816	-2.901	0.6498184E 07	27.1
-24.184	-38.368	-18.340	-4.037	0.2558674E 08	28.0
-28.668	-48.059	-21.887	-7.708	0.9565482E 08	29.1
-41.284	-51.932	-27.827	-10.047	0.3015027E 09	30.0
-23.021	-34.701	-18.979	-4.867	0.2338917E 08	31.2
-31.831	-44.320	-21.335	-8.478	0.8418930E 08	32.1
-48.026	-47.651	-20.101	-9.377	0.2829284E 09	33.0
-28.476	-38.247	-16.537	-5.144	0.2339274E 08	34.0
-30.730	-42.806	-21.482	-6.352	0.8135183E 08	35.1
-46.719	-41.961	-21.683	-8.175	0.2668704E 09	36.0
-25.526	-33.200	-15.026	-8.872	0.2071602E 08	37.1
-34.112	-38.790	-18.073	-9.540	0.7298242E 08	38.1
-48.663	-45.230	-12.869	-10.261	0.2398449E 09	39.0

17614

NUSSELT NUMBER VERSUS GRASHOF NUMBER

NUSSELT NUMBER NODE 301	NUSSELT NUMBER NODE 302	NUSSELT NUMBER NODE 303	NUSSELT NUMBER NODE 304	GRASHOF NUMBER	RUN NUMBER
-4.392	-6.531	-8.051	9.311	0.1363074E 07	18.0
-8.261	-4.964	-9.696	15.071	0.4926023E 07	19.0
-7.990	-12.811	-10.193	14.164	0.5901717E 07	20.1
-4.967	-7.679	-9.476	9.398	0.1473230E 07	21.0
-8.205	-7.088	-9.882	9.218	0.1372414E 07	22.0
-11.177	-9.757	-12.654	14.272	0.6368430E 07	23.0
-13.545	-11.407	-13.060	12.746	0.6536687E 07	24.0
-8.509	-8.012	-10.780	9.893	0.1583025E 07	25.0
-7.430	-9.256	-11.274	6.167	0.1371040E 07	26.1
-15.447	-9.605	-15.457	10.550	0.6498184E 07	27.1
-22.844	-12.499	-18.171	17.485	0.2558674E 08	28.0
-27.527	-24.199	-18.149	28.615	0.9565482E 08	29.1
-32.761	-28.046	-18.345	43.646	0.3015027E 09	30.0
-17.929	-17.383	-14.279	19.989	0.2338917E 08	31.2
-23.996	-21.763	-15.243	30.608	0.8418930E 08	32.1
-27.656	-27.900	-10.784	49.289	0.2829284E 09	33.0
-5.242	-20.512	-8.962	24.799	0.2339274E 08	34.0
-24.940	-20.847	-13.092	30.733	0.8135189E 08	35.1
-31.987	-23.967	-8.154	50.622	0.2668704E 09	36.0
-14.006	-14.450	-11.106	21.212	0.2071602E 08	37.1
-21.271	-19.319	-9.792	31.827	0.7298242E 08	38.1
-33.002	-14.822	-7.752	51.337	0.2398449E 09	39.0

D180-15048-1

NUSSELT NUMBER VERSUS GRASHOF NUMBER

NUSSELT NUMBER NODE 305	NODE 306	NODE 307	NODE 308	GRASHOF NUMBER	RUN NUMBER
15.649	108.573	168.109	93.858	0.1363074E 07	18.0
21.826	151.796	149.346	124.039	0.4926023E 07	19.0
25.890	148.155	157.618	130.141	0.5901717E 07	20.1
17.800	109.367	105.222	97.935	0.1473230E 07	21.0
17.341	112.811	88.481	100.079	0.1372414E 07	22.0
24.236	166.050	136.402	140.198	0.6368430E 07	23.0
24.390	164.212	133.792	142.164	0.6533687E 07	24.0
16.341	117.880	90.578	101.504	0.1583025E 07	25.0
15.684	114.643	91.587	95.007	0.1371040E 07	26.1
22.054	168.542	133.839	137.415	0.6498184E 07	27.1
33.226	236.249	202.957	192.877	0.2558674E 08	28.0
54.673	326.045	342.486	272.136	0.9565482E 08	29.1
86.456	431.101	542.497	351.629	0.3015027E 09	30.0
37.196	220.758	216.559	186.676	0.2338917E 08	31.2
55.651	309.713	347.581	258.884	0.8418930E 08	32.1
91.620	422.524	580.387	333.226	0.2829284E 09	33.0
44.679	207.180	234.035	176.177	0.2339274E 08	34.0
54.205	207.414	354.649	251.686	0.8135189E 08	35.1
84.648	431.429	570.586	331.280	0.2668704E 09	36.0
34.233	215.395	229.880	175.422	0.2071602E 08	37.1
50.303	301.517	352.611	239.804	0.7298242E 08	38.1
79.794	439.647	554.488	326.366	0.2398449E 09	39.0

NUSSELT NUMBER VERSUS GRASHOF NUMBER

NUSSELT NUMBER NODE 309	NODE 310	NODE 311	NODE 312	GRASHOF NUMBER	RUN NUMBER
62.176	37.696	21.433	13.362	0.1363074E 07	18.0
79.461	49.171	27.299	20.366	0.4926023E 07	19.0
83.801	51.565	26.163	12.520	0.5901717E 07	20.1
64.628	39.444	20.287	12.330	0.1473230E 07	21.0
63.804	38.852	18.933	7.825	0.1372414E 07	22.0
87.211	52.680	26.512	12.309	0.6368430E 07	23.0
89.128	52.635	25.954	10.119	0.6536687E 07	24.0
66.748	39.104	20.509	5.779	0.1583025E 07	25.0
63.467	38.773	18.675	4.770	0.1371040E 07	26.1
89.218	52.673	26.903	11.002	0.6498184E 07	27.1
119.646	67.123	32.142	17.689	0.2558674E 08	28.0
160.492	86.918	40.157	16.350	0.9565482E 08	29.1
205.443	103.922	44.770	23.903	0.3015027E 09	30.0
116.202	65.607	34.629	14.310	0.2338917E 08	31.2
155.391	84.723	41.506	19.018	0.8418930E 08	32.1
200.910	102.925	43.501	35.849	0.2829284E 09	33.0
109.243	64.178	31.928	14.833	0.2339274E 08	34.0
151.941	83.653	39.862	21.064	0.8135189E 08	35.1
199.451	103.531	40.657	41.305	0.2668704E 09	36.0
110.488	65.124	33.944	19.704	0.2071602E 08	37.1
148.629	81.496	40.398	22.039	0.7298242E 08	38.1
196.767	102.732	45.067	43.215	0.2398449E 09	39.0

NUSSELT NUMBER VERSUS GRASHOF NUMBER

NUSSELT NUMBER				GRASHOF	RUN
NODE 401	NODE 402	NODE 403	NODE 404	NUMBER	NUMBER
-9.092	-14.126	-15.633	-17.279	0.1363074E 07	18.0
-10.984	-18.917	-20.044	-23.398	0.4926023E 07	19.0
-11.163	-19.807	-22.003	-26.303	0.5901717E 07	20.1
-8.412	-15.646	-16.163	-17.069	0.1473230E 07	21.0
-8.754	-14.233	-16.437	-16.544	0.1372414E 07	22.0
-12.289	-20.200	-20.692	-26.350	0.6368430E 07	23.0
-10.275	-20.874	-21.740	-25.958	0.6536687E 07	24.0
-8.449	-15.632	-15.533	-18.658	0.1583025E 07	25.0
-7.081	-14.538	-15.194	-17.720	0.1371040F 07	26.1
-9.281	-20.905	-21.083	-25.804	0.6498184E 07	27.1
-12.594	-26.300	-27.733	-36.612	0.2559674E 08	28.0
-16.010	-35.463	-37.199	-50.840	0.9565482E 08	29.1
-21.641	-43.007	-49.651	-68.784	0.3915027E 09	30.0
-11.522	-26.257	-27.697	-35.467	0.2338917E 08	31.2
-15.675	-34.456	-37.087	-51.900	0.8418930E 08	32.1
-25.092	-46.185	-50.178	-69.035	0.2829284E 09	33.0
-13.251	-26.804	-28.259	-36.192	0.2339274E 08	34.0
-17.747	-34.332	-37.763	-51.107	0.8135189E 08	35.1
-26.771	-46.237	-51.139	-67.967	0.2668704E 09	36.0
-10.267	-25.457	-28.993	-34.772	0.2071602E 08	37.1
-16.606	-33.128	-38.195	-49.700	0.7298242E 08	38.1
-26.897	-43.579	-51.617	-68.410	0.2398449E 09	39.0

NUSSELT NUMBER VERSUS GRASHOF NUMBER

NUSSELT NUMBER NODE 405	NODE 406	NODE 407	NODE 408	GRASHOF NUMBER	RUN NUMBER
-21.745	-16.585	-24.460	-3.203	0.1363074E 07	18.0
-31.354	-26.614	-32.281	-6.464	0.4926023E 07	19.0
-31.536	-30.884	-34.326	-7.683	0.5901717E 07	20.1
-23.346	-19.253	-24.792	-6.031	0.1473230E 07	21.0
-22.545	-18.682	-25.663	-5.504	0.1372414E 07	22.0
-33.429	-31.402	-35.979	-8.289	0.6368430E 07	23.0
-34.917	-30.524	-37.741	-7.596	0.6536687E 07	24.0
-23.145	-19.385	-25.591	-5.281	0.1583025E 07	25.0
-23.233	-19.510	-24.764	-5.448	0.1371040E 07	26.1
-35.050	-30.936	-35.842	-8.216	0.6498184E 07	27.1
-50.936	-48.747	-49.701	-12.177	0.2558674E 08	28.0
-77.173	-79.392	-76.700	-17.441	0.9565482E 08	29.1
-108.223	-119.596	-106.437	-24.021	0.3015027E 09	30.0
-49.603	-47.911	-50.272	-12.925	0.2338917E 08	31.2
-73.085	-74.590	-71.247	-17.019	0.8418930E 08	32.1
-114.879	-116.537	-97.049	-22.843	0.2829284E 09	33.0
-49.303	-46.776	-48.435	-12.707	0.2339274E 08	34.0
-73.047	-72.069	-69.900	-16.902	0.8135189E 08	35.1
-114.814	-112.364	-91.960	-21.919	0.2668704E 09	36.0
-47.172	-50.441	-54.353	-12.430	0.2071602E 08	37.1
-71.375	-68.499	-65.430	-15.390	0.7298242E 08	38.1
-109.084	-106.214	-87.871	-20.394	0.2398449E 09	39.0

17618

NUSSELT NUMBER VERSUS GRASHOF NUMBER

NUSSELT NUMBER NODE 409	NODE 410	NODE 411	NODE 412	GRASHOF NUMBER	RUN NUMBER
0.850	2.549	0.830	2.221	0.1363074E 07	18.0
0.752	3.542	2.288	4.978	0.4926023E 07	19.0
-0.700	2.694	2.373	1.260	0.5901717E 07	20.1
1.431	0.102	1.548	1.881	0.1473230E 07	21.0
0.399	0.776	1.000	1.716	0.1372414E 07	22.0
-0.497	2.176	1.180	2.239	0.6368430E 07	23.0
-1.847	2.588	0.965	4.823	0.6536687E 07	24.0
-1.066	1.097	0.943	2.377	0.1583025E 07	25.0
-1.500	1.425	0.253	3.184	0.1371040E 07	26.1
-1.344	2.135	0.660	6.551	0.6498184E 07	27.1
-1.601	3.160	0.968	8.498	0.2558674E 08	28.0
-3.639	4.398	2.251	4.081	0.9565482E 08	29.1
-4.814	4.535	3.420	5.364	0.3015027E 09	30.0
-0.692	2.253	1.895	2.998	0.2338917E 08	31.2
-2.919	3.531	2.621	3.144	0.8418930E 08	32.1
-3.060	5.041	3.297	3.430	0.2829284E 09	33.0
-1.346	3.065	1.721	1.487	0.2339274E 08	34.0
-2.632	3.615	2.586	4.138	0.8135189E 08	35.1
-3.290	4.950	3.555	4.168	0.2668704E 09	36.0
0.128	2.500	3.018	1.621	0.2071602E 08	37.1
-2.254	3.811	3.781	2.613	0.7298242E 08	38.1
-2.801	5.712	4.953	3.574	0.2398449E 09	39.0

PART III

SPACECRAFT DOCKING THERMAL INTERFACE

Table of Contents

III.1 INTRODUCTION

The spacecraft docking thermal interface may be critical when a controlled temperature spacecraft is being docked to a spacecraft without temperature control. For example the heat transfer from the controlled temperature spacecraft to a cold spacecraft during docking may result in local moisture condensation on the inside wall of the controlled spacecraft. Disregarding the possibility of convective heat transfer between the docked spacecraft, the spacecraft docking thermal interface involves both radiative and conductive heat transfer. The thermal interface may be separated into a "local" interface and a "distant" interface. The "local" interface involves both radiation and conduction, whereas; the "distant" interface involves only radiation heat transfer.

Thermal scale modeling application to the "distant" interface is within the present state-of-the-art. This modeling application can be used to simulate the radiant interchange and blockage effects for complex multiple docking configurations. Thermal scale modeling application to the "local" thermal interface may be more difficult due to the possible complexities in the docking mechanisms. In particular the contact conductance at the docking interface may be difficult to simulate in a thermal scale model.

This report presents the results of an investigation of transient thermal scale modeling applied to the spacecraft docking thermal interface. The thermal scale modeling criteria and scaling techniques applicable to the docking interface are described. An investigation of a typical AAP docking configuration was made and the details of the spacecraft docking thermal interface were defined. This definition includes the conduction and radiation heat transfer processes with particular emphasis on the contact conductance at the mating flanges.

III.2 THERMAL SCALE MODELING CRITERIA

The thermal scale modeling criteria for the spacecraft docking thermal interface are the same as those for any radiation-conduction system with the additional complexity of the contact conductance scaling criteria. The radiation-conduction scaling criteria are given in Part II of this report. The contact conductance scaling criteria are easily derived by relating the contact conductance to the heating rate per unit area.

$$h_c \Delta T = q \tag{1}$$

where

h_c = contact conductance coefficient

ΔT = temperature difference across joint

q = heating rate per unit area

The scaling criteria for q is that $(q/\sigma T_o^4)$ remain invarient, where T_o is the characteristic temperature. Consequently the scaling criteria for contact conductance is

$$\left(\frac{h_c}{\sigma T_o^3}\right)^* = 1 \tag{2}$$

where the superscript * refers to the model to prototype parameter ratio.

For the temperature preservation scaling technique

$$h_c^* = 1 \tag{3}$$

and for material preservation

$$h_c^* = (T_o^3)^* = (L^*)^{-1} \tag{4}$$

where L is the characteristic length.

Rice (reference 1) has shown that the contact conductance can be represented by an equation of the form

$$h_c = c\,k\,\frac{m}{\sigma}\left(\frac{P}{H}\right)^a \tag{5}$$

where

c = constant

k = mean thermal conductivity

m = mean rms slope of surface roughness

σ = mean rms height of surface roughness

P = pressure at interface

H = micorhardness of material

a = constant

The microhardness H may be approximated, in terms of yield strength S, by

$$H \approx S/3 \tag{6}$$

and by plotting experimental data on log-log coordinates Rice obtained

$$h_c = 0.55\,k\left(\frac{m}{\sigma}\right)\left(\frac{P}{3S}\right)^{0.85} \tag{7}$$

This equation holds for ideal surfaces in contact, i.e., surfaces which do not have waves or distortions. Surfaces of 'O' ring groove quality are examples of the type surface for which the contact conductance is given by equation (7).

The conditions required for meeting the contact conductance scaling criteria may be found from equations (3), (4) and (7).

The criteria for temperature preservation scaling then becomes

$$k^*\left(\frac{m}{\sigma}\right)^*\left(\frac{P^*}{S^*}\right)^{0.85} = 1 \tag{8}$$

or in terms of pressure

$$P^* = \left(\frac{1}{k^*}\,\frac{\sigma^*}{m^*}\right)^{1.18} S^* \tag{9}$$

If the mating surfaces of both the prototype and model are machined to the same roughness then the scaling requirement for temperature preservation becomes

$$P^* = S^* \, (k^*)^{-1.18} \tag{10}$$

The required pressure at the mating surfaces for temperature preservation scaling is thus a function of the yield strength and thermal conductivity.

The criteria for material preservation scaling can be written using equations (4) and (7) as

$$\left(\frac{m}{\sigma}\right)^* (P^*)^{0.85} = (L^*)^{-1} \tag{11}$$

or in terms of pressure at the interface, assuming identical surface conditions for model and prototype,

$$P^* = (L^*)^{-1.18} \tag{12}$$

The material preservation scaling technique thus requires the interface pressure to be increased to model the contact conductance.

III.3 DOCKING INTERFACE DEFINITION

The docking interface definition was based on the Apollo Command Module (CM) docking system. In this study the thermal effects of the docking probe and drogue were considered insignificant and emphasis placed on the heat transfer through the basic docking ring structures. In the docking of the Apollo CM to another spacecraft the Apollo docking ring is held to the mating spacecraft docking ring by twelve spring loaded latches. The docking ring is a 35 inch diameter tube with flanges at both ends. There are two O-ring grooves in the mating flange and one O-ring groove in the flange which is held permanently to the CM with metal to metal contact along its surface.

The heat transfer between the docked spacecraft occurs primarily by conduction through the docking ring structures and radiation through the docking tunnel. The most complex heat transfer process occurs at the mating flanges where contact conductance effects may be significant. These contact conductance effects depend on the details of the docking latches, in particular on the amount of docking force generated by the latching system. In the accomplishment of this task the details of the docking latches were unavailable until late in the program. Consequently the docking interface was defined, except for the latches, and thermal analyses conducted for various values of contact conductance at the mating surfaces. When the details of the docking latches became available their effect on the interface was also determined.

III.3.1 Thermal Analyses

A thermal math model was developed for the docking interface between the CM and the Subsystem Test Bed (STB). Since the conduction through the Apollo docking ring is a major heat transfer mode for the thermal interface, a detailed analysis was performed to determine the total thermal conductance of the CM docking ring. The results of this analysis was then used to design a thermally equivalent docking ring that replaces the complex CM docking ring cross section with a simple cross section. This thermally equivalent CM docking ring cross section is shown in Figure III-1. The overall dimensions are the same as the actual docking ring.

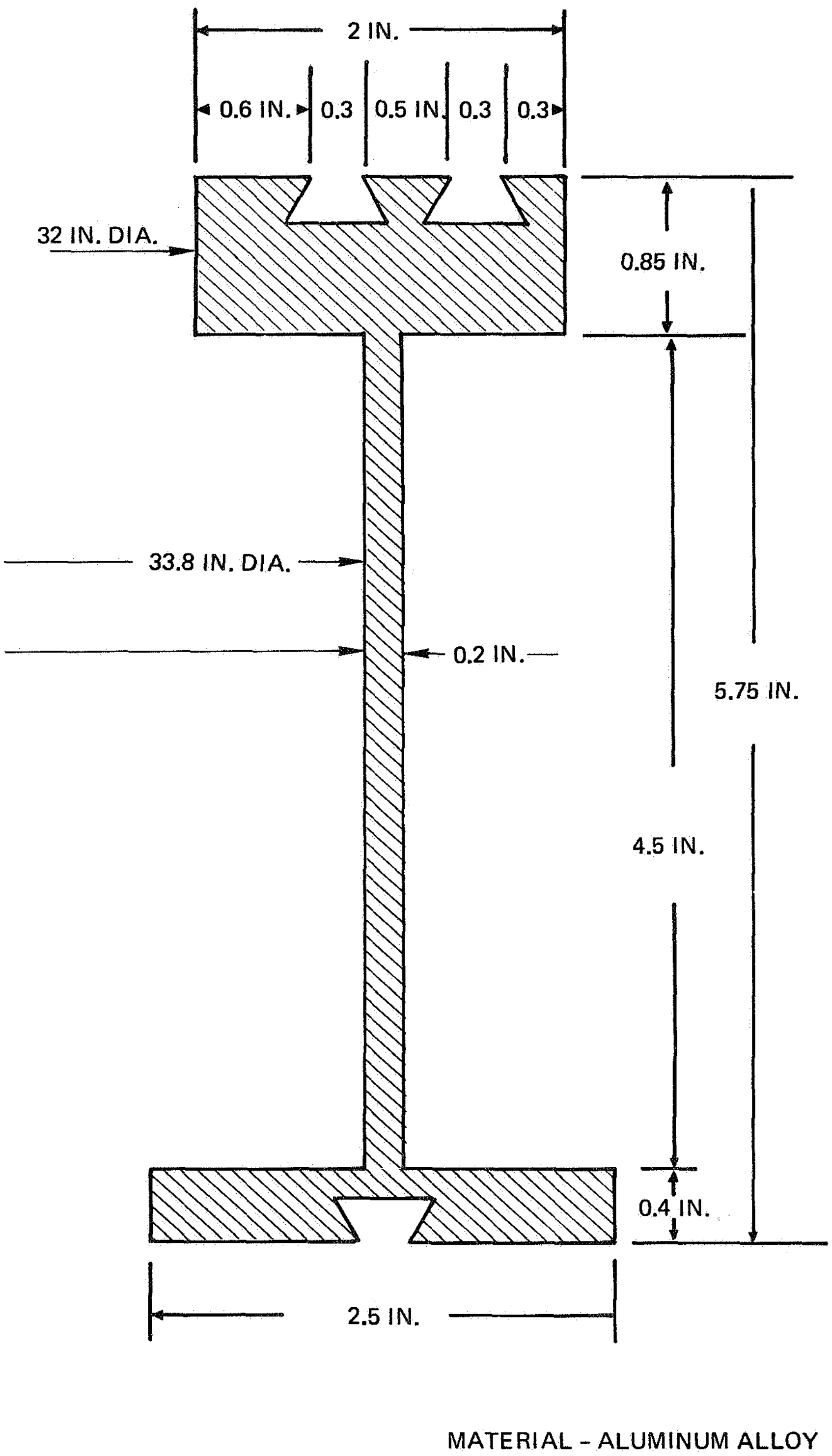

FIGURE III-1 THERMALLY EQUIVALENT CM DOCKING RING

The thermal math model nodes used for the CM/STB thermal interface is shown in Figure III-2. This math model includes convection from the STB atmosphere to the STB pressure shell and docking hatch; conduction along the STB pressure shell to the docking tunnel; conduction along the tunnel wall; variable contact conductance across the mating interface and conduction along the CM docking ring to the CM structure. The radiation heat transfer inside the docking tunnel was also included in the math model. The radiative interchange factors (script - F values) for the tunnel nodes were determined from The Boeing Company's Thermal Radiative Interchange Factor Computer Program (reference 2). The STB tunnel surfaces were assumed to have an emissivity of 0.2 and the CM thermal hatch surface an emissivity of 0.4. The radiation exchange between the mating flanges was also included for cases in which there is no metal to metal contact.

The conductive heat transfer across the mating flanges was considered for two cases. In one case the O-rings are not completely compressed and there is no metal to metal contact at the interface. In this case the conduction across the interface depends on the degree to which the O-rings are compressed. As the distance between the mating flanges is decreased the contact area between the surfaces and the O-rings is increased due to the flattening of the O-rings. This increase in contact area and reduction in conduction path length was included in the determination of the O-ring conductance versus the CM/STB interface separation shown in Figure III-3. The band of values shown is due to the uncertainties in exact sizes and materials used in the docking system.

The other case considered occurs when the O-rings are completely compressed and the mating flanges contact each other. In this case there is metal to metal contact and the dominant mode of heat transfer is by contact conductance. This contact conductance is very sensitive to the contact pressure exerted at the interface (see equation 7).

Thermal analyses of the CM/STB docking interface were made using the Boeing Engineering Thermal Analyzer (BETA) computer program (reference 3). These analyses assumed the gas atmosphere in the STB to be maintained at 530°R and the CM structure to be at 490°R. Three convective heat transfer coefficient

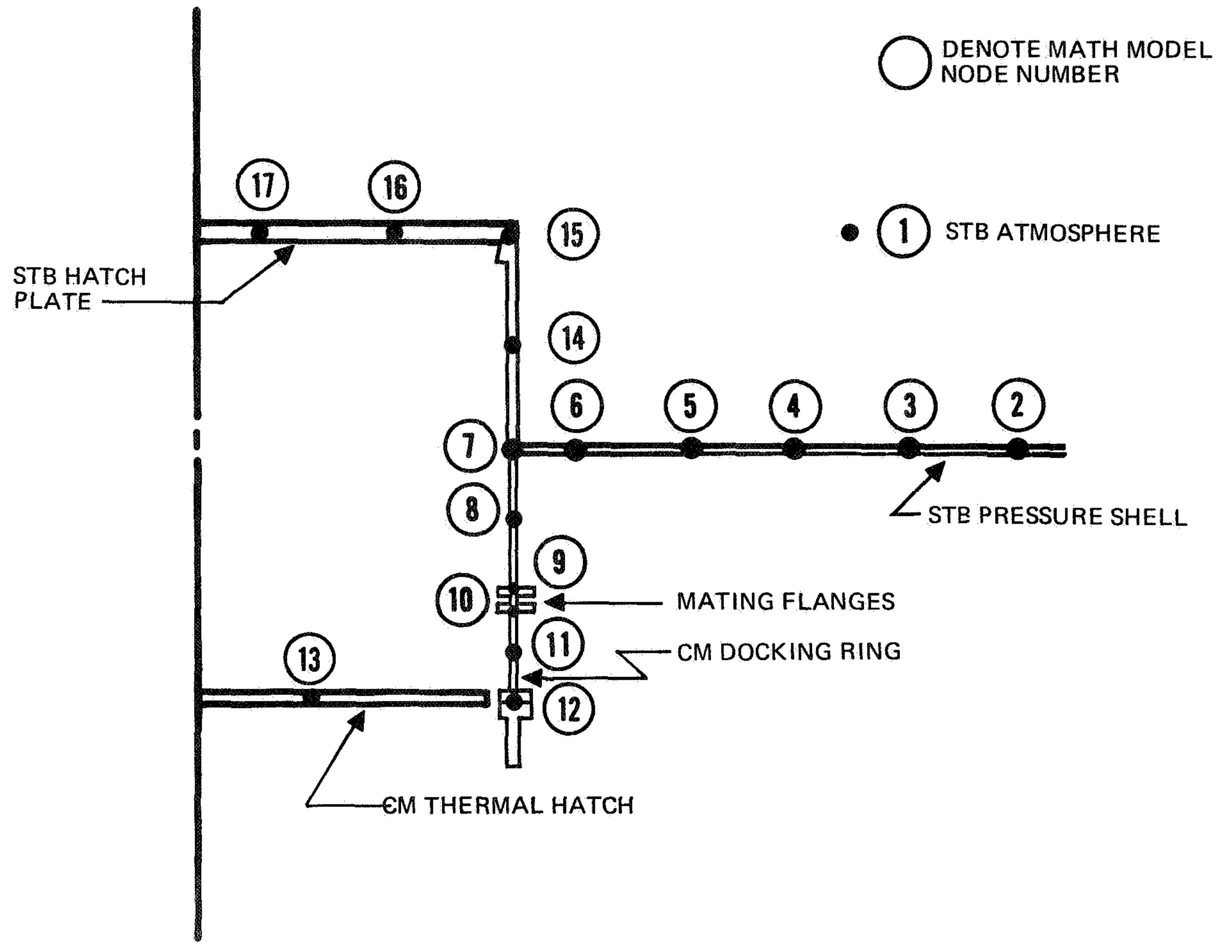

FIGURE III– 2 CM/STB DOCKING INTERFACE

FIGURE III–3 O-RING CONDUCTANCE

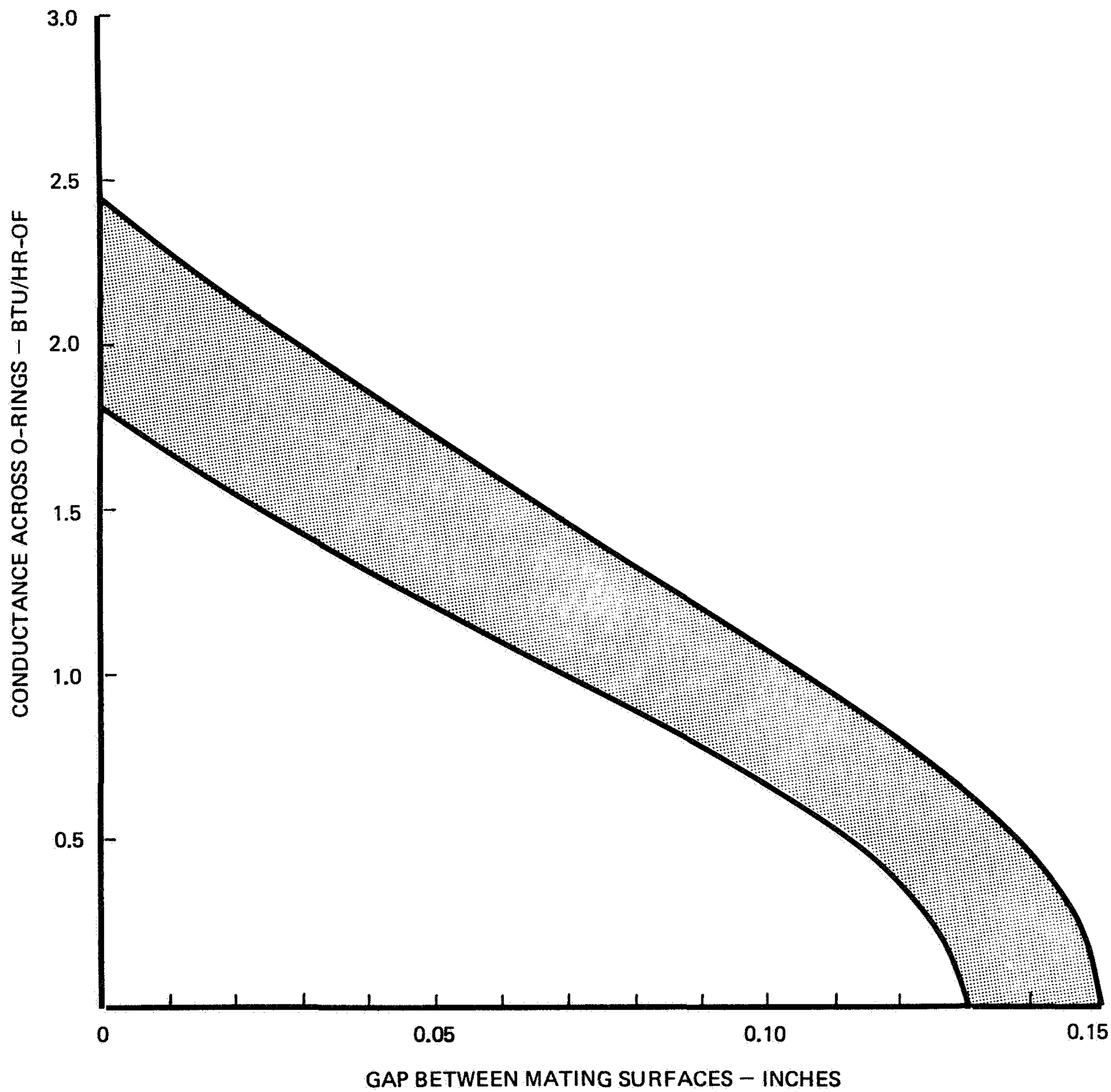

values (0.05, 0.5 and 1.0 BTU/FT^2-HR-°F) were used for the STB atmosphere/wall thermal interface and various values of conductance, ranging from 0 to 10^4 BTU/HR-°F, were used for the mating flange interface. Typical steady state temperature distributions calculated for the docking tunnel are shown in Figure III-4 for a convective heat transfer coefficient of 0.5 BTU/FT^2-HR-°F. This figure shows that there is a substantial temperature drop at the mating interface for all cases except for intimate metal to metal contact where the interface conductance is greater than 100 BTU/HR-°F. The heat transfer rate between the STB and CM is shown in Figure III-5 as a function of the conductance at the mating interface for the three heat transfer coefficients. This figure shows the heat transfer rate to be independent of conductance for both high and low conductance values. This was expected since at high values of interface conductance the heat transfer rate is fixed by the conduction in the tunnel wall and at low values of interface conductance it is fixed by the radiation heat transfer. In the intermediate range of contact conductance (from about 1. to 100 BTU/HR-°F) the magnitude of this conductance has a significant effect on the spacecraft docking thermal interface. If the contact conductance is either large or small then its magnitude does not have a significant effect on the docking interface.

III.3.2 Conductance At The Mating Interface

When the details of the docking latches became available it was determined that the total conductance for the twelve latches is about 0.5 BTU/HR-°F if they are made of stainless steel and about 4.0 BTU/HR-°F if made of aluminum. This conductance is important only if there is no metal to metal contact at the mating flanges.

The contact conductance at the mating flanges may be found from equation (7) using the following values for the CM/STB docking interface

k = 79 BTU/FT-HR-°F

S = 45,000 PSI

$\sigma = 32 \times 10^{-6}$ inches

$m = 1$

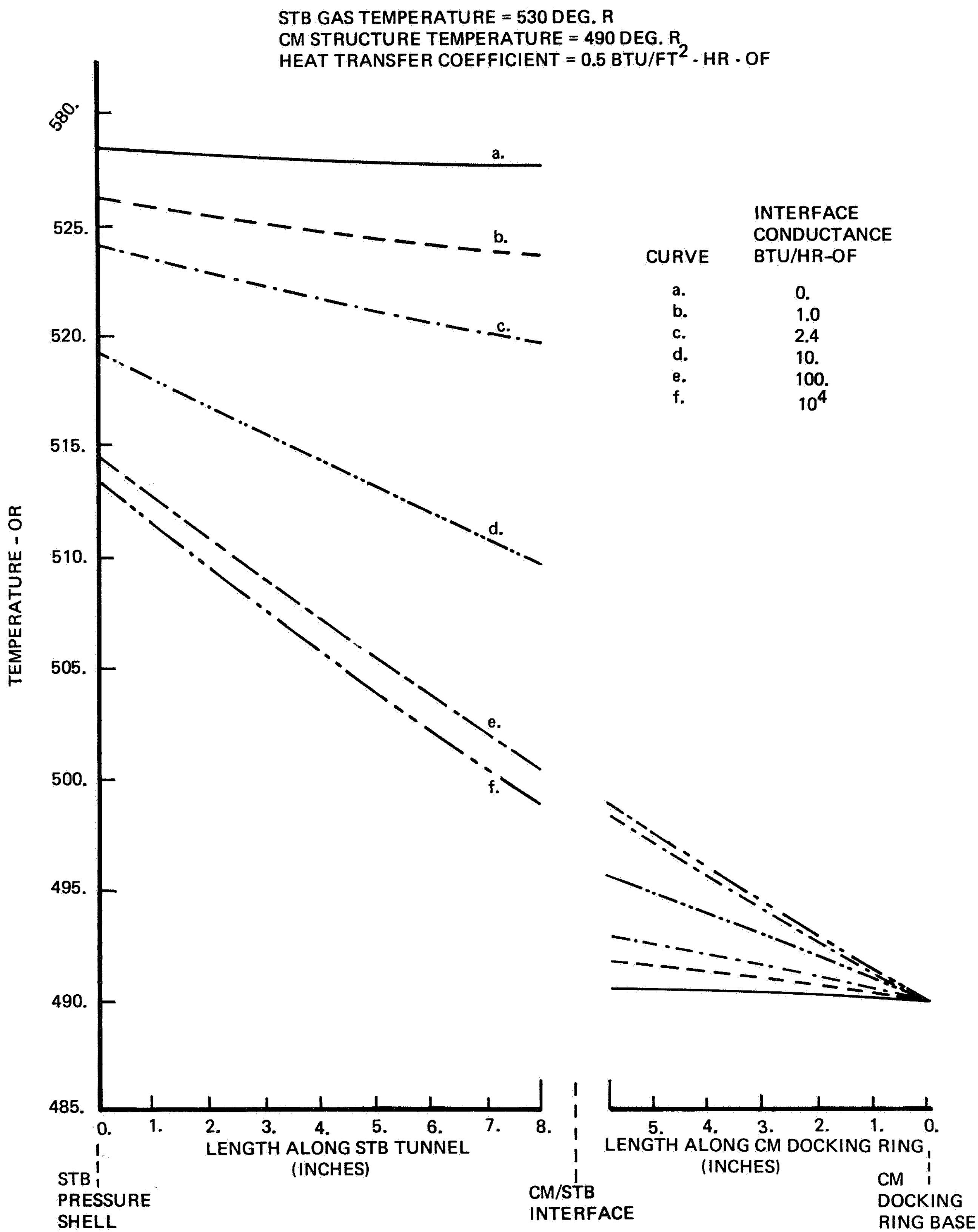

FIGURE III–4 DOCKING TUNNEL TEMPERATURE DISTRIBUTION

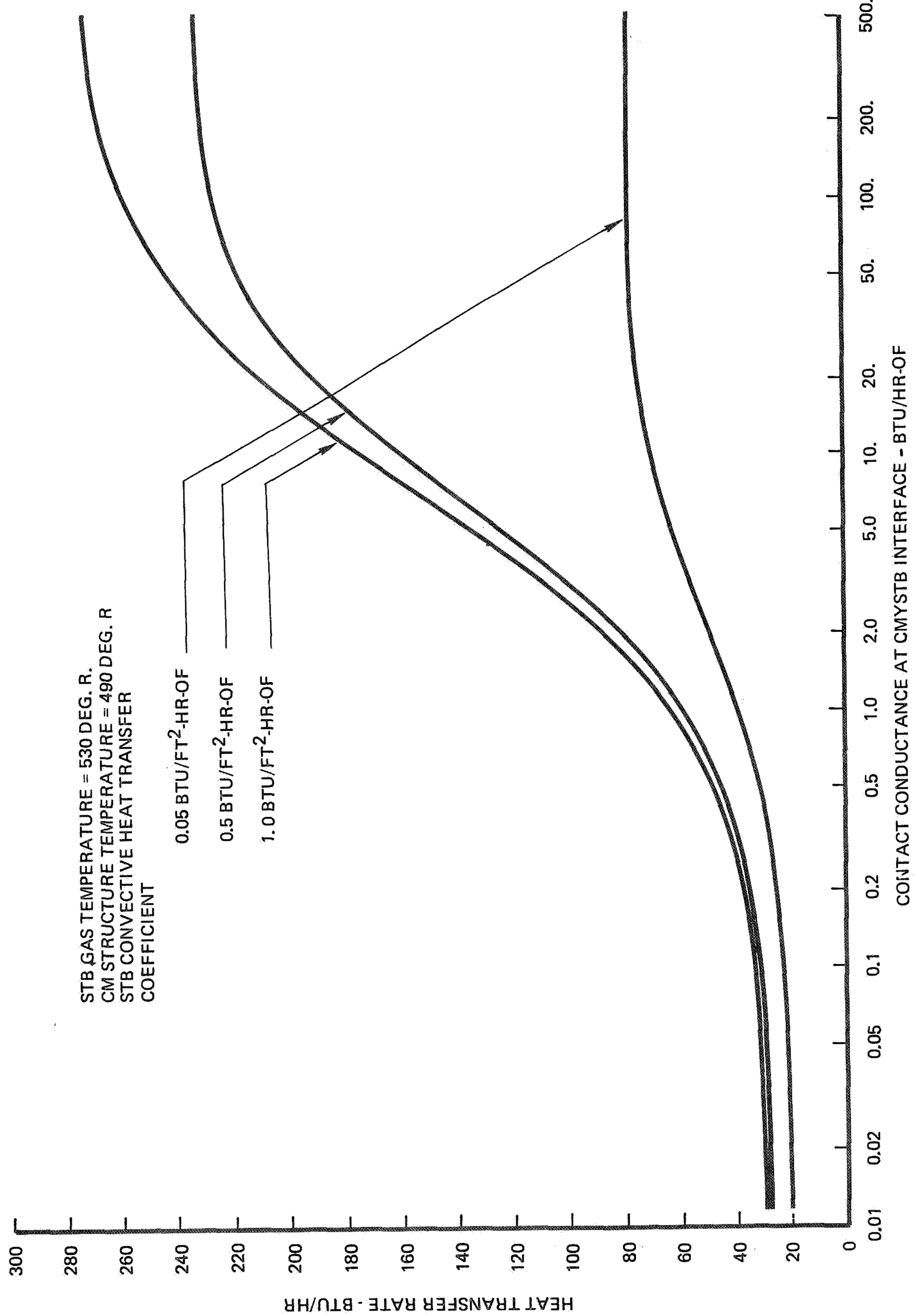

FIGURE III-5 HEAT TRANSFER RATE BETWEEN STB AND CM

The contact conductance coefficient at the mating interface is then given as

$$h_c = 710\ P^{0.85}\ \text{BTU/FT}^2\text{-HR-°F} \tag{13}$$

where P is the interface contact pressure in PSI.

The contact conductance ($h_c A$) at the interface is thus related to the net docking force by

$$K = 4.9F^{0.85}A^{0.15}\ \text{BTU/HR-°F} \tag{14}$$

where

K = contact conductance at mating flanges
F = net docking force lb
A = contact area of mating surfaces in^2

The net docking force is the force exerted by the docking latches minus that required to compress the O-rings (about 1000 lbs) and that required to overcome the pressurization of the tunnel (about 5500 lbs). The total force exerted by the docking latches is reported to be about 38,000 lbs. Consequently the net docking force is about 31,500 lbs. Using this net force along with the flange area of 94.5 in^2 in equation (14) gives a contact conductance of

$$K = 6 \times 10^4 A_*^{0.15}\ \text{BTU/HR-°F} \tag{15}$$

where A_* = fraction of total area in contact.

Equation (15) shows that even with a small fraction of the flange area in metal to metal contact the value of the contact conductance is large enough to assume intimate contact. Consequently contact conductance has an insignificant effect on the docking interface.

III.4 CONCLUSIONS

Thermal scale modeling of systems involving contact conductance is a problem area where further investigation is needed. However the contact conductance at the mating flanges is too large to have a significant effect on the Spacecraft Docking Thermal Interface. Consequently the application of thermal scale modeling to this interface presents no special problems and thermal similitude may be achieved using existing scale modeling techniques.

REFERENCES

1. "Thermal Conductance of Metallic Joints," Rice, R. E., M. S. Thesis, Mechanical Engineering Department, University of California at Berkeley, May 1966.

2. "Thermal Radiative Interchange Factor Program (AS2814)," MacGregor, R. K., Lester, A. B. and Drake, R. T., The Boeing Company, D2-114470-1, May 1970.

3. "Boeing Engineering Thermal Analyzer (A51917)," Bullock, R. H., Brossard, J. J. and MacGregor, R. K., The Boeing Company, D180-10016-1, August 8, 1970.

PART IV

PRELIMINARY STUDY FOR THERMAL SCALE MODELING OF LIQUID LOOP SPACE RADIATORS

TABLE OF CONTENTS

Nomenclature

c	=	specific heat of fluid
D	=	tube diameter
$\vec{e}_g$	=	unit vector in direction of gravity
f	=	friction factor
$f_{c.p}$	=	constant property friction factor
$f(Re)$	=	friction factor as function of Reynolds number
g	=	acceleration of gravity
h	=	heat transfer coefficient
Gr	=	Grashof number
	=	$\dfrac{\rho g \beta (\bar{T} - T_w) D^3}{\mu^2}$
Gz	=	Graetz number
	=	$RePr\dfrac{D}{X}$
k	=	thermal conductivity of fluid
L	=	characteristics length
L_F	=	radiator fin width (or tube spacing)
Nu	=	Nusselt number
	=	$\dfrac{hD}{k}$
$Nu_{c.p}$	=	Nusselt number for constant fluid properties
$Nu(Gz)$	=	Nusselt number as function of Graetz number
Nu_q	=	Nusselt number for constant wall heat flux
p	=	pressure
p_*	=	nondimensional pressure
	=	$\dfrac{\rho L^2 p}{\mu^2}$

Pr	=	Prandtl number
	=	$\frac{\mu c}{k}$
Q	=	heat rejection rate
Re	=	Reynolds number
	=	$\frac{\rho \bar{v} D}{\mu} = \frac{4w}{\pi D \mu}$
t	=	time
T	=	fluid temperature
T_i	=	inlet fluid temperature
T_o	=	characteristic temperature
T_R	=	radiator fin root (tube wall) temperature
T_S	=	radiator sink temperature
v	=	fluid velocity
v_*	=	nondimensional velocity
	=	$v/\bar{v}$
w	=	fluid mass flow rate
x	=	axial distance from tube inlet

Greek Symbols

β	=	coefficient of thermal expansion
ε	=	emissivity
η_F	=	radiator fin effectiveness
θ	=	nondimensional temperature
	=	$\frac{T - T_w}{\bar{T} - T_w}$

θ' = nondimensional temperature

= $\frac{T}{T_o}$

μ = fluid viscosity

ρ = fluid density

σ = Stefam-Boltzmann constant

τ = nondimensional time

= $\frac{Kt}{\rho \; cL^2}$

Subscripts

m refers to model

p refers to prototype

R refers to fin root

w refers to wall

Superscript * Refers to model to prototype ratio

bars denote average values (or evaluation at average fluid temperature)

Operators

∇ = gradient operator

= $\vec{e}_i \frac{\partial}{\partial x_i}$

∇_* = nondimensional gradient operator

= L_∇

IV.1 INTRODUCTION

Liquid loop space radiators are critical elements in the thermal control of manned spacecraft. These radiator systems are quite complex and costly design problems have been associated with their development. Thermal scale modeling may represent a means of minimizing the development costs involved in the design, fabrication and testing of large, complex liquid loop space radiator systems.

A literature search conducted at the start of this study failed to reveal any thermal scale modeling studies of liquid loop radiators reported in the literature. However, near the end of this study, two spacecraft radiator scale modeling investigations were found. In a recent study Colvin and Maples, reference 9, have initiated experiments with thermal modeling of fluid flow in tubes with a radiation boundary condition. They derived "scaling criteria" based on the thermal conduction in the tube wall and the convection and radiation boundary conditions for the tube wall. Based on these "scaling criteria" they designed and tested prototype and model radiator tubes. Their test results for identical Reynolds numbers in model and prototype showed a lack of thermal similitude. This lack of similitude is related to their neglection of the fluid thermal energy balance in deriving "scaling criteria." Fluid energy balance considerations are of primary importance in deriving proper scaling criteria. More recently Dietz and Fleming, reference 10, have derived scaling criteria and performed an analytical investigation of scale modeling a space shuttle radiator panel at a 0.4 scale ratio using two scaling techniques. One scaling technique uses a fluid change model and the other uses a fluid preservation model. The results of their analytical investigation show good agreement between the model and prototype temperatures during transient and steady state operation for both scale modeling techniques. The scaling techniques described by Dietz and Fleming are closely related to those described in this report.

This report presents the results of a preliminary investigation of thermal scale modeling of liquid loop radiators. The characteristics of fluid flow in tubes are reviewed and their effects on liquid loop radiator performance and tests are discussed. The thermal scale modeling criteria are developed and possible scaling techniques discussed. Based on this preliminary study, recommendations for further work are made.

IV.2.0 FLUID FLOW IN TUBES (A BRIEF REVIEW)

Investigations of heat transfer for fluid flow in tubes date back to the 1870's and those of pressure drop date back to even earlier times. These investigations are still continuing and accurate predictions for heat transfer and pressure drop for all flow conditions are not yet possible even though a great amount of literature has been published on the subject.

Aside from the transitional flow regime, which most designers avoid, the major uncertainties in predicting the heat transfer and pressure drop are caused by the variable fluid property effects. This is especially true for laminar flow where theoretical solutions have been verified for constant properties fluids. These variable property effects are less important for turbulent flow, however, the theory for turbulent flow is less developed than for laminar flow and the emperical correlations are subject to considerable uncertainty.

The variable fluid properties having the largest effect on heat transfer and pressure drop are the viscosity and, when in the presence of a gravity field, the density. In fluids such as water that have a well defined freezing point the variable viscosity effects on the heat transfer coefficient and the local pressure gradient are generally small. However, in fluids such as oils, which are characterized by a pour point instead of a freezing point, the variable viscosity effects can be quite significant. The density variations give rise to free convection effects that can be significant for all fluids in a gravity field environment.

IV.2.1 Governing Equations

The heat transfer and pressure drop are governed by the energy and momentum equations. The energy equation can be written (for constant thermal conductivity, negligible viscous dissipation and no internal heat sources) as

$$\rho c \frac{\partial T}{\partial t} + \rho c \vec{v} \cdot \nabla T = k \nabla^2 T \qquad (1)$$

The momentum equation, Navier-Stokes equation for incompressible fluid, may be written, considering buoyancy as the only body force, as

$$\rho\left(\frac{\partial \vec{v}}{\partial t} + \vec{v}\cdot\nabla\vec{v}\right) = -\nabla p - \rho g\,\beta(T-\bar{T})\vec{e}_g - \nabla\times(\mu\,\nabla\times\vec{v}) \qquad (2)$$

These equations may be written in nondimensional form as:

energy

$$\frac{\partial \theta}{\partial \tau} + Re\,Pr\,\vec{v}_*\cdot\nabla_*\theta = \nabla_*^2\theta \qquad (3)$$

momentum

$$\frac{Re}{Pr}\frac{\partial \vec{v}_*}{\partial \tau} + Re^2\,\vec{v}_*\cdot\nabla_*\vec{v}_* = -\nabla_* p_* - Gr\,\theta\,\vec{e}_g - Re\,\nabla_*\times\left(\frac{\mu}{\bar{\mu}}\nabla_*\times\vec{v}_*\right) \qquad (4)$$

These equations are used directly for laminar flow problems, however, for turbulent flow, time averaged terms are used and the flow fluctuations are accounted for by the addition of turbulent stress terms (Reynolds Stresses).

IV.2.2 Laminar Flow

Numerical solutions have been developed for the energy and momentum equations for laminar flow in tubes under various boundary conditions. These solutions generally relate to constant property fluids under steady state conditions. Tribus and Klein, reference 1, reviewed the solutions for prescribed wall temperature boundary conditions. Siegel, Sparrow and Hallman, reference 2, present the solution for the uniform wall heat flux boundary condition. The radiant heat flux boundary condition case was solved by Chen, reference 3. He also relates his numerical solution for the local Nusselt number to that for the uniform wall heat flux case to within ± 2 percent by a simple relationship. These results are of particular interest in the design of liquid loop space radiators.

The verification of these numerical solutions with experimental data has been limited by the variable fluid property effects on heat transfer and pressure drop. These effects have also obscured many experimental data correlation attempts. The variable viscosity effects are generally taken into account by using the emperical correlations developed by Sieder and Tate (reference 4). Their correlations for laminar flow are:

heat transfer

$$Nu = Nu_{c.p.}\left(\frac{\bar{\mu}}{\mu_w}\right)^{0.14}$$

pressure drop

$$f = f_{c.p.}\left(\frac{\bar{\mu}}{\mu_w}\right)^{-0.25}$$

They also correlated turbulent flow data with the same viscosity ratio exponent for the Nusselt number correction and with an exponent of -0.14 for the friction factor correction. More recently Shannon and Depew, reference 5, developed a numerical solution for the variable vicosity effects for laminar flow in a tube with uniform wall heat flux. Their solution, which was verified with experimental data, shows that the viscosity ratio exponent is a function of the Graetz number and is also a weak function of the viscosity ratio itself. For fully developed flow the Nusselt number correction is in close agreement with the Sieder-Tate correlation for viscosity ratios greater than about 0.1. However, the Sieder-Tate correlation for the friction factor does not fully account for the variable viscosity effects. The numerical analysis and experimental data show that the viscosity ratio exponent is about -0.5 for fully developed flow as compared to the Sieder-Tate value of -0.25.

The free convection effects on heat transfer and pressure drop depend on the tube orientation. Vertical tubes lend themselves to theoretical analyses because of the symmetry, whereas, the asymmetric effects in horizontal tubes make the problem much more complex. Free convection effects in vertical tubes have been investigated by Hallman, reference 6, for the uniform wall flux case and by Rosen and Hanratty, reference 7, for the uniform wall temperature case. These investigations related the free convection effects to the magnitude of the Grashof to Reynolds number ratio, Gr/Re.

Shannon and Depew, references 5 and 8, experimentally investigated the free convection effects in horizontal tubes with a uniform heat flux boundary condition. The results of these investigations show that the free convection effects are independent of the Reynolds number and depend on the magnitude of the Rayleigh number (Ra = GrPr) for fully developed flow. Free convection effects become significant for a Rayleigh number between 2 x 10^3 and 5 x 10^3. The free convection effects increase the Nusselt number by as much as a factor of 2 at a Rayleigh number of 2 x 10^4.

In many practical applications both the variable viscosity and free convection effects are significant. These combined effects make theoretical analyses very difficult and obscure the emperical data correlations.

IV.2.3 Turbulent Flow

Since the temperature difference between the fluid and tube wall is generally small for turbulent flow, the free convection and variable viscosity effects are generally small. However the theory for turbulent flow heat transfer is less developed that that for laminar flow and there remains some uncertainty in the emperical data correlations. The turbulent flow Nusselt number correlations generally refer to an average Nusselt number for the entire tube length and are expressed in the form

$$\overline{Nu} = C\,Re^{n}\,Pr^{m}\left(\frac{\bar{\mu}}{\mu_w}\right)^{l} g\left(\frac{L}{D}\right) \tag{5}$$

Various correlations use different values for the parameters in this equation. Typical values for the constant C range from .021 to .025; the exponent n on the Reynolds number from 0.7 to 0.9; the exponent m on the Prandtl number from 0.3 to 0.6; the viscosity ratio exponent l for liquids from 0.1 to 0.2; and the function of length to diameter ratio g(L/D) is given in various forms. Perhaps the most widely used correlation is the Sieder-Tate equation

$$\overline{Nu} = 0.023\,Re^{0.8}\,Pr^{0.4}\left(\frac{\bar{\mu}}{\mu_w}\right)^{0.14} \tag{6}$$

IV.3 LIQUID LOOP SPACE RADIATOR PERFORMANCE

Consider the simple case of a circular tube attached to a radiator fin with one side radiating to a constant temperature sink. The thermal balance between the fluid heat losses and the convection to the radiator fin is given by

$$-wc\frac{d\bar{T}}{dX} = \pi k \, Nu\,(\bar{T} - T_R) \tag{7}$$

and the balance between the convective and radiative heat transfer is given by

$$\pi k \, Nu\,(\bar{T} - T_R) = \epsilon\sigma\eta_F L_F\,(T_R^4 - T_S^4) \tag{8}$$

This set of equations can be numerically integrated to determine the overall heat rejection rate and the average fluid and tube wall (radiator fin root) temperatures as functions of distance down the tube.

For laminar flow in the tube the local Nusselt number can be used taking into account the variable viscosity effects. At present the best Nusselt number representation would be to use that developed by Chen (reference 3) for the radiant flux boundary condition in terms of the uniform wall flux Nusselt number, i.e.,

$$Nu(Gz) = \left[0.928 + \ln\left(\frac{\epsilon\sigma\eta_F L_F T_i^3}{k}\right)\right] Nu_q(Gz) \tag{9}$$

The variable viscosity effects should be well represented by using the results of Shannon and Depew (reference 5) to modify the constant property uniform wall flux Nusselt number Nu_q, i.e.,

$$Nu(Gz) = \left[0.928 + \ln\left(\frac{\epsilon\sigma\eta_F L_F T_i^3}{k}\right)\right] \left(\frac{\bar{\mu}}{\mu_w}\right)^{m(Gz)} Nu_q(Gz) \tag{10}$$

The viscosity ratio exponent as a function of Graetz number m(Gz) is given in reference 5 and the uniform wall heat flux Nusselt number as a function of Graetz number $Nu_q(Gz)$ is given in reference 2.

Having calculated the tube wall and average fluid temperatures as a function of distance down the tube, the pressure drop may be calculated including the variable viscosity effects from

$$\frac{dp}{dx} = - \frac{128 W \bar{\mu}}{\pi \rho D^4} \left(\frac{\bar{\mu}}{\mu_w} \right)^{n(Gz)} \tag{11}$$

where the viscosity ratio exponent as a function of the Graetz number n(Gz) is given in reference 5 and the viscosities are evaluated at the local temperatures (i.e., at $\bar{T}(x)$ and $T_R(x)$).

Due to the lack of data correlations for the local Nusselt number the calculations for turbulent flow are less refined that those for laminar flow. The overall heat rejection rate and tube wall and average fluid temperature variation with distance along the tube may be determined using the average Nusselt number given by equation (6). The pressure drop may be calculated from

$$\frac{dp}{dx} = - \frac{\rho \bar{v}^2}{2D} f(Re) \left(\frac{\bar{\mu}}{\mu_w} \right)^{-0.14} \tag{12}$$

where f(Re) is taken from the "Moody Diagram."

An actual liquid loop radiator system involves much more than the single tube radiator considered in the preceding paragraphs. However the proper treatment of the fluid flow in a single tube is critical to the overall radiator system performance. Under nominal heat load conditions the heat transfer and pressure drop considerations for the radiator tubes can be of primary importance. In order to achieve maximum flexibility radiator designers strive to achieve as large of a heat load range as possible while maintaining temperature control. Several techniques are used for controlling the temperature at low heat load conditions, among them are:

- o Bypass Control

  A value is used to bypass the fluid around the radiator at low heat load conditions. This type of control is usually unacceptable due to the possible freeze up of the radiator.

- o Regenerative Control

  Full flow is maintained through the radiative and a regenerative heat exchanger is used to control the fluid temperature. This technique generally results in very large pressure drops at low heat loads and is limited by the pump capabilities.

- o Selective Stagnation Radiators

  This technique uses parallel flow passages in the radiator panel and allows the fluid to stagnate (freeze) in selected passages as the heat load is reduced. The successful implementation of this technique depends on the accurate prediction of the pressure drop in each flow passage. Flow instabilities may arise which cause progressive freeze up of the panel.

All of these control techniques depend on the accurate assessment of the pressure drop through the radiator tubes. This is a critical problem for fluids that are characterized by a pour point temperature. Since their viscosities are extremely temperature dependent, fluid temperature variations in both the radial and axial directions have large nonlinear effects on the pressure drop. These effects are accentuated by the fact that these fluids are in the laminar flow regime at the low heat load conditions. Fluids that are characterized by a freezing point temperature usually have viscosities that are not strongly temperature dependent. Consequently, the variable viscosity effects are less critical for these fluids especially if they are in the turbulent flow regime. However, the use of these fluids in selective stagnation radiators requires the freezing and thawing phenomena to be understood in relationship to possible flow instabilities in the radiator panels.

Free convection effects are absent for liquid loop radiators operating under zero-g conditions. However, the design verification tests are conducted in a 1-g environment where free convection may significantly affect the radiator performance.

IV.4 THERMAL SCALE MODELING CRITERIA

The thermal scale modeling criteria for liquid loop space radiators may be developed from the energy equation, momentum equation and the boundary conditions. For steady state conditions and constant fluid properties the energy equation (3) may be written as:

$$Re\,Pr\,\vec{v}_* \cdot \nabla_* \theta' = \nabla_*^2 \theta' \tag{13}$$

the momentum equation (4) as

$$Re^2\,\vec{v}_* \cdot \nabla_* \vec{v}_* = -\nabla_* P_* + Re\,\nabla_*^2 \vec{v}_* \tag{14}$$

and the boundary conditions, equations (7) and (8), as

$$-Re\,Pr\,\frac{D}{L}\,\frac{d\bar{\theta}'}{dx_*} = 4\,Nu\,(\bar{\theta}' - \theta_R') \tag{15}$$

and

$$4\,Nu\,(\bar{\theta}' - \theta_R') = \frac{4\epsilon\sigma\eta_F L_F T_o^3}{\pi k}\,(\theta_R'^4 - \theta_s'^4) \tag{16}$$

Thermal similitude with geometric scaling then requires the following parameters to be preserved in the scale model:

$$Re,\; Pr,\; \frac{\epsilon\sigma\eta_F L_F T_o^3}{k}$$

If free convection effects are present then the Grashof number Gr must also be preserved in the scale model. For the variable viscosity effects to be preserved in the scale model the $(\mu/\bar{\mu})$ term (see equation 4) must be preserved. For a quasi real fluid (a fluid for which the viscosity is exponentially dependent on temperature, see reference 5) this term may be written as

$$\frac{\mu}{\bar{\mu}} = \left(\frac{\mu_W}{\bar{\mu}}\right)^{1-\theta} \tag{17}$$

Consequently, since most real fluid viscosities may be represented by this quasi real fluid over given temperature ranges, the preservation of the variable viscosity effects requires the preservation of the wall to bulk viscosity ratio.

The thermal scale modeling criteria for liquid loop space radiators under steady state conditions can be summarized as

$$Re^* = Pr^* = \left(\frac{\epsilon \sigma \eta_F L_F T_o^3}{k} \right)^* = 1 \tag{18}$$

when free convection and variable viscosity effects are important the additional scaling criteria are

$$Gr^* = \left(\frac{\mu_w}{\bar{\mu}} \right)^* = 1 \tag{19}$$

The detailed consideration of radiator freeze up for fluids characterized by a freezing point temperature is beyond the scope of the present study. However it is obvious that the nondimensional freezing point temperature must be preserved in the scale model. Other factors involving transients may also be involved.

IV.5.0 THERMAL SCALE MODELING TECHNIQUES

The material preservation and temperature preservation thermal scale modeling techniques commonly used for radiation-conduction scaling are inappropriate for liquid loop radiators. The strong dependence of the fluid properties on temperature precludes the use of material preservation and it is extremely doubtful that a fluid could be found to exactly meet the scaling criteria for temperature preservation. Consequently, compromised scaling techniques must be considered. This is also true for scaling of systems involving gaseous convection (see Part II of this report) however, the scaling of liquid loop radiators is further complicated by the variable viscosity effects on heat transfer and pressure drop.

The thermal scale modeling compromises to be used depend on the radiator characteristics of interest. Since flow instabilities and radiator flow stagnation are critical aspects for radiator concepts applicable to AAP and other advanced spacecraft, these aspects should be preserved as well as possible in scale model radiators. Various potential scaling techniques are developed in the following paragraphs.

IV.5.1 Fluid Preservation

Since the fluid properties are critical to the radiator performance, it may be desirable to preserve the fluid in the scale model and use compromised scaling techniques to approximately preserve the temperatures.

IV.5.1.1 Reynolds Number Preservation

If the radiator operates with the coolant flow in different flow regimes for different heat load conditions, then the Reynolds number must be preserved in the scale model to preserve the operating conditions. Preservation of the Reynolds number may also be required for radiators with parallel flow paths in order to preserve the flow distribution pattern.

IV.5.1.1.1 Radiator Fin Geometry Distortion

If the radiator geometry is scaled geometrically except for the radiator fin width (tube spacing) which is kept full scale, then the radiator performance may be preserved in the scale model.

The scale modeling requirements for this scaling technique are

$$\begin{aligned} Re^* &= L_F^* = 1 \\ W^* &= Q^* = L^* \\ \Delta P^* &= (L^*)^{-2} \end{aligned} \tag{20}$$

This technique preserves the fluid and radiator fin temperatures

$$T^* = (T - T_R)^* = \Delta T^* = 1 \tag{21}$$

Since the temperatures are preserved the variable viscosity effects are also preserved

$$\left(\frac{\mu_w}{\bar{\mu}}\right)^* = 1 \tag{22}$$

however the free convection effects are not preserved since

$$Gr^* = (L^*)^3 \tag{24}$$

This scaling technique has the advantage of preserving the radiator performance including the variable viscosity effects. Also the reduction of the Grashof number in the scale model may represent a way to simulate operation in a zero-g field. The disadvantage of this technique is the geometric distortion that doesn't allow reduction of the radiator width.

IV.5.1.1.2 Radiator Tube Diameter Distortion

If the radiator fin geometry is scaled geometrically approximate thermal similitude can be achieved in the model by a distoriton in the scaling of the tube diameter. Dietz and Fleming (reference 10) investigated the use of this technique in preserving the fluid temperature change through the system. The scaling requirements for this case are:

$$\begin{aligned} Re^* &= 1 \\ D^* = W^* = Q^* &= (L^*)^2 \\ \Delta P^* &= (L^*)^{-5} \end{aligned} \tag{25}$$

This technique preserves the radiator fin temperature and the fluid temperature change through the system

$$T_R^* = \Delta T^* = 1 \tag{26}$$

however the temperature difference between the fluid and tube wall is not preserved

$$(T - T_R)^* = L^* \tag{27}$$

Consequently the variable viscosity effects are not preserved and the Grashof number is reduced

$$Gr^* = (L^*)^7 \tag{28}$$

The major disadvantage of this technique is the large pressure drop requirements for small scale sizes.

IV.5.1.1.3 Exact Geometric Scaling

Exact geometric scaling results in reduced temperature changes in the fluid. The scaling requirements for this technique are

$$\begin{aligned} Re^* &= 1 \\ W^* &= L^* \\ Q^* &= (L^*)^2 \\ \Delta P^* &= (L^*)^{-2} \end{aligned} \tag{29}$$

This technique preserves the average radiator fin temperature

$$\bar{T}_R^* = 1 \tag{30}$$

however the fluid temperatures are not preserved

$$\Delta T^* = (T - T_R)^* = L^* \tag{31}$$

consequently the variable viscosity effects are not preserved and the Grashof number is reduced

$$Gr^* = (L^*)^4 \tag{32}$$

The similitude achieved with this technique is not quite as good as that for the radiator tube diameter distortion technique (IV.5.1.1.2), however, the pressure drop requirements are much less severe.

IV.5.1.2 Mass Flux Preservation

If the Reynolds number is not preserved it is possible to preserve the fluid temperature change through the system while using exact geometric scaling. The scaling requirements for this technique are

$$\begin{aligned} Re^* &= L^* \\ W^* = Q^* &= (L^*)^2 \\ \Delta P^* &= (L^*)^{-1} \quad \text{LAMINAR} \\ &= f^* \quad \text{TURBULENT} \end{aligned} \tag{33}$$

This technique preserves the average radiator fin temperature and the fluid temperature change through the system

$$\bar{T}_R^* = \Delta T^* = 1 \tag{34}$$

however the temperature difference between the fluid and the tube wall is not preserved

$$(T - T_R)^* = \frac{L^*}{Nu^*} \tag{35}$$

For fully developed laminar flow equation (35) can be written as

$$(T - T_R)^* = L^* \tag{36}$$

and for turbulent flow as

$$(T - T_R)^* = (L^*)^{0.2} \tag{37}$$

The temperature preservation is fairly good in turbulent flow, however, in laminar flow where variable viscosity effects can be important, the lack of temperature preservation precludes the preservation of variable viscosity effects. The major disadvantage of this scaling technique is the lack of Reynolds number preservation.

IV.5.1.3 Heat Transfer Coefficient Preservation

Whereas the mass flux preservation scaling technique preserved the fluid temperature change through the system while using exact geometric scaling, the heat transfer coefficient preservation technique preserves the temperature difference between the fluid and the tube wall.

IV.5.1.3.1 Turbulent Flow

The heat transfer coefficient preservation scaling requirements for the turbulent flow case are

$$\begin{aligned} Re^* &= (L^*)^{1.25} \\ W^* &= (L^*)^{2.25} \\ Q^* &= (L^*)^2 \\ \Delta P^* &= (L^*)^{0.5} f^* \end{aligned} \tag{38}$$

This technique preserves the temperature difference between the fluid and tube wall

$$(T - T_R)^* = 1 \tag{39}$$

However the fluid temperature change through the system is only approximately the same

$$\Delta T^* = (L^*)^{-0.25} \tag{40}$$

The major disadvantage of using this technique for turbulent flow is that the lack of Reynolds number preservation may result in laminar flow for the scale model.

IV.5.1.3.2 Laminar Flow

The heat transfer coefficient preservation scaling technique is not applicable to fully developed laminar flow where the Nusselt number is independent of the Reynolds number. For developing laminar flow the average Nusselt number is generally taken as proportional to the cube root of the Graetz number.

$$\overline{Nu}^* = (Gz^*)^{1/3} \tag{41}$$

For this case the scaling requirements are

$$\begin{aligned} Re^* &= (L^*)^3 \\ W^* &= (L^*)^4 \\ Q^* &= (L^*)^2 \\ \Delta P^* &= L^* \end{aligned} \tag{42}$$

This technique preserves the temperature difference between the fluid and tube wall

$$(T - T_R)^* = 1 \tag{43}$$

however the fluid temperature change through the system is not preserved

$$\Delta T^* = (L^*)^{-2} \tag{44}$$

The major disadvantage of using this technique for laminar flow is the non-preservation of fluid temperature change through the system. While this technique preserves the variable viscosity effects caused by radial temperature gradients those caused by axial temperature gradients are not preserved.

IV.5.2 Fluid Change

IV.5.2.1 Temperature Preservation

Use of the temperature preservation scaling technique depends on finding a suitable fluid for the scale model. Dietz and Fleming (reference 10) selected R-13B1 fluid for a 0.384 scale model of a space shuttle radiator panel which uses R-21 fluid. The slight difference in fluid Prandtl numbers neccessitated a slight distortion in the scaling of the tube diameter. Even though the freezing point of R-13B1 is -270¼F as compared to -211¼F for R-21, the results of their analytical investigation showed good thermal similitude over the entire range of radiator operation. The major disadvantage of this scaling technique is that the scale ratio is fixed at a given value depending on the model fluid.

The use of this technique, in scale modeling a system in which variable viscosity effects are important, would probably be precluded by the lack of a suitable fluid for the model.

IV.5.2.2 Matched Viscosity Scaling Technique

The thermal scale modeling techniques described in the preceding paragraphs are unsuited for laminar flow with variable viscosity effects with the exception of the radiator fin geometry distortion technique (IV.5.1.1.1). This technique, however, does not allow the radiator fin width to be reduced in size. A solution to this problem might be found in a "matched viscosity scaling technique". This technique would use a fluid in the scale model that has a much larger viscosity than that of the prototype fluid at any given temperature and the prototype performance would be simulated by operating the scale model at a higher temperature. This would allow the radiator fin width to be scaled down in size.

The scale model fluid would be chosen such that its viscosity dependence on nondimensional temperature matches that of the prototype fluid, i.e.,

$$\mu^* = 1 \quad \text{FOR} \quad \theta'^* = 1 \tag{45}$$

This fluid selection fixes the characteristic model temperature since the model fluid viscosity at this temperature must equal that of the prototype fluid at the characteristic prototype temperature.

The product of fin effectiveness and fin width is given by

$$(\eta_F L_F)^* = (T_o^*)^3 k^* \tag{46}$$

As can be seen from equation (46) the fluid thermal conductivity ratio has a strong effect on the scaling of the fin width and may counteract the reduction in size resulting from the increased model temperature.

The local Nussett number, the nondimensional temperature difference between the fluid and tube wall and the nondimensional fluid temperature change through the system may be preserved by preserving the Graetz number. This can be accomplished by setting the model flow rate such that

$$w^* = \left(\frac{k}{c}\right)^* L^* \tag{47}$$

This technique geometrically scales the radiator except for the fin width which is distorted according to equation (46). Further study of this technique is required before its applicability can be ascertained.

IV.6 CONCLUSIONS AND RECOMMENDATIONS

Thermal scale modeling of liquid loop space radiators operating in the turbulent flow regime appears quite promising. Three scaling techniques may be used in one geometrically scaled model radiator configuration. These techniques use the same fluid as the prototype and preserve the radiator fin temperature. The heat rejection is scaled as the square of the scale ratio. The fluid temperature and temperature gradients vary somewhat between the scaling techniques. These techniques are implemented by adjusting the model flow rate as follows:

Reynolds number preservation	$w^* = L^*$
Mass flux preservation	$w^* = (L^*)^2$
Heat transfer coefficient preservation	$w^* = (L^*)^{2.25}$

The freeze up phenomena scaling requires further study.

Thermal scale modeling of liquid loop space radiators operating in the laminar flow regime where variable viscosity effects are important is not as promising. One scaling technique that preserves the radiator performance does not allow a reduction in the radiator width dimension. Another technique, "Matched Viscosity Scaling Technique," shows some promise, however, it depends on the selection of a proper fluid for the scale model and further investigation of this technique is required.

It is recommended that the thermal scale modeling study of liquid loop radiators be continued with emphasis on the high load ratio radiator systems required for AAP and other advanced spacecraft. The results of this study should then be used to experimentally verify and demonstrate the use of thermal scale modeling in the design, development and test verification of liquid loop radiator systems.

References

1. M. Tribus and J. Klein, "Forced Convection from Nonisothermal Surfaces," Heat Transfer Symposium, pp 211-235, University of Michigan, 1953.

2. R. Siegel, E. M. Sparrow and T. M. Hallman, "Steady Laminar Heat Transfer in a Circular Tube with Prescribed Wall Heat Flux," Applied Scientific Research, Section A, Vol. 7, 1958 p. 586.

3. J. C. Chen, "Laminar Heat Transfer in a Tube with Nonlinear Radiant Heat Flux Boundary Condition," Int. J. Heat Mass Transfer, Vol. 9, pp. 433-440, 1966.

4. E. N. Sieder and G. E. Tate, "Heat Transfer and Pressure Drop of Liquids in Tubes," Industrial and Engineering Chemistry, Vol. 28, 1936 p. 1429.

5. R. L. Shannon and C. A. Depew, "Forced Laminar Convection in a Horizontal Tube with Variable Viscosity and Free-Convection Effects," Journal of Heat Transfer, ASME, May 1969, pp. 251-258.

6. T. M. Hallman, "Combined Forced and Free Convection in a Circular Tube," PhD Thesis, Department of Mechanical Engineering, Purdue University, Lafayette, Indiana, May 1968.

7. E. M. Rosen and T. J. Hanratty, "Use of Boundary Layer Theory to Predict the Effect of Heat Transfer on the Laminar - Flow Field in a Vertical Tube with Constant Wall Temperature," AICRE Journal, 7, 112, 1961.

8. R. L. Shannon and C. A. Depew, "Combined Free and Forced Laminar Convection in a Horizontal Tube with Uniform Heat Flux," Journal of Heat Transfer, ASME, August 1968. pp 353-357.

9. D. P. Colvin and D. Maples, "Thermal Scale Modeling of a Spacecraft Radiator with Coupled Convection-Conduction-Radiation Heat Transfer", Institute of Environmental Sciences Proceedings, 1971, pp 428-434.

10. J. B. Dietz and M. L. Fleming, "Thermal Scale Modeling of Spacecraft Radiators", to be presented at Second Intersociety EC/LSS Conference (ASME, AIAA, SAE) San Francisco, California, August 1972.

PART V

EVALUATION OF EXISTING NASA/MSC FACILITIES

TABLE OF CONTENTS

V.1 INTRODUCTION

Thermal verification tests of Apollo Application Program spacecraft will be both demanding and difficult. The physical size and complexity of the AAP configurations are such that full scale testing of the assembled vehicles is not possible utilizing existing thermal/vacuum test facilities.

Consequently, scaled thermal model testing as an alternative to full scale testing must be considered. Scaled model tests may provide certain advantages in terms of reducing test facility and test model costs.

V.2 AAP CONFIGURATIONS

The Apollo Applications Program is primarily concerned with the Skylab Spacecraft configuration as shown in Figure 1. The figure shows the completely assembled spacecraft with a docked command and service module. The physical complexity of the assembled spacecraft and the potential for significant solar shadowing are apparent from the figure.

In addition to the AAP-Skylab other large manned spacecraft presently being studied include the Space Station, the Space Base and the Space Shuttle.

All of these spacecraft configurations present similar thermal simulation test problems because of their size and physical arrangement. Practical thermal testing of the assembled spacecraft can probably only be accomplished with scaled models.

V.3 EXISTING NASA/MSC FACILITIES

Existing NASA/MSC facilities for thermal/vacuum testing are located in both the Space Environment Simulation Laboratory and the Space Environment Effects Laboratory. The Space Environment Simulation Laboratory consists of chambers A & B. The Space Environment Effects Laboratory consists of chambers D & E and six smaller chambers. A description of the capabilities and characteristics of all of the space environment test chambers is included in reference 1.

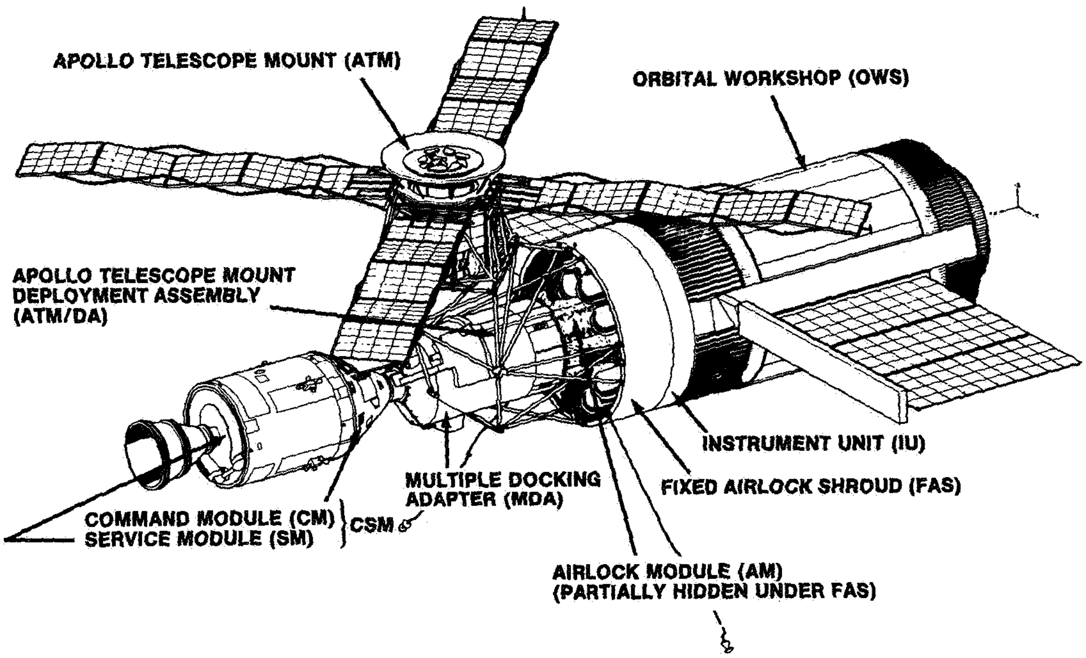

FIGURE 1 SKYLAB SPACECRAFT

V.4 FACILITY REQUIREMENTS FOR SCALE MODEL THERMAL TESTS

Facilities required for spacecraft thermal performance tests consist of vacuum chambers with a cold wall to simulate deep space and some form of thermal simulation. Solar thermal energy simulation requires simulation in terms of total energy, spectral distribution and collimation. Planetary thermal emission and albedo simulation are usually not required except for special tests.

General requirements of test facilities for scaled model thermal tests relate to vacuum chamber size, pressure and thermal environment. The required chamber size is determined by the scale model size. Recent research (reference 2) has indicated that scaled models smaller than 1/10 prototype size incur unacceptable temperature errors, while scaled models smaller than 1/6-1/8 prototype size are increasingly error sensitive to small changes in model scale ratio. This indicates that thermal testing of the Skylab cluster would require a scaled thermal model approximately 12-20 feet in length and 4-6 feet in diameter, not including solar arrays. While the Space Shuttle Orbiter would require a scaled model 15-20 feet in length and 7-9 feet wide.

Vacuum chamber pressure requirements for scaled thermal models will not differ from the requirements for full scale thermal model tests.

Proper thermal environment simulation is an important requirement for scaled thermal model tests. Both the solar simulator and the deep space simulator cold wall must effectively simulate the actual thermal environment. The actual cold wall temperature and emittance are not any more critical than what is required for full size thermal models. However, large temperature gradients in the cold wall or large variations in the wall emittance could have a significant though local effect for a case where the model and chamber are approximately the same size.

Solar simulator errors in intensity, uniformity, collimation and spectral match can all seriously affect the results of thermal tests. However, these errors do not affect scaled models anymore than full size models. However, scaled models tested in large chambers will normally utilize only a small section of the solar simulator which may have different characteristics than the overall simulator. Consequently, thermal simulator characteristics must be accurately determined for all thermal tests and particularly so for scaled model tests.

V.5 EVALUATION OF NASA/MSC FACILITIES IN COMPARISON TO REQUIREMENTS

There are four existing NASA/MSC facilities which can be considered for use in thermal scaled model testing. Chambers A & B in the Space Environment Simulation Laboratory and chambers D & E in the Space Environmental Effects Laboratory. The remaining chambers in the Space Environmental Effects Laboratory (FGHIK & N) are either limited in size, used for special functions or do not have adequate thermal simulation.

Table I shows the interior working dimensions and solar simulator dimensions for chambers A, B, D & E.

TABLE I

	CHAMBER			
	A	B	D	E
Working Dimensions	75'L 25'D	27'L 13'D	15'L 6'D	10'L 4'D
Solar Simulator Dimension	Top 13'D Side 13'x33'	7.5'D	3.5'D	3'D

The approximate dimensions of the Skylab cluster are 120' x 40'. Space Shuttle orbiter dimensions are approximately 120' x 60' while the assembled orbiter/ booster is approximately 200' x 140'. Table II shows the various size scaled models of Skylab and Space Shuttle that could be tested in the NASA/MSC chambers.

This table indicates that chamber "A" can be used to test any realistic size scaled thermal model of either Skylab or Space Shuttle. Chamber B however, can be used for testing these models only with modifications to provide more extensive thermal simulation capability. Chamber D with modifications to the thermal simulation capability, can be used for tests of small models of Skylab or Space Shuttle. Chamber E can be used only for tests of very small sized models, for example, a 1/12 scale model of Skylab or the Space Shuttle orbiter would be necessary. Such small models would incur probable temperature errors of approximately 6-8 percent of absolute temperature. Chamber E could however, be used to test a small scaled model of the Skylab cluster minus the CSM and ATM.

TABLE II

CHAMBER

Config.	A	B	D	E
SKYLAB				
1/4	X	(X)		
1/6	X	(X)		
1/8	X	(X)	(X)	
1/10	X	X	(X)	*
SPACE SHUTTLE ORBITER				
1/4	(X)			
1/6	X	(X)		
1/8	X	(X)		
1/10	X	(X)	(X)	

X - Test with no mod

(X) - Test with mod to chamber

* - Skylab Test minus CSM & ATM

V.6 CONCLUSIONS

Thermal scale model tests of reasonable sized models (1/4-1/10) of both Skylab and Space Shuttle Orbiter can readily be performed in NASA/MSC chambers A & B. Chamber A modifications to the thermal simulator are required only in the case of a large (1/4) model of the Space Shuttle Orbiter. Extension of the thermal simulator capability of Chamber B will be required for most proposed model tests.

A significant saving in test costs can probably be made by using chamber D where possible. Table II indicates that only quite small models of either Skylab or Space Shuttle can be tested in this facility and then only with major modifications to the thermal simulation capability. However it is possible that wider use could be made of chamber D by confining thermal model testing to include only the areas of the vehicle which have critical temperature control requirements.

REFERENCES

1. "Major Test Facilities of the Engineering and Development Directorate," NASA/MSC-03415; Section 6, Space Environment Test Division, October 1970.
2. "Limitations in Thermal Similitude," R. K. MacGregor, The Boeing Company, D2-121352-1, December 1969.